Universitat Internacional de Catalunya
Facultat de Medicina i Ciències de la Salut -
Departament de Ciències Bàsiques

Tesi doctoral

Nutrient-mediated regulation of AMPAR receptors' trafficking through the malonyl-CoA – CPT1C axis

Rocío Rojas Martín

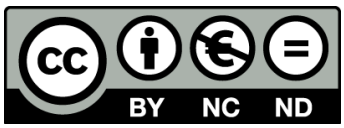

UNIVERSITAT INTERNACIONAL DE CATALUNYA

MEDICINE AND HEALTH SCIENCE FACULTY

BASIC SCIENCE DEPARTMENT

NUTRIENT-MEDIATED REGULATION OF AMPA RECEPTORS' TRAFFICKING THROUGH THE MALONYL-COA – CPT1C AXIS

Rocío Rojas Martín

2023

NUTRIENT-MEDIATED REGULATION OF AMPA RECEPTORS' TRAFFICKING THROUGH THE MALONYL-COA – CPT1C AXIS

Doctoral thesis manuscript presented by Rocío Rojas Martín to opt for the degree of Doctor of Philosophy (PhD) awarded by the International University of Catalonia.

This thesis has been conducted in the Basic Science Department from the Medicine and Health Science Faculty of the International University of Catalonia, under the direction of Dr. Núria Casals Farré and Dr. Rut Fadó Andrés.

This thesis is part of the Doctoral program of Health Sciences included in the Neuroscience Research line of the International University of Catalonia.

Sant Cugat del Vallès, 2023

Dr. Núria Casals Farré	**Dr. Rut Fadó Andrés**	**Rocío Rojas Martín**
Director	Director	PhD student

No temas a las dificultades. Lo mejor surge de ellas.

Rita Levi Montalcini

ACKNOWLEDGMENTS

¡Qué rápido pasa el tiempo! Parece mentira que esta etapa de tesis doctoral haya llegado a su fin. Echo la vista atrás y hace nada estaba empezando en el laboratorio cual "pollito" nuevo. Desde entonces han pasado cuatro años y, para mí, han supuesto una gran aventura en la cual he adquirido nuevos conocimientos y he estado rodeada de la mejor compañía posible. Tengo que dar las gracias a muchísimas personas ya que, sin su ayuda y apoyo incondicional, no habría sido posible recorrer este camino y llegar hasta la meta final.

En primer lugar, quiero agradecer a mis directoras de tesis, Núria y Rut, dado que sin ellas no habría sido posible llegar hasta aquí. Me disteis una oportunidad para convertirme en doctora y ha dado sus frutos. Todo empezó con vosotras.

Nada más comenzar mi camino para convertirme en doctora conocí a Marta y Andrea y enseguida me di cuenta que eran un pilar fundamental para el buen funcionamiento del laboratorio. Gracias por la "ayudasión" constante siempre que la necesitaba y por hacer las cosas más fáciles de lo que parecían al principio. Además, en mi último año, conocí también a Meritxell dispuesta a seguir con la tarea de Andrea ayudando en todo momento.

Dentro del "Neurolipid Group" me encontré con personas maravillosas. La primera de ellas fue Maria y, aunque estuvimos poco tiempo a la vez en el laboratorio, aprendí todo lo posible de ella. ¡Fue una gran profesora! También tengo que agradecer a los post-docs del grupo: a Rosi, por todos los consejos que me dio; a Miguel, por sus clases en el departamento de clonajes y, a Sebas, por estar dispuesto a echarme una mano con temas del estabulario. ¡Aprendí mucho de vosotros! Aunque ya no están en el grupo, tengo que dar las gracias a Anna Fosch, por sus palabras de aliento en los momentos difíciles y, a Helena, por alegrarme siempre el día con su buen humor.

Mis compañeros pre-docs también han sido igual de importantes en esta carrera hacia el doctorado. Anna Molins, mi confidente de batallitas, compartimos tantos momentos juntas, gracias por estar siempre ahí. Te deseo mucha suerte y ánimo en estos últimos meses. Piensa que, al final, todo acaba (porque sí, hay una meta, aunque parezca inalcanzable y esté muy lejos). Jesús, Cris y Xavi, han sido innumerables los momentos

compartidos con vosotros, llenos de risas y aprendizajes. Me he divertido mucho.

Las últimas incorporaciones del grupo fueron María Rodríguez y David. Os tengo que decir a ambos que el camino pre-doc no es un camino de rosas, sino que está lleno de obstáculos, pero estoy segura que los podréis saltar sin problemas. Además, tuve la oportunidad de tener un estudiante a mi cargo: Marc. Espero haberte enseñado de la mejor manera posible y que disfrutaras de tu periodo en nuestro grupo.

Mi carrera hacia el doctorado no hubiera sido lo mismo sin mis "trabajadores de montaña": Ana, Alessandro, Joan y Ferrán. No tengo palabras para describir lo fantásticamente genial que me lo he pasado durante este tiempo con vosotros. Me llevo tantos buenos recuerdos a vuestro lado: viajes llenos de risas, salidas inolvidables, videollamadas increíbles, quedadas improvisadas…

Tiempo después llegaron dos nuevas incorporaciones a la mesa del despacho. Blanca, mi compañera runner. Siempre que salíamos a correr me decías una frase que se puede aplicar a la vida en general: "el límite lo pones tú". Gracias por adaptar tu paso al mío y no parar de hablar para que no pudiera pensar en otra cosa. Y Tadeo, mi compañero de prácticas, gracias por estar dispuesto a ayudarme y hacer las prácticas más amenas.

También tengo que agradecer a los compis del otro lado del pasillo. Lídia, Dani y Laura, gracias por apoyarme e invitarme a los seminarios de grupo que organizáis. ¡Nunca defraudan! Eva, te encargaste de hacer justicia a pesar de acabar prácticamente de entrar aquí, te debemos todos tanto. ¡Eres el mejor sindicato! Toni, me salvaste con los cultivos y lo sabes. Aprendí muchas cosas de ti y te deseo todo lo mejor en tu futuro.

A las demás personas del laboratorio: Núria, Sara P, Ainhoa, Eva Q, Bárbara, Samu, Reyes, Bob, Vero, Gonzalo y Xènia. Por los buenos consejos que me dieron Marta Pera y Pau, lecciones reales de vida que siempre tendré en cuenta.

La carrera hacia la meta se hizo mucho más liviana gracias al "proyecto Mayhem" y las magníficas galas del club de cine que se alargaban hasta que salía el sol al día siguiente y terminábamos desayunando churros. Por

las calçotadas, los *correbars*, las salidas de despedidas, las “cerves” de los jueves/martes, los bocatas del primer viernes de mes… Han sido tantos momentos compartidos, me he divertido tanto con vosotros que os voy a echar muchísimo de menos.

In my final stretch, I was able to cross the pond and go on a research stay to New York in Pablo Castillo's group. I cherish wonderful memories from those three intense months I spent there. Pablo, thank you so much for the opportunity to be temporarily part of your research group. I’ll always be grateful to you for giving me a hand with all the administrative procedures I had to do to enroll there. A special thanks to Manuel for teaching me everything I know about electrophysiology and for having patience with me. To the post-docs Coralie, Kaoutsar and Asma, each of you contributed your bit to my training. And, of course, to the rest of the group – Michelle, Aubrey, Shivani and Czarina – always ready to help whenever needed. Lastly, a thank you to Ernesto, although we never met in person, your assistance with the pending experiments was invaluable.

A Carlos, mi primer gran mentor. Me enseñaste todo lo que era necesario para poder trabajar en un laboratorio. Me inculcaste las habilidades necesarias. Esta carrera ha sido llevadera por tus grandes enseñanzas.

A mis amigos de toda la vida, Iván y Ricardo. Hace muchos años que nos conocemos ya y, a pesar de la distancia, habéis estado ahí. A Estefanía, sabes que ahora tengo una “nueva misión” que pasará de estado pasivo a activo. A mis “okupas del pasillo”, hace nueve años que nos conocimos y, aunque ahora nos veamos menos, también habéis sido una base fundamental para mí.

Por último, pero no menos importante, quiero agradecer a mi familia por todo el apoyo que me ha dado durante este tiempo. A mis padres, que me dieron la oportunidad de poder estudiar y hacer de mí la persona que soy hoy. Siempre habéis creído en mí y me habéis animado a perseguir mis sueños. ¡Quién iba a decir que todo comenzaría con el “ce-hache-loro-plast”! Además, tengo que dar las gracias, en especial, a mi hermana, la persona que más me ha ayudado y que ha estado ahí en todo momento. No hubiera superado esta etapa de mi vida sin ti. Eres una persona muy importante para mí. Me has demostrado tu cariño y apoyo todos los días. Siempre me decías que nunca estabas ocupada y podíamos hablar en

cualquier momento y hora pasase lo que pasase. Gracias por aguantarme en las llamadas infinitas hablando de todo y nada a la vez. Has hecho que mi moral siempre estuviera alta.

Estas palabras se quedan cortas para expresar todo lo agradecida que estoy. Habéis sido parte muy importante de mi vida. ¡Muchísimas gracias a tod@s por ayudarme a alcanzar la meta!

RESUMEN/ABSTRACT

Resumen

Actualmente existe un creciente interés sobre el impacto de las dietas en la cognición. Es ampliamente conocido que el cerebro requiere una gran cantidad de energía para llevar a cabo sus funciones vitales. La gran mayoría de esta energía es consumida por las neuronas para mantener las sinapsis, donde los receptores AMPA desempeñan un papel significativo. Nuestro grupo ha demostrado recientemente que el tráfico de la subunidad GluA1 de estos receptores AMPA hacia la membrana plasmática se reduce en situaciones de escasez de glucosa. De acuerdo con esto, esta tesis se centra en dilucidar los efectos de diferentes nutrientes en el tráfico de la subunidad GluA1 de los receptores AMPA, las funciones sinápticas y los procesos cognitivos. Para poder abordarlos, se utilizaron cultivos primarios de neuronas y cortes de hipocampo para analizar el efecto de nutrientes intentando imitar diferentes dietas. También se llevaron a cabo experimentos *in vivo* para examinar el impacto de estas dietas en procesos de memoria. Los resultados de esta tesis mostraron que, por un lado, el ácido palmítico, un ácido graso saturado, disminuyó la cantidad de niveles de GluA1 en la superficie, mientras que el ácido oleico y el ácido docosahexaenoico ω-3, dos ácidos grasos insaturados, aumentaron la cantidad de GluA1 en la membrana plasmática. Por otro lado, el β-hidroxibutirato, un cuerpo cetónico utilizado como fuente de energía en el cerebro durante una dieta cetogénica (basada en la ingesta baja de carbohidratos y alta en grasas), elevó los niveles de GluA1 en la superficie. Además, este cuerpo cetónico contrarrestó los efectos negativos del ácido palmítico en los niveles sinápticos de GluA1, la transmisión sináptica y la excitabilidad neuronal. De igual manera, la administración oral de BHB fue capaz de revertir el deterioro cognitivo mediado por una dieta rica en grasas saturadas. También se exploró si el eje malonil-CoA - CPT1C está involucrado en los efectos del ácido palmítico y del β-hidroxibutirato. Finalmente, se identificó la región de SAC1 que interactúa con CPT1C, ya que estas dos proteínas forman parte del macrocomplejo de los AMPARs y están involucradas en la regulación del tráfico de dichos receptores. En conclusión, los resultados confirman el importante papel de los nutrientes en la neurotransmisión, brindando nuevas perspectivas sobre por qué ciertas dietas son capaces de retrasar los deterioros cognitivos.

Abstract

Nowadays there is an increasing interest about the impact of diets on cognition. It is widely known that brain demands huge amount of energy to carry out its vital functions. The vast majority of this energy is consumed by neurons to maintain synapses, where AMPA receptors assume a significant role. Our group has recently shown that the AMPAR subunit GluA1 trafficking toward the plasma membrane is downregulated upon glucose depletion. In agreement with this, this thesis is focused on elucidating the effects of different nutrients on GluA1 trafficking, synaptic functions and cognitive processes. To address so, primary neuronal cultures and hippocampal slices were used to analyze the effect of nutrients imitating different diets. *In vivo* experiments were also conducted to examine the impact of diets in memory processes. Results of this thesis showed that, on the one hand, palmitic acid, a saturated fatty acid, decreased the amount of surface GluA1 levels, while oleic acid and ω-3 docosahexaenoic acid, two unsaturated fatty acids, increased the amount of GluA1 at the plasma membrane. On the other hand, β-hydroxybutyrate, a ketone body used as a source of energy in the brain during ketogenic diet (based on low carbohydrate and high fat intake), raised surface GluA1 levels. Furthermore, this ketone body counteracted the negative effects of palmitic acid on synaptic GluA1 levels, synaptic transmission and neuronal excitability. Moreover, β-hydroxybutyrate oral administration was able to reverse the cognitive impairment mediated by saturated high fat diet. It has been explored whether malonyl-CoA – CPT1C axis is involved in palmitic acid and β-hydroxybutyrate effects too. Finally, it has been identified the region of SAC1 interacting with CPT1C, since these two proteins form part of the AMPAR macrocomplex and are involved in the regulation of its trafficking. Overall, results confirm the important role of nutrients in neurotransmission, providing new insights into why certain diets are able to delay cognitive impairments.

TABLE OF CONTENTS

INTRODUCTION

1. Synaptic transmission

The human brain stands as the most intricate and enigmatic organ within the body, functioning as the core of our thoughts, emotions, memories and behaviors. Although the brain represents only 2% of the total body weight, this vital organ consumes approximately 20% of the total body's energy expenditure. All this energy is mainly used for ion and neurotransmitter transport, which predominantly takes place in synapses (Attwell & Laughlin, 2001).

Neurons are the fundamental units of the nervous system, responsible for transmitting information from one part of the body to another thanks to the synapses. It is well-known that they establish communication through the release of neurotransmitters from their presynaptic terminals into the synaptic cleft (Di Maio, 2008). Subsequently, these molecules are detected by the receptors on the postsynaptic neuron's membrane and the chemical signal is expanded throughout the neuron.

However, they are not the only cells that take part in synapses. Astrocytes also modulate synaptic neurotransmission through their internal Ca^{2+} levels. Their increase triggers the release of chemical neurotransmitters from the glial cells themselves. This fact led to introduce a novel concept that completely transformed the understanding of synaptic transmission known as the "tripartite synapse" (Araque et al., 1999). Later on, microglia, the resident immune cells of the central nervous system (CNS), has been proposed as synaptic sensors also participating in the process called "quad-partite synapse" (Paolicelli & Gross, 2011; Schafer et al., 2013). Indeed, it has been recently suggested the concept of "multipartite synapse" where oligodendrocytes and the extracellular matrix would have a further role (Louail et al., 2023).

As mentioned earlier, neurons are the main character of the synapse due to their huge electrical excitability. These crucial components of synapses can fire an action potential (also known as spike) as it is represented in figure 1. It is an all-or-none firing event where there are voltage changes across the plasma membrane (Hodgkin & Huxley, 1952).

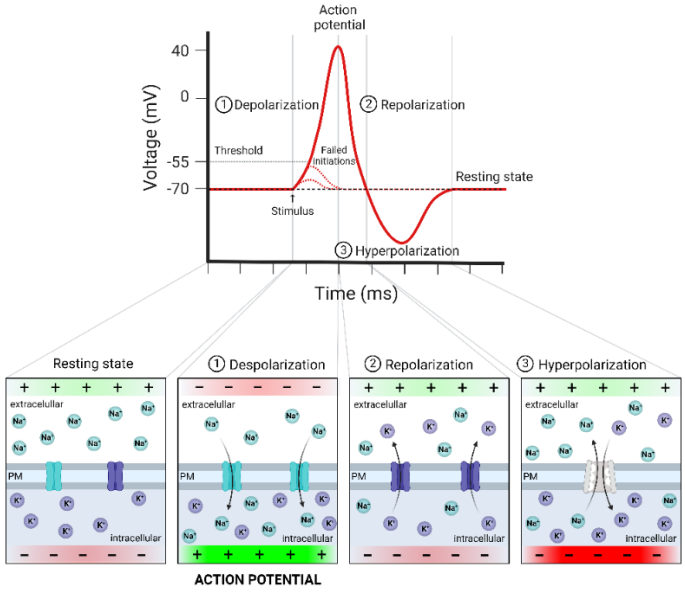

Figure 1. Events on the plasma membrane during an action potential. The membrane voltage is determined by the relative ratio of ions both extracellular and intracellular. A chemical signal triggers the opening of sodium ion (Na^+) channels and it initiates the action potential (despolarization). The resting potential is restored by the opening of potassium ion (K^+) channels (repolatization). There may be a brief hyperpolarization, making it temporarily more challenging to trigger another action potential. Finally, the sodium-potassium pump actively transports three sodium ions out while bringing two potassium ions into the cell, restoring the proper ion balance.

These local voltage changes (postsynaptic potentials) in the plasma membrane represent the neuron's response to incoming signals from other neurons through the release of neurotransmitters. The majority of neurons receive inputs from both excitatory and inhibitory synapses leading to excitatory postsynaptic potentials (EPSPs) and inhibitory postsynaptic potentials (IPSPs). EPSPs cause temporary depolarization of the postsynaptic membrane, bringing it closer to the threshold for firing an action potential (Vadakkan, 2016). In contrast, IPSPs produce a temporary hyperpolarization, making it more difficult for the neuron to reach the action potential threshold. The balance between these opposing potentials is crucial for the complex computations performed by neurons, allowing them to integrate incoming information and determine whether or not to transmit signals to downstream neurons (Taub et al., 2013).

EPSPs are graded, they have an additive effect. Thus, the summation of several EPSPs increase the likelihood for the initiation of an action potential in a neuron. If the cumulative inputs are frequent and strong enough, they can effectively push the membrane potential past the threshold, leading to the firing of an action potential.

EPSPs can be measured using various electrophysiological techniques that offer valuable insights into synaptic signaling within neural circuits (Acker et al., 2016; Richardson & Silberberg, 2008; Sayer et al., 1990; Stuart & Häusser, 2001). Furthermore, field EPSPs (fEPSPs) can also be analyzed collecting the electrical activity generated by a population of neurons rather than the activity of a single one even *in vivo* (Heim et al., 2022).

1.1. Mechanisms of neurotransmitters' release

When the action potential reaches the axon terminal, it triggers the opening of voltage-gated calcium channels in the presynaptic membrane. They are the responsible for the fusion of vesicles and the posterior exocytosis of neurotransmitters (Katz, 1969). Calcium ions bind to synaptotagmin signaling vesicle fusion (Fernández-Chacón et al., 2001). This promotes the assembly of the soluble N-ethylmaleimide-sensitive factor (NSF) attachment protein receptors (SNARE) complex, where each membrane has its own SNARE proteins, generating mechanical force that overcomes lipid bilayer repulsion, forming the stalk and leading to fusion (Chernomordik & Kozlov, 2008). This involves vesicle-SNAREs (synaptobrevin, also known as VAMP) and target-SNAREs (syntaxin and SNAP-25) zippering, bringing the synaptic vesicle and the presynaptic membrane close (Söllner et al., 1993) as it is shown in figure 2. Apart from the SNARE complex itself, there are other proteins such as Munc and complexin which play complementary roles. Munc ensures the proper formation of the SNARE complex, preventing premature vesicle fusion (Wang et al., 2019), while complexin acts as a brake, inhibiting full zippering until calcium ions trigger its release (Chen et al., 2002).

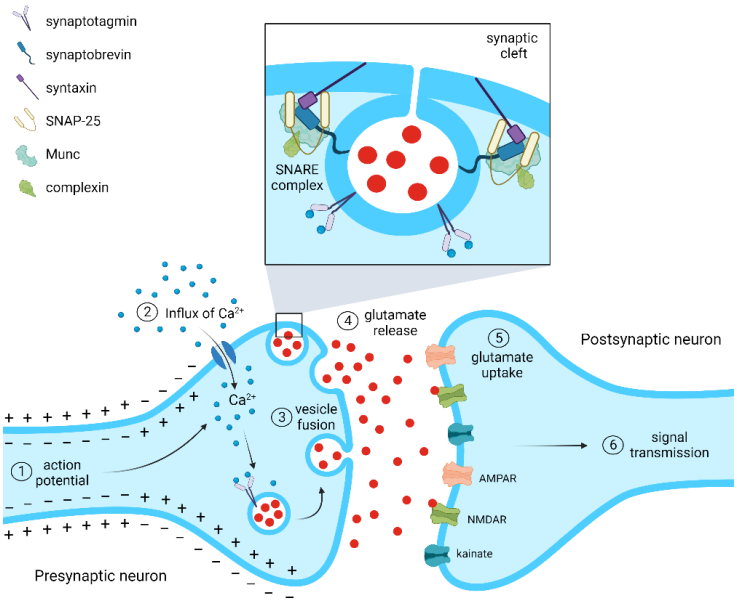

Figure 2. Neurotransmitters' release during a synapse. The action potential facilitates the entrance of calcium ions into the cells. This movement of ions allow synaptic vesicles to fuse with the presynaptic membrane and release neurotransmitter which will bind the postsynaptic receptors.

Once docked and fused, the synaptic vesicles undergo exocytosis releasing neurotransmitters into the synaptic cleft. They diffuse across it and bind to specific receptor molecules on the postsynaptic membrane. In the case of an excitatory synapses, glutamate, the main excitatory neurotransmitter, binds to the three types of ionotropic receptors: α-amino-3-hydroxy-5-methyl-4-isoxazolepropionic acid receptors (AMPARs), N-methyl-D-aspartate receptors (NMDARs) and kainate receptors (Traynelis et al., 2010).

Among these receptors, AMPARs predominantly mediate rapid neurotransmission driving postsynaptic depolarization. They will be explained in detail in section 2. It is remarkable that the postsynaptic exocytosis of AMPARs also requires the SNARE-mediated fusion machinery but it is different from the mechanism used during presynaptic neurotransmitter release (Jurado et al., 2013).

NMDARs have relatively slow kinetics compared to AMPARs'. Moreover, they are known as "coincidence detector" because their activation needs, apart from the ligand binding, the removal of magnesium ion which is blocking the channel. This ion is only displaced when neuron experiences an adequate depolarization (Furukawa et al., 2005). By contrast, kainate receptors can modulate both presynaptic glutamate and γ-aminobutyric acid (GABA) release (Negrete-Diaz et al., 2022). Furthermore, in addition to these ionotropic receptors, there are metabotropic glutamate receptors which are involved in "slower" neurotransmission. They are linked to G proteins and modulate cell excitability through second messenger signaling pathways (Niswender & Conn, 2010).

After neurotransmitter molecules have communicated their signal, they are typically taken back up into the presynaptic neuron through transporters and repackaged into synaptic vesicles for future release (Andersen et al., 2021).

However, it can occur that in the absence of any neurotransmission signal, synaptic vesicles release its content taking place miniature excitatory postsynaptic currents (mEPSCs). They are not evoked by an action potential in the presynaptic neuron but rather result from the spontaneous release of a single synaptic vesicle containing glutamate. They are the smallest unit of excitatory synaptic transmission and their study allows to analyze the properties of individual synapses.

1.2. Synaptic plasticity

The capacity of neurons to change the strength of their connections is known as synaptic plasticity. This mechanism is essential for the development of brain networks (Stampanoni Bassi et al., 2019). It shapes brain connectivity regulating cognitive functions such as learning and memory (Magee & Grienberger, 2020). Donald Hebb proposed a groundbreaking concept that has influenced our understanding of neurotransmission: the connection between two neurons should increase when neuron A consistently contributes to the firing of neuron B (Hebb, 1949). He emphasized causality and repetition as the basis for these modifications, highlighting that it is not simultaneous firing but the consistent triggering of one neuron by another that strengthens their connection. This notion of causation anticipated the understanding of

spike-timing-dependent plasticity, emphasizing the temporal precedence of events (Caporale & Dan, 2008). Traditionally, Hebbian plasticity is summarized as “neurons that fire together wire together” (Shatz, 1992).

It is important to take into account that the strengths of all synapses in a neuron must be globally adjusted to maintain a stable level of activity. That is what is known as homeostatic plasticity (synaptic scaling). If a neuron is underactive, all of its synapses could be strengthened proportionally to restore its firing rate to a normal range (Turrigiano & Nelson, 2004). Thus, homeostatic plasticity returns neurons to their initial state after any alteration, including those from Hebbian plasticity. It prevents neurons from being overloaded in one direction or the other. Hence, there is a potential significance in integrating Hebbian and homeostatic plasticity (Fox & Stryker, 2017).

Neuronal networks have the characteristic of producing rhythmic oscillations in distinct frequency ranges (Buzsáki & Watson, 2012). Neurons’ excitability fluctuates during these oscillations, leading to increased firing likelihood during the depolarization phase. In contrast, during the hyperpolarizing phase, they are less likely to respond to excitatory inputs (Wang & Buzsáki, 1996). When a population of neurons engages in synchronous bursting, it leads to alterations in the network. Specifically, high-frequency activity induces long-term potentiation (LTP), while low-frequency bursting, long-term depression (LTD).

Both LTP and LTD are anti-homeostatic activity and the most studied types of plasticity. In the case of LTP, it is involved in creating highly interconnected neural structures influencing learning and memory processes (Lynch, 2004). This enables the formation of precise connections by remodeling dendritic spines in volume and clustering (Hill & Zito, 2013). Moreover, AMPARs increase their number on the postsynaptic membrane during LTP due to an increase in their exocytosis. They are involved in the initial phase of LTP by enhancing synaptic strength, while NMDARs play a crucial role in the late phase of LTP which is related with structural changes in synapses, such as the growth and stabilization of dendritic spines (Luscher & Malenka, 2012). On the other hand, LTD is characterized by a significant spine shrinkage that can result in the removal of dendritic spines (Zhou et al., 2004). Despite their opposing effects, LTP and LTD

interact reciprocally to fine-tune neural connections regulating cognitive processes.

There are other types of plasticity which have no long-lasting changes compared to LTP and LTD: the short-term potentiation and the short-term depression. The alterations they caused in synaptic strength are relatively short-lived and tend to decay relatively quickly, from a few milliseconds to several minutes (Zucker & Regehr, 2002). Paired-pulse facilitation and depression are examples of this plasticity (Citri & Malenka, 2008).

The AMPA/NMDA ratio is considered an indicator of plasticity in the excitatory glutamatergic synapses because it reflects the relative contributions of the two major types of glutamate receptors in neurotransmission (Watt et al., 2004). Their balance can signal whether synaptic strength is potentiated or weakened.

Hence, synaptic transmission is a dynamic process that underlies our ability to learn, remember and adapt to our ever-changing environment. Its intricate mechanisms allow for the strengthening and weakening of synaptic connections. This process is regulated by postsynaptic receptors (mainly AMPARs), signaling pathways and structural changes within neurons.

2. AMPARs

AMPARs are the main glutamate-gated ion channels and mediate fast excitatory synaptic transmission in the CNS of mammals. For this reason, they are the perfect targets for the modulation of synaptic excitation. Upon glutamate activation, AMPARs swiftly undergo desensitization (Traynelis et al., 2010). Their functions are carried out in the millisecond timescale (Twomey et al., 2019) and their activation results in the influx of cations, predominantly sodium ions (Na^+), into the postsynaptic neuron. This influx of positive ions leads to membrane depolarization, which (if it reaches the threshold) can trigger the generation of an action potential.

Moreover, they participate in synaptic strength and plasticity which underlies more advanced cognitive processes such as learning and memory (Barry & Ziff, 2002; Malinow & Malenka, 2002).

AMPARs are dynamically regulated in number and properties at synapses through various mechanisms such as receptor trafficking, post-translational modifications and interactions with other proteins which will be discussed later. Indeed, alterations in AMPARs cause a wide range of neurological disorders (Guo & Ma, 2021). Their overexpression leads to neuroexcitotoxicity and, eventually, neuronal death (Kwak et al., 2010). On the contrary, neuronal dendritic arborization decreases when their levels are downregulated (Yoon et al., 2012).

Therefore, the intracellular transport of AMPARs is rigorously controlled during synaptic plasticity and it is probably the responsible of the amount of AMPARs present at the plasma membrane (Hangen et al., 2018). There are three different pathways through which AMPARs can reach plasma membrane (figure 3).

The first of them is the canonical ER-trans Golgi network (TGN) secretory pathway. The trafficking of newly synthesized AMPARs involves a huge network of internal membrane compartments (Choquet & Triller, 2013). Initially, the receptor is synthesized in the ER, where it undergoes assembly into tetramers and goes through protein quality control mechanisms. This fact ensures that only properly folded receptors are exported (Greger et al., 2007). For instance, palmitoylation process occurs here contributing to the stabilization of the receptor' structure and protecting it from degradation. Subsequently, AMPARs are transported to the Golgi where further processing takes place. At this stage, palmitoylation specifically at cysteine 585 promotes the accumulation of the receptor in this compartment. It is noteworthy that the ER transmembrane protein CPT1C, which will be explained in detail in section 4, is a modulator of this post-translational modification (Gratacos-Batlle et al., 2015).

After budding from the Golgi, secretory vesicles with AMPARs go to the plasma membrane, thanks to the participation of microtubules and motor proteins associated with them, such as kinesin and dynein (Kapitein et al., 2010). Moreover, electrophysiological recordings have indicated that

AMPAR-mediated synaptic transmission relies on both proteins. When LTP occurs, the increase of AMPARs is due to an increase in their secretory transport (Esteves da Silva et al., 2015; Hangen et al., 2018).

The second pathway consists of the endo- and exocytosis of recycled AMPARs. The internalization of already existing AMPARs from the plasma membrane allows a rapid response to any stimuli by either removing or inserting the receptors as needed (Moretto & Passafaro, 2018). Once AMPARs are internalized, they become part of early endosomes, which have the potential to undergo acidification and transform into late endosomes (Parkinson & Hanley, 2018). Alternatively, these early endosomes can either return directly to the plasma membrane or travel through recycling endosomes before reintegration with the participation of some vesicle-associated SNARE proteins (Bakr et al., 2021). Just as the previous pathway, this route can also be modulated by activity-dependent post-translational modifications. In addition, it has been corroborated that the suppression of AMPARs exocytosis contributes to LTD (Fujii et al., 2018; Hirano, 2018).

The third and last known pathway to date is the Golgi-independent transport route as approximately 80% of dendrites lack the Golgi apparatus (Krijnse-Locker et al., 1995). This mechanism enables the swift insertion of AMPARs into the plasma membrane. AMPARs leave ER and they are promptly conveyed to recycling endosomes (Bowen et al., 2017). Subsequently, they reach the plasma membrane.

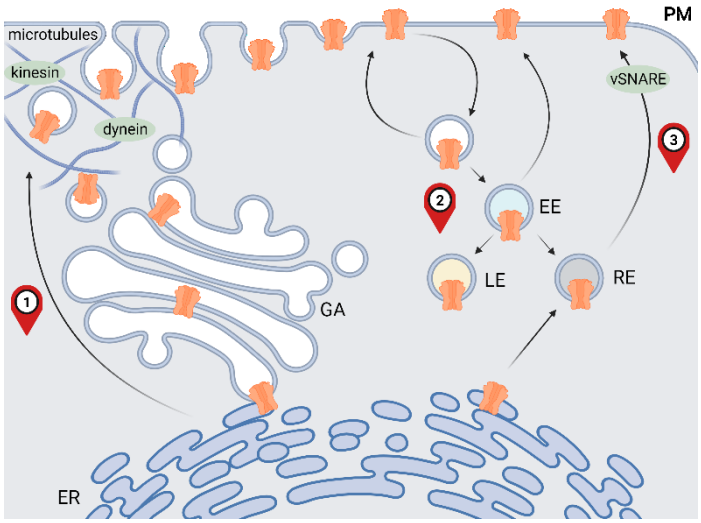

Figure 3. AMPARs' secretory trafficking pathways. 1) Canonical ER-TGN secretory route. 2) Endo- and exocytosis of recycled receptors. 3) The Golgi-independent transport. EE: early endosomes. ER: endoplasmic reticulum. GA: Golgi apparatus. LE: late endosomes. PM: plasma membrane. RE: recycling endosomes.

2.1. Structure

AMPARs are made up of different subunits from GluA1 to GluA4 constituting homo- or heterotetramers. Each subunit contributes in different ways to AMPARs giving them distinct channel kinetics, ion selectivity and trafficking characteristics. Nevertheless, all subunits have a common structural topology based on four domains: an extracellular N-terminal domain (NTD), which is sometimes known as the amino-terminal domain (ATD), a ligand-binding domain (LBD), a transmembrane domain (TMD) and a short cytoplasmic C-terminal domain (CTD). (Greger et al., 2017; Twomey et al., 2019).

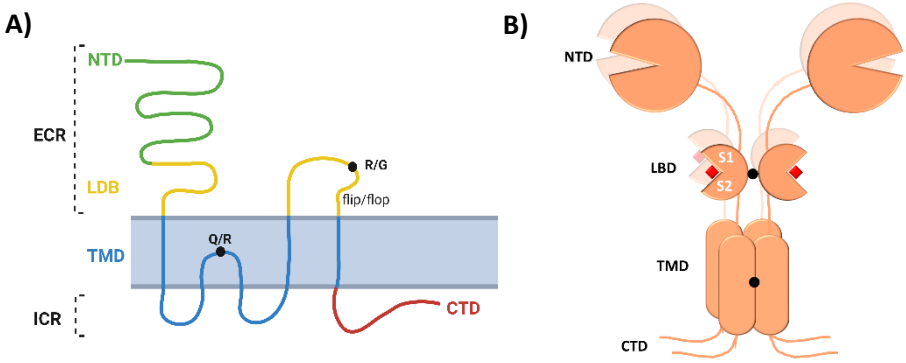

Figure 4. AMPARs topology. A) Common subunit structure of AMPARs with domain architecture. B) Organization of an AMPAR tetramer. mRNA editing sites (R/G and Q/R) are represented with black dots. The ligand glutamate is shown as a red square. S1 and S2 represent stretches of the LBD separated by the plasma membrane. CTD: C-terminal domain. ECR: extracellular region. ICR: intracellular region. LBD: ligand-binding domain. NTD: N-terminal domain. TMD: transmembrane domain.

These four domains are constituted by three different layers: the extracellular region (ECR), the transmembrane region and the intracellular region (ICR). The ECR includes the largest portion of AMPAR (approximately 85%) and it is formed by the NTD and the LBD. On the one

hand, the NTD has a two-fold symmetric architecture and it is necessary for the assembly, regulation and trafficking. On the other hand, the LBD folds into a bilobate structure too capturing the ligand (glutamate) within this interlobe cleft. Its clamshell-like structure is made up of two polypeptide stretches (S1 and S2) divided by TMDs. The S2 stretch presents two different isoforms (flip or flop) relying on alternative splicing. Each isoform exhibits unique gating kinetics and respond in very different ways to allosteric modulators (Sommer et al., 1990). Just located before the flip/flop site is the R/G mRNA editing site, which also modulate gating properties (Lomeli et al., 1994).

This type of ionotropic transmembrane receptors has an overall organization where the connection between NTD and LBD is notably less compact, resulting in the receptor taking on a distinctive “Y-shaped” configuration (figure 4B). The two NTD dimers extend outward from the LBD (Mayer, 2006). Nevertheless, GluA2/3 and GluA2/4 heteromers have the ability to assume a vertically compressed NMDAR-like structure. Here, the NTD is constrained in a compact “O-shaped” configuration, achieved through a cysteine cross-link (Herguedas et al., 2016). Moreover, in the case of homomeric GluA2 structures, they present a “N-shaped” form too (Herguedas et al., 2016).

The TMD is the responsible for forming the ion channel. Among them, TMD1, TMD3 and TMD4 span the entire cellular membrane, whereas TMD2 forms a sort of reentrant loop which plays a crucial role in shaping the channel pore. The Q/R mRNA editing site is found in this TMD significantly reducing the permeability of GluA2-containing AMPARs to calcium ions and makes them more resistant to polyamine block (Hume et al., 1991). Therefore, in the absence of GluA2 subunits, an AMPAR will be permeable for calcium ions (in addition to sodium and potassium ions).

The cytoplasmic CTD, which constitute ICR, is the most heterogeneous domain. It differs between subunits: GluA1 and GluA4 have a long tail, whereas GluA2 and GluA3 present a short one (Granger et al., 2013). It is involved in subunit-specific protein interactions and trafficking. Its phosphorylation affects channel conductance although its role in LTP remains unclear (Hosokawa et al., 2015; Kristensen et al., 2011).

Moreover, the expression of the subunits varies depending on the development stage. In the first phases, there is a notable presence of AMPARs lacking the GluA2 subunit leading to a high calcium permeability. GluA1 and GluA3 subunits are also low during this period but higher during adulthood. Therefore, GluA4 is the subunit which is most abundantly expressed during early developmental stages (Lilliu et al., 2001; Zhu et al., 2000).

2.2. Post-translational modifications

AMPARs are regulated by several post-translational modifications including phosphorylation, palmitoylation, ubiquitination, nitrosylation or even O-GlcNAcylation (Diering & Huganir, 2018). Numerous modifications have been described to occur in tandem. As a result, particular combinations of these post-translational modifications may be either favored or inhibited.

Among post-translational modifications, phosphorylation is the most completely studied and abundant type. Many sites have been described to undergo this modification affecting serine (S), threonine (T) and tyrosine (Y) residues as it can be shown in figure 5. AMPARs' CTD serves as substrates for various protein kinases including cAMP-dependent kinase (PKA) at GluA1 S845 and GluA4 S842; protein kinase C (PKC) at GluA1 S818/S831/T840, GluA2 S863/S880, GluA3 S885 and GluA4 T830; Ca^{2+}/calmodulin-dependent kinase II (CAMKII) at GluA1 S831 and GluA4 S842; p21-activated kinase 3 (PAK3) at GluA1 S863 and Src family tyrosine kinase at GluA2 Y876 and GluA3 Y881 (Diering & Huganir, 2018). Indeed, one site can be phosphorylated by more than one kinase.

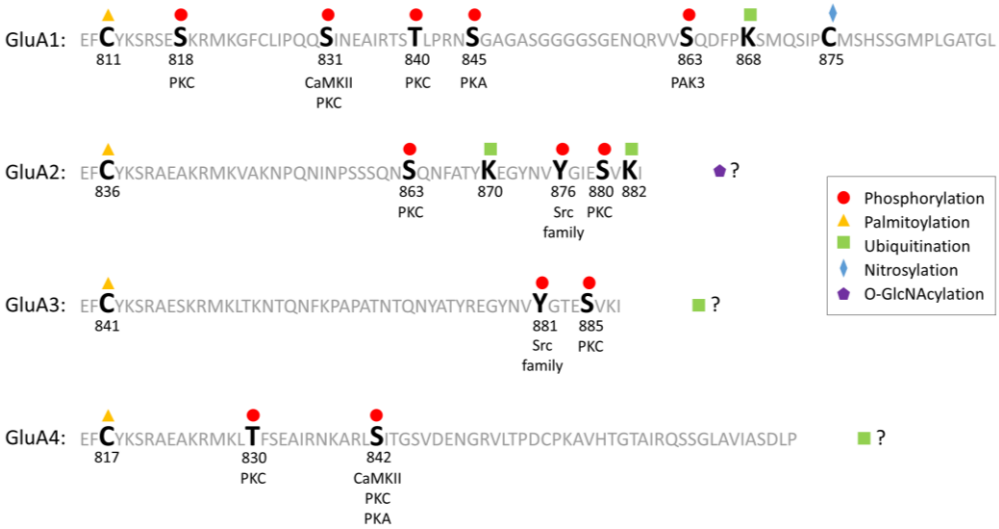

Figure 5. Amino acid sequences of GluA1-GluA4 CTD with their post-translational modifications indicated. Symbol "?" represents the changes confirmed to occur but the specific amino acid undergoing the modification has not been identified yet. In the cases of phosphorylation, the specific kinase that causes it is indicated. Modified from (Diering & Huganir, 2018).

Moreover, the phosphorylation sites of GluA2 are conserved in GluA3 subunit. Nevertheless, the better known and analyzed post-translational modifications are the ones that take place in GluA1 subunit at S831 and S845 residues (Park, 2018). Both of them are highly related to synaptic plasticity and learning and memory processes. Knock-in mice with mutations in S831 and S845 (S831A/S845A) show partial impairment in hippocampal LTP (Lee et al., 2003). Therefore, either of them alone could potentially facilitate LTP but it has been published that S845 plays a crucial role in the expression of LTD (Lee et al., 2010).

Phosphorylated GluA1 at S831 (but not at S845) is notably concentrated within PSD contributing to the targeting and stability of receptors in this area (Diering et al., 2016). It also increases single-channel conductance and the regulation of receptor trafficking in synaptic integration (Summers et al., 2019). S845 phosphorylation is responsible for receptor recycling between intracellular endosomes and the extrasynaptic plasma membrane (Traynelis et al., 2010) facilitating the endosomal recycling of

GluA1 subunits. This process halts their sorting to late endosomes and lysosomes for degradation (Fernandez-Monreal et al., 2012).

Upon normal conditions in cultured neurons, around 15-20% of GluA1 goes through phosphorylation at either S831 or S845 and just a tiny portion of this subunit experiences dual phosphorylation (Diering et al., 2016; Oh et al., 2006). However, these results seem to be controversial because in another study less than 1% of GluA1 was phosphorylated at S831 and even less than 0.1% at S845 in hippocampal tissues (Hosokawa et al., 2015) These data force the scientific community to reevaluate the mechanisms that underlie synaptic plasticity.

Additionally, as mentioned earlier, post-translational modifications can influence each other. For instance, T840 phosphorylation hinders the increase in S845 phosphorylation by PKA and the consequent potentiation of AMPARs (Gray et al., 2014). There can be influences even between different types of post-translational modifications: S831 phosphorylation by CaMKII is enhanced by S-nitrosylation at C875 (Selvakumar et al., 2013).

The potential combinations of these modifications open up a vast landscape of regulatory possibilities, allowing for precise control over receptor properties. As the understanding of these modifications deepens, it is likely that mechanisms underlying synaptic transmission and plasticity could be explained with more detail.

2.3. Protein interactors and regulation

AMPARs are not only built up by their four basic subunits forming the described tetramers. Indeed, they are macromolecular complexes requiring the presence of many other proteins (Bissen et al., 2019; Schwenk et al., 2012). Like post-translational modifications do, these protein interactors modulate AMPARs' trafficking, gating properties and maturation. Thus, they carry out functions such as being auxiliary proteins or scaffolding ones.

Due to the large amount of proteins forming the macrocomplex, only the most well-known and recent discovered ones will be explained here. AMPAR's macrocomplex comprises an "inner core" constituted of the most tightly bound proteins, including transmembrane AMPA-regulatory

proteins (TARPs), cornichon proteins (CNIHs) and postsynaptic density protein 95 (PSD95). In addition, there is an “outer core” containing more variable peripheral components (Schwenk et al., 2012).

TARPs family (with stargazin being particularly noteworthy) and CNIHs are the typical auxiliary subunits of AMPARs. On the one hand, in the case of stargazin, it binds AMPARs both inside and outside the cell (Bedoukian et al., 2006) and its interaction with the glutamate-binding region of the receptor plays a significant role in channel desensitization (Tomita et al., 2007). When AMPARs are in the ER, this protein can act as a chaperone being the responsible for the proper folding of AMPAR subunits (Vandenberghe et al., 2005). On the other hand, CNIHs participate in both trafficking and gating kinetics maintaining the channel in an active state (Boudkkazi et al., 2014; Schwenk et al., 2009).

PSD95 is a scaffold protein which modifies spine density and morphology. Spine dimensions increase with its overexpression, but when reducing PSD95 levels hinders not only spine morphology development but also spine growth (Ehrlich et al., 2007). Thus, PSD95 plays a role in the maturation of glutamatergic synapses and synaptic strength (Beique & Andrade, 2003). Moreover, it has been described that this protein can interact with stargazin controlling surface AMPARs trafficking (Bats et al., 2007).

Regarding GluA1 subunit, which is the focus of study in this thesis, synapse-associated protein 97 (SAP97) and protein 4.1 seem to be important for this subunit. SAP97 has the particularity to only bind GluA1 due to a novel sequence motif in its C-terminus (Leonard et al., 1998). It controls early trafficking of GluA1 to the dendritic membrane and synaptic and extrasynaptic reservoirs of AMPARs at the cell surface (Sans et al., 2001). Protein 4.1 binds GluA1’s CTD linking AMPARs to actin cytoskeleton ensuring their presence on cell surface (Shen et al., 2000).

Recently, it has been published that when AMPARs are in the ER there is a novel complex transiently formed made up of ABHD6, FRRS1l and CPT1C (Brechet et al., 2017; Schwenk et al., 2019). Indeed, these proteins do not participate in AMPARs macrocomplex when the receptors leave the ER. ABHD6 enhances the stability of GluA monomers, whereas FRRS1l/CPT1C complex facilitates the formation of GluA tetramers with CNIHs and TARPs

preparing the receptors for their exit from the ER (Schwenk et al., 2019). Moreover, our group has recently demonstrated CPT1C regulates the transport of GluA1 to the plasma membrane through the canonical pathway in collaboration with another protein, SAC1, which will be described in detail in section 5.

The trafficking of GluA1 is regulated by the complex CPT1C-SAC1 based on malonyl-CoA, a precursor of fatty acids. Its levels fluctuate depending on the nutritional status of the cells and CPT1C can sense it by the binding to malonyl-CoA. When nutrients are available and malonyl-CoA levels are high, CPT1C inhibits SAC1 phosphatase activity, so there is more PI4P in the TGN allowing a correct transport of GluA1 to the plasma membrane. However, in a fasting situation, there is a decrease in malonyl-CoA levels and CPT1C no longer inhibits SAC1. Consequently, there is less PI4P in the TGN preventing the transport of AMPARs (Casas et al., 2020).

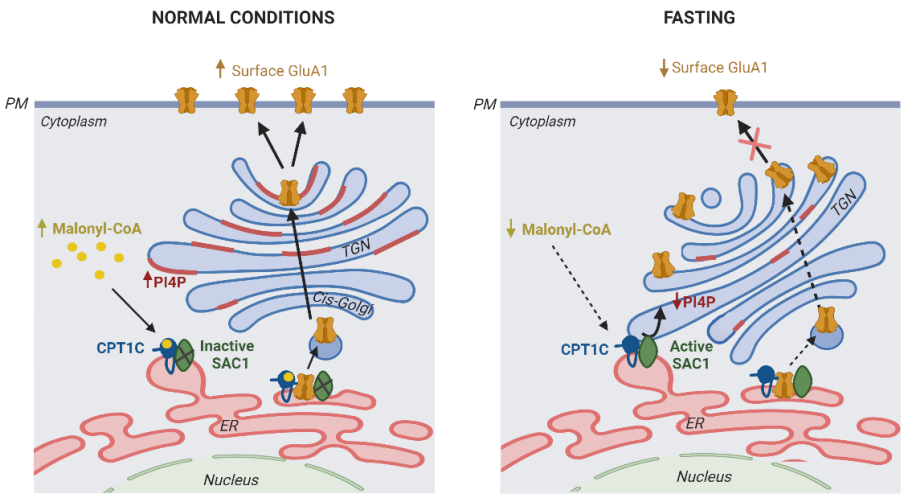

Figure 6. Regulation of GluA1 trafficking through CPT1C. In a normal situation, malonyl-CoA – CPT1C axis inhibits SAC1 activity allowing the correct transport of GluA1 to the plasma membrane. Nevertheless, in a fasting situation, SAC1 is active due to low malonyl-CoA levels. CPT1C: Carnitine palmitoyltransferase 1C. ER: endoplasmic reticulum. PI4P: phosphatidylinositol 4-phosphate. PM: plasma membrane. TGN: trans-Golgi network. Modified from (Casas et al., 2020).

It is noteworthy to wonder whether there are other nutritional situations that modify malonyl-CoA levels that can also regulate the transport of AMPAR through CPT1C-SAC1 axis.

3. Diets' effects on AMPARs, synaptic function and cognition

Similar to the way fasting has demonstrated to regulate the transport of AMPARs, several metabolic conditions and nutrients have an influence on the functionality of these glutamatergic receptors, synaptic plasticity, and subsequently, on cognition, as it has been recently reviewed in our group (Fado et al., 2022). As it was mentioned before, the brain consumes a lot of energy and this energy comes from the nutrients we daily eat. They play a crucial role in modulating brain functions, with their impact reaching far beyond simply providing energy (Gardener & Rainey-Smith, 2018; Spencer et al., 2017). There are important evidences from animal studies and emerging findings from research involving humans which corroborate this point of view (Gómez-Pinilla, 2008; Klimova et al., 2020; Puri et al., 2023).

The brain, a highly metabolically active organ, depends on a consistent supply of essential nutrients to function optimally. Its main source of energy are carbohydrates, particularly glucose. They provide a readily available and efficient fuel for neurons supporting various cognitive processes, including learning and memory.

However, upon situations with a low carbohydrate intake, such as fasting, the brain shifts to using ketone bodies (β-hydroxybutyrate (BHB), acetoacetate and acetone), produced by the liver from fats, as an alternative energy source (Kolb et al., 2021; Puchalska & Crawford, 2017).

Various dietary patterns have been studied for their effects on cognition. For instance, the Mediterranean diet, rich in fruits, vegetables, whole grains and healthy fats, like olive oil and fatty fish, has been associated with improved cognitive function and a reduced risk of cognitive decline (Sikalidis et al., 2021). On the other hand, Western diets, high in saturated fats, sugars and processed foods, have been linked to cognitive impairments and an increased risk of conditions like Alzheimer's disease (Lopez-Taboada et al., 2020). This thesis has focused on the impact of fats as they have both negative and positive effects on cognition.

3.1. Saturated high fat diet

Saturated fatty acids have generated increasing attention for their potential influence on cognition and brain health. Among these, palmitic acid (PA), has emerged as a subject of particular interest. It is present in red meats (beef, lamb…), butter and palm oil, which is used in many processed foods.

In vitro studies show that the co-treatment with PA and insulin induces lower levels of GluA1's phosphorylation and increases palmitoylation, altering the trafficking of AMPARs towards the plasma membrane (Spinelli et al., 2017). Therefore, PA affects AMPARs in cortical neurons without any observed changes in NMDARs levels (Loehfelm et al., 2020).

Moreover, PA treatment alters neuronal morphology and reduces dendritic arborization in neuronal primary cultures (McLean et al., 2019). Neurons present swelling in their somas and the formation of axonal and dendritic blebs with a significant decrease in synaptic connections weakening the excitability of these cells (Loehfelm et al., 2020). The morphological changes caused by PA are driven by the activation of phosphoinositide 3-kinase (Loehfelm et al., 2020). It phosphorylates the phosphoinositide $PI(4,5)P_2$, which directly enhances the stability of GluA1 on the surface of the plasma membrane (Seebohm et al., 2014).

Nevertheless, when studying the effects of saturated fatty acids *in vivo*, the composition of fats used is not always specified. In most cases, a high fat diet (HFD) consists of a mix of fats, with a predominance of saturated fats over unsaturated ones. Despite the fact that short period of HFD does not cause any change in short-term memory, it does in long-term memory (Wang et al., 2020). The same results are found when using HFD for a long time: a decrease in spine density and weakened cognitive processes (Hahm et al., 2020; Kim et al., 2020; Wang et al., 2015; Wu et al., 2022).

Young animals fed with a saturated fatty acid diet (SFAD) for a few days, have demonstrated that LTP is decreased and the long-term memory is impaired. With short-term SFAD, cognitive deficits are also found when memory is analyzed with several tests such as the Morris water maze, novel object recognition, object place recognition and Y-maze (Fernandez-Felipe et al., 2021; Spinelli et al., 2017; Spinelli et al., 2020). The analysis of LTD reveals that this kind of synaptic plasticity is increased with SFAD

(Fernandez-Felipe et al., 2021). Over an extended period on this particular diet (more than 2 months), young animals do not exhibit alterations in learning, but they do experience changes in cognitive flexibility (Leyh et al., 2021).

Feeding with SFAD for 2 weeks results in impaired memory in adult animals (Beilharz et al., 2016). Consuming SFAD for 8 weeks also leads to memory deficits and dendritic loss in the hippocampus (Granholm et al., 2008).

Although it seems that saturated fatty acids have detrimental effects on cognition, there is controversy on the topic because several studies do not suggest this. In diet-induced obesity with HFD, surface GluA1 levels are increased (Osborne et al., 2016) and, in another study, no changes in memory were detected at all (Lee et al., 2021). The lack of effect of mixed HFD could be due to the presence of unsaturated fatty acids, which will be described below.

Regarding human studies, a stronger and more evident correlation between diminished memory performance is observed in both younger and older age groups when they have a higher habitual consumption of unhealthy saturated fats. This association is notably more pronounced in these age groups compared to the healthier adult population (Baym et al., 2014; Gibson et al., 2013; Golomb & Bui, 2015; Martin et al., 2018; Okereke et al., 2012).

In addition, this type of fats not only affect neurotransmission, but also other physiological mechanisms. It is related with an increase in microglia's inflammation (Butler et al., 2020), cell stress (McLean et al., 2019) and decreased BDNF levels in hippocampus (Spinelli et al., 2020). However, as it has been explained, the biochemistry mechanisms and pathways, by which these changes that influence memory occur, are poorly understood with just a few experiments conducted in the field.

3.2. Unsaturated high fat diet

Nevertheless, it is worth noting that not all the effects of fatty acids can be negative. Unsaturated fatty acids, crucial components of a balanced diet, have beneficial impacts on cognition. It is important to take into account

the two categories of unsaturated fatty acids: monounsaturated fatty acids (MUFAs) and polyunsaturated fatty acids (PUFAs), each with different properties and health implications.

MUFAs, such as the oleic acid (OA), are found in sources like olive oil, avocados and nuts, whereas PUFAs are present in foods like fatty fish (salmon, sardines…), flaxseeds and walnuts. Indeed, they are classified in two main types: omega-3 (ω-3) and omega-6 (ω-6) such as docosahexaenoic acid (DHA) and araquidonic acid (AA), respectively. The balance between these two types of PUFAs is critical, as an excessive intake of ω-6 fatty acids relative to ω-3s can lead to an inflammatory response (D'Angelo et al., 2020).

To examine the impact of MUFAs, specifically OA, several studies have been carried out involving mice subjected to diets rich in this fatty acid for more than two months. Nevertheless, none of them have demonstrated any alterations in the total AMPARs expression or the levels of GluA1 phosphorylation (Lauretti et al., 2020; Thomas et al., 2017).

By contrast, the detrimental effects in dendritic morphology showed by the saturated fatty acids (PA) in primary neuron cultures can be reversed when treated with DHA (Loehfelm et al., 2020; McLean et al., 2019). Therefore, it is implied that consuming a balanced combination of unsaturated and saturated fatty acids, might have the potential to counteract the negative cognitive effects of SFAD.

Under an ω-3-enriched diet, AMPARs levels are increased in the hippocampus, the region related to learning and memory processes (Dyall et al., 2007; Lee et al., 2012). DHA administration induces the increase in the number of dendritic spines and the expression of synaptic proteins in cultured neurons (Cansev et al., 2008). In aged mice, ω-3 PUFAs also increase dendritic arborization and, even, neurogenesis process (Cutuli et al., 2014).

According to these cellular changes, older mice show improved cognitive performance in spatial learning and memory when they have a daily administration of ω-3 PUFAs (Cutuli et al., 2014; Lee et al., 2012). Indeed, in mouse models of some neurodegenerative diseases such as Alzheimer's disease, this type of unsaturated fatty acids can restore the deleterious

effects of amyloid-β peptide oligomers (Lee et al., 2016; Thomas et al., 2017).

Similar to the effect of saturated fatty acids, unsaturated ones also impact on other biological processes. They lead to elevated BDNF levels and a decrease in astrocytosis (Cutuli et al., 2014; Lee et al., 2016)

In reference to human studies, a Mediterranean diet supplemented with extra-virgin olive oil (rich in OA) and mixed nuts has neuroprotective effects on cognition (Martínez-Lapiscina et al., 2013). In young adults, supplementing the diet with DHA does not enhance working memory (Bauer et al., 2014). Nevertheless, ω-3 PUFAs exhibit beneficial results on cognitive functions among older adults (Kulzow et al., 2016; Power et al., 2022) but it remains unclear whether they can prevent cognitive decline in healthy elderly people (Rangel-Huerta & Gil, 2018). In the case of patients with early Alzheimer's disease, ω-3 supplementation improves brain functions (Canhada et al., 2018).

All these data underline the impact of different types of dietary fats, both saturated and unsaturated fatty acids, on brain's cognitive functions, as it is summarized in figure 7.

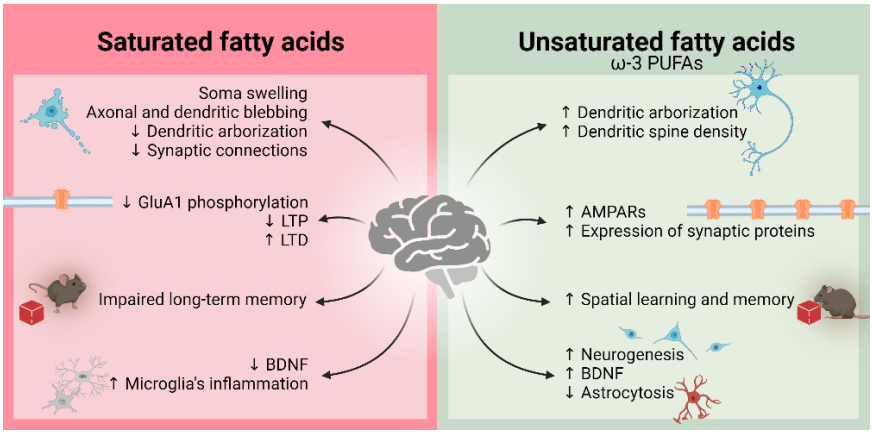

Figure 7. Fatty acids effects on brain's functions. Main changes reported in neuronal morphology, neuroplasticity, cognitive processes and other mechanisms involved when saturated fatty acids and ω-3 PUFAs are present in the diet.

3.3. Ketogenic diet

In the case of the previous diets, fat typically comprises 40-60% of the calorie intake, with glucose remaining the primary energy source for neurons. In contrast, the ketogenic diet involves a composition where fats constitute 90% of calories, while carbohydrates are restricted to 5-15%. As a result, ketone bodies become the principal energy source for neurons. Traditionally, ketonegenic diet has been associated to decrease seizures of epilepsy (Sampaio, 2016). Recently, accumulating evidence suggests that this diet results effective in decreasing cognitive decline.

On the one hand, young animals fed with ketogenic diet improve their short-term memory, but no changes are found in the long-term memory (Fukushima et al., 2015). GluA1 subunit levels are increased in the hippocampus without any alterations in GluA2's levels (Fukushima et al., 2015) but no differences are found in learning processes (Rodenas-Gonzalez et al., 2022; Silva et al., 2005). However, there are other studies where ketogenic diet leads to impaired memory and a decrease in LTP magnitude (Blaise et al., 2015; Miles & Skelton, 2020; Zhao et al., 2004).

Adults rodents exhibit enhanced memory under ketogenic diet (Hernandez et al., 2018; Newman et al., 2017), but no changes in learning and LTP (Huang et al., 2019). By contrast, in an Alzheimer's disease mouse model, this diet results in improved learning and memory with an increased in hippocampal dendritic spines (Xu et al., 2021).

On the other hand, BHB supplementation also shows effects in cognition. In young animals, it induces higher levels of BDNF in the hippocampus (Hu et al., 2018). This supplementation ameliorates memory in aged mice (Wang & Mitchell, 2016) and improves it in animals with Alzheimer's disease (Kashiwaya et al., 2010; Yin et al., 2016; Zhang et al., 2013). Thus, it is important to emphasize the differences between ketogenic diet, which can vary widely in composition, and ketone body supplementation.

Regarding human studies, no changes in cognitive performance have been reported in adults following a ketogenic diet (Iacovides et al., 2019), whereas it improves paired associate learning in elderly people (Krikorian et al., 2012). Ketone body supplementation also enhances working memory in older adults (Yomogida et al., 2021) and in patients with Alzheimer's disease (Ota et al., 2019).

Therefore, it seems like ketone bodies can mitigate adverse effects in the presence of brain damage linked to neurodegenerative diseases, as it is summarized in figure 8. BHB, the main ketone body and the most efficiently used one as energy source, prevents the oxidative stress-induced impairments in hippocampal LTP (Kimura et al., 2012; Maalouf & Rho, 2008). In epilepsy, the anticonvulsant effectiveness of the ketogenic diet is associated with the serum concentration of BHB, which can directly activate the potassium voltage-gated channels (Manville et al., 2020). The supplementation with this ketone body causes an enhancement in cognitive functions in patients with Alzheimer's disease (Henderson et al., 2009; Newport et al., 2015). In the case of Parkinson's disease, BHB has the potential to reduce the dopaminergic neurodegeneration by increasing the bioavailability of L-DOPA (Tieu et al., 2003). Moreover, in multiple sclerosis, BHB increases BDNF levels, the primary neurotrophic growth factor generated by neurons involved in myelin repair (Di Majo et al., 2022).

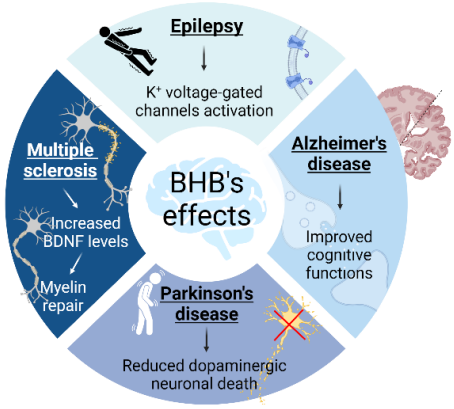

Figure 8. BHB's effects on neurological diseases. This ketone body is able to counteract the negative effects brain disorders cause.

Nevertheless, the precise mechanism by which these diets influence synaptic processes remains unclear and has yet to be fully elucidated. It becomes evident that further studies are required to gain a more comprehensive understanding of how these diets influence AMPAR function, synaptic plasticity and cognition.

4. Carnitine palmitoyltransferase 1C

CPT1C was the latest member of the carnitine palmitoyltransferases (CPTs) family to be found out (Price et al., 2002). This family of proteins carry out the transport of fatty acids towards the mitochondria in order to break them down and obtain energy from β-oxidation. There are different proteins with carnitine acyltransferase activity based on the length of the fatty acid they catalyze: carnitine acetyltransferase (CrAT) for short-chain fatty acids, carnitine octanoyltransferase (COT) for medium-chain fatty acids and CPT for long-chain fatty acids. Furthermore, this last group is composed of 4 isoforms: CPT1A, CPT1B, CPT1C and CPT2.

CrAT is located in the mitochondrial matrix, endoplasmic reticulum (ER) and peroxisomes. COT is only found in peroxisomes. However, members of CPT family differ in tissue and subcellular localization (figure 9). Meanwhile CPT2 is ubiquitously expressed throughout the organism and found in the inner membrane of the mitochondria (Demaugre et al., 1990), CPT1A is only expressed in lungs, pancreas, liver, intestine, ovaries and brain (McGarry & Brown, 1997); whereas CPT1B is highly found in muscle, brown adipose tissue and testis (Esser et al., 1996). Both of them are in the outer membrane of the mitochondria while CPT1C, the isoform this project is focused on, is in the ER and it is only expressed in mammalian neurons (Sierra et al., 2008), tumor cells (Zaugg et al., 2011) and stem cells (Roa-Mansergas et al., 2018).

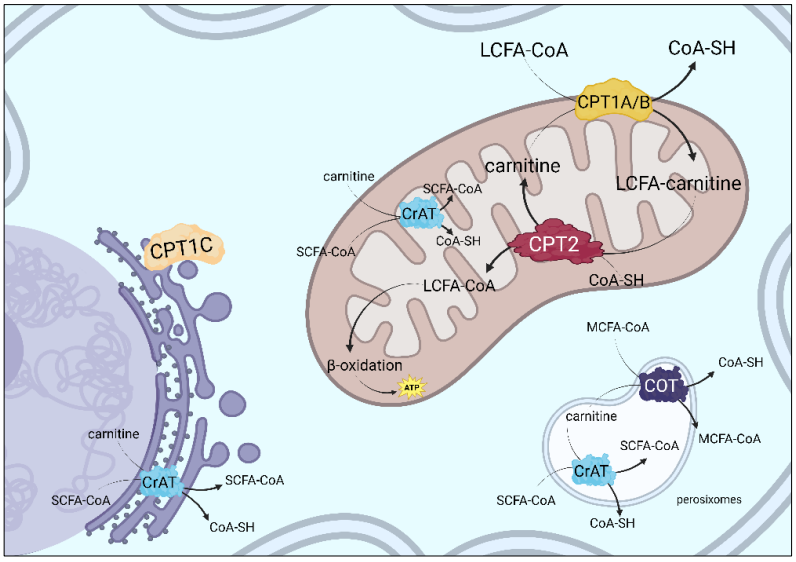

Figure 9. Cellular location of carnitine transferases. SCFA: short-chain fatty acids. MCFA: medium chain fatty acids. LCFA: long-chain fatty acids. Adapted from (Casals et al., 2016).

CPT1C shares 86% and 85% of coding sequence identity with CPT1A and CPT1B respectively (Price et al., 2002). These enzymes consist of two transmembrane domains associated with a short intraluminal loop allowing the N- and C-terminal regions to be both towards the cytoplasm. Table 1 describes the different domains of CPT1C. This protein has a unique characteristic compared with the other two canonical isoforms: it has a longer C-terminal consisting of 39 extra amino acids. Recent studies have revealed that this extended tail plays a critical role in facilitating interactions between CPT1C and other proteins of the ER, such as SAC1 (Casas et al., 2020) modulating its function.

Table 1. Domain's features of mouse CPT1C.

Region	Amino acids	Description
N-terminus	1-52	Cytoplasmic
Transmembrane	53-75	Helical
Topological domain	76-103	Luminal
Transmembrane	104-126	Helical
C-terminus	127-803	Cytoplasmic

The tiny N-terminal domain has an important function too. It is the responsible of the ER localization (Sierra et al., 2008). In addition, it can be in two different conformations, Nα and Nβ, alternating between them based on the physiological conditions (feeding or fasting) of the cell (Rao et al., 2011; Samanta et al., 2014).

4.1. Catalytic activity and regulation by malonyl-CoA

CPT1s specially catalyze the transesterification process between acyl-CoA esters and carnitine, resulting in the formation of acylcarnitine esters and coenzyme A (CoA). This step facilitates the translocation of fatty acids to the mitochondria as it was mentioned before. Subsequently, CPT2 carries out the reverse reaction by converting acylcarnitines back into acyl-CoA within the mitochondrial matrix. This transformation allows the acyl-CoA to undergo β-oxidation (figure 9).

Nevertheless, despite having all the motifs that are essential for CPT activity conserved along with the acyl-CoA binding sites, CPT1C seems not to have catalytic activity and does not participate in the fatty acid oxidation. It has been demonstrated that CPT1C has limited enzymatic function in the presence of different acyl-CoA esters and carnitine (Price et al., 2002; Wolfgang et al., 2006). Moreover, CPT1C shows a catalytic efficiency 20-300 times lower than that of CPT1A (Sierra et al., 2008).

Although CPT1C has minimal catalytic activity, it can bind malonyl-CoA with the same affinity as CPT1A does (Price et al., 2002). Malonyl-CoA is the first intermediate in the fatty acid biosynthesis. This metabolite is synthesized by the acetyl-CoA carboxylase (ACC) from acetyl-CoA, which is then used by the fatty acid synthase (FAS) to produce long-chain fatty acids. It can be converted again to acetyl-CoA by the malonyl-CoA decarboxylase (MCD).

The nutritional status of the organism modulates the levels of malonyl-CoA (figure 10). During periods of reduced nutrient availability, the activation of AMP-activated protein kinase (AMPK) results in the inhibition of ACC (by its phosphorylation) and a subsequent decrease in malonyl-CoA levels. In these conditions, long-chain fatty acids will not be generated, leading to energy conservation within the organism (Hardie, 2015). However, under feeding conditions its levels increase again (Tokutake et al., 2010). This dynamic regulation has been observed in different brain regions, such as the hypothalamus, cortex, hippocampus and cerebellum.

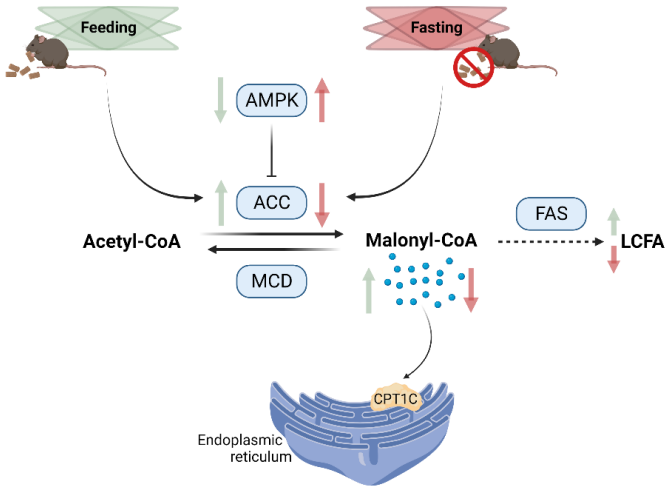

Figure 10. Levels of malonyl-CoA depend on feeding/fasting conditions. In a feeding situation, there is an increase in ACC activity, leading to high levels of malonyl-CoA. Conversely, during fasting, ACC is phosphorylated and inhibited, resulting in a decrease in malonyl-CoA levels and the corresponding reduction in the synthesis of LCFA. ACC: acetyl-CoA carboxylase, CPT1C: carnitine palmitoyltransferase 1C, FAS: fatty acid synthase, LCFA: long-chain fatty acids, MCD: malonyl-CoA decarboxylase.

Considering all these aspects, CPT1C is a malonyl-CoA sensor (Fado et al., 2021). When CPT1C senses malonyl-CoA levels, it does modify the activity of its interactors such as SAC1, ABHD6 or protudin. In normal conditions (feeding), CPT1C inhibits SAC1 and ABHD6 enzymes. A fasting situation triggers decreased levels of malonyl-CoA (figure 10) blunting the inhibitory effect of CPT1C on ABHD6 (Miralpeix et al., 2021) or SAC1 (Casas et al., 2020). This results in increased levels of endocannabinoid 2-arachidoniyglycerol (2-AG), the substrate of ABHD6, and PI4P, the substrate of SAC1. In the case of protudin, in the same fasting situation, CPT1C would slow down axon growth (Palomo-Guerrero et al., 2019), a process where protudin participates as it will be explained later.

4.2. Implication in cognition

As it was mentioned above, CPT1C is widely distributed throughout the nervous system, specifically in neurons (Sierra et al., 2008). It presents significant levels in key brain region such as the hypothalamus, hippocampus, cortex, cerebellum and amygdala (Dai et al., 2007). It is well-known the relationship between the hippocampus and learning and memory processes, with CPT1C playing an important physiological role in this context. CPT1C's effects at synaptic, cellular and molecular level explain its involvement in cognition.

CPT1C KO mice show a delayed learning in the Morris water maze demonstrating an impaired spatial learning (Carrasco et al., 2012). Open field and object location tests were also evaluated with the same results (Iborra-Lazaro et al., 2023). Nevertheless, no anxiety- and depression-like behavior is found when CPT1C KO mice are tested in the elevated plus maze (Iborra-Lazaro et al., 2023).

It has been published that the absence of CPT1C induces impairments in dendritic spine morphology in hippocampal neurons (Carrasco et al., 2012). These cells have a strong enhancement in filopodia (being an indicator of immature spines) and a significant decrease in mature spines (both, mushroom and stubby ones). This phenotype of CPT1C KO neurons can be rescue by CPT1C overexpression (Carrasco et al., 2012), suggesting that dendritic spine maturation requires CPT1C. Moreover, cortical neurons from CPT1C KO mice have shorter axons and reduced branching than WT neurons, indicating that CPT1C is essential for an adequate neurite growth (Palomo-Guerrero et al., 2019).

Furthermore, as expected, synaptic plasticity is also altered in CPT1C deficient neurons. On the one hand, mEPSCs are decreased in hippocampal neurons from CPT1C KO mice (Fado et al., 2015) and LTP is also disrupted at the CA3-CA1 synapse of the hippocampus from slices of CPT1C KO mice (Iborra-Lazaro et al., 2023). On the other hand, the CPT1C overexpression is able to improve glutamate-evoked whole-cell currents of GluA1 (Gratacos-Batlle et al., 2015).

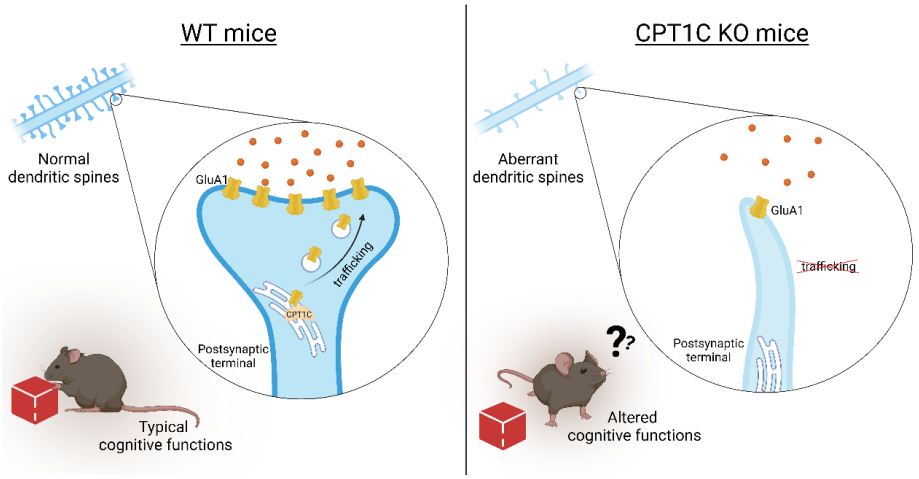

Figure 11. CPT1C's role in cognition. There are normal dendritic spines with normal cognitive functions due to the correct trafficking of GluA1 to the plasma membrane in WT animals. However, under CPT1C deficiency in KO mice, the number of filopodia increase, surface GluA1 levels decrease and cognition is impaired.

As explained previously (see section 2.), CPT1C was identified as part of the AMPAR complex (Brechet et al., 2017; Schwenk et al., 2012). This protein can modulate the post-transcriptional GluA1 protein synthesis and AMPAR trafficking to the cell surface (Casas et al., 2020; Fado et al., 2015; Gratacos-Batlle et al., 2015). In fact, CPT1C deficiency results in a reduction of AMPARs at the synaptic level in cultured hippocampal neurons (Fado et al., 2015). However, CPT1C does not participate in the gating properties of AMPARs (Gratacos-Batlle et al., 2015).

For CPT1C regulation of surface AMPAR levels, the palmitoylable cysteine residue located at position 585 of GluA1 plays a critical role (Gratacos-Batlle et al., 2015), because its mutations blocks CPT1C-induced GluA1 trafficking towards plasma membrane.

4.3. Other functions

Beyond the effects in cognition, CPT1C is also involved in motor functions, food intake and cancer. Regarding the first one, CPT1C deficiency causes impaired coordination associated with a reduction in muscle strength, hypoactivity and decreased daily locomotor activity in mice (Carrasco et al., 2013). Moreover, another study provides further evidence of muscle weakness and altered coordination (Iborra-Lazaro et al., 2023).

These motor deficits that CPT1C KO mice present correlate with some of the symptoms of human CPT1C mutations. In fact, a form of hereditary spastic paraplegia (HSP) has been related to CPT1C mutations in patients (Hong et al., 2019; Rinaldi et al., 2015). HSP is described by impaired functions of corticospinal motor neurons with lower extremity weakness (Fink, 2013). There have been no reports of significant cognitive deficits in these patients, but more exhaustive tests are needed. This neurological disorder is also characterized by the impairment of organelle transport along the axon (Blackstone et al., 2011; Boutry et al., 2019).

Among the identified mutations in HSP related to CPT1C, one of them (Q76X) is a missense mutation that introduces a premature stop (Hong et al., 2019) and the other one (R37C) is an amino acid substitution in the N-terminal regulatory domain of CPT1C (Rinaldi et al., 2015). This mutated CPT1C impairs the formation of lipid droplets which are the responsible for the storage of fatty acids, further corroborating the key role of CPT1C

in lipid metabolism. Moreover, R37C mutation reduces axon growth in neurons. In fact, CPT1C has recently been implicated in the anterograde transport of late endosomes/lysosomes at the axonal tip, necessary for axon growth. This effect of CPT1C is malonyl-CoA dependent (Palomo-Guerrero et al., 2019).

Additionally, CPT1C regulates food intake and energy balance. It has been demonstrated that CPT1C KO mice have reduced body weight and decreased food intake compared to WT (Wolfgang et al., 2006). However, these animals are much more susceptible to gain body weight when fed with HFD, even when consuming nearly the same amount of food as the WT (Rodriguez-Rodriguez et al., 2019; Wolfgang et al., 2008).

Under HFD, these animals present insulin resistance, characterized by increased hepatic gluconeogenesis and reduced glucose uptake in skeletal muscle (Gao et al., 2009). These alterations cause a decrease in fatty acids oxidation storing lipids in these tissues, explaining the obesogenic phenotype.

Furthermore, under fasting conditions, CPT1C KO mice display a lower degree of body weight loss (Pozo et al., 2017). Strikingly, when CPT1C is overexpressed in the hypothalamus of WT mice, it provides protection from diet-induced obesity (DIO) without any decrease in food intake (Dai et al., 2007).

Moreover, CPT1C is essential in the regulation of ghrelin and leptin, the two mayor hormonal regulators of food intake. On the one hand, the intracerebroventricular (icv) administration of the orexigenic peptide ghrelin, which stimulates appetite, promotes a food-seeking behavior and food intake in fully satiated WT mice (Ramirez et al., 2013). However, these effects are attenuated in CPT1C KO mice corroborating the key role of CPT1C in mediating the impact of ghrelin on feeding behavior. On the other hand, the effects of the anorexigenic hormone leptin, which reduces appetite and promotes satiety, are impaired in CPT1C KO mice (Gao et al., 2011). These animals do not have a proper activation of leptin-induced brown adipose tissue thermogenesis that counteracts the development of obesity (Rodriguez-Rodriguez et al., 2019).

Finally, CPT1C is also related to cancer. When depleting CPT1C in cancer cells, tumor growth is inhibited (Zaugg et al., 2011). Moreover, CPT1C is a downstream target of the AMPK/p53 pathway establishing a direct connection with the metabolic adaptation of tumor cells to environmental changes, especially hypoxia and nutrient deficiency (Sanchez-Macedo et al., 2013). Recently, it has been published that a lower CPT1C expression directly correlates with a lower pathological tumor response to anthracyclines, suggesting CPT1C as a new predictive biomarker for breast cancer treatment (Muley et al., 2023). Most published studies suppose that CPT1C activates β-oxidation in cancer cells adapting them to survive to the dynamic conditions of tumor microenvironment. Nevertheless, CPT1C would rather play a more indirect role in tumors regulating CPT1A-mediated fatty acid oxidation at mitochondria-ER contact sites by sequestering malonyl-CoA (Fado et al., 2023). It is noteworthy to consider that neurons and cancer cells do not use fatty acids as the primary source of energy. Cancer cells could benefit from CPT1C as a nutritional sensor to control lipid metabolism for membrane synthesis when they are dividing (Fado et al., 2023).

5. SAC1

SAC1 is an enzyme that plays a crucial role in regulating lipid metabolism and cellular processes within cells. It is a lipid phosphatase which dephosphorylates phosphatidylinositol 4-phosphate (PI4P) into phosphatidylinositol (PI) *in vivo* and it is conserved in protein sequence, subcellular localization and function. However, *in vitro* studies have shown that SAC1 can remove phosphate groups from PI3P and PI(3,5)P_2 too (Guo et al., 1999).

It was discovered and named as a "suppressor of actin 1" defects in yeast cells of *Saccharomyces cerevisiae* more than 25 years ago (Novick et al., 1989). SAC1 yeast mutants are viable but show sensitivity to cold temperatures, disordered intracellular actin and decreased chitin secretion rate (Novick et al., 1989; Schorr et al., 2001). They are inositol auxotrophs despite exhibiting no abnormalities in inositol biosynthesis (Whitters et al., 1993) and present ATP transport alterations (Kochendörfer et al., 1999). Despite the fact that SAC1 is not essential for

yeast, it is fundamental in flies and mice. In the case of flies, SAC1 deletion leads to embryonic lethality attributed to dorsal closure, a crucial stage in the development of *Drosophila melanogaster* (Wei et al., 2003). In mice, SAC1 knock-down causes early embryonic lethality by mitotic defects in formation of multipolar spindles, resulting in atypical chromosome separation (Liu et al., 2008). Moreover, the viability and growth of cell lines are compromised when silencing SAC1 with siRNA (Cheong et al., 2010).

Mammalian SAC1 is ubiquitously expressed throughout adult and embryonic tissues, with elevated levels in cerebellar Purkinje cells (Nemoto et al., 2000). As regards its subcellular distribution, it is mainly localized at the ER, Golgi apparatus and membrane contact sites (ER-plasma membrane and ER-Golgi) (Del Bel & Brill, 2018).

Most of the studies carried out to explore SAC1 distribution within the cell have been conducted in yeast. The overexpression of this protein at the ER in yeasts results in a reduction of PI4P levels with no defects over this organelle (Konrad et al., 2002). However, when a dysfunctional SAC1 variant is overexpressed, PI4P levels are increased impairing protein processing and affecting cellular functions (Tahirovic et al., 2005).

In Golgi apparatus, SAC1 has an expression gradient because it is differently distributed among the three distinct compartments (cisternae). SAC1 presents higher levels in cis-regions than in trans-ones resulting in an increasing gradient of PI4P from cis- to trans-parts of the Golgi (Cheong et al., 2010; Wood et al., 2012).

This capacity of SAC1 to regulate PI4P levels within the Golgi apparatus depends on an effector molecule known as GOLPH3 in mammalian cells (or Vps74 in yeasts). SAC1 interacts with this molecule, which simultaneously binds PI4P (Cai et al., 2014). In cases of SAC1 mutations, the Golgi's ability to confine GOLPH3 is compromised. Furthermore, the high levels of PI4P disrupt the anterograde transport of Golgi's enzymes, leading to an abnormal redistribution at the plasma membrane (Dippold et al., 2009; Wood et al., 2009).

SAC1 also plays a crucial role at membrane contact sites. They are important for non-vesicular transport of molecules. The plasma membrane is tethered to the ER through the action of mammalian ORP5/8

(Osh6/7 in yeasts) exchanging PI4P and the lipid phosphatidylserine (PS) (Chung et al., 2015). The SAC1-mediated hydrolysis of PI4P is vital for efficient countertransport by ORP proteins (Moser von Filseck, Copic, et al., 2015). This transfer of PI4P from the plasma membrane to the ER (against its concentration gradient) leads to its hydrolysis by SAC1 in cis-region, helping the uptake of PS by ORP proteins. This process facilitates constant levels of this lipid in the plasma membrane where they are necessary for several biological process (Chung et al., 2015). Nevertheless, it was also described that SAC1 can modulate PI4P in trans-region (Stefan et al., 2011).

In the case of ER-Golgi contact sites, VAP proteins are the responsible for tethering these two organelles (Wakana et al., 2015) and sterols are exchanged for PI4P instead of PS (Moser von Filseck, Vanni, et al., 2015). Nevertheless, there is a debate whether SAC1 regulates PI4P pool at these contact sites through the cis- or trans-region. On the one hand, it is published that SAC1 dephosphorylates PI4P at the ER suggesting an obligate “cis” activity of SAC1 (Zewe et al., 2018). On the other hand, it is also proposed that SAC1 operates in trans-regions, especially at ER-TGN, thanks to the FAPP1 protein (Venditti et al., 2019). Indeed, it has been published that the trans-activity of SAC1 regulates the AMPAR’s transport depending on the presence of nutrients (Casas et al., 2020).

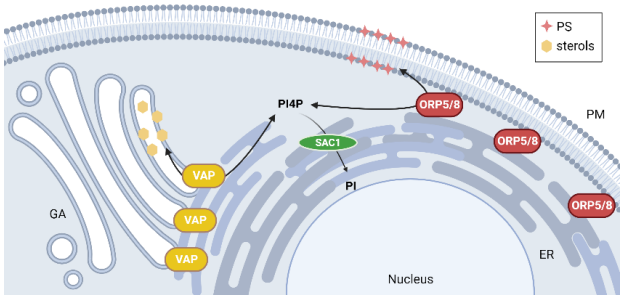

Figure 12. Implication of SAC1 at membrane contact sites. ORP5/8 are in charge of the exchange of PI4P and PS between the ER and the PM. VAP mediate the exchange of PI4P and sterols between the ER and the GA. ER: endoplasmic reticulum. GA: Golgi apparatus. PM: plasma membrane. PS: phosphatidylserine.

Finally, SAC1’s control of PI4P is essential for the correct formation and trafficking of vesicles at the TGN (Del Bel & Brill, 2018). SAC1 is also present

at endolysosomal membranes and has different functions such as membrane tubule formation and mediation of autophagosome-lysosome fusion (Liu et al., 2021; Zhang et al., 2021).

5.1. Structure

SAC1 has a primary sequence similarity to a subfamily of cytosolic/peripheral membrane phosphoinositide phosphatases known as synaptojanins. It has a long N-terminal domain, 2 transmembrane domains and a short C-terminal domain (table 2). Recently, its structure has been resolved with the high-resolution cryo-EM (Schafer et al., 2023).

Table 2. Domain's features of mouse SAC1.

Region	Amino acids	Description
N-terminus	1-520	Cytoplasmic
Transmembrane	521-541	Helical
Topological domain	542-548	Lumenal
Transmembrane	549-569	Helical
C-terminus	570-587	Cytoplasmic

This distribution of domains facilitates a "J" topology allowing the N- and C-terminus face the cytosol and the transmembrane regions bind the protein to the membrane (Del Bel & Brill, 2018). SAC1 is characterized by a domain of approximately 500 amino acids known as SAC1 domain containing the phosphatase activity (Guo et al., 1999). This domain presents seven highly maintained motifs among different species (figure 13).

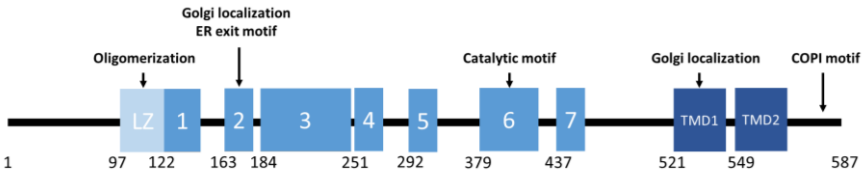

Figure 13. Schematic mammalian SAC1 protein domains with their main characteristics. Numbers 1-7 correspond to conserved motifs within the phosphatase domain in mammals. LZ: putative leucine zipper. TMD: transmembrane domain. Based on (Del Bel & Brill, 2018).

Firstly, mammalian SAC1 has a putative leucine zipper at the N-terminal domain responsible for oligomerization and its localization at the Golgi apparatus (Blagoveshchenskaya et al., 2008). In addition, the second conserved motif of SAC1 domain together with the first transmembrane domain are also implicated in Golgi localization (Wang et al., 2013). The catalytic motif ($CX_5R(T/S)$ is found in the 6^{th} motif characterized by a unique P-loop conformation, where the phosphatase activity takes place (Manford et al., 2010). SAC1 has a large cationic catalytic groove where the catalytic cysteine is distantly positioned from the conserved arginine responsible for the phosphate group binding (Zhong et al., 2012), suggesting a conformational change: the catalytic residues must move closely to each other to allow PI4P hydrolysis. Thus, it is proposed an allosteric activation of SAC1 activity by anionic phospholipids, such as PS, which could induce the conformational alteration necessary to bring the cysteine and arginine together (Zhong et al., 2012).

Regarding the C-terminal extreme, it has a coat protein I (COPI) binding motif (583-KEKIDD) accountable for the presence of SAC1 in the ER (Blagoveshchenskaya et al., 2008). This motif is not present in yeasts and flies.

Several studies have been done comparing SAC1 protein sequence within different species. Human SAC1 exhibits 32% identity with yeast SAC1 and 95%, with rat SAC1 (Rohde et al., 2003). Figure 14 shows a scheme of the conservative domains of SAC1 among species. In the case of human SAC1 domain, it starts from amino acid 121 to 500 and the putative leucine zipper, from amino acid 98 to 126 (Rohde et al., 2003). Moreover, the leucine zipper motif is perfectly conserved in mammalian SAC1 family members. The conservation of SAC1 sequence suggests that its function has been preserved throughout evolution due to the importance this protein has in cellular processes.

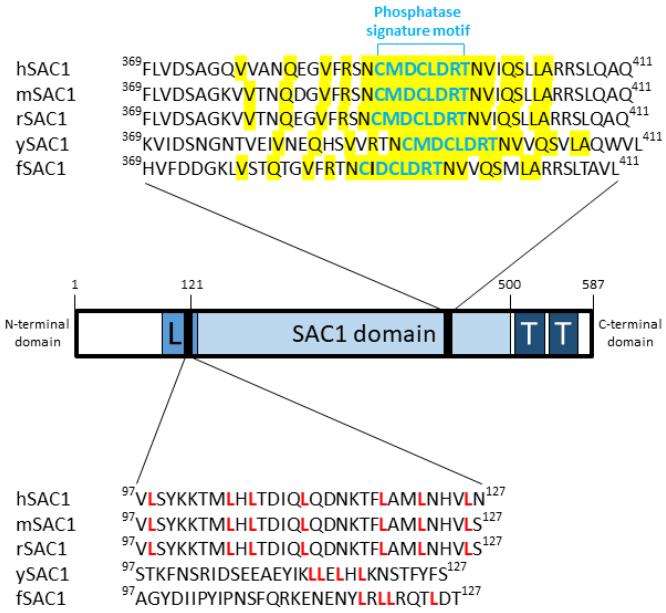

Figure 14. Comparison between the phosphatase signature motif and the leucine zipper motif of different species. Phosphatase signature motif is in blue in the SAC1 homology domain. Identical amino acids are highlighted. Conserved leucines are in red. hSAC1: human SAC1. mSAC1: mouse SAC1. rSAC1: rat SAC1. ySAC1: yeast SAC1. fSAC1: fly SAC1. L: putative leucine zipper. T: transmembrane domains.

A detailed analysis of the yeast SAC1 crystal structure shows a N- (SacN) and C-terminal (SacC) subdomains (1-182 and 183-503 amino acids, respectively) within N-terminus (Manford et al., 2010). SacN is composed of 3 layers of β-sheets and 4 α-helices facilitating protein interactions, whereas SacC presents 9 β-sheets surrounded by 5 α-helices (Manford et al., 2010).

5.2. Metabolic regulation

As it was mentioned before, SAC1 is expressed in the ER, Golgi apparatus and membrane contact sites. The presence of SAC1 in these compartments relies on the nutrients' provisions in the cellular environment (Mayinger, 2009). When there are enough growth factors, SAC1 localizes to the ER and, when there is nutrient deprivation, it is in the Golgi (Blagoveshchenskaya & Mayinger, 2009).

On the one hand, when there is nutrient availability, SAC1 is quickly re-located from the Golgi to the ER, facilitating Golgi PI4P levels to increase and the rapid enhancement of secretion. To do so, SAC1 needs the interaction of COPI vesicles through the dilysine motif (KEKIDD) at its C-terminal domain (Rohde et al., 2003).

The SAC1's translocation to the ER is regulated by the p38 MAPK pathway (Blagoveshchenskaya et al., 2008). To remain in the Golgi, SAC1 requires to oligomerize. However, p38 separates these oligomers and SAC1 can be easily transported to the ER thanks to COPI vesicles. Under these conditions, there is a decreasing PI4P gradient from the Golgi to the ER.

On the other hand, in starved mammalian cells, SAC1 remains in the Golgi and halts the increase of PI4P levels here, resulting in a slowdown of constitutive secretion. In addition, the absence of nutrients triggers SAC1 oligomerization thanks to its N-terminal LZ motif in the Golgi (Blagoveshchenskaya et al., 2008). This SAC1's accumulation in the organelle needs COPII-dependent vesicular trafficking along with the involvement of 14-3-3 protein.

Moreover, c-Jun N-terminal kinase 3 (JNK3), a protein kinase predominantly expressed in the brain (Nakano et al., 2020), binds to SAC1 oligomers in the Golgi inhibiting anterograde transport (Yang & Cynader, 2014). The second conserved motif (figure 13) is the responsible for the ER exit of SAC1 (Del Bel & Brill, 2018). Upon this type of situation, an increasing PI4P gradient is generated from Golgi to ER. This adaptive shuttling between the different compartment is summarized in figure 15.

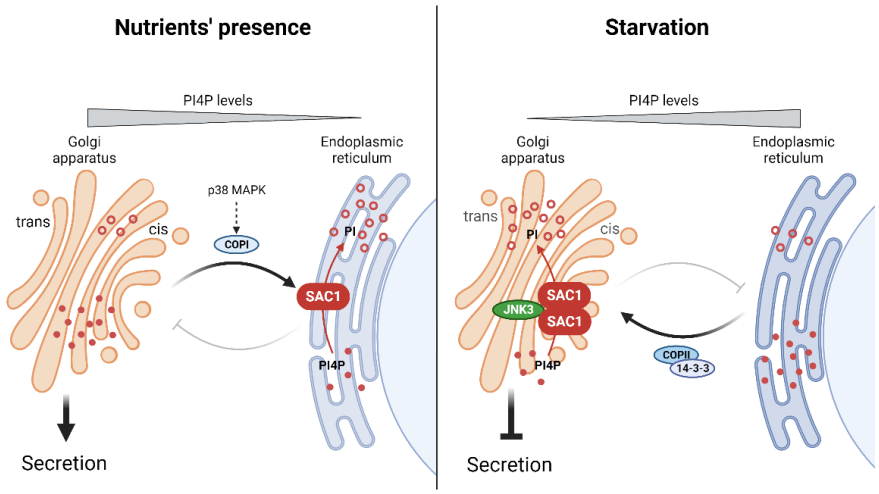

Figure 15. Dynamic regulation of SAC1 in ER-Golgi in mammalian cells. The localization of SAC1 depends on the nutritional status of the cells. In nutrients' presence, it is translocated to ER increasing PI4P levels in the Golgi and enabling secretion. Under starvation situation, SAC1 is in the Golgi decreasing PI4P levels and blocking secretion.

5.3. Cellular functions

SAC1 participates in a variety of complex processes such as membrane trafficking, cytoskeletal distribution and intracellular communication (Del Bel & Brill, 2018).

It has been published that SAC1 participates in regulating axon guidance within the embryonic CNS in *D. Melanogaster* (Lee et al., 2011). When SAC1 is mutated, it leads to an aberrant crossing of cell adhesion molecule axon tracts at the midline (Lee et al., 2011). Furthermore, SAC1 is also essential for maintaining the structural integrity of the retinal floor in *D. Melanogaster* (Griffiths et al., 2020). These data emphasize the critical function of SAC1 in tissue development.

In post-embryonic synapses, SAC1 downregulation causes disruptions in the distribution of various postsynaptic components, synaptic growth and the integrity of microtubules (Forrest et al., 2013). SAC1 knock-down cells provoke the aggregation of an essential factor in axons' synaptic active zones (Wagh et al., 2006). Hence, SAC1 is crucial for the proper functioning of axonal processes.

It has been reported that cultured primary rat neurons treated with an excitotoxic concentration of NMDA (mimicking a metabolic stress) lead to the palmitoylation of JNK3 and its attachment to the Golgi complex (Yang et al., 2013). Upon physiological conditions, the kinase is not palmitoylated and remains in the cytosol without interacting with SAC1. Under metabolic dysregulation, JNK3 is palmitoylated and binds SAC1, decreasing PI4P necessary for the exit of GluA1-vesicles from the Golgi (Yang et al., 2013). These data underscore the relevance of SAC1 in the secretory pathway.

SAC1 is also important in lipid homeostasis. Yeast SAC1 mutants present a 40% reduction in the cellular PS levels (Tani & Kuge, 2010) and an aberrant accumulation in intracellular membranes (Tani & Kuge, 2014). Conversely, PS allows SAC1 to dephosphorylate PI4P facilitating the phospholipid transfer to the plasma membrane (Zhong et al., 2012). This self-regulation links PS distribution and abundance to PIP metabolism through SAC1 activation. Moreover, yeast SAC1 mutants show a reduced rate of sphingolipid biosynthesis resulting in higher ceramide levels (Brice et al., 2009; Tani & Kuge, 2010).

Finally, SAC1 has been related to cancer cell metastasis. Reducing SAC1 levels leads to decreased cell-cell adhesion with cytoskeletal reorganization and increased cell migration in breast cancer cells (Tokuda et al., 2014). Therefore, SAC1 is a critical protein that regulates phosphoinositide lipid metabolism, membrane trafficking and synaptic function. Its proper function is essential for maintaining neuronal health and synaptic plasticity.

5.4. SAC1 – CPT1C interaction

As previously mentioned, SAC1 interacts with CPT1C, which senses malonyl-CoA depending on the nutritional status of the cell. This interaction is permanent, CPT1C is always tethering SAC1 independently of malonyl-CoA presence. Nevertheless, the connection is inhibitory when there is malonyl-CoA in the cell. In the absence of the molecule, SAC1 can carry out its phosphatase activity although CPT1C remains linked to it.

The interaction between these two proteins predominantly takes place within the ER-TGN contacts. It has also been published that the presence

of CPT1C at these contact sites corresponds to an increased abundance of SAC1 in these regions (Casas et al., 2020).

In addition, CPT1C, through its binding to SAC1, regulates the exit of AMPARs from TGN to the plasma membrane. CPT1C senses malonyl-CoA levels and SAC1 is released from CPT1C's inhibition when they decrease, retaining AMPARs in TGN. Thus, SAC1 – CPT1C interaction modulates AMPARs' trafficking toward the plasma membrane.

CPT1C does not interact with SAC1 through its last 40 amino acids, the C-terminus (Casas et al., 2020). However, this part of the protein is very important as CPT1C uses it to bind to GluA1 subunit (Casas et al., 2020), but it is unknown which motifs SAC1 and CPT1C use to interact with each other.

HYPOTHESIS

Cognition can be affected by diets, especially at young and old ages. Our hypothesis is that unsaturated fats and ketone bodies enhance AMPA receptors' trafficking and synaptic plasticity, while saturated fats are detrimental. The effects of nutrients on AMPAR trafficking is partially mediated by the interaction between CPT1C and SAC1.

OBJECTIVES

1. To explore the effects of different fatty acids and ketone bodies on AMPA receptor trafficking and synaptic transmission

    1.1. To examine whether unsaturated and saturated diets can contribute to the phosphorylation of GluA1 in brain hippocampus and cortex

    1.2. To determine the effect of fatty acids and ketone bodies' treatments on surface GluA1 in primary cortical neurons

    1.3. To study whether BHB can reverse the saturated fatty acids' effects on synaptic GluA1 in primary hippocampal neurons

    1.4. To characterize the effects of fatty acids and ketone bodies on excitatory synaptic transmission in brain slices

    1.5. To demonstrate the implication of fatty acids and ketone bodies in memory

    1.6. To establish whether the malonyl-CoA – CPT1C axis is involved in nutrient-mediated GluA1 regulation

2. To elucidate the interaction between SAC1 and CPT1C

    2.1. To check the correct expression and subcellular localization of truncated proteins

    2.2. To analyze the interaction between SAC1 and CPT1C proteins through FRET techniques

    2.3. To describe the interaction between SAC1 and CPT1C proteins via pull-downs

METHODOLOGY

1. Animal procedures

C57BL/6J wild type (WT) mice were used for experiments. They were kept in a controlled environment with a 12h light-12h dark cycle (light on at 8 a.m., light off at 8 p.m.) maintaining the same temperature and humidity conditions. Mice were fed with a standard laboratory chow diet (other case indicated as it is described in table 3) and had unrestricted access to water.

Table 3. Composition of diets used for this thesis.

Diet	Composition (% kcal)			Reference
	Fats	Carbohydrates	Proteins	
Standard diet (SD)	10	70	20	D12450J, Research Diets
High fat diet (HFD)	60	20	20	D12492, Research Diets
Saturated fat diet (SFAD)	49	31	20	D19121204, Research Diets
Monounsaturated fat diet (MUFAD)	49	31	20	D19121203, Research Diets

For primary neuron cultures, pregnant mice with embryos of E15.5 were sacrificed by cervical dislocation. The embryos' heads were cut off as soon as they were taken out of the uterus. All animal procedures were performed in agreement with European guidelines (2010/63/EU) and approved by the Research Ethical Committee of the International University of Catalonia (CBAS-2020-05).

1.1. Behavioral and cognitive tests

5 weeks-old mice were fed with SD (10% of kcal from fat) or SFAD (49% of kcal from saturated fatty acids) for a period of 7 weeks. Simultaneously, they received intragastric administrations of either vehicle (water) or BHB (100 mg/kg/day). Throughout the study, animals had unrestricted access to food and water. Animals were also weighed every week to analyze their gain in body weight. After that, three different tests were conducted: novel object recognition test (NORT), object location test (OLT) and open field test (OFT) in collaboration with Christian Griñán Ferré from University of Barcelona.

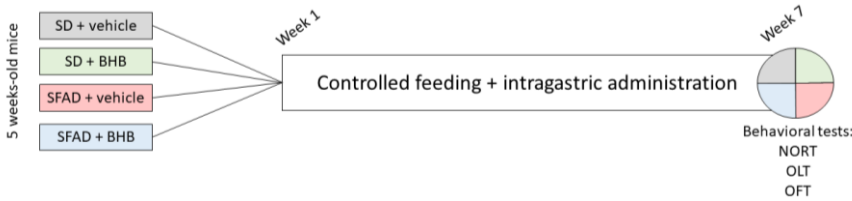

Figure 16. Schematic representation of the experimental design before conducting behavioral tests.

1.1.1. Novel object recognition test

NORT allows the analysis of both short- and long-term recognition memory involving cortical areas as well as the hippocampus. As previously described (Grinan-Ferre et al., 2020), it was performed in a 90º, two-arm, 25 cm-long and 20 cm-high maze. Before the real test took place, mice underwent a 3-day habituation period, spending 10 minutes per day in the maze individually. On the fourth day, they were allowed to freely explore it during a 10-minute acquisition trial (habituation phase). During this phase, they examined two identical novel objects placed at the end of each arm. Short-term memory was evaluated 2 hours after the habituation phase with another 10-minute retention trial, where one of the two identical objects was replaced by a novel one. 24 hours later, mice were tested again, using a new objet along with an object that was identical to the new one used in the previous trial as shown in figure 17.

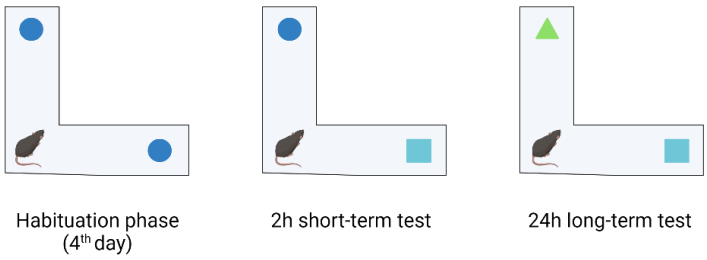

Figure 17. Scheme of the NORT indicating the differences in objects used in the habituation phase, 2h and 24h trials.

The exploration time of the novel object (TN) and the exploration time of the old object (TO) were quantified by reviewing video recordings of each trial session. Object exploration was defined as the mouse's nose touching the object or pointing it toward the object at a distance ≤ 2cm. The

cognitive performance was analyzed using the discrimination index (DI) calculated as (TN-TO)/(TN+TO).

1.1.2. Object location test

OLT evaluates spatial learning which mostly depends on hippocampal activity. This test is based on the spontaneous decision of mice to spend more time exploring a novel object location compared to a familiar one (Ennaceur & Meliani, 1992). It was performed in a box (50 x 50 x 25 cm). Three of the wall were white, while the fourth wall was black (figure 18). The box remained empty the first day allowing mice to acclimate to it for 10 minutes. The following day, two identical 10-cm high objects were positioned equidistant from each other and the black wall. Mice explored them for 10 minutes too. The last day, one of the objects was relocated in front of the white wall, serving as a test of spatial memory. The evaluation of the cognitive performance was done in the same way as the NORT.

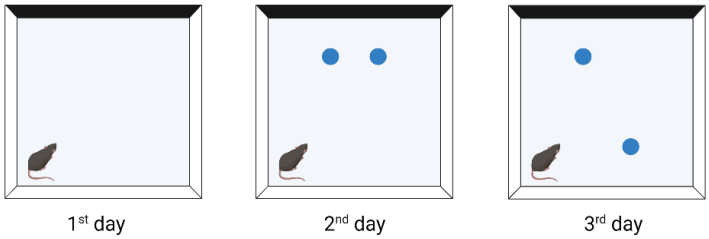

Figure 18. Scheme of the experimental design for the OLT.

1.1.3. Open field test

OFT is also used to study spatial learning apart from an anxiety-like behavior (Grinan-Ferre et al., 2016). In this case, the ground of the box (50 x 50 x 25 cm) was divided into central and peripheral zones to facilitate the analysis of the distance travelled. Mice were positioned either at the center or at one of the corners of the open field. They explored it for 5 minutes and the distance travelled was considered as a primary indicator of locomotion.

2. Cellular biology

2.1. Cells and maintenance

In this thesis, both cell lines and primary cortical/hippocampal neurons were used. All cell types were always maintained at a temperature of 37°C, with a CO_2 concentration of 5% and humidity of 95%.

2.1.1. Cell lines

The cell lines used were the following:

HEK293T cells: they are a stable clone from the human embryonic kidney 293T cell line. Its genome expresses the simian virus 40 (SV40) large T antigen which allows them to generate recombinant proteins using plasmid vectors that incorporate the SV40 promoter. For this reason, they are widely used for lentiviral production and expression of eukaryotic proteins.

SH-SY5Y cells: they were derived from the SH-SY subclone of the parental SK-N-SH human neuroblastoma cell line. They can be converted from neuroblast-like state into mature human neurons by the addition of specific compounds. SH-SY5Y were differentiated into a neuron-like type by adding 10 µM of retinoic acid (R2622 Sigma) diluted in DMSO (1029521011 Merck) to normal medium. For the control group, 20 000 cells/mL were seeded in a 24-well plate and, for the differentiated group, 40 000 cells/mL. The medium was changed every 2-3 days. These cells were seeded in coverslips previously treated with 1/50 diluted collagen (354236 Corning). The coverslips were incubated for 1h at 37°C and then, washed 3 times with 1X PBS.

Both cells lines were maintained with DMEM (Dulbecco's Modified Eagle Medium) with high glucose concentration (D5671 Sigma-Aldrich) supplemented with 10% of fetal bovine serum (FBS; FBS12A Capricorn Scientific), 1% glutamax (X0551-100 Biowest) and 1% penicillin-streptomycin (P0781 Sigma-Aldrich).

2.1.2. Primary cortical/hippocampal neurons

Primary cortical/hippocampal cultures were prepared from mouse embryos (E15.5) of C57BL/6J mice. Brain dissection was carried out in sterile conditions as previously described (Parcerisas et al., 2020).

The coverslips used for the culture were cleaned with nitric acid overnight with agitation. The next day, 3 washes with water and one wash with ethanol were done. Once the coverslips were completely dried, they were sterilized. Lastly, the same day of the culture, coverslips in plates for immunochemistry studies were incubated with 0.1 mg/mL poly-D-lysine and plates for molecular and biochemical assays (with no coverslips), with 0.05 mg/mL of poly-D-lysine. After an hour of incubation at 37ºC and before seeding, they were washed 3 times with 1X PBS.

First of all, embryos were extracted by caesarean section and placed into cold 1X PBS supplemented with 3% of glucose. Cortices and hippocampi were extracted using a stereoscopic microscope and placed in 2.7 mL of 1X PBS-glucose and 300 µL of trypsin (15400054 ThermoFisher) for 8 minutes at 37ºC inverting the falcon tube every 2 minutes to facilitate cell disaggregation.

In order to stop the digestion reaction, 1.6 mL of horse serum (10368902 Fisher) were added. Afterwards, 500 µL DNase (4716728001 Merk) were added and the falcon tube was incubated for 8 minutes at 37ºC being inverted every 2 minutes.

Later, tissues were mechanically dissociated with a pipette 30 times and passed through a 40 µm cell strainer (542040 ddBiolab). The cell suspension was then centrifuged at 800 rpm for 5 minutes. The supernatant was removed and the pellet was re-suspended in 1 mL of culture medium.

The culture medium was composed of Neurobasal (21103049 ThermoFisher), 1% glutamax, 1% penicillin-streptomycin, 2% B27 (17504044 ThermoFisher) and 1/5 of glia conditioned medium. Depending on the amount of brains dissected, 5-10 mL of culture medium were added to the cell suspension after centrifugation.

Finally, trypan blue was used to count viable cells in a Neubauer chamber. For molecular and biochemical assays, 300 000 cells/mL were seeded in poly-D-lysine (P7886 Sigma-Aldrich) coated plates. However, for immunochemistry studies, 180 000 cortical cells/mL and 150 000 hippocampal cells/mL were seeded in poly-D-lysine coated coverslips-

containing plates. Neurons were maintained for 2 weeks and one-fifth of the culture medium was changed every 3-4 days.

To obtain the glia conditioned medium, the rest of the neurons that were not used for culture were seeded in a T-75 flask with a medium composed of Neurobasal, 1% glutamax, 1% penicillin-streptomycin and 10% FBS to avoid the growth of neurons and stimulate glia proliferation. The day after the seeding, it was necessary to change the medium in order to eliminate all the neurospheres formed. A week later, this medium was replaced by a medium containing Neurobasal, 1% glutamax, 1% penicillin-streptomycin and 2% B27. After 10 days, the conditioned medium containing factors secreted by glia was harvested: it was centrifuged for 10 minutes at 1500 rpm, filtered and stored at -20ºC. This process can be repeated twice because the glia in the flask will continue proliferating and generating new factors.

2.2. Transfection

Transfection was used to introduce exogenous genetic material into cultured cells. It is based on the opening of temporary pores in the cell membrane to facilitate the uptake of the genetic material. There are several methods to approach transfection. The ones used in this thesis were the calcium phosphate and polyethylenimine (PEI) for FRETse and pull-down, respectively.

2.2.1. Calcium phosphate

When HEK293T had a confluence of 60-80% they were transfected with calcium phosphate. The culture medium was removed 2 hours before the transfection and new medium was added. The following amount of reagents for a 6-well plate was added in this order: 1 µg of DNA, 86.5 µL of 0.1X TE, 48.5 µL of buffered water, 15 µL of 2.5M $CaCl_2$ and 150 µL of 2X HeBS. This last reagent was added dropwise while vortexing. The total volume of transfection for 6-well plate was 300 µL.

0.1X TE: 1 mM Tris-HCl pH 8 and 0.1 mM EDTA pH 8
Buffered water: milliQ water supplemented with 2.5 mM HEPES pH 7.3
2XHeBS: 280 mM NaCl, 50 mM HEPES and 1.5 mM $Na_2HPO{\cdot}2H_2O$ pH 7

The transfection mixes were left 20 minutes at RT before being added to HEK293T dropwise. The medium was changed after 24 hours and the experiments were performed 24 hours later.

2.2.2. Polyethylenimine

Polyethylenimine (PEI) is a highly efficient transfection reagent. It has a very low cytotoxicity and breaks cell membrane minimally. The ratio of PEI:DNA used was 3:1 and the amount of DNA was 15 µg (7.5 µg in the case of being transfected with two different plasmids) for 100 mm Ø dishes.

Once cells had a confluence of 60-80% approximately, they were transfected with PEI (24765 Polysciences). The medium used to prepare the transfection mixture was DMEM with just 1% glutamine (DMEMg).

The first transfection mixture was composed of 15 µg of DNA and 450 µL of DMEMg. The second transfection mixture consisted of 45 µL of PEI and 450 µL of DMEMg. Both mixtures were incubated for 5 minutes at RT and then, the second mixture was added over the first one. The final mixture was incubated for 15 minutes at RT and the 900 µL were added to cells. After 48 hours, the experiments (pull-down) were performed.

2.3. Infection with lentivirus

2.3.1. Production

Primary cortical neurons were infected with lentivirus to silence CPT1C. Lentiviruses have an RNA-based genome and replicate by forming a temporary DNA copy through reverse transcription. They also rely on integrases to insert their DNA into the genome of host cells. Moreover, they are highly efficient in infecting not only dividing cells but also non-dividing cells such as neurons. Nevertheless, they lack the ability to self-replicate.

The pLVTHM plasmid (Addgene #12247) was used as a lentiviral vector to introduce RNA interference sequences (RNAi). Previously in the research group, short hairpin-loop RNA of mCPT1C (shCPT1C) and a short hairpin-loop RNA with a random sequence (shRandom) were cloned into pLVTHM plasmid using ClaI/MluI as the cloning site. Thus, pLVTHM_shmCPT1C-GFP

was used for silencing CPT1C protein and pLVTHM_shRandom-GFP, for control group (see figure 19).

In addition to the lentiviral vector, a viral packaging vector (capsid) and a viral envelope vector are required to generate lentiviruses. They allow virus to fuse with the host cell membrane and introduce the capsid containing the genome. The viral packaging vectors used in this thesis were psPAX2 (Addgene #12260) and pMD2.G (Addgene #12259). Their maps are shown in figure 19.

A)

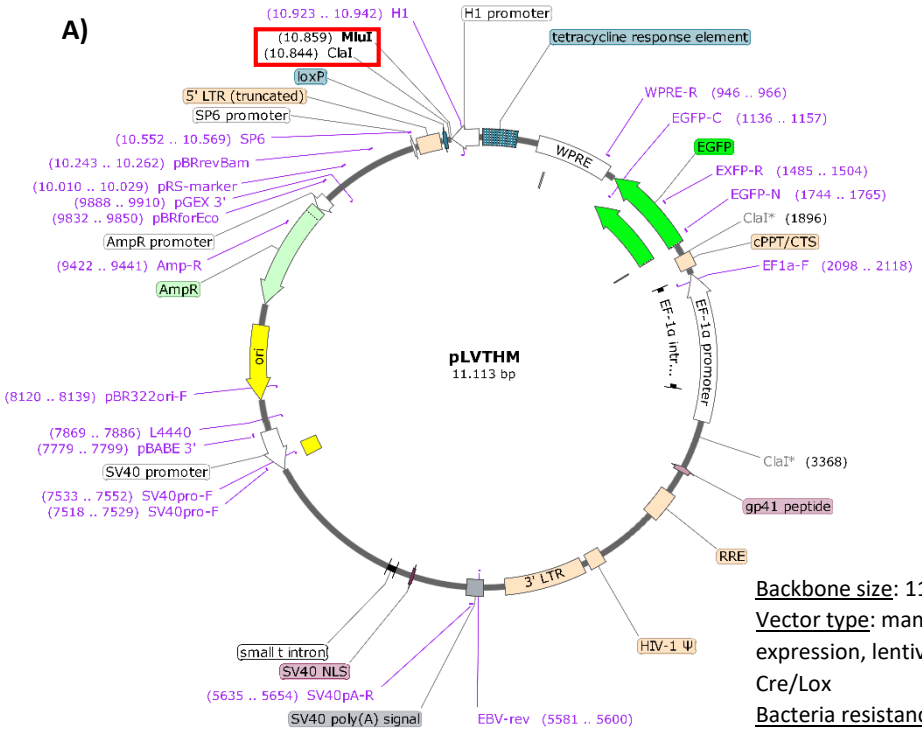

Backbone size: 11 113 bp
Vector type: mammalian expression, lentiviral, RNAi, Cre/Lox
Bacteria resistance: ampicillin
Copy number: high copy

B)

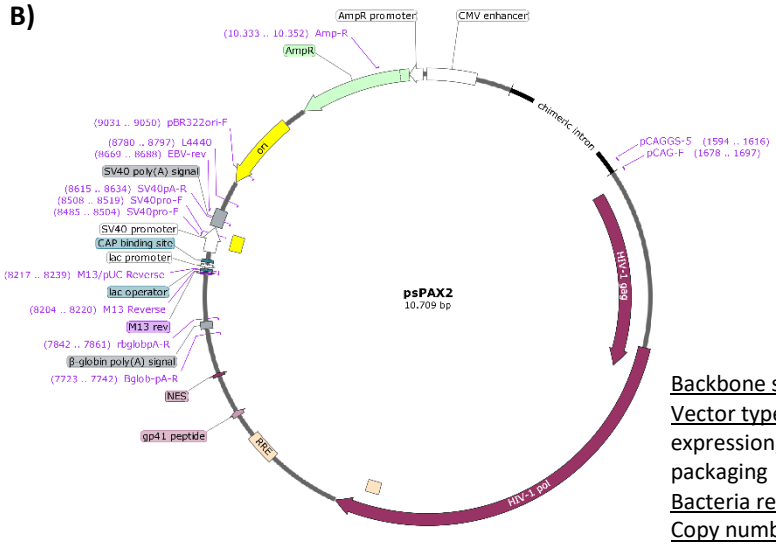

Backbone size: 10 703 bp
Vector type: mammalian expression, lentiviral, packaging
Bacteria resistance: ampicillin
Copy number: high copy

C)

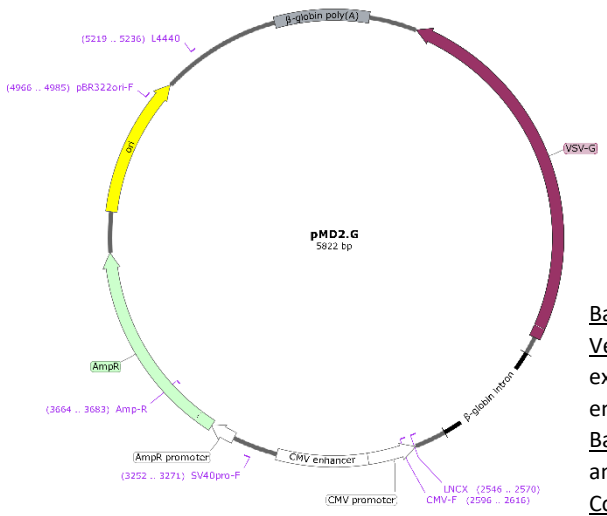

Backbone size: 5 822 bp
Vector type: mammalian expression, lentiviral, envelope
Bacteria resistance: ampicillin
Copy number: low copy

Figure 19. Plasmids' map created with *SnapGene*. A) Backbone of pLVTHM plasmid use for generate shCPT1C and shRandom viruses. B) Viral packaging vector psPAX2. C) Viral envelope vector pMD2.G.

The calcium phosphate method was used to produce lentiviruses. For each generated virus three 100 mm Ø dishes were seeded with 500 000

cells/mL of HEK293T per each dish. After 24 hours, cells had to be 80% confluence in order to be transfected.

Two hours before the transfection, the medium was changed and half of the maximum volume of the dish was added fresh. For each dish the volumes of the reagents were the following:

Table 4. Amount of each reagent used for calcium phosphate transfection in a 100 mm Ø dish.

		[stock]	Volume
Lentivirus vector		1 µg/µL	45 µL
Packaging vectors	**pMD2.G**	1 µg/µL	15.9 µL
	psPAX2	1 µg/µL	29.1 µL
TE 0.1X		0.1X	1.3 mL
Buffered water		-	727 µL
$CaCl_2$		2.5 M	223 µL
HeBS		2x	2.25 mL

The medium was replaced by 5 mL of new medium a day after the transfection, and 8 hours later, the first virus-containing medium was collected and stored at 4°C. This process was repeated the next day in the morning and in the afternoon. Then, the virus-containing medium was centrifuged at 3000 g 1h at 4°C using filtered tubes (VS2042 Sartorius), aliquoted and stored at -80°C.

2.3.2. Titulation

For titulation, cells were infected with different volumes of viruses to know the concentration of viral particles in a given volume. HEK293T were seeded at a final concentration of 50 000 cells/mL in 24-well plate. The next day, cells from two wells were counted again to know the number of cell per well at 1DIV. Furthermore, 250 µL of medium was removed from each well to facilitate the infection. Afterwards, HEK293T were infected with different amount of viruses: 0.015, 0.03, 0.06, 0.125, 0.25, 0.5, 1, 2, 3 and 4 µL.

After 24 hours, 1 mL of new medium was added to each well to stop the infection. Two days later, HEK293T were detached and GFP positive cells

were counted using the fluorescent-activated cell sorting (FACS) through BD FACSCalibur™. FACS is a type of flow cytometry which enables the detection of cells emitting fluorescence.

The data analysis for titulation was done with *Flowing Software*. Taking into account the percentages of GPF^+ cells, a dilution curve was generated and the concentration of virus in transduction units per milliliter (TU/mL) was obtained according to this formula:

$$\frac{\text{TU}}{\text{mL}} = \frac{\%\ \text{GFP positive cells} \cdot \text{counted cells at 1DIV}}{\mu\text{L of viral solution added in the well}}$$

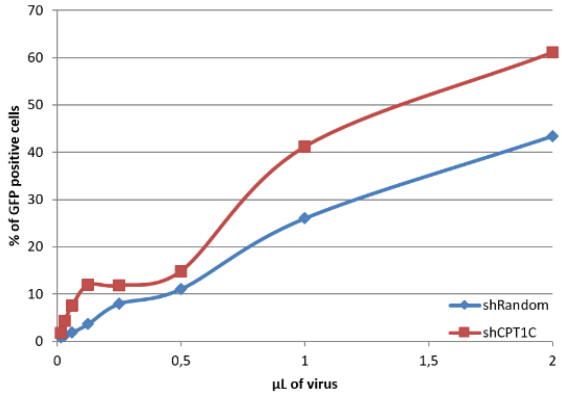

Figure 20. Graph of the dilution curve for virus titulation.

2.3.3. Infection

Cortical neurons were infected at 7DIV and the experiments were performed at 14-15DIV. For shCPT1C or shRandom virus, 1 MOI was used to infect cells.

2.4. Cellular treatment with fatty acids and ketone bodies

On the one hand, oleic acid (OA; O7501 Sigma), palmitic acid (PA; P9767 Sigma) and docosahexaenoic acid (DHA; D8768 Sigma) were prepared with a final concentration of 3 mM. First, 0.5 g deffated BSA (126575 Millipore) were added in 5 mL of 0.9% NaCl at 37ºC with agitation and the corresponding amount of the fatty acid was added to 500 µL of 0.1N NaOH at 80ºC. Once everything had been dissolved properly, the fatty acids were added dropwise to the BSA solution and left 5 more minutes at 37ºC. Then,

the solutions were filtered and stored at -20ºC. It is important to take into account that 500 µL of 0.1N NaOH had to be added to another BSA solution as a control group known as the "vehicle".

On the other hand, β-hydroxybutyrate (BHB; H6501 Sigma) was prepared at a final concentration of 250 mM in water.

Cortical/hippocampal neurons were treated for 2h or 24h at 14DIV and 13DIV respectively with the different treatments. In the case of differentiated SH-SY5Y cells, treatments of 2h and 24h were also done after seven and six days after seeding, respectively.

3. Molecular biology

3.1. Protein detection

3.1.1. Cellular lysis

To extract protein from cultured cells, they were first washed with 1X PBS three times. Then, lysis buffer (20 mM Tris pH 7.5, 5 mM EDTA, 150 mM NaCl, 1% NP40) with phosphatase inhibitor (ratio 1:40 in lysis buffer; A32957 Fisher Scientific) and protease inhibitor (ratio 1:40 in lysis buffer; A32955 Fisher Scientific) was added (50 µL of lysis buffer per well in 12-well plate).

The scraped cells were collected and incubated for 30 minutes at 4ºC with agitation. After it, they were centrifuged at 10 000 rpm at 4ºC for 10 minutes to eliminate the not-lysed cells and stored at -20ºC.

3.1.2. Tissue homogenization

Hippocampal samples and 10-20 mg of cortical samples were homogenized. The lysis buffer used was RIPA buffer (R0268 Sigma-Aldrich) complemented with phosphatase and protease inhibitor in a ratio of 1/40 to RIPA buffer too. For each sample 120 µL of RIPA buffer with inhibitors were added. Moreover, samples were sonicated 8 times (0.6 cycle and 80% amplitude) to break intact cell components. Then, they were incubated for 20 minutes at 4ºC with agitation. Finally, they were centrifuged in the same way as the lysed cells and stored at -20ºC.

3.1.3. Protein quantification

Protein quantification was conducted in different ways depending on the type of biological sample. On the one hand, proteins from cell lines were measured using Bradford (5000006 Bio-Rad). A 1/5 dilution of Bradford reagent was used and 200 µL were added per well. After an incubation of 5 minutes at RT, the absorbance at 595 nm was read with a plate reader.

On the other hand, proteins from neurons and tissues were quantified with Pierce™ BCA Protein Assay Kit (23225 ThermoFisher). A 1/50 dilution of BCA reagent was used and 200 µL were added per well. After an incubation of 30 minutes at 37°C, the absorbance at 562 nm was read with a plate reader.

The BSA stock for the calibration curve (0, 2, 5, 10, 15, 20, 25, 30 µL) was prepared in water at 0.1 mg/mL. This calibration curve was then used to interpole the concentrations of the samples.

3.1.4. Western blot

Western blot allows the detection of a specific protein from the total extract of proteins in a sample.

The first step of the technique is the preparation of the sample. After protein quantification, samples were prepared with a final concentration of 0.5 µg/µL by adding water and 5X loading buffer (125 mM Tris pH 6.8, 25% glycerol, 10% SDS, 10% β-mercaptoethanol, 2.5% H_2O and bromophenol blue). In addition, they were boiled at 95°C for 5 minutes to denaturalize proteins.

The second step is the electrophoresis allowing the protein separation according to their molecular weight among a polyacrylamide gel (Midi-PROTEAN BioRad). Electrophoresis was run with a voltage of 200V in electrophoresis buffer (25 mM Tris-HCl pH 8.3, 192 mM glycine and 0.05% SDS).

The third step is the transference to a PVDF membrane (IPVH00010 Merck). To do so, a “sandwich” consisting of a sponge, Whatman paper (11330744 Fisher Scientific), SDS-PAGE gel, PVDF membrane, Whatman paper and a sponge was created. This “sandwich” was put in a tray

containing transfer buffer (25 mM Tris pH 8.3, 192 mM glycine and 10% methanol) and a current of 400mA was applied for 90 minutes at 4ºC.

The fourth step is the blocking of the membrane to avoid unspecific binding of antibodies. The blocking was done with 5% fat-free powdered-milk in TBS-T (0.1 % Tween20 (P9416 Sigma-Aldrich) in 1X TBS (20 mM Tris, 137 mM NaCl and 3.9 mM HCl). The membrane was incubated with blocking solution for 30 minutes at RT on a shaker.

The fifth step is the primary antibody incubation. Once the membrane was blocked and all the empty spaces were filled with milk's proteins, the membrane was incubated with the correspondent primary antibody overnight at 4ºC in plastic-sealed bags with permanent agitation. Each antibody was diluted following the instructions provided in the data sheet (table 5).

Table 5. Primary antibodies used in this thesis with their dilution factor and reference. All of them were prepared in TBS-T with 0.2% BSA solution (10735078001 Roche).

Antibody	Dilution	Host	Reference
α-ACC	1:1000	Rabbit	3676 Cell Signalling
α-p(Ser79)-ACC	1:2000	Rabbit	3661 Cell Signalling
α-β-actin	1:5000	Mouse	MA1-91399 Fisher
α-BDNF	1:1000	Rabbit	SC-546 Santa Cruz
α-calnexin	1:1000	Rabbit	ab22595 abcam
α-CPT1C	1:6000	Rabbit	Produced by Dolors Serra's laboratory
α-CREB	1:1000	Rabbit	sc-58 Santa Cruz
α-p(Ser129)-CREB	1:1000	Rabbit	sc-101662 Santa Cruz
α-FAS	1:1000	Mouse	sc-48357 Santa Cruz
α-GFP	1:1000	Rabbit	2956S Cell Signalling
α-GluA1	1:1000	Rabbit	PC246 Millipore
α-p(Ser831)-GluA1	1:1000	Rabbit	ab76321 abcam
α-p(Ser845)-GluA1	1:1000	Rabbit	ab109464 abcam
α-SAC1	1:1000	Rabbit	13033-1-AP ProteinTech

The next step is the secondary antibody incubation (see table 6) that allows the visualization of the protein's band through an indirect enzymatic reaction. The secondary antibody has conjugated a horseradish

peroxidase which reacts with luminata (WBLUF0500 Merck) and emits light. The incubation of secondary antibody was done for 1 hour at RT with agitation.

Tabla 6. Secondary antibodies used in this thesis with their dilution factor and reference.

Antibody	Dilution	Host	Reference
α-mouse-HRP	1:20 000	Goat	115-035-003 Jackson
α-rabbit-HRP	1:10 000	Goat	111-035-144 Jackson

After the incubation with the primary and secondary antibodies, membranes were washed three times with TBS-T solution for 5 minutes in agitation at RT.

Finally, emitted light was detected using Syngene G:Box system and quantified by densitometry with *ImageJ Software*. The housekeeping gene actin was used as a control to normalize protein expression levels.

3.2. Plasmid constructs

Cloning was conducted making copies of the desired DNA by PCR amplification and inserting it into the plasmid of interest by recombination. The figure 21 shows a diagram with every step of this process.

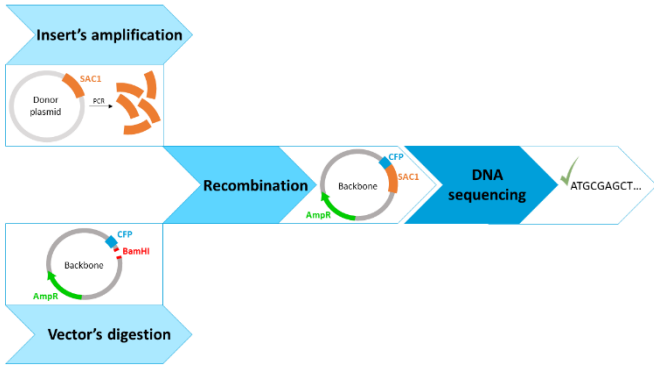

Figure 21. Schematic representation of cloning's steps.

Deletions in SAC1 protein were conducted in this thesis to study the interaction with CPT1C. The plasmid used as a backbone for the insertion

of SAC1's deletions was pcDNA3.1(+)-MycHis_A (see figure 22). Moreover, a fluorescent protein (mTurquoise2) was inserted in this plasmid to facilitate the visualization of transfected cells. The restriction enzyme used for that was KpnI (R3142 New England BioLabs) and the primers to amplify the insert mTurquoise2 are detailed in table 7.

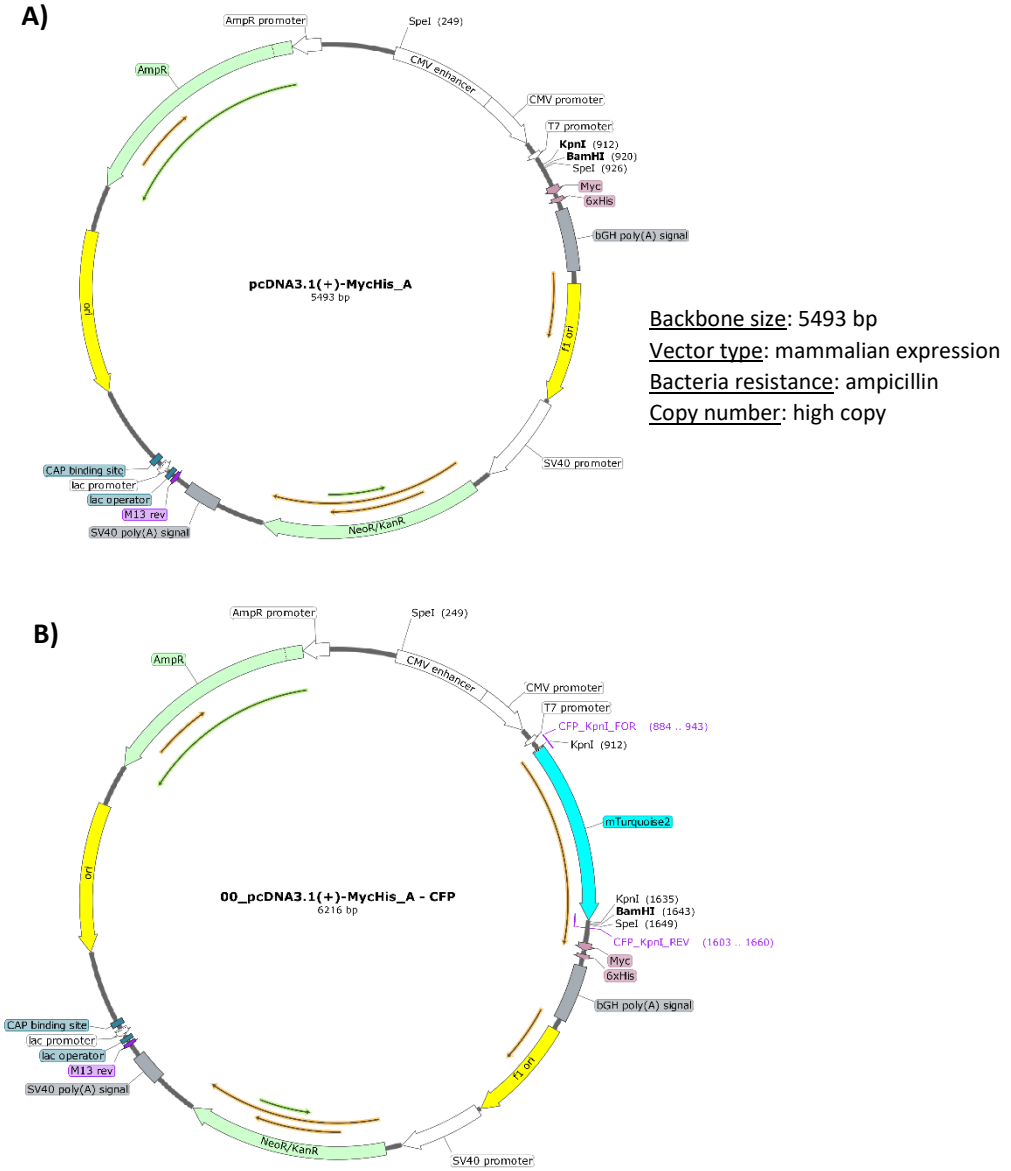

Figure 22. Design for backbone plasmid. A) Map of pcDNA3.1(+)-MycHis_A plasmid created with *SnapGene.* B) Map of pcDNA3.1(+)-MycHis_A plasmid with the mTurquoise2 protein inserted created with *SnapGene.*

Table 7. Amplifying primers for mTurquoise2 insert. The purple part corresponds to the restriction site of KpnI enzyme and the green one, the start codon. They were designed taking into account a 40-60% of G/C.

Primer		Sequence (5'→3')
CFP-KpnI	Forward	GACCCAAGCTGGCTAGTTAAGCTT**GGTACC** **ATG**GTGAGCAAGGGCGAGGAGCTGTTCACC
	Reverse	CACTGGACTAGTGGATCCGAGCTC**GGTACC** CTTGTACAGCTCGTCCATGCCGAGAGTG

Seven constructs (C1-C7) codifying for mouse SAC1 protein with different deletions were generated: C1 (1-587aa; the full-length protein), C2 (89-587aa), C3 (189-587aa), C4 (275-587aa), C5 (378-587), C6 (436-587aa) and C7 (520-587aa). They are shown in figure 23.

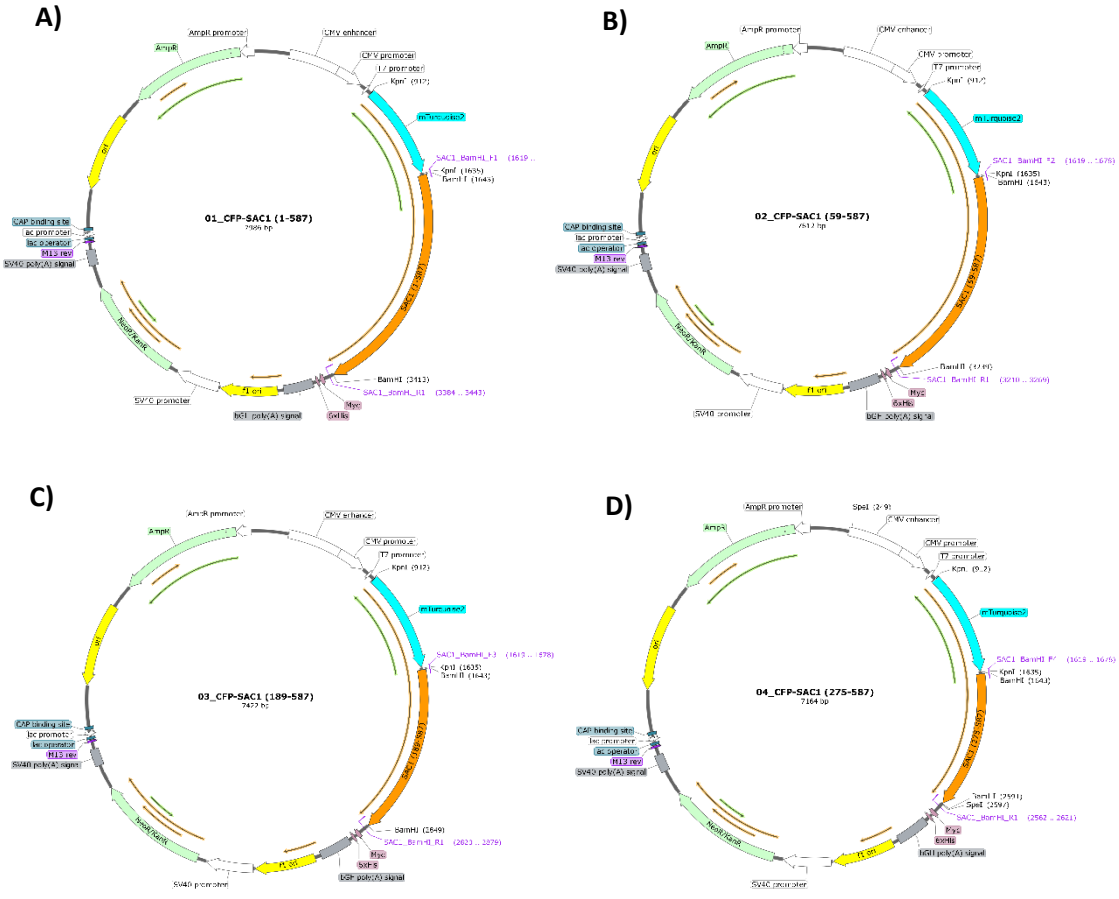

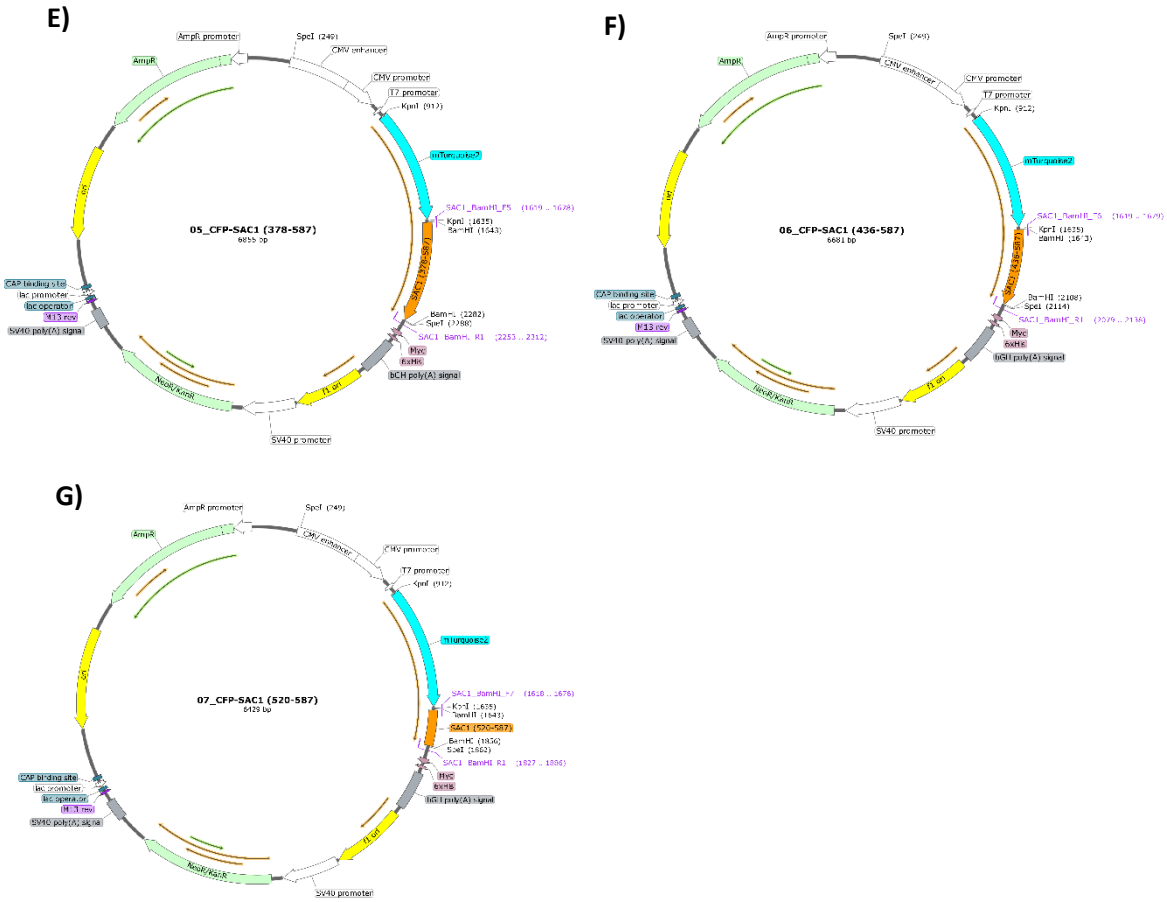

Figure 23. Maps of pcDNA3.1(+)-MycHis_A-mTurq2 plasmid with SAC1 inserts. A) C1 (1-587aa) which corresponds to the whole SAC1 protein. B) C2 (89-587aa). C) C3 (189-587aa). D) C4 (275-587aa). E) C5 (378-587). F) C6 (436-587aa). G) C7 (520-587aa) which corresponds to just the two transmembrane domains and the C-terminus.

3.2.1. DNA amplification

The SAC1 DNA fragment was amplified with the polymerase chain reaction (PCR) to obtain many copies of it. Depending on the length of the SAC1 DNA fragment to be amplified, different primers were used (table 8). They were re-suspended according to the datasheet to a final concentration of 100 µM.

Table 8. Primers' sequences for cloning SAC1. The purple part corresponds to the restriction site of KpnI enzyme and the blue one, the restriction site of BamHI. The green part represents the start codon and the red one, the stop codon. They were designed taking into account a 40-60% of G/C.

Primer		Sequence (5'→3')	Insert's size
C1	Forward	GAGCTGTACAAGGGTACCGAGCTCGGATCC ATGGCGGCCGCAGCCTACGAGCATCTGAAG	1764 bp
	Reverse	CAGAATTCCACCACACTGGACTAGTGGATCC TCAGTCTATCTTTTCTTTCTGGACCAGTC	
C2	Forward	GAGCTGTACAAGGGTACCGAGCTCGGATCC GGGATACTGGGCACAATCCATCTGGTGGCA	1590 bp
	Reverse	CAGAATTCCACCACACTGGACTAGTGGATCC TCAGTCTATCTTTTCTTTCTGGACCAGTC	
C3	Forward	GAGCTGTACAAGGGTACCGAGCTCGGATCC GTGTTGCATGGCTTTATTACTATGCACTCA	1200 bp
	Reverse	CAGAATTCCACCACACTGGACTAGTGGATCC TCAGTCTATCTTTTCTTTCTGGACCAGTC	
C4	Forward	GAGCTGTACAAGGGTACCGAGCTCGGATCCC ATCCACAGATCAGCAAAGTAGCAAATCAC	942 bp
	Reverse	CAGAATTCCACCACACTGGACTAGTGGATCC TCAGTCTATCTTTTCTTTCTGGACCAGTC	
C5	Forward	GAGCTGTACAAGGGTACCGAGCTCGGATCC GTGACAAACCAGGACGGAGTTTTCCGCAGC	633 bp
	Reverse	CAGAATTCCACCACACTGGACTAGTGGATCC TCAGTCTATCTTTTCTTTCTGGACCAGTC	
C6	Forward	GAGCTGTACAAGGGTACCGAGCTCGGATCC AATGCCTGGGCCGATAATGCTAATGCTTGTG	459 bp
	Reverse	CAGAATTCCACCACACTGGACTAGTGGATCC TCAGTCTATCTTTTCTTTCTGGACCAGTC	
C7	Forward	CGAGCTGTACAAGGGTACCGAGCTCGGATCC AAATTCCTGGCGTTGCCTATCATCATGG	207 bp
	Reverse	CAGAATTCCACCACACTGGACTAGTGGATCC TCAGTCTATCTTTTCTTTCTGGACCAGTC	

The final volume of the reaction was 50 µL. Table 9 has the volumes for each reagent and table 10, the steps for the PCR. After the first 5 minutes of denaturalization, 6 µL of PFU enzyme (EMBL Heidelberg core facility)

diluted 1/10 were added. The PFU enzyme is a DNA polymerase that replicates DNA catalyzing the polymerization of nucleotides in the 5'→3' direction in the presence of magnesium.

Table 9. Volumes of reagents used for PCR.

Reagent	Volume (µL)
10X PFU buffer*	5 µL
2.5 mM dNTPs	6 µL
50 mM $MgCl_2$	1.5 µL
50 ng of SAC1 DNA	2 µL
DEPC H_2O*	28.5 µL
10 µM primer mix (forward + reverse)	1 µL

*10X PFU buffer: 200 mM Tris-HCl (pH 8.8), 100 mM $(NH_4)_2SO_4$, 100 mM KCl, 1% (v/v) Triton-X100, 20 mM $MgSO_4$

*DEPC H_2O: 10 µL of diethyl pyrocarbonate (DEPC; D5758 Sigma-Aldrich) in 100 mL of MQ H_2O (18 mΩ)

Table 10. Description of PCR steps.

	Process	Temperature	Time
	Initial denaturalization	95°C	5'
x25 cycles	**Denaturalization**	95°C	30''
	Annealing	65°C	45''
	Elongation*	72°C	2'
	Final elongation	72°C	10'
	Hold	12°C	∞

*For the elongation step it is recommended 1 minute per kb

On the other hand, the backbone vector was digested with BamHI (R3136 New England BioLabs) to introduce the SAC1 insert on it. The digestion mix contained: 1 µL of DNA (pcDNA3.1(+)-MycHis_A – mTurq2), 1 µL of BamHI as the restriction enzyme, 5 µL of 10X CutSmart Buffer and 44 µL of DEPC H_2O. The digestion was carried out in a thermal cycler for 15 minutes.

3.2.2. DNA purification and extraction

To isolate the amplified gene and the digested vector, an electrophoresis in agarose gel was done. Samples were prepared with 10X loading buffer (0.42% bromophenol blue, 0.42% xylene cyanol FF, 50% glycerol in bidistilled water) and the electrophoresis was conducted at 120V using 1X TAE electrophoresis buffer (40 mM Tris-acetate pH 8.3, 1 mM EDTA, 0.5 µg/mL ethidium bromide (GX12420 Genaxis).

Then, the desired DNA fragment was cut off and purified with the Nucleo Spin Gel and PCR clean up kit (740609.250 Machery Nagel) following the manufacturer's instructions. Finally, to check if the purification was done properly, the samples (80 ng of DNA) were charged in an agarose gel.

3.2.3. Recombination

The final step was the recombination of the insert DNA (in this case the different deletions of SAC1 protein) with the vector backbone. To do so, 25 ng of vector DNA and 50 ng of insert DNA (the amount of insert is recommended to be twice the amount of vector) were added in a final volume of 10 µL. The reaction took place in the thermal cycler at 50ºC for 70 minutes in the presence of the 5X In-Fusion HD recombinase (638948 Takara).

3.2.4. DNA spectrophotometric quantification

DNA was measured using a micro-plate reader. In addition, it was taken into account that the absorbance ratio between 260/280 was around 1.8 to be sure that all the constructs were well-purified.

Furthermore, an analytical restriction digestion was performed to the obtained plasmid and 200 ng of DNA were charged in an agarose gel to visualize the correct fragment's size of the digested DNA.

3.2.5. DNA sequencing

As the polymerase can introduce some mutations in the insert, the new generated constructs were sequenced. 2 µL of 5 µM primer (table 11) and 1 µg of DNA added to a maximum final volume of 10 µL were sent to Macrogen for sequencing.

Table 11. Primers used for sequencing the new constructs.

Constructs	Primers' sequence (5'→3')
C1/C2/C3	GGATTTCCAAGTCTCCACCCCATTG
C1/C2/C3/C4/C5/C6/C7	CGATCACATGGTCCTGCTGGAGTTC
C1/C2/C3	GTTTGTCCAGACTCGAGGATCAATAC
C1/C2/C3/C4/C5	GGAAATTCCTGGCGTTGCCTATCATC

3.3. Protein-protein interaction by pull-down

To study the interaction between two proteins, a type of co-immunoprecipitation based on the union of the protein of interest (tagged with streptavidin) to the Strep-Tactin® Superflow® high capacity resin (2-1208-002, IBA Lifesciences) was used to purify its interacting proteins. If this protein of interest is able to interact with another one, the two interacting proteins will be purified together with the streptavidin resin (figure 24).

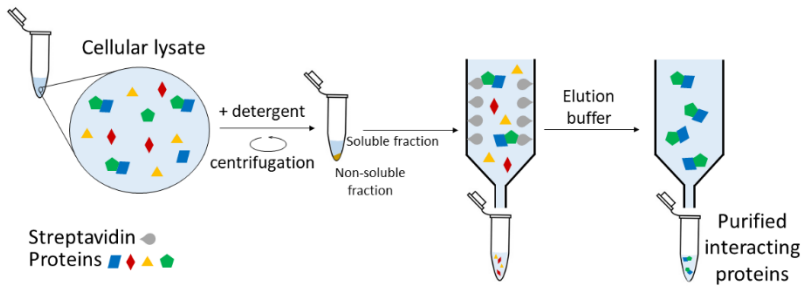

Figure 24. Schematic representation of pull-down done for this thesis.

First of all, HEK293T were seeded in a 100 mm Ø dish at a final concentration of 150 000 cells/mL. Two dishes per condition were seeded. Cells were transfected with PEI two days after the seeding with mCPT1C-eGFP-streptavidin or calnexin-eGFP-streptavidin plasmids (both engineered by Xavier Fontanals Palacios) to study the interaction. Calnexin-eGFP-streptavidin was used as a control. Two days after, the pull-down was conducted.

HEK293T were washed with 5 mL of 1X PBS at 4°C and centrifuged at 600 g for 5 minutes at 4°C (each step of the protocol was done at this temperature). This process was repeated two more times. Then, the pellet

was re-suspended in 0.5 mL of lysis buffer/dish (100 mM pH 7.5, 150 mM NaCl, 10% glycerol and inhibitors of proteases) and samples were sonicated for 30 seconds/seeded dish.

In order to degrade any nucleic acid, 250 U of benzonase (E1014 Sigma) per gram of pellet were added and the sample was incubated for 10 minutes with agitation. Later, it was centrifuged at 10 000 g for 10 minutes to eliminate non-lysed cells. GDN detergent (GDN101 Anatrace) was added with a final concentration of 1% and incubated for 2 hours with agitation to solubilize proteins.

Afterwards, the sample was centrifuged at 200 000 g for 1 hour and the supernatant containing the solubilized proteins was added to a 2 mL columns (89896 Thermo Scientific) previously equilibrated with the resin.

When the sample passed through the resin, the protein of interest tagged with streptavidin (mCPT1C or calnexin) was retained in the resin. The columns were washed three times with wash buffer (purification buffer with 0.2% of GDN).

Finally, proteins were eluted with 300 µL of elution buffer (purification buffer, GDN diluted 1:1000 and 2.15 mg/mL of desthiobiotin). The desthiobiotin (2-1000-001 IBA Lifesciences) must be sonicated for 10 seconds before its addition. Results were checked by Western blot.

4. Microbiology

4.1. Bacterial transformation

To achieve the bacterial transformation with exogenous DNA, the *Escherichia coli* (E. coli) DH5α competent cells were used allowing an efficient taking up of foreign DNA from their environment. They were grown in sterile LB liquid or agar plates with the corresponding antibiotic.

Firstly, 15 µL of the recombined plasmid were added to 150 µL of DH5α (no more than this 1:10 proportion can be added to the bacteria because otherwise it can be toxic for them). The bacteria with the DNA were left on ice for 30 minutes.

Afterwards, a heat-shock was done for 75 seconds at 42ºC allowing that the cell membrane became permeable to facilitate the insertion of the plasmid. Then, they were incubated at 4ºC for 5 more minutes.

An enriched medium like SOC (500 µL) was added to the bacteria and they were incubated 1h at 37ºC with strong agitation. In order to concentrate bacteria, they were centrifuged 2 minutes at 12000 rpm and the pellet was re-suspended in 100 µL of medium.

This volume containing the bacteria with the plasmid of interest was plated in a LB agar plate with the corresponding antibiotic. Then, the plate was incubated overnight at 37ºC.

The next day, a colony was picked up and it was cultivated in 5 mL of liquid LB with the corresponding antibiotic at 37ºC overnight with agitation.

4.2. Bacterial glycerol stocks

For long-term storage of plasmids, it is necessary to glycerinate them. In a cryotube, 300 µL of 80% glycerol were added to 1200 µL of bacteria containing the plasmid of interest. This cryotube was stored at -80ºC.

4.3. Plasmidic DNA extraction

The extraction of plasmidic DNA was conducted using the Miniprep DNA purification kit (A1330 Promega) following the instructions provided by the manufacturer. If bigger amounts of DNA were needed, the Midiprep (MB14101 NZYtech) or Maxiprep (740414.50 Cultek) DNA purification kit were used following the instructions provided by the manufacturer too.

5. Microscopy

5.1. Immunocytochemistry

Immunocytochemistry can detect proteins in fixed cells using a specific primary antibody and an appropriate secondary antibody conjugated with

a fluorophore. The desired protein can be then visualized under a fluorescent microscope.

First of all, cells were washed three times with cold 1X PBS and fixed with 4% paraformaldehyde (252549 Sigma-Aldrich) for 15 minutes at 4ºC. After that, they were washed three times again.

If the protein was localized inside the cell, a permeabilization step was performed to provide access to that protein. To do so, cells were incubated with 0.1% triton solution (X100 Sigma-Aldrich) for 30 minutes at RT. However, when the target protein was localized in the plasma membrane, this step was skipped.

In order to prevent non-specific binding of antibodies, cells were incubated with a blocking solution composed of 2% goat serum (g-9023 Sigma-Aldrich) for 20 minutes at 37ºC.

Then, 24 µL of primary antibody per coverslip were added in a wet chamber. The incubation lasted 1 hour and it was carried out at 37ºC. The dilution used for each antibody is detailed in table 12. After this incubation, coverslips were washed three times with 1X PBS.

Table 12. Primary antibodies used for immunocytochemistry. They were diluted in blocking solution.

Antibody	Dilution	Host	Reference
α-GluA1	1:300	Mouse	ab174785 abcam
α-PSD95	1:30	Rabbit	ab18258 abcam
α-GFP	1:1000	Chicken	ab13970 abcam
α-Calnexin	1:200	Rabbit	ab22595 abcam

Later, 300 µL of the secondary antibody (table 13) were added to the 24-well plate containing the coverslips with cells. This incubation lasted also 1 hour at 37ºC and then cells were washed three times with 1X PBS.

Table 13. Secondary antibodies used for immunocytochemistry. They were diluted in blocking solution.

Antibody	Dilution	Host	Reference
α-mouse 488	1:150	Goat	A11001 Invitrogen

α-rabbit 568	1:300	Goat	A11011 Invitrogen
α-chicken 488	1:1000	Goat	A11039 Invitrogen

To label the cellular nuclei, a short incubation of 5 minutes with 1:1000 Hoescht solution (1 mg/mL; 14530 Sigma-Aldrich) was conducted. Additionally, coverslips were washed with 1X PBS three times again.

Finally, coverslips were mounted with Fluoromount-G® (0100-01 Southern Biotech) and the immunocytochemistry was stored at 4°C until imaged.

5.2. Image acquisition and analysis

All images were acquired using a LEICA DMi8 confocal microscope. They were taken under a 63x oil- objective using type F immersion liquid (11513859 Leica) with a size of 1024x1024 pixels resolution. The lasers used were 405, 488 and 594 nm of wavelength. Approximately 15 stacks with 0.5 µm-distance were taken per each image.

Imaris Software (9.3 version Bitplane) was used for the analysis. In cultured neurons, the quantification of surface GluA1 was performed on primary dendrites (the first ones branched from the main axon). A region of interest (ROI) measuring 15 µm x 5 µm was chosen and the intensity sum of GluA1's dots was measure inside this area. In the case of SH-SY5Y cell line, the ROI was 7.5 µm x 5 µm as the neurites are much shorter.

For synaptic GluA1 quantification in cultured neurons, the intensity sum of GluA1 was quantified inside the ROI generated by PSD95 channel (used as a synaptic marker).

5.3. Protein-protein interaction by Föster resonance energy transfer

Föster resonance energy transfer or fluorescence resonance energy transfer (FRET) is a technique used to study the interaction between two proteins in both living or fixed cells. It is based on the energy transfer between two fluorophores tagged to the target proteins. This method can only be used when: 1) the emission spectrum of the donor overlaps with

the excitation spectrum of the acceptor and 2) the distance between the donor and the acceptor is less than 10 nm (figure 25). There are two variations of FRET studied in this thesis: the sensitized emission and the acceptor bleaching.

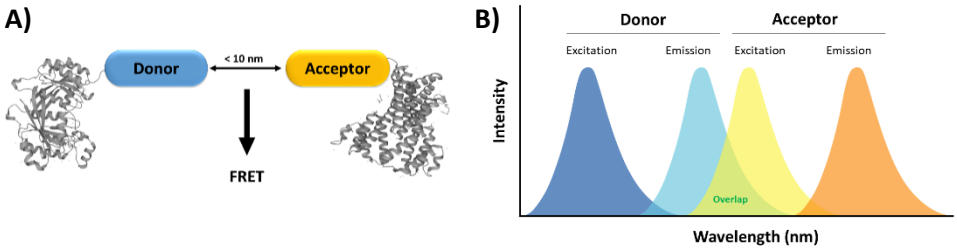

Figure 25. Conditions necessary for a FRET. A) Minimum distance between fluorophores. B) Wavelengths' representations where donor's emission spectrum and acceptor's excitation spectrum overlaps.

5.3.1. FRET sensitized emission

FRET sensitized emission (FRETse) is measured in living cells by three different combinations of excitation (ex) and emission (em) filters: donor channel (D_{ex} and D_{em}), FRET channel (D_{ex} and A_{em}) and acceptor channel (A_{ex} and A_{em}). It is highly recommended for membrane protein-protein interaction studies (Qian et al., 2014).

For that, HEK293T were transfected with calcium phosphate (see section 2.2.1.). The donors were the plasmids pcDNA3.1(+)-MycHis_A-mTurq2-SAC1 or CPT1C_pmTurquoise2-N1 and the acceptors, CPT1C-EYFP and SAC1-EYFP.

The donors containing SAC1 as the protein of interest were engineered specifically for this thesis and the ones containing CPT1C were engineered by Ana Cristina Reguera Moreno (as part of her thesis project) and Dr. Marta Palomo Guerrero (Palomo-Guerrero et al., 2019). Regarding the acceptors, the CPT1C-EYFP plasmid was kindly provided by Dr. Dolors Serra and SAC1-EYFP was engineered by Dr. Maria Casas Prat (Casas et al., 2020).

The amount of DNA used for donors was adjusted depending on the molecular weight of the plasmids, but the control group was always 0.4

µg. In the case of acceptors, increasing amounts of DNA were used (from 0.25 µg to 6 µg).

Before starting the experiment, cells were washed twice with Hank's balanced salt solution (HBSS; 14025-050 Fisher) to eliminate any color from the medium that could interfere with the fluorometric assay. Then, 1 mL of HBSS containing glucose (1 mg/mL) was added per well to remove cells from the plate. Once detached, they were centrifuged at 3200 rpm for 5 minutes and pellets were re-suspended in 250 µL of HBSS-glucose.

In order to use the same concentration for each condition, a Bradford assay was performed loading a 96-well plate with 10 µL of sample. The concentration was adjusted to 0.2 mg/mL adding more HBBS-glucose until reaching the appropriate volume for that.

Afterwards, 100 µL of cellular suspension were added to a black 96-well plate and 3 reads with different wavelengths were used to do the FRETse:

- Read 1 (CFP): excitation 420/50 nm – emission 485/20 nm
- Read 2 (FRETse): excitation 420/50 nm – emission 530/25 nm
- Read 3 (YFP): excitation 495/10 nm – emission 530/25 nm

Finally, a saturation curve for each studied interaction was represented. The x axis corresponds to the fluorescence ratio emitted by basal YFP and CFP in mols, and the y axis shows the basal ratio of read2/read1. The basal data refer to the difference between the read (donor-acceptor transfected cells) and the control read (only donor transfected cells).

5.3.2. FRET acceptor photobleaching

FRET acceptor photobleaching (FRETap) is based on the increase of donor fluorescence intensity when eliminating the acceptor's in a specific ROI (5 µm x 5 µm).

After 24 hours of transfection (see section 2.2.1.), HEK293T were fixed and mounted using Fluoromount-G®. FRETap was conducted in the Scientific and technological center of the University of Barcelona (CCiTUB). The data were analyzed with *ImageJ Software* using the following formula:

$$\text{FRET efficiency (\%)} = \frac{\text{Post bleaching donor intensity} - \text{Pre bleaching donor intensity}}{\text{Post bleaching donor intensity}} \cdot 100$$

6. Electrophysiology

Electrophysiology studies the electrical activity of living neurons decoding the molecular and cellular processes that cause their signaling. Patch clamp and extracellular recordings were conducted for this thesis.

6.1. Recording in primary cultures: miniature excitatory synaptic current (mEPSC)

Miniature excitatory postsynaptic currents (mEPSCs) are the current events that can be recorded from a postsynaptic neuron as a consequence of the spontaneous release of one single vesicle from presynaptic neurons contacting the recorded neuron. This type of electrophysiological recordings was done using cultured cortical neurons (see section 2.1.2.) in collaboration with David Soto and Aida Castellanos from University of Barcelona as previously described (Fado et al., 2015).

Coverslips were mounted in a recording chamber placed on the stage of an inverted microscope (Olympus IX50). Whole-cell patch-clamp currents were recorded using an Axopatch 200B amplifier-Digidata1440A Series interface board with pClamp10 software (Molecular Devices Corporation). Recordings were conducted at RT (25-26^{o}C). The extracellular solution used for bathing the cells contained the following (in mM): 140 NaCl, 3.5 KCl, 10 HEPES, 20 glucose, 1.8 $CaCl_2$, and 0.8 $MgCl_2$ (pH 7.4 adjusted with NaOH).

To isolate AMPAR-mediated mEPSCs, specific blockers were added to the extracellular solution: 1 µM tetrodotoxin (TTX; ab120054 Abcam) to inhibit evoked synaptic transmission, 50 µM D-(-)-2-amino-5-phosphonopentanoic acid (D-AP5; ab120003 Abcam) to block NMDA receptors and 100 µM picrotoxin (PTX; P1675 Sigma-Aldrich) to block $GABA_A$ receptors.

Recordings were performed with electrodes made from borosilicate glass (1.2 mm o.d., 0.69 mm i.d.; GC120F-10 Harvard Apparatus) with a final resistance of 4-5 MΩ, pulled using a puller P-97 (Sutter Instrument Co.). These electrodes were filled with an internal solution containing (in mM): 116 K-Gluconate, 6 KCl, 8 NaCl, 10 HEPES, 0.2 ethylene glycol tetraacetic acid (EGTA), 2 MgATP, 0.3 Na2GTP (pH 7.2 with KOH).

Series resistance (Rs) from the recordings was 17.71 ± 0.92 MΩ and was controlled at the beginning and at the end of the experiment. Cells exhibiting a change in Rs greater than 20% were excluded from the analysis. Moreover, mEPSCs were filtered at 2 KHz and digitized at 5 KHz. Events were detected using amplitude threshold of 5 pA.

From the recorded miniature events, several parameters were analyzed: amplitude, frequency, rise time and deactivation kinetics (figure 26). The amplitude of the events was calculated as the difference between the baseline current 5 ms before the event and the peak current of such event (measured in picoamperes; pA). For the amplitude, only events with monotonic fast rise and uncontaminated decay were included. The frequency was calculated by dividing the number of detected events by the recorded time. The rise time is the time (in ms) that takes one event to reach the minimum current once the current deflection is observed (note that the events are detected as a downward deflection). Finally, the deactivation kinetics (showed as weighted kinetics) is the measure of the decaying phase of the current and the τ represents the time that the current takes to diminish at one third of its maximum value at the peak (figure 26).

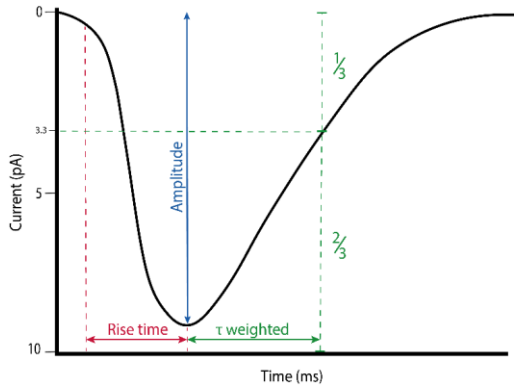

Figure 26. Schematic representation of the parameters measured in mEPSCs.

These parameters give us important information. The frequency refers to whether there are changes at the presynaptic level, while the amplitude, rise time and the time weighted are related to postsynaptic changes. More specifically, amplitude is typically related to changes in the number of receptors, while rise time and time weighted are kinetic parameters

associated with the subunit composition of postsynaptic receptors. The analysis of mEPSCs was performed with IGOR Pro 6.06 (Wavemetrics) using NeuroMatic 2.03 (Rothman & Silver, 2018).

6.2. Recording in slices

Whole-cell recordings in slices were performed in Pablo E. Castillo's laboratory in the Albert Einstein College of Medicine (New York).

Once the hippocampus of 1 month-old male mice was extracted on ice, it was put over a 4% agarose gel and slices were cut using a vibratome (model VT 1200S Leica Microsystems) with a thickness of 300 µm. Then, the slices were first incubated with a sucrose solution and extracellular artificial cerebrospinal fluid (aCSF) solution (1:1 proportion) for 20 minutes at 37ºC oxygenated with a 95% O_2/5% CO_2 mixture (carbogen). Afterwards, they were incubated with both solutions in the same proportion again for 10 minutes at RT with carbogen. The last incubation was only done with aCSF solution for 20 minutes at RT with carbogen too. After these three incubations, slices were ready to start the recordings.

> Sucrose solution: 2.5 mM KCl, 1 mM $CaCl_2$, 4 mM $MgSO_4$, 4 mM $MgCl_2$, 1.6 mM NaH_2PO_4, 26 mM $NaHCO_3$, 20 mM glucose and 215 mM sucrose
> aCSF solution: 124 mM NaCl, 2.5 mM KCl, 2.5 mM $CaCl_2$, 1.3 mM $MgSO_4$, 1 mM NaH_2PO_4, 26 mM $NaHCO_3$ and 10 mM glucose

Field excitatory postsynaptic potentials (fEPSPs) were recorded from CA1 pyramidal neurons at stratum radiatum while stimulating Schaffer collateral (SC) fibers to evoke synaptic responses in dorsal hippocampal slices. The recordings were done with glass pipettes-containing electrodes: the stimulating one was filled with aCSF and the recording one, with NaCl, as shown in figure 27. The distance between the electrodes was 100 µm.

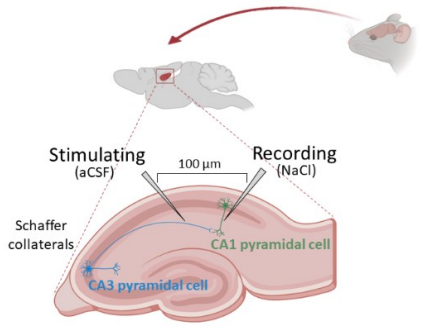

Figure 27. Schematic representation of the circuit recorded for fEPSPs.

During the recordings, the slices were placed in an immersion chamber constantly perfused (2 mL/min) with aCSF, carbogen and 50 µM PTX. The total volume recirculating through the chamber was 200 mL. In addition, the temperature was continuously monitored and maintained at 28 ± 1°C.

Before any recording, slices were incubated at RT for two hours with different treatments: 200 µM PA, 200 µM vehicle (BSA), 2 mM BHB and 200µM PA + 2mM BHB. Unlike the treatments' preparation for cells, the stock solutions of the fatty acid and the ketone body were prepared more concentrated (50 mM and 800 mM respectively) to use the minimum volume when incubating the slices in the immersion chamber in order to avoid alterations in the recordings.

6.2.1. Field excitatory postsynaptic potentials (fEPSP)

The LTP was induced using a high-frequency stimulation (HFS) protocol composed of 2 trains of bursts (100 pulses at 100 Hz with a 10 seconds interval). Data acquisition was carried out with an amplifier (model MultiClamp 700A, Molecular Devices). Data analysis (slope and amplitude) was performed using *IgorPro* (WaveMetrics).

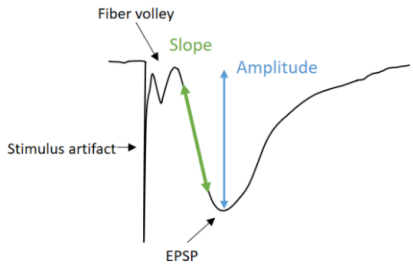

Figure 28. Evoked synaptic response for a fEPSP indicating the stimulus artifact, fiber volley, slope and amplitude.

6.2.2. Input-Output curves

Evoked synaptic responses were measured increasing stimulus intensities to generate input/output (I/O) curves from 10 to 90 volts (V). Data acquisition and analysis were done as the previous section.

6.2.3. Paired-pulse ratio

Paired-pulse ratio (PPR) is the ratio between the slope (or amplitude) of the second response to that of the first after performing two stimuli. These stimuli were separated by 100 milliseconds (ms). Data acquisition and analysis were done as explained before.

6.2.4. AMPA/NMDA ratio

Once the voltage clamp seal was achieved, the membrane potential was held at -70 mV. Subsequently, using an extracellular electrode, SC fibers were stimulated to evoke AMPA-mediated EPSCs in the recorded neuron. After 5-10 minutes, the neuron was depolarized to +30 mV to record NMDA-mediated EPSCs for another 5-10 minutes.

The AMPA/NMDA ratio was obtained by dividing the amplitude of AMPA-mediated EPSCs by the amplitude of NMDA-mediated EPSCs. Previously, electronic subtraction was performed to remove any residual AMPA current in the recordings conducted at +30 mV. This step was necessary since an AMPA receptor antagonist was not employed to record NMDA-mediated EPSCs.

7. Data processing and statistical analyses

Data analysis was conducted using *Graphpad Prism 9.0 Software*. Results were presented as mean ± SEM and the statistical test depended on the number of groups that were compared. A Student t-test was used for comparisons between two groups when data followed a normal distribution or, a non-parametric Mann Whitney U test, in the case one group did not follow a normal distribution. One-way or two-way ANOVA test (followed by Bonferroni test) was used for comparisons between more than two groups. Statistical significance was considered at a p value less than 0.05 (*$p<0.05$, **$p<0.01$, ***$p<0.001$ and ****$p<0.0001$). The statistical test for each experiment is specified.

RESULTS

Chapter I

Effects of nutrients on GluA1 trafficking and synaptic transmission

As it was mentioned in the introduction section, our group has provided evidences showing that the basal transport of AMPAR subunit GluA1 to the plasma membrane is downregulated upon glucose depletion, through the sensing of malonyl-CoA by CPT1C (Casas et al., 2020). For that reason, this chapter is focused on the effects that different nutrients have on neurotransmission. Furthermore, our group tries to elucidate the molecular mechanisms responsible for these changes through the malonyl-CoA – CPT1C axis.

To address the impact of nutrients on synaptic transmission, three different approaches were used: 1) to measure levels of surface and synaptic GluA1 using *in vivo* and *in vitro* models, 2) to analyze synaptic function through electrophysiological recordings and 3) to explore cognitive processes in mice models.

1. Diets' effect *in vivo*

To study the effect of diets on GluA1 levels *in vivo*, 9-11 weeks-old mice were sacrificed after being fed for seven days with different types of diets (see composition of diets in table 3 in methodology section 1). Firstly, the effects of a low-fat diet (SD; 10% kcal from fat, 70% carbohydrates and 20% proteins) and a high-fat diet (HFD; 60% kcal from fat, 20% carbohydrates and 20% proteins) were compared. Secondly, for a better study of the impact of different fatty acids on GluA1 levels, special diets with distinct proportion of unsaturated and saturated fatty acids were also used: a high-fat diet enriched only with unsaturated fatty acids (MUFAD, 49% kcal from fat) and a high-fat diet enriched only with saturated fatty acids (SFAD, 49% kcal from fat).

1.1. Effect of HFD in WT or CPT1C KO animals

Initially, it was decided to explore whether there were differences in total and surface GluA1 between WT and CPT1C KO mice. As an approximation to measure the levels of GluA1 at the surface, p(S845)-GluA1 was analyzed since the phosphorylation in this residue causes GluA1 to translocate to the plasma membrane (Purkey & Dell'Acqua, 2020). Mice were fed for 1 week with SD and brains were dissected extracting the hippocampus and the cortex.

In hippocampus, total GluA1 levels were reduced in KO mice (figure 29A) but no clear differences were observed when analyzing its phosphorylation ratio. In contrast, the results in cortical samples were the opposite: the levels of total GluA1 did not change between the two groups of mice while the pGluA1/GluA1 ratio was reduced in KO mice (figure 29E). Results suggest that total GluA1 decreased in the hippocampus of CPT1C KO mice while surface GluA1 is decreased in the cortex. Results also suggest that AMPAR synthesis and trafficking are impaired in CPT1C KO mice.

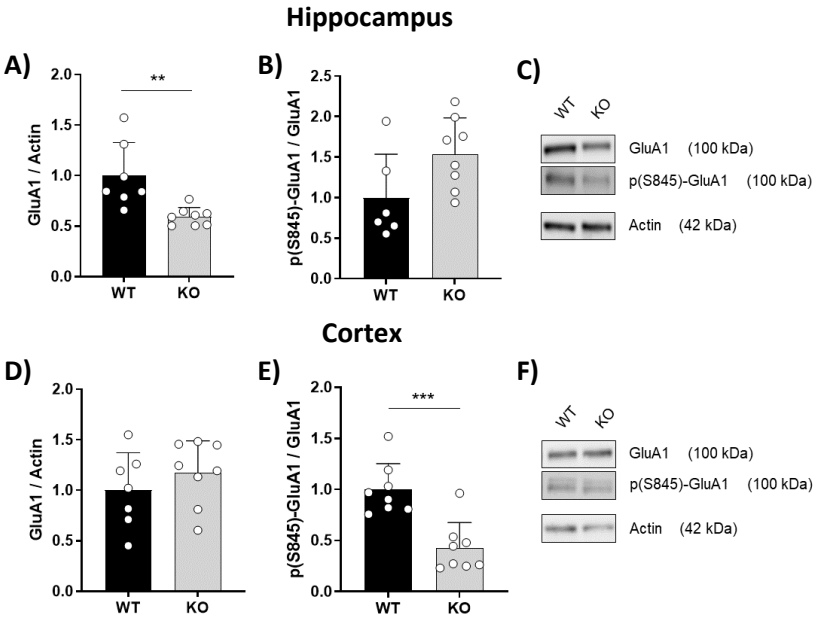

Figure 29. Expression of total GluA1 and p(S845)-GluA1 levels in different parts of the brain. A-B) Hippocampal levels of GluA1 and ratio of p(S845)-GluA1. C) Representative blots of total hippocampal GluA1, p(S845)-GluA1 and actin. D-E) Cortical levels of GluA1 and ratio of p(S845)-GluA1. F) Representative blots of total cortical GluA1, p(S845)-GluA1 and actin. Actin was used as housekeeping to normalize protein levels. Data are represented as mean ± SD, n=6-8/group. The results are from one independent experiment. Hippocampal GluA1: WT (1.000 ± 0.326, n=7) and KO (0.594 ± 0.090, n=8). Hippocampal ratio of p(S845)-GluA1: WT (1.000 ± 0.537, n=6) and KO (1.540 ± 0.442, n=8). Cortical GluA1: WT (1.000 ± 0.371, n=7) and KO (1.170 ± 0.319, n=8). Cortical ratio of p(S845)-GluA1: WT (1.000 ± 0.252, n=8) and KO (0.430 ± 0.246, n=8). Statistical significance was performed by Student t-test. **p<0.01, ***p<0.001.

Then, the effect of short-term HFD (7 days) on the levels of GluA1 phosphorylation in the cortex was further investigated. As it was mentioned in the introduction section, this thesis is focused on S845 and S831 GluA1 phosphorylations. The phosphorylation in residue 845 increases exocytosis, whereas S831 increases single-channel conductance (Purkey & Dell'Acqua, 2020).

Results show that HFD did not change the phosphorylation ratio of GluA1, neither in WT or CPT1C KO mice. This suggests that HFD treatment for only 1 week is not enough to impact the surface transport of GluA1 in the cortex. On the other hand, changes in p(S845)-GluA1 ratio between WT and KO mice were observed in SD, as previously shown in figure 29. However, these changes were no longer evident in animals fed with a HFD.

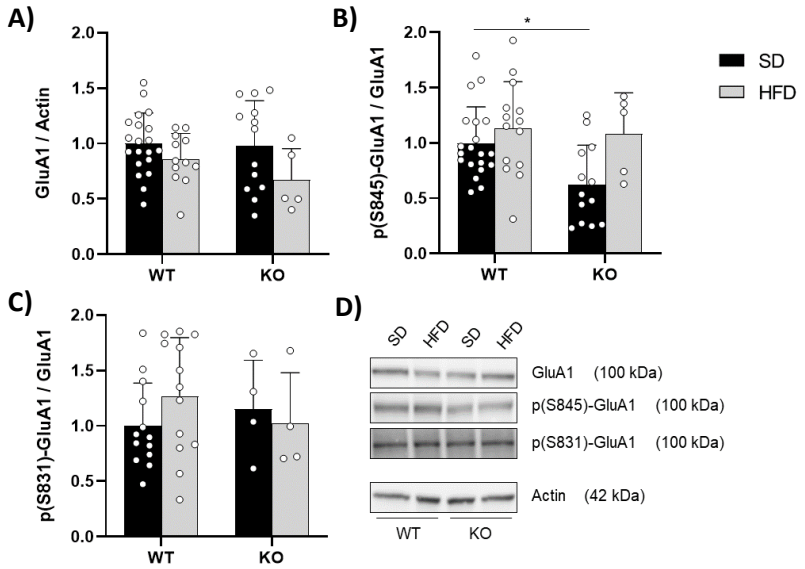

Figure 30. Cortical levels of GluA1 after seven days of HFD in WT and CPT1C KO mice. A) Levels of total GluA1. B) Levels of phosphorylated GluA1 (S845). C) Levels of phosphorylated GluA1 (S831). D) Representative blots of GluA1, p(S845)-GluA1, p(S831)-GluA1 and actin. Actin was used as housekeeping to normalize protein levels. Data are represented as mean ± SD, n=4-20/group. The results are from one (KO + HFD), two (WT + HFD and KO + SD), or three (WT + SD) independent experiments. GluA1: WT SD (1.000 ± 0.276, n=20), WT HFD (0.862 ± 0.229, n=12), KO HFD (0.984 ± 0.403, n=13) and KO HFD (0.671 ± 0.284, n=5). Ratio p(S845)-GluA1: WT SD (1.000 ± 0.326, n=20), WT HFD (1.132 ± 0.422, n=14), KO SD (0.625 ± 0.356, n=13) and KO HFD (1.085 ± 0.370, n=5). Ratio p(S831)-GluA1: WT SD (1.000 ± 0.388, n=13), WT HFD (1.270 ± 0.527, n=13), KO SD (1.154 ± 0.439, n=4) and KO HFD (1.026 ± 0.455, n=4). Statistical analysis was performed by two-way ANOVA followed by Bonferroni's post correction. *p<0.05.

1.2. SFAD and MUFAD do not alter GluA1 phosphorylation

As no differences were observed between SD and HFD (composed by a mix of saturated and unsaturated fats) when analyzing the expression of GluA1 in the cortex, HFD was replaced with a specific diet with only saturated fatty acids (SFAD) or only monounsaturated fatty acids (MUFAD).

As it can be observed in the figure 31, short-term feeding with SFAD and MUFAD did not change the levels of phosphorylated GluA1 (both for serine 845 and serine 831) compared to SD. A similar observation is noted when comparing total GluA1 levels of the three diets.

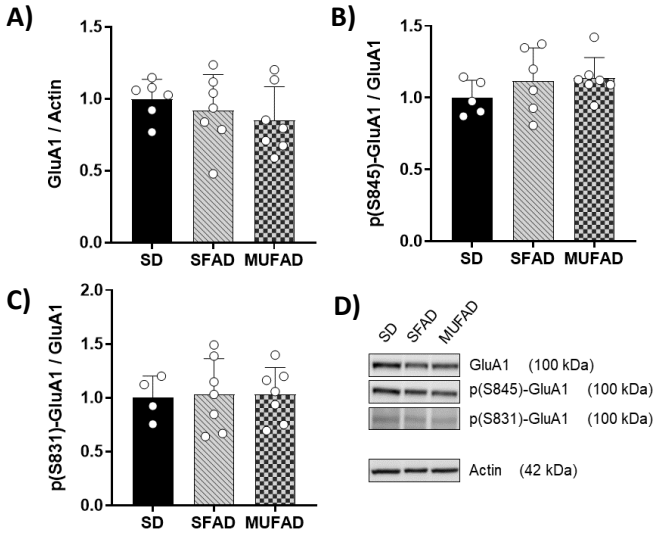

Figure 31. Levels of GluA1 in WT mice's cortex after 1 week of SFAD/MUFAD. A) Levels of total GluA1. B) Levels of phosphorylated GluA1 (S845). C) Levels of phosphorylated GluA1 (S831). D) Representative blots of GluA1, p(S845)-GluA1, p(S831)-GluA1 and actin. Actin was used as housekeeping to normalize protein levels. Data are represented as mean ± SD, n=4-7/group. The results are from one independent experiment. GluA1: SD (1.000 ± 0.136, n=6), SFAD (0.918 ± 0.249, n=7) and MUFAD (0.850 ± 0.233, n=7). Ratio p(S845)-GluA1: SD (1.000 ± 0.121, n=5), SFAD (1.118 ± 0.229, n=6) and MUFAD (1.137 ± 0.144, n=7). Ratio p(S831)-GluA1: SD (1.000 ± 0.202, n=4), SFAD (1.030 ± 0.335, n=7) and MUFAD (1.029 ± 0.252, n=7). Statistical analysis was performed by one-way ANOVA followed by Bonferroni's post correction.

Since short-term diet did not affect GluA1 levels or its phosphorylation, a long-term diet (1 month) was conducted in order to check its potential

impact on AMPAR. Interestingly, no significant differences were obtained although there appears to be a slight tendency to increase total GluA1 in SFAD (p=0.1331).

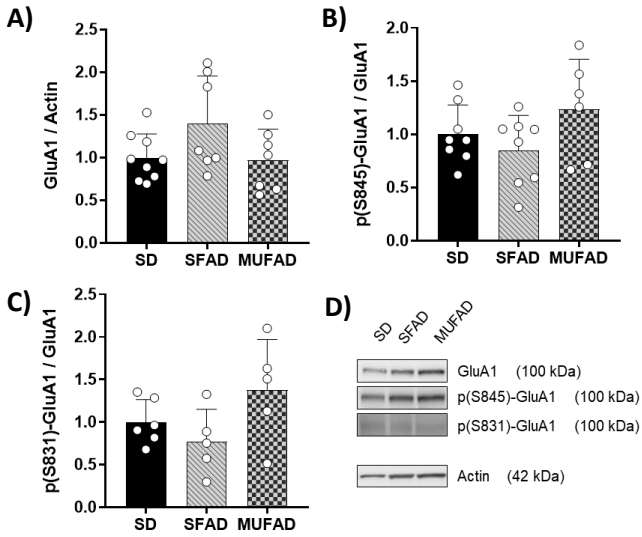

Figure 32. Levels of GluA1 in WT mice's cortex after 1 month of SFAD/MUFAD. A) Levels of total GluA1. B) Levels of phosphorylated GluA1 (S845). C) Levels of phosphorylated GluA1 (S831). D) Representative blots of GluA1, p(S845)-GluA1, p(S831)-GluA1 and actin. Actin was used as housekeeping to normalize protein levels. Data are represented as mean ± SD, n=5-9/group. The results are from one independent experiment. GluA1: SD (1.000 ± 0.277, n=9), SFAD (1.395 ± 0.560, n=7) and MUFAD (0.971 ± 0.360, n=7). Ratio p(S845)-GluA1: SD (1.000 ± 0.276, n=8), SFAD (0.850 ± 0.327, n=8) and MUFAD (1.237 ± 0.467, n=6). Ratio p(S831)-GluA1: SD (1.000 ± 0.266, n=6), SFAD (0.768 ± 0.383, n=5) and MUFAD (1.376 ± 0.594, n=5). Statistical analysis was performed by one-way ANOVA followed by Bonferroni's post correction.

Overall, these results indicate that short-term diets do not affect phosphorylated GluA1 levels at the cortex but that long-term diets could have some kind of impact. More animals should be analyzed to further confirm these preliminary results.

2. Nutrients' effect *in vitro*

To simulate the different types of diets (SFAD and MUFAD) in an *in vitro* model, different fatty acids were chosen to treat primary cultures of cortical neurons. Palmitate was used as a saturated fatty acid; oleate, as a monounsaturated fatty acid and DHA, as a polyunsaturated fatty acid. Moreover, to simulate an exclusively fat-based diet, such as the ketogenic diet, BHB (a ketone body) was employed.

2.1. Short-term treatments

Primary cortical neurons obtained from mouse embryos were treated at 14 DIV with different nutrients just for two hours to simulate a short-term diet.

The effects of palmitate in surface GluA1 were first analyzed. For measuring them, an antibody against an external domain of GluA1 was used without permeabilizing the cells. Figure 33A shows a reduction in surface GluA1 levels due to palmitate. However, no effects were observed in total or phosphorylated GluA1, suggesting the absence of correlation between surface and phosphorylation levels of GluA1.

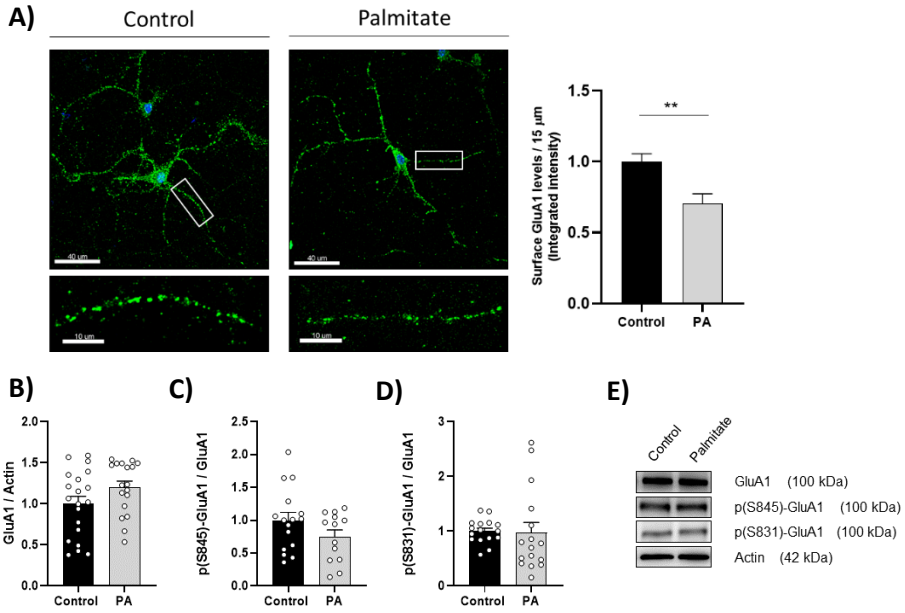

Figure 33. Palmitate's short-term effects on surface GluA1 levels in cortical neurons. A) Surface GluA1 quantified by immunocytochemistry in cortical neurons (n=45 cells) under 2h palmitate treatment (200 µM). Hoechst was used

to detect nuclei. Results of integrated intensity in 15 µm of primary dendrites were normalized by the control treatment. Data are represented as mean ± SEM of 90 dendrites from three independent experiments. Control (BSA; 1.000 ± 0.056, n=79) and PA (0.704 ± 0.069, n=82). Scale bar = 40 µm; scale bar of inset magnifications = 10 µm. B) Cortical levels of total GluA1. C) Cortical levels of phosphorylated GluA1 (S845). D) Cortical levels of phosphorylated GluA1 (S831). D) Representative blots of GluA1, p(S845)-GluA1, p(S831)-GluA1 and actin after 2h incubation with 200 µM palmitate. Actin was used as housekeeping to normalize protein levels. Data are represented as mean ± SEM, n=13-20 from four independent experiments. GluA1: control (BSA; 1.000 ± 0.091, n=20) and PA (1.202 ± 0.075, n=18). Ratio p(S845)-GluA1: control (BSA; 1.000 ± 0.119, n=16) and PA (0.749 ± 0.104, n=13). Ratio p(S831)-GluA1: control (BSA; 1.000 ± 0.055, n=16) and PA (0.971 ± 0.190, n=16). Statistical analysis was performed by Student t-test. **p<0.01.

When analyzing the results of the monounsaturated fatty acid oleate, no significant differences were found (figure 34). This could be due to the brief duration of the treatment.

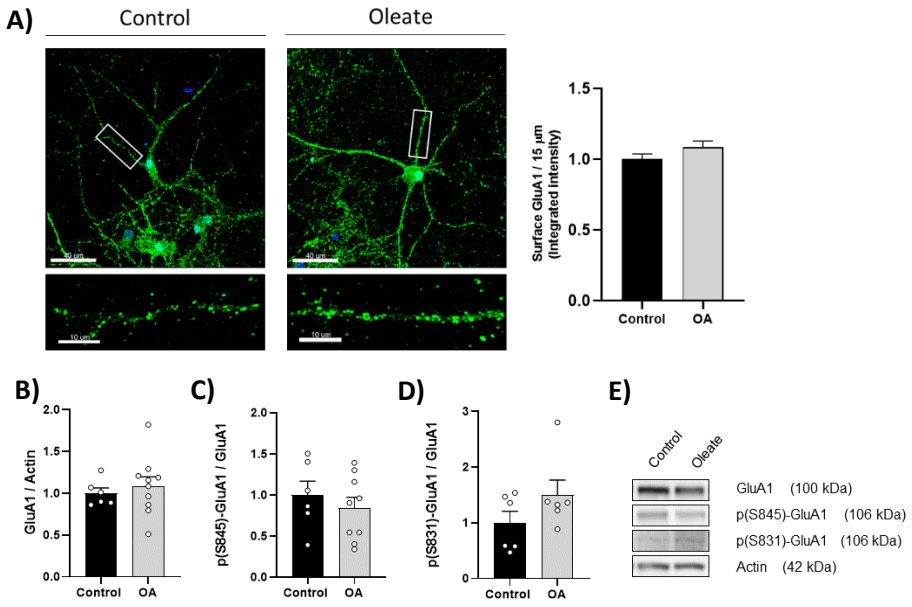

Figure 34. Oleate's short-term effects on surface GluA1 levels in cortical neurons. A) Surface GluA1 quantified by immunocytochemistry in cortical neurons (n=45 cells) under 2h oleate treatment (200 µM). Hoechst was used to detect nuclei. Results of integrated intensity in 15 µm of primary dendrites were normalized by the control treatment. Data are represented as mean ± SEM of 90 dendrites from three independent experiments. Control (BSA; 1.000 ± 0.037, n=84) and OA (1.084

± 0.044, n=86). Scale bar = 40 µm; scale bar of inset magnifications = 10 µm. B) Cortical levels of total GluA1. C) Cortical levels of phosphorylated GluA1 (S845). D) Cortical levels of phosphorylated GluA1 (S831). D) Representative blots of GluA1, p(S845)-GluA1, p(S831)-GluA1 and actin after 2h incubation with 200 µM oleate. Actin was used as housekeeping to normalize protein levels. Data are represented as mean ± SEM, n=6-10 from two independent experiments. GluA1: control (BSA; 1.000 ± 0.064, n=6) and OA (1.088 ± 0.110, n=10). Ratio p(S845)-GluA1: control (BSA; 1.000 ± 0.169, n=6) and OA (0.840 ± 0.132, n=9). Ratio p(S831)-GluA1: control (BSA; 1.000 ± 0.205, n=6) and OA (1.497 ± 0.272, n=6). Statistical analysis was performed by Student t-test (GluA1 and p845) and Mann-Whitney U test (p831).

Then, a polyunsaturated fatty acid, the DHA, was studied. As it was mentioned in the introduction, the DHA is the most abundant ω-3 fatty acid on the brain. This fatty acid did not cause any change in total or surface GluA1 (figure 35A-B), but it increased GluA1's phosphorylation at the serine 831 (figure 35D).

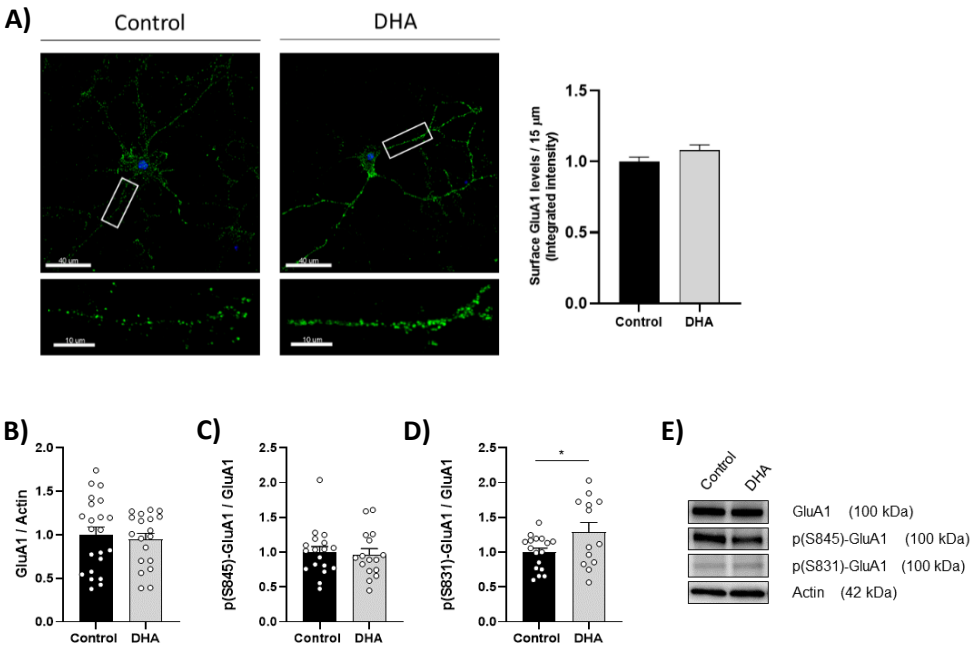

Figure 35. DHA's short-term effects on surface GluA1 levels in cortical neurons. A) Surface GluA1 quantified by immunocytochemistry in cortical neurons (n=45 cells) under 2h DHA treatment (200 µM). Hoechst was used to detect nuclei. Results of integrated intensity in 15 µm of primary dendrites were normalized by the control treatment. Data are represented as mean ± SEM of 90 dendrites from three

independent experiments. Control (BSA; 1.000 ± 0.032, n=93) and DHA (1.081 ± 0.037, n=114). Scale bar = 40 µm; scale bar of inset magnifications = 10 µm. B) Cortical levels of total GluA1. C) Cortical levels of phosphorylated GluA1 (S845). D) Cortical levels of phosphorylated GluA1 (S831). D) Representative blots of GluA1, p(S845)-GluA1, p(S831)-GluA1 and actin after 2h incubation with 200 µM DHA. Actin was used as housekeeping to normalize protein levels. Data are represented as mean ± SEM, n=13-22 from four independent experiments. GluA1: control (BSA; 1.000 ± 0.089, n=22) and DHA (0.948 ± 0.070, n=19). Ratio p(S845)-GluA1: control (BSA; 1.000 ± 0.081, n=18) and DHA (0.967 ± 0.083, n=16). Ratio p(S831)-GluA1: control (BSA; 1.000 ± 0.059, n=17) and DHA (1.289 ± 0.136, n=13). Statistical analysis was performed by Student t-test. *p<0.05.

On the other hand, treating cortical neurons with the ketone body (BHB) for 2h was enough to increase the surface GluA1 levels as it is shown in figure 36A. However, no changes were observed in total GluA1 or its phosphorylated forms (figure 36B-D).

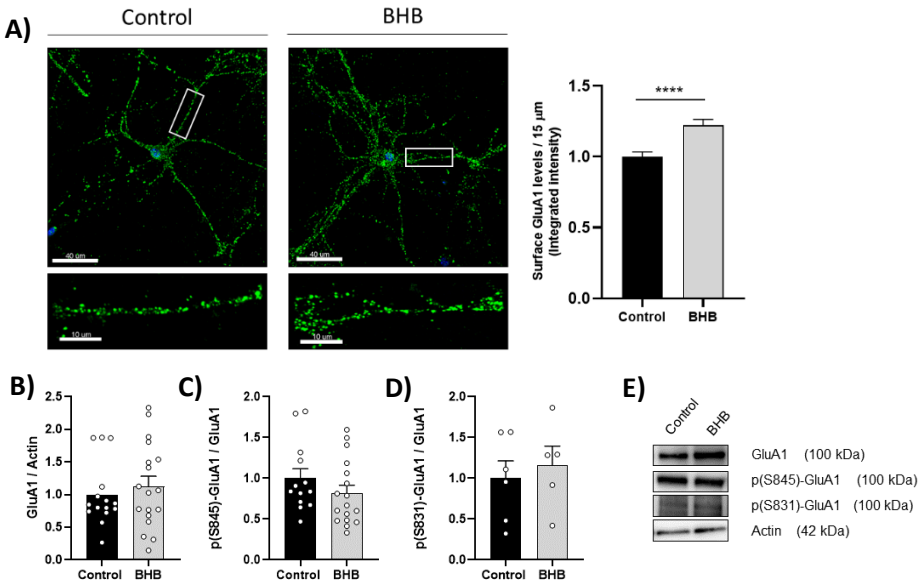

Figure 36. BHB's short-term effects on surface GluA1 levels in cortical neurons. A) Surface GluA1 quantified by immunocytochemistry in cortical neurons (n=45 cells) under 2h BHB treatment (5 mM). Hoechst was used to detect nuclei. Results of integrated intensity in 15 µm of primary dendrites were normalized by the control treatment. Data are represented as mean ± SEM of 90 dendrites from three independent experiments. Control (1.000 ± 0.035, n=98) and BHB (1.221 ± 0.042, n=86). Scale bar = 40 µm; scale bar of inset magnifications = 10 µm. B) Cortical levels of total GluA1. C) Cortical levels of phosphorylated GluA1 (S845). D) Cortical levels of phosphorylated GluA1 (S831). D) Representative blots of GluA1, p(S845)-

GluA1, p(S831)-GluA1 and actin after 2h incubation with 5 mM BHB. Actin was used as housekeeping to normalize protein levels. Data are represented as mean ± SEM, n=5-18 from two (p(S831)-GluA1) to three independent experiments. GluA1: control (1.000 ± 0.126, n=15) and BHB (1.129 ± 0.154, n=18). Ratio p(S845)-GluA1: control (1.000 ± 0.117, n=13) and BHB (0.817 ± 0.097, n=17). Ratio p(S831)-GluA1: control (1.000 ± 0.215, n=6) and BHB (1.156 ± 0.239, n=5). Statistical analysis was performed by Student t-test. ****p<0.0001.

Considering the results of short-term treatments, only the palmitate and the BHB have an effect on surface GluA1. Unsaturated fatty acids, including both monounsaturated and polyunsaturated forms, have no effect in the short-term.

2.2. Long-term treatments

Considering that some nutrients of interest in this thesis did not show any effect on GluA1 levels during the short incubation period, it was deemed necessary to explore the impact of these nutrients under a long-term treatment. Therefore, the same treatments explained above were repeated for 24 hours. In this case, with the same concentration of palmitate (200 µM), the decrease of surface GluA1 was even bigger as it is represented in figure 37A. Nevertheless, total and phosphorylated GluA1 levels did not present any change again (figure 37B-D).

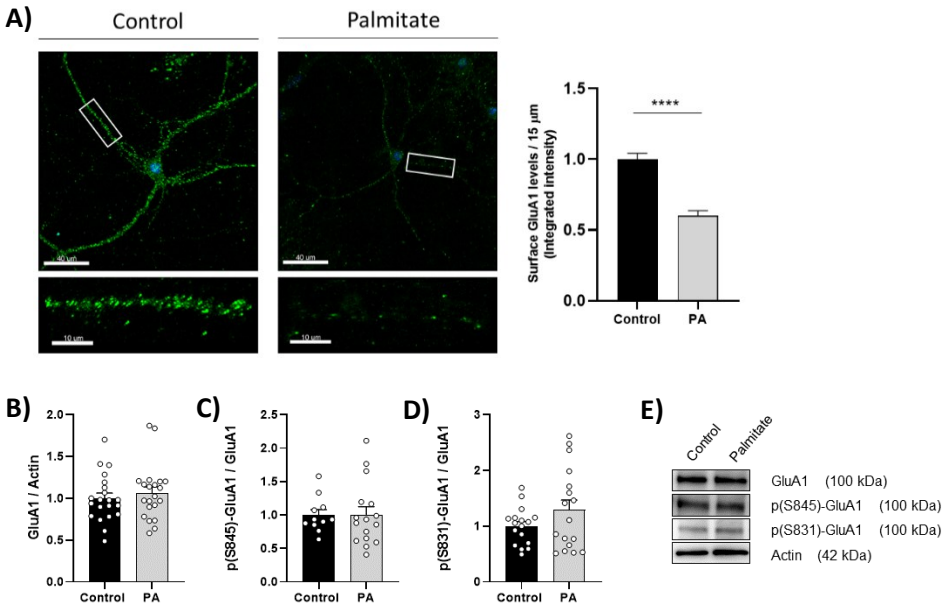

Figure 37. Palmitate's long-term effects on surface GluA1 levels in cortical neurons. A) Surface GluA1 quantified by immunocytochemistry in cortical neurons (n=45 cells) under 24h palmitate treatment (200 µM). Hoechst was used to detect nuclei. Results of integrated intensity in 15 µm of primary dendrites were normalized by the control treatment. Data are represented as mean ± SEM of 90 dendrites from three independent experiments. Control (BSA; 1.000 ± 0.041, n=77) and PA (0.602 ± 0.033, n=72). Scale bar = 40 µm; scale bar of inset magnifications = 10 µm. B) Cortical levels of total GluA1. C) Cortical levels of phosphorylated GluA1 (S845). D) Cortical levels of phosphorylated GluA1 (S831). D) Representative blots of GluA1, p(S845)-GluA1, p(S831)-GluA1 and actin after 24h incubation with 200 µM palmitate. Actin was used as housekeeping to normalize protein levels. Data are represented as mean ± SEM, n=11-21 from four independent experiments. GluA1: control (BSA; 1.000 ± 0.062, n=21) and PA (1.064 ± 0.072, n=21). Ratio p(S845)-GluA1: control (BSA; 1.000 ± 0.080, n=11) and PA (1.004 ± 0.120, n=16). Ratio p(S831)-GluA1: control (BSA; 1.000 ± 0.081, n=17) and PA (1.290 ± 0.178, n=17). Statistical analysis was performed by Student t-test. ****p<0.0001.

Contrary to the short-term treatment, treating cortical neurons for 24h with unsaturated fatty acids, oleate or DHA (figure 38 and figure 39, respectively), did increase surface GluA1. Furthermore, total GluA1 levels were diminished in both cases (figure 38B and 39B), suggesting that a substantial portion of GluA1 is directed towards the membrane surface. Notably, the phosphorylated levels remained unchanged.

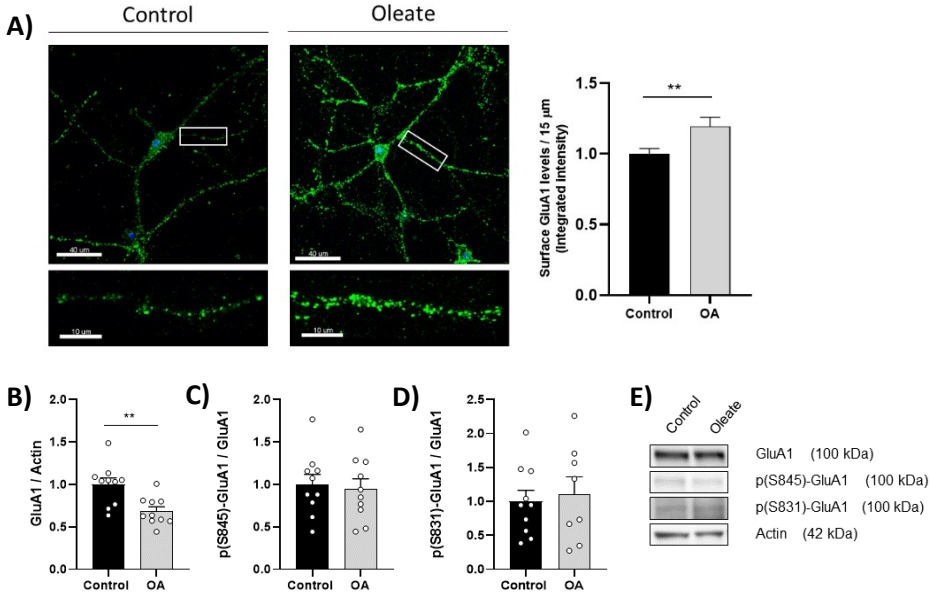

Figure 38. Oleate's long-term effects on surface GluA1 levels in cortical neurons. A) Surface GluA1 quantified by immunocytochemistry in cortical neurons (n=45 cells) under 24h oleate treatment (200 µM). Hoechst was used to detect nuclei. Results of integrated intensity in 15 µm of primary dendrites were normalized by the control treatment. Data are represented as mean ± SEM of 90 dendrites from three independent experiments. Control (BSA; 1.000 ± 0.038, n=80) and OA (1.194 ± 0.064, n=60). Scale bar = 40 µm; scale bar of inset magnifications = 10 µm. B) Cortical levels of total GluA1. C) Cortical levels of phosphorylated GluA1 (S845). D) Cortical levels of phosphorylated GluA1 (S831). D) Representative blots of GluA1, p(S845)-GluA1, p(S831)-GluA1 and actin after 24h incubation with 200 µM oleate. Actin was used as housekeeping to normalize protein levels. Data are represented as mean ± SEM, n=8-10 from two independent experiments. GluA1: control (BSA; 1.000 ± 0.077, n=10) and OA (0.684 ± 0.052, n=10). Ratio p(S845)-GluA1: control (BSA; 1.000 ± 0.117, n=10) and OA (0.948 ± 0.120, n=10). Ratio p(S831)-GluA1: control (BSA; 1.000 ± 0.163, n=10) and OA (1.111 ± 0.252, n=8). Statistical analysis was performed by Student t-test. **p<0.01.

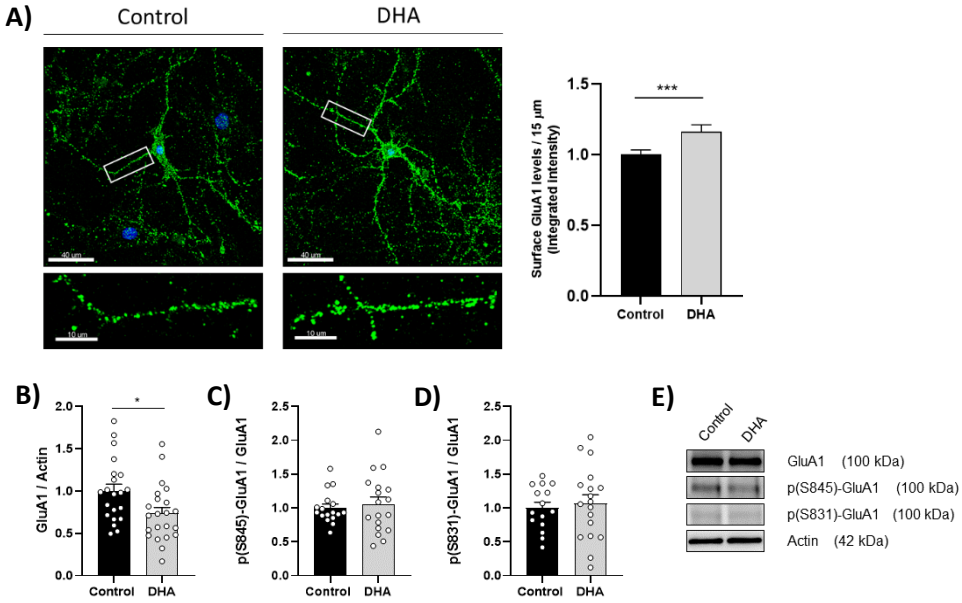

Figure 39. DHA's long-term effects on surface GluA1 levels in cortical neurons. A) Surface GluA1 quantified by immunocytochemistry in cortical neurons (n=45 cells) under 24h DHA treatment (200 µM). Hoechst was used to detect nuclei. Results of integrated intensity in 15 µm of primary dendrites were normalized by the control treatment. Data are represented as mean ± SEM of 90 dendrites from three independent experiments. Control (BSA; 1.000 ± 0.033, n=100) and DHA (1.160 ± 0.051, n=99). Scale bar = 40 µm; scale bar of inset magnifications = 10 µm. B) Cortical levels of total GluA1. C) Cortical levels of phosphorylated GluA1 (S845). D) Cortical levels of phosphorylated GluA1 (S831). D) Representative blots

of GluA1, p(S845)-GluA1, p(S831)-GluA1 and actin after 24h incubation with 200 µM DHA. Actin was used as housekeeping to normalize protein levels. Data are represented as mean ± SEM, n=15-22 from three independent experiments. GluA1: control (BSA; 1.000 ± 0.075, n=21) and DHA (0.684 ± 0.067, n=22). Ratio p(S845)-GluA1: control (BSA; 1.000 ± 0.057, n=17) and DHA (1.059 ± 0.104, n=18). Ratio p(S831)-GluA1: control (BSA; 1.000 ± 0.085, n=15) and DHA (1.069 ± 0.127, n=18). Statistical analysis was performed by Student t-test. *p<0.05, ***p<0.001.

Regarding the ketone body, the same increase observed at the short-term treatment was obtained at long-term (figure 40A). It seems like BHB has a strong effect in both the short and the long-term treatments (20% of increase at 2h and 30% at 24h approximately), highlighting the essential role that ketone bodies might have in the brain. However, prolonged incubation with BHB resulted in a reduction in serine 831 phosphorylation (figure 40D).

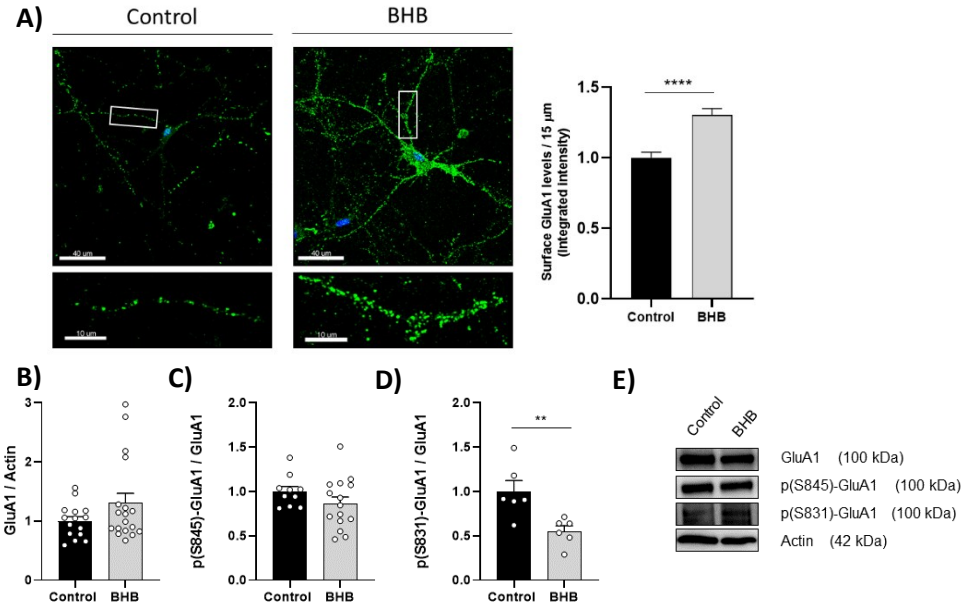

Figure 40. BHB's long-term effects on surface GluA1 levels in cortical neurons. A) Surface GluA1 quantified by immunocytochemistry in cortical neurons (n=45 cells) under 24h BHB treatment (5 mM). Hoechst was used to detect nuclei. Results of integrated intensity in 15 µm of primary dendrites were normalized by the control treatment. Data are represented as mean ± SEM of 90 dendrites from three independent experiments. Control (1.000 ± 0.038, n=95) and BHB (1.303 ± 0.046, n=93). Scale bar = 40 µm; scale bar of inset magnifications = 10 µm. B) Cortical levels of total GluA1. C) Cortical levels of phosphorylated GluA1 (S845). D) Cortical

levels of phosphorylated GluA1 (S831). D) Representative blots of GluA1, p(S845)-GluA1, p(S831)-GluA1 and actin after 24h incubation with 5 mM BHB. Actin was used as housekeeping to normalize protein levels. Data are represented as mean ± SEM, n=6-18 from two (p(S831)-GluA1) to three independent experiments. GluA1: control (1.000 ± 0.074, n=15) and BHB (1.303 ± 0.166, n=18). Ratio p(S845)-GluA1: control (1.000 ± 0.057, n=10) and BHB (0.864 ± 0.074, n=15). Ratio p(S831)-GluA1: control (1.000 ± 0.122, n=6) and BHB (0.550 ± 0.062, n=6). Statistical analysis was performed by Student t-test. **p<0.01, ****p<0.0001.

Overall, these results establish a distinct cellular impact of the studied nutrients. In addition, each nutrient showed a stronger effect with the long-term treatment than with the short one, suggesting that a continuous consumption of these nutrients can influence the brain at a cellular level.

2.3. Alternative model in differentiated SH-SY5Y

Taking into account primary cultures of cortical neurons are difficult to obtain, an alternative model to study the effect of nutrients was developed. Despite the fact that SH-SY5Y are a neuroblastoma cell line, they can be converted into a neuron-like type by adding retinoic acid to the medium. Once differentiated, they show extensions simulating dendrites and axons which are called neurites.

Figure 41 shows the effect of short-term treatments with different fatty acids and the ketone body. In this cell model, nutrients did not alter the surface GluA1 levels except in the case of the oleate, in which an increase in surface GluA1 was observed. The great changes observed in primary cultures are not present here. As differentiated SH-SY5Y are a neuron-like type, they probably need more time to be influenced with palmitate and BHB.

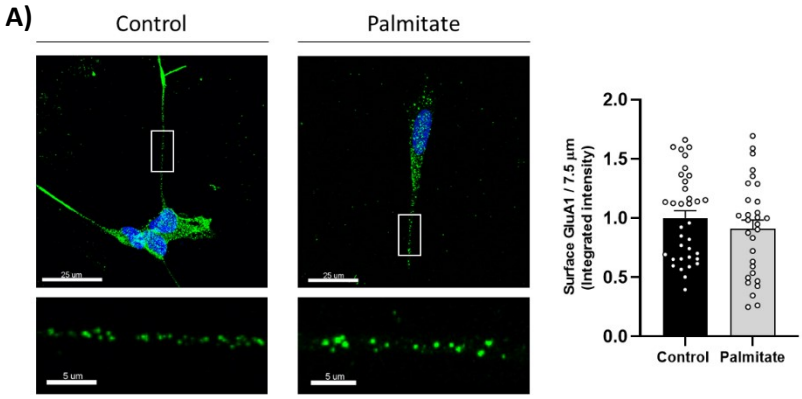

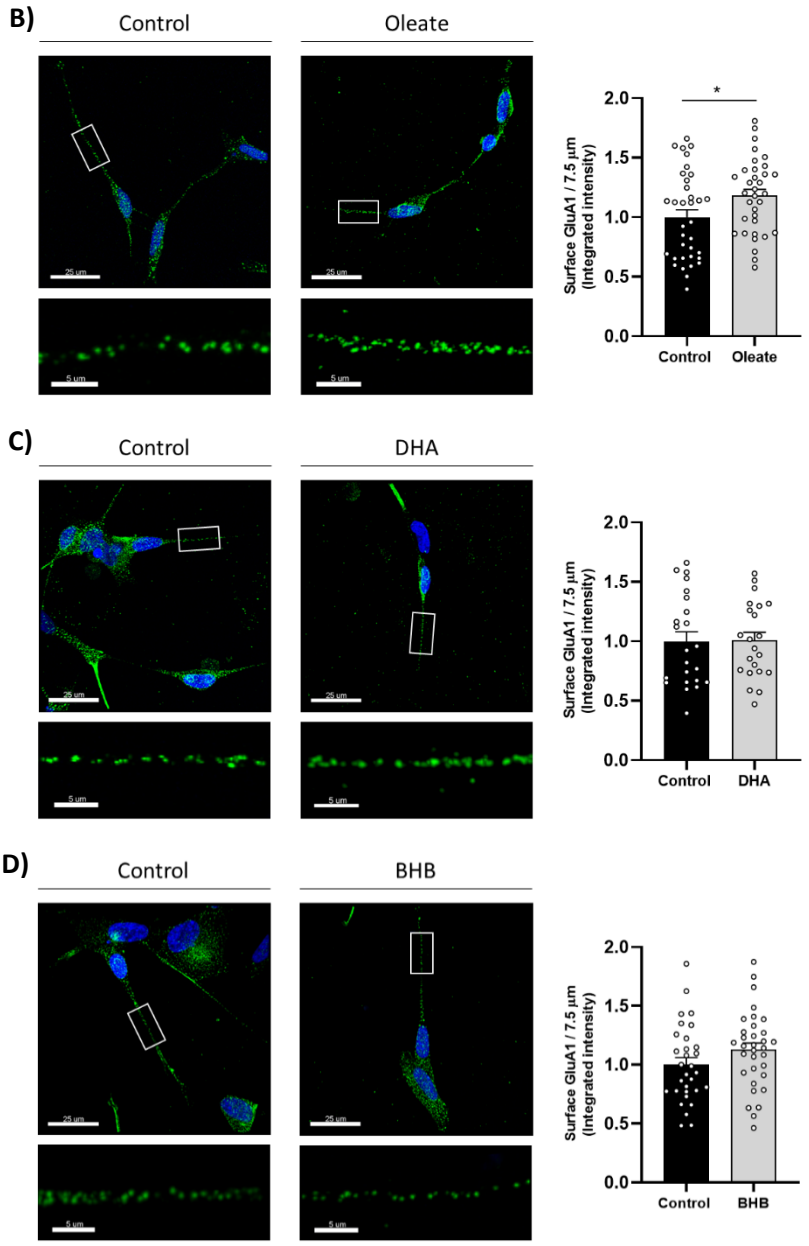

Figure 41. Short-term effects on surface GluA1 levels in differentiated SH-SY5Y treated with different nutrients. A) Surface GluA1 quantified by immunocytochemistry in differentiated SH-SY5Y under 2h palmitate treatment (200 µM). Control (BSA; 1.000 ± 0.062, n=35) and PA (0.910 ± 0.074, n=30). B) Surface GluA1 quantified by immunocytochemistry in differentiated SH-SY5Y under 2h oleate treatment (200 µM). Control (BSA; 1.000 ± 0.062, n=35) and OA (1.180 ± 0.054, n=34). C) Surface GluA1 quantified by immunocytochemistry in differentiated SH-SY5Y under 2h DHA treatment (200 µM). Control (BSA; 1.000 ±

0.080, n=23) and DHA (1.007 ± 0.069, n=22). D) Surface GluA1 quantified by immunocytochemistry in differentiated SH-SY5Y under 2h BHB treatment (5 mM). Control (1.000 ± 0.059, n=31) and BHB (1.128 ± 0.057, n=33). Hoechst was used to detect nuclei. Results of integrated intensity in 7.5 µm of neurites were normalized by the control treatment. Data are represented as mean ± SEM of 22-35 neurites from one (DHA) to two independent experiments. Scale bar = 25 µm; scale bar of inset magnifications = 5 µm. Statistical analysis was performed by Student t-test. *p<0.05.

However, the same significant effects observed in primary cultures were found with the long-term treatment using the same concentration of nutrients (200 µM for fatty acids and 5 mM for BHB). The palmitate decreased surface GluA1 levels while the unsaturated fatty acids (oleate and DHA) and the ketone body (BHB) increased them (figure 42).

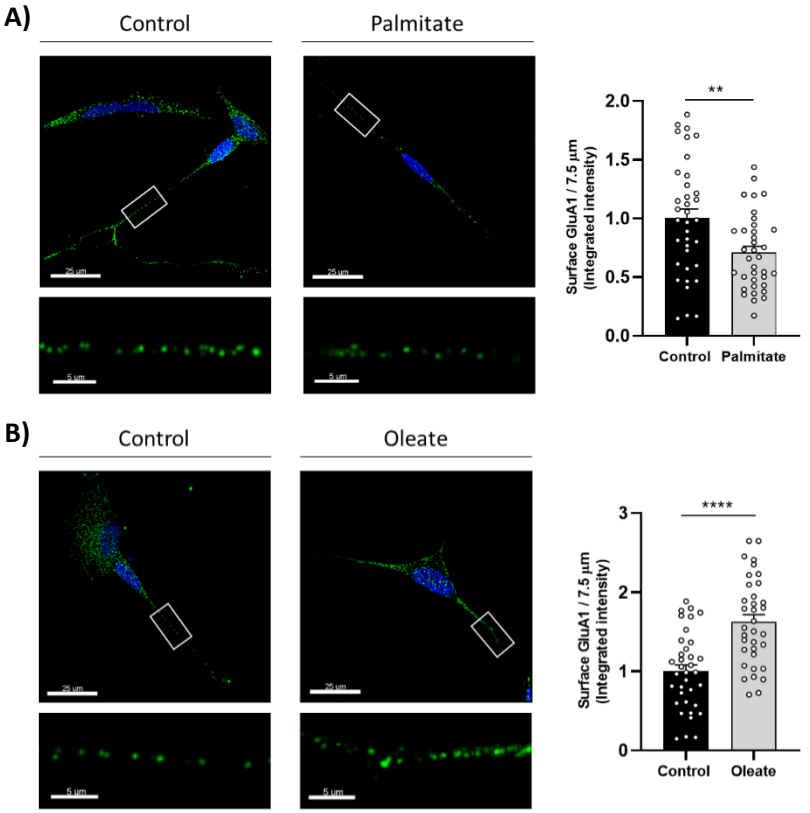

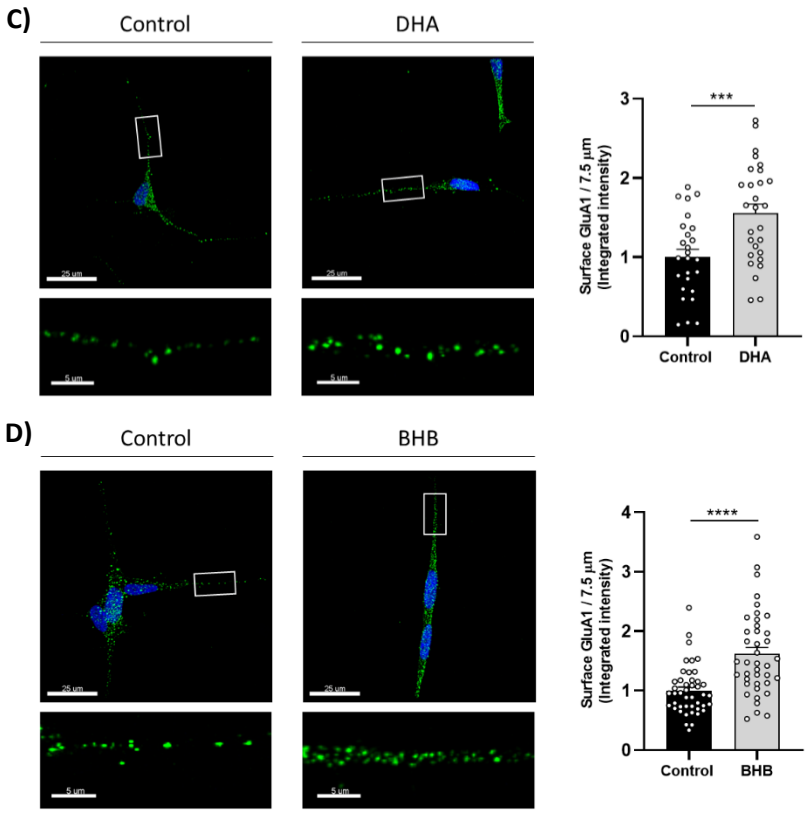

Figure 42. Long-term effects on surface GluA1 levels in differentiated SH-SY5Y treated with different nutrients. A) Surface GluA1 quantified by immunocytochemistry in differentiated SH-SY5Y under 24h palmitate treatment (200 µM). Control (BSA; 1.000 ± 0.082, n=36) and PA (0.709 ± 0.053, n=36). B) Surface GluA1 quantified by immunocytochemistry in differentiated SH-SY5Y under 24h oleate treatment (200 µM). Control (BSA; 1.000 ± 0.082, n=36) and OA (1.626 ± 0.093, n=35). C) Surface GluA1 quantified by immunocytochemistry in differentiated SH-SY5Y under 24h DHA treatment (200 µM). Control (BSA; 1.000 ± 0.100, n=26) and DHA (1.556 ± 0.118, n=28). D) Surface GluA1 quantified by immunocytochemistry in differentiated SH-SY5Y under 24h BHB treatment (5 mM). Control (1.000 ± 0.062, n=44) and BHB (1.617 ± 0.111, n=40). Hoechst was used to detect nuclei. Results of integrated intensity in 7.5 µm of neurites were normalized by the control treatment. Data are represented as mean ± SEM of 26-44 neurites from one (DHA) to two independent experiments. Scale bar = 25 µm; scale bar of inset magnifications = 5 µm. Statistical analysis was performed by Student t-test. **p<0.01, ***p<0.001, ****p<0.0001.

Considering the results with the long incubation period in differentiated SH-SY5Y, these neuron-like cells are a suitable alternative model to study the effect of nutrients. In addition, they avoid the use of animals.

3. PA and BHB's effects on synaptic GluA1

Since palmitate and BHB showed short-term effects in cortical cultured neurons and had a stronger effect than oleate or DHA in the long-term, the study of these two nutrients was continued analyzing the effect in primary hippocampal neurons. Moreover, different concentrations of BHB were tested, all of them in the range of physiological levels found in mice. In addition, synaptic GluA1 levels were analyzed by the co-localization of this protein with PSD95, used as a post-synaptic density marker.

Figure 43A shows a decrease in synaptic GluA1 due to palmitate's short-term treatment. This suggests that palmitate is a critical nutrient that negatively affects synaptic function.

In the case of BHB, several concentrations were evaluated (1 mM, 2 mM and 5 mM) in hippocampal neurons. As observed in figure 43B, surface GluA1 was increased by 5 mM of BHB, the concentration used in cortical neurons, but synaptic GluA1 was not affected by any of the concentrations used. This suggests that short-term treatment with physiological concentration of BHB does not enhance synaptic GluA1, even though at higher concentrations is able to increase surface GluA1, indicating that BHB mainly increases perisynaptic GluA1 levels.

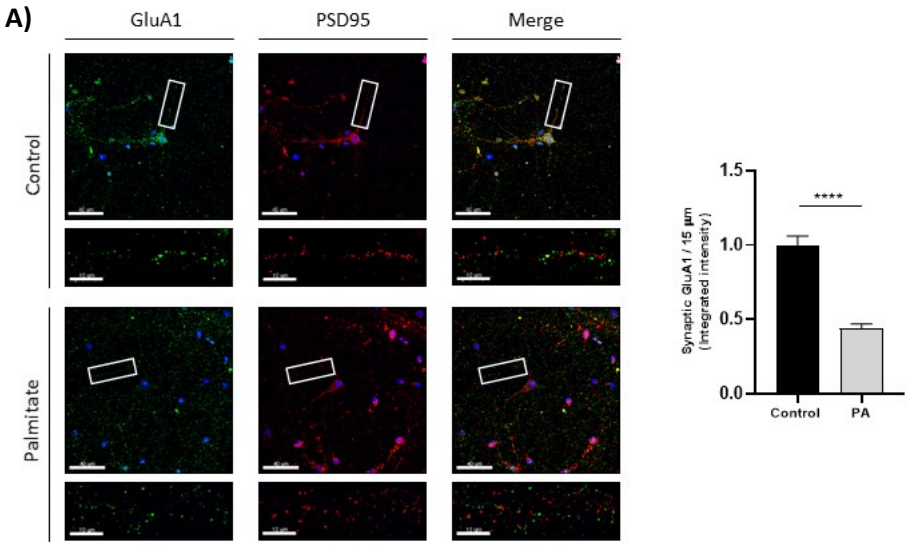

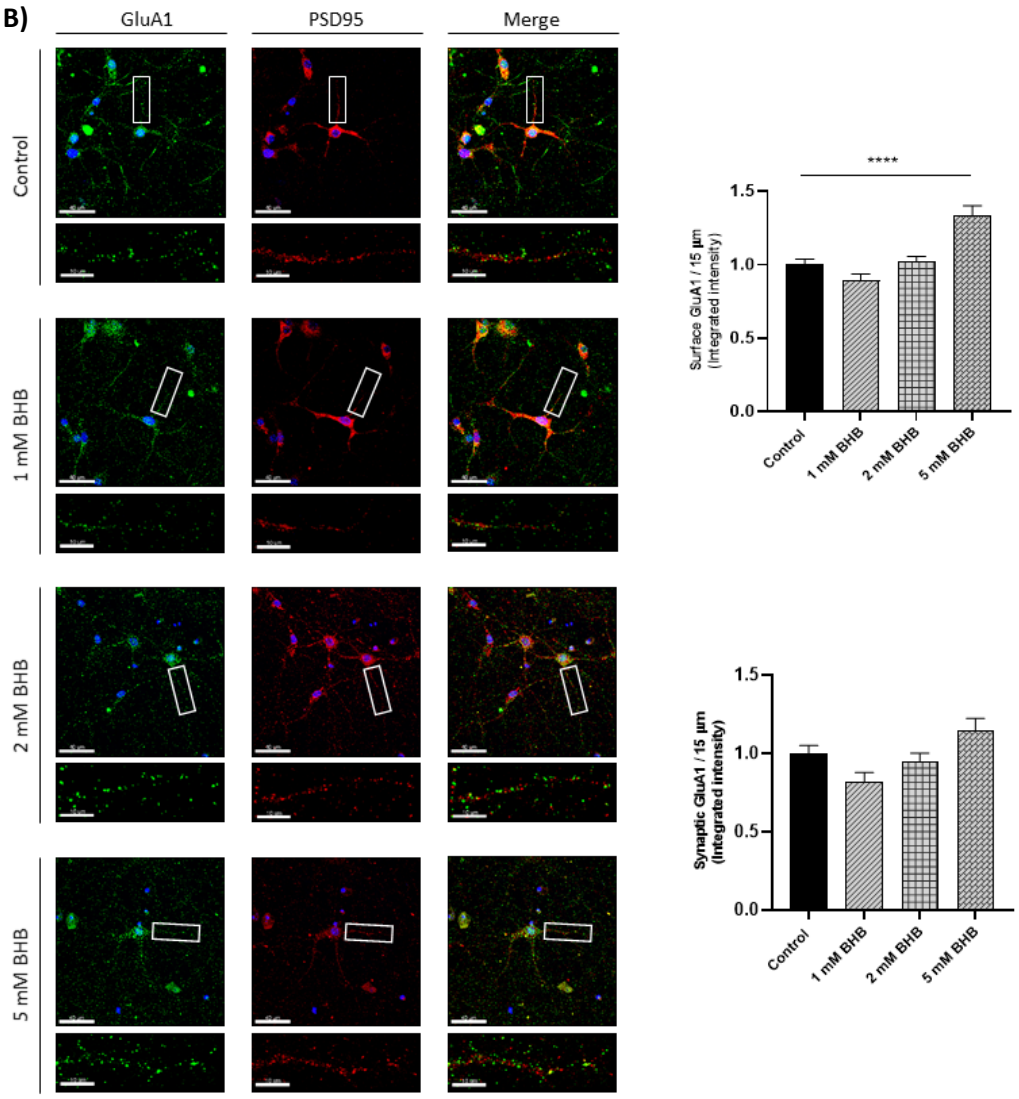

Figure 43. Short-term effects on synaptic/surface GluA1 levels in hippocampal neurons. A) Synaptic GluA1 quantified by immunocytochemistry in hippocampal neurons (n=30 cells) under 2h palmitate treatment (200 µM). Control (BSA; 1.000 ± 0.061, n=49) and PA (0.439 ± 0.030, n=58). B) Synaptic/surface GluA1 in hippocampal neurons (n=30 cells) under 24h BHB treatment (1 mM, 2 mM and 5 mM). Surface GluA1: control (1.000 ± 0.037, n=66), 1 mM BHB (0.890 ± 0.047, n=53), 2 mM BHB (1.019 ± 0.038, n=65) and 5 mM BHB (1.337 ± 0.065, n=53). Synaptic GluA1: control (1.000 ± 0.050, n=61), 1 mM BHB (0.816 ± 0.062, n=45), 2 mM BHB (0.951 ± 0.049, n=59) and 5 mM BHB (1.142 ± 0.081, n=46). Hoechst was used to detect nuclei. Results of integrated intensity in 15 µm of primary dendrites were normalized by the control treatment. Data are represented as mean ± SEM of 60 dendrites from two independent experiments. Scale bar = 40 µm; scale bar

of inset magnifications = 10 µm. Statistical analysis was performed by Student t-test (A) or one-way ANOVA followed by Bonferroni's post correction (B). ****p<0.0001.

Furthermore, when hippocampal neurons were treated with palmitate for 24h, synaptic GluA1 was also significantly reduced (figure 44A). In the case of BHB, similar to the results of the short-term treatment, no alterations in synaptic GluA1 were observed (figure 44B). However, lower concentrations of BHB (1 mM and 2 mM) led to an increase in surface GluA1. As the effect of 2 mM BHB was stronger than that of 1 mM, synaptic transmission experiments in hippocampus described later were conducted using this concentration.

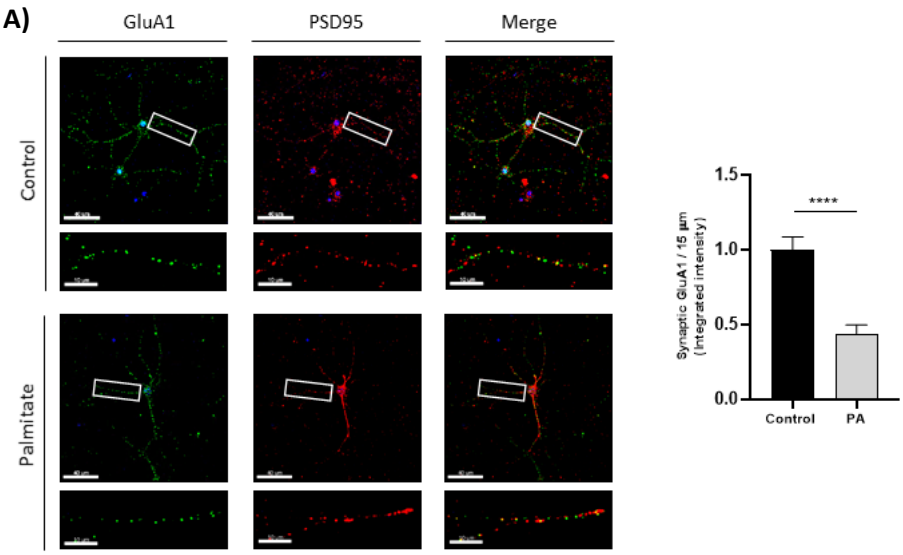

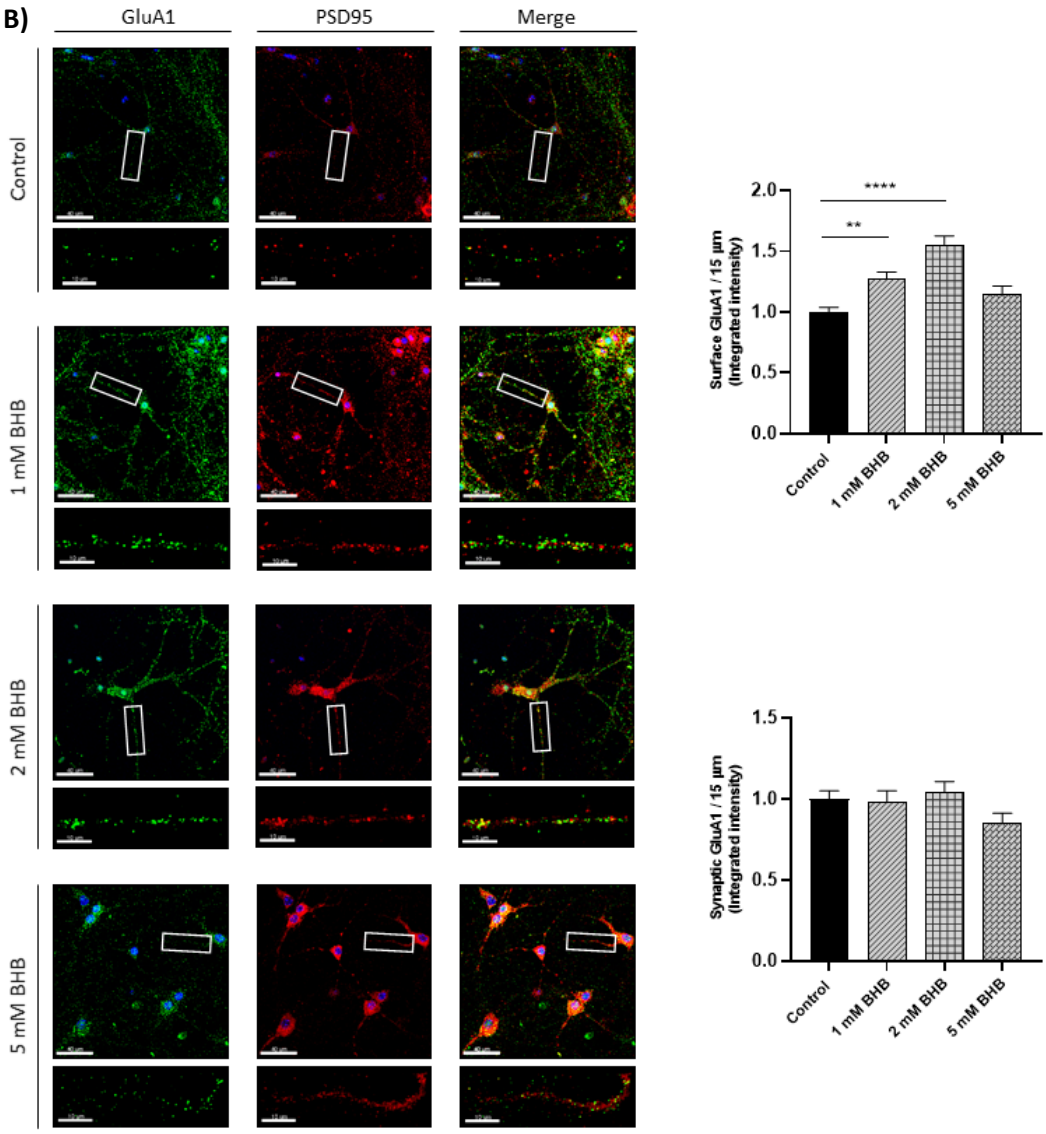

Figure 44. Long-term effects on synaptic/surface GluA1 levels in hippocampal neurons. A) Synaptic GluA1 quantified by immunocytochemistry in hippocampal neurons (n=30 cells) under 24h palmitate treatment (200 µM). Control (BSA; 1.000 ± 0.086, n=54) and PA (0.439 ± 0.058, n=56). B) Synaptic/surface GluA1 in hippocampal neurons (n=30 cells) under 24h BHB treatment (1 mM, 2 mM and 5 mM). Surface GluA1: control (1.000 ± 0.037, n=66) 1 mM BHB (1.269 ± 0.060, n=67), 2 mM BHB (1.557 ± 0.070, n=65) and 5 mM BHB (1.147 ± 0.066, n=44). Synaptic GluA1: control (1.000 ± 0.050, n=61) 1 mM BHB (0.982 ± 0.068, n=56), 2 mM BHB (1.040 ± 0.067, n=57) and 5 mM BHB (0.855 ± 0.057, n=43). Hoechst was used to detect nuclei. Results of integrated intensity in 15 µm of primary dendrites

were normalized by the control treatment. Data are represented as mean ± SEM of 60 dendrites from two independent experiments. Scale bar = 40 µm; scale bar of inset magnifications = 10 µm. Statistical analysis was performed by Student t-test (A) or one-way ANOVA followed by Bonferroni's post correction (B). **p<0.01, ****p<0.0001.

In order to analyze if BHB can counteract palmitate deleterious effects on GluA1 synaptic levels, co-treatment of palmitate and BHB were performed in hippocampal neurons. As it can be observed in figure 45, 1 mM and 2 mM of BHB effectively counteracted the adverse effects of palmitate on synaptic GluA1. However, a 5 mM concentration of BHB, which falls outside the physiological range, did not exhibit this beneficial effect in the presence of the saturated fatty acid.

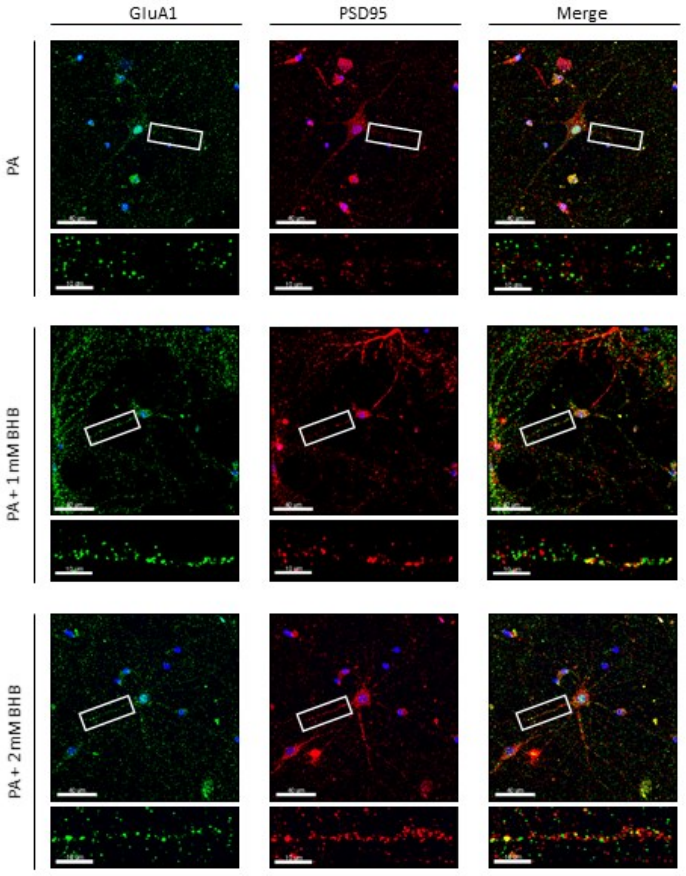

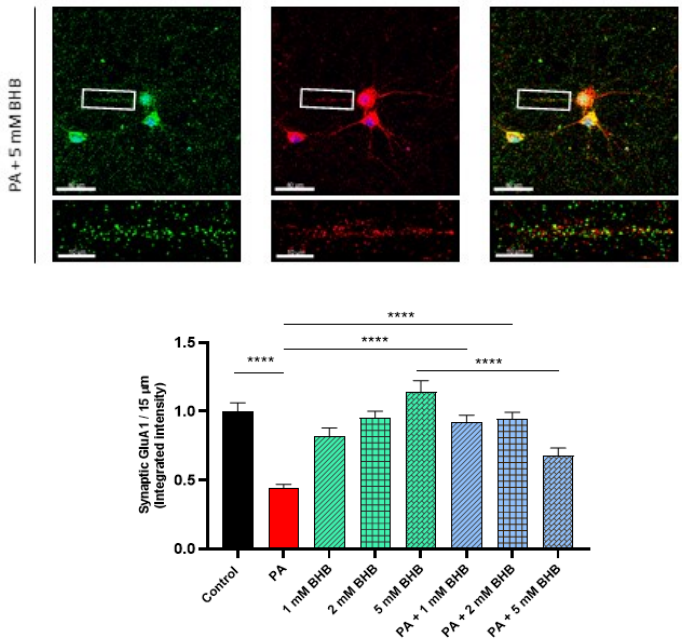

Figure 45. Short-term effects on synaptic GluA1 levels in hippocampal neurons co-treated with palmitate and BHB. Synaptic GluA1 was quantified by immunocytochemistry in hippocampal neurons (n=30 cells) under 2h palmitate (200 µM) and BHB (1 mM, 2 mM and 5 mM) treatment. Control, PA and BHB's have been extracted from figure 43. Hoechst was used to detect nuclei. Results of integrated intensity in 15 µm of primary dendrites were normalized by the control treatment. Data are represented as mean ± SEM of 60 dendrites from two independent experiments. PA + 1 mM BHB (0.922 ± 0.050, n=52), PA + 2 mM BHB (0.943 ± 0.050, n=45) and PA + 5 mM BHB (0.676 ± 0.057, n=47). Scale bar = 40 µm; scale bar of inset magnifications = 10 µm. Statistical analysis was performed by one-way ANOVA followed by Bonferroni's post correction. ****p<0.0001.

4. Synaptic transmission under PA and BHB treatments and cognitive evaluations

4.1. mEPSCs

To study the role of the saturated fatty acid (palmitate) and the ketone body (BHB) in synaptic transmission, AMPAR-mediated mEPSCs were measured in primary cortical neurons (at 14-15 DIV) treated with these nutrients for 24h. In order to detect them, recordings were carried out in the presence of TTX in extracellular solution to block evoked transmission.

D-AP5 and PTX were also added in the solution to block NMDA and $GABA_A$ receptors. Moreover, to use the same control group for both treatments, BHB group also contained BSA.

These recordings were performed by David Soto and Aida Castellanos at the University of Barcelona. Results point out that AMPAR-mediated mEPSCs amplitudes were decreased in cortical neurons treated with palmitate but no changes were found in BHB's (figure 46A-C). This result aligns perfectly with earlier observations regarding the lack of BHB's effects on synaptic GluA1 levels. Cumulative amplitude histograms for mEPSCs (figure 46D) demonstrate a significant shift in the amplitude distribution towards smaller values in palmitate treated neurons, indicating a reduction in the number of postsynaptic AMPARs.

Figure 46E shows the frequency of AMPAR-mediated mEPSCs and no significant differences are observed indicating no presynaptic alteration is present in neurons treated with palmitate or BHB. Some kinetic parameters from mEPSCs were also studied: rise time and τ-weighted (figure 46F-G). Neither of them was affected with the treatments suggesting that there is not any alteration in the AMPAR subtype composition underlying mEPSCs.

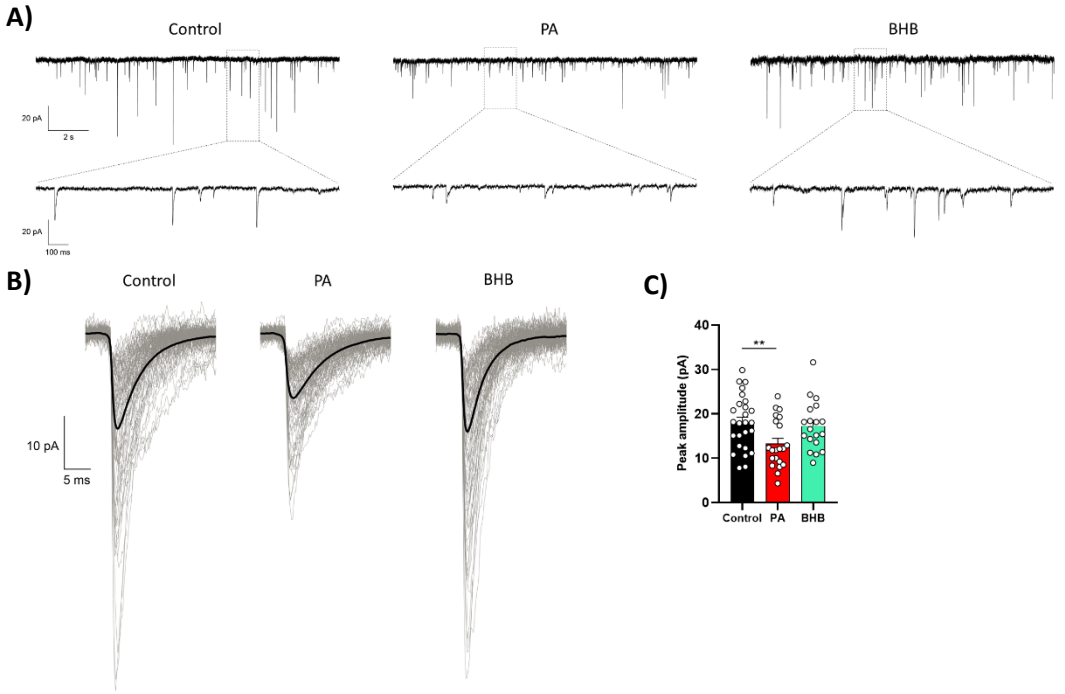

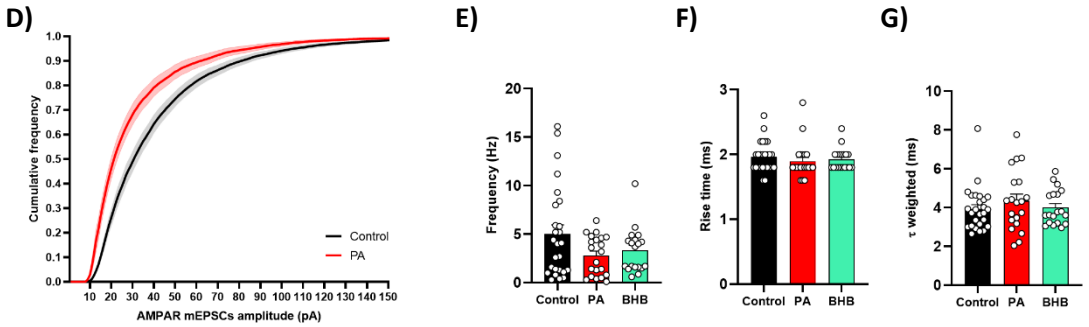

Figure 46. mEPSCs recordings. A) Representative whole-cell recordings of AMPAR-mediated mEPSCs of 15 seconds duration from cultured cortical neurons (14-15 DIV) treated with palmitate or BHB for 24h. The control group contains BSA (vehicle). Inset magnifications correspond to 1.5 seconds. Membrane potential was held at -70 mV. B) Examples of averaged mEPSCs (bold lines) from 11, 7 and 5 minutes' time period (vehicle, palmitate and BHB respectively) of the recordings shown in A. The neuron treated with vehicle (left traces) exhibited mean mEPSCs amplitude of –18 pA (average of 2815 miniature events). The neuron treated with palmitate (central traces) exhibited mean mEPSCs amplitude of –12.1 pA (average of 1967 miniature events). The neuron treated with BHB (right traces) exhibited mean mEPSCs amplitude of –18.38 pA (average of 1098 miniature events). 100 random individual mEPSCs (events) for the three recordings are showed in grey. Note that the smaller events are found in the neuron treated with palmitate. C) AMPAR mEPSCs amplitude was decreased in palmitate treated cells compared with vehicle treated (-18.07 ± 1.195 pA; -13.28 ± 1.2 pA and -17.25 ± 1.269 pA for vehicle, palmitate and BHB treated neurons respectively; n=26, 21 and 19 neurons respectively). **p<0.01. Statistical analysis was performed by Student t-test by only comparing each condition with the control. D) Cumulative probability distribution of mEPSCs amplitude showing a leftward shift in amplitude for events of neurons treated with palmitate. Continuous lines represent the average for control (black line; 26 neurons containing an average of 1104 events/neuron) and palmitate (red line; 21 neurons containing an average of 768 events/neuron). Discontinuous lines denote SEM. E) AMPAR mEPSCs frequency was not altered neither with palmitate nor with BHB (5.042 ± 0.923 Hz; 2.816 ± 0.441 Hz and 3.319 ± 0.5306 Hz for vehicle, palmitate and BHB treated neurons respectively; n=26, 21 and 19 neurons respectively too). Statistical analysis was performed by Mann-Whitney test by only comparing each condition with the control. F) AMPAR mEPSCs rise time was not altered neither with palmitate nor with BHB (1.962 ± 0.046 ms; 1.895 ± 0.06 ms and 1.926 ± 0.038 ms for vehicle, palmitate and BHB treated neurons respectively; n=26, 21 and 19 neurons respectively too). Statistical analysis was performed by Mann-Whitney test by only comparing each condition with the control. G) AMPAR mEPSCs τ-weighted was not altered neither with palmitate nor with BHB (3.938 ± 0.213 ms; 4.349 ± 0.347 ms and 4.003 ± 0.207 ms for vehicle, palmitate and BHB treated neurons respectively; n=26, 21

and 19 neurons respectively too). Statistical analysis was performed by Mann-Whitney test by only comparing each condition with the control.

4.2. fEPSPs

After studying the effect of palmitate and BHB on mEPSCs in cortical neurons, synaptic plasticity was explored in hippocampal slices recording field-EPSPs. For these electrophysiological experiments, the stimulating electrode was positioned in stratum radiatum to stimulate SC fibers and the recording electrode, onto CA1 pyramidal neurons (the distance between them was 100 μm). Slices were from P27-P34 mice and were continuously perfused (2 mL/min) with aCSF, carbogen and PTX to block $GABA_A$ receptors. Moreover, they were incubated for 2h with palmitate or BHB before doing any recording. To further explore whether the beneficial effects found with BHB treatment could ameliorate the deleterious ones of palmitate treatment, a special group combining both nutrients was also analyzed.

It is important to reiterate that palmitate is insoluble in water, being necessary the use of BSA as the vehicle. In contrast, BHB is soluble in aqueous solution. Therefore, it was used a control condition without BSA and a vehicle condition with BSA.

After a stable long-term baseline of 15 minutes, LTP was induced using a HFS protocol composed of 2 trains of bursts (100 pulses at 100 Hz with a 10 seconds interval). Two different parameters were measured. On the one hand, the slope which is the steepness of an electrical signal or potential over time. It is useful in understanding the speed of a signal's change. On the other hand, the amplitude which refers to the magnitude or height of an electrical signal. It describes the intensity or strength of a signal. The obtained data (figure 47A-B) prove that there is no any significant difference in LTP when treating slices with palmitate or BHB. Although there is a noticeable disparity between the recordings from the initial 5 minutes and the final 5 minutes in the control, BHB, and palmitate+BHB treated slices, no discernible differences are observed when compared to palmitate's LTP (figure 47C). This lack of effect in synaptic plasticity could be due to the small number of slices recorded (just 3 or 4 per group) and the fact that only a short treatment (2h) could be carried out. However, when the curve of palmitate was compared with the

curve of palmitate+BHB, statistical differences were observed ($p<0.01$, Student t-test), suggesting that the addition of BHB is able to improve the synaptic plasticity of palmitate condition.

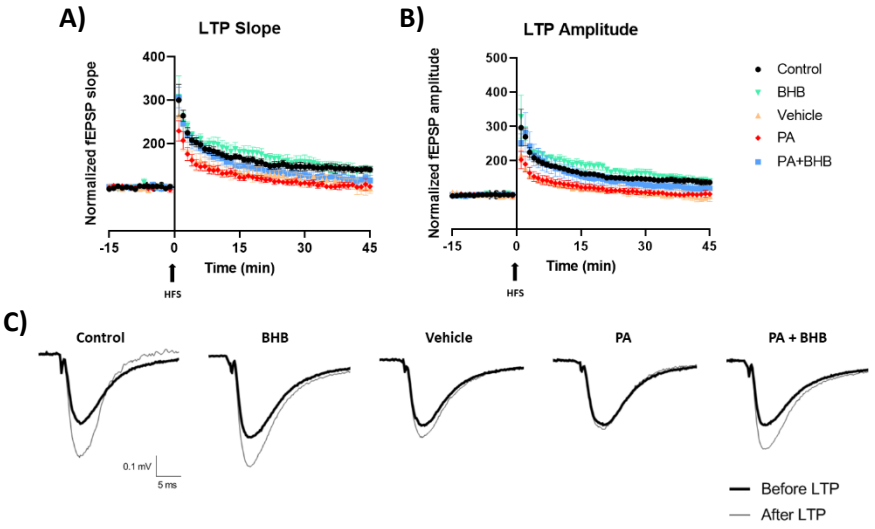

Figure 47. LTP induced by HFS in slices treated with PA, BHB and PA+BHB. A) Time course of normalized slope of AMPAR-mediated EPSCs from baseline and after induction of LTP. B) Time course of normalized amplitude of AMPAR-mediated EPSCs from baseline and after induction of LTP. C) Representative traces before induction (thick lines) and for the last 5 minutes of the time course (thin lines). n = 3-4 slices from four mice per condition. Statistical analysis was performed by two-way ANOVA followed by Bonferroni's post correction.

In order to determine the involvement of presynaptic terminals in synaptic plasticity after incubating with palmitate, BHB or palmitate+BHB, PPRs were calculated from fEPSPs. The findings shown in figure 48 reinforce the idea that the effects of these nutrients are completely postsynaptic as there is not any difference between groups.

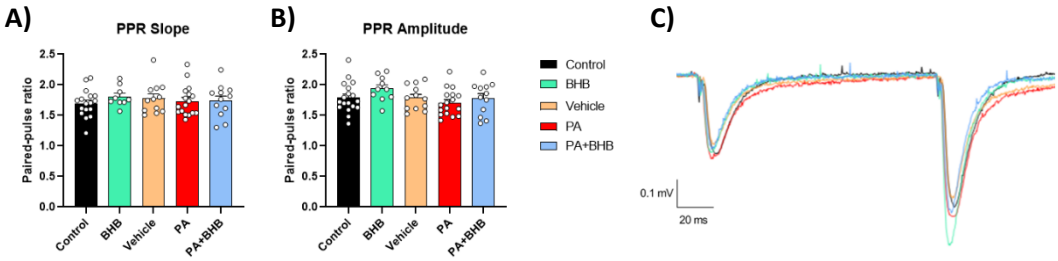

Figure 48. Postsynaptic contributions to fEPSPs. A-B) Average values of PPRs from fEPSP recordings from PA, BHB and PA+BHB treated slices with 100 ms interstimulus interval. Individual values for each condition are displayed as a dot plot. C) Representative traces for each condition. Data are represented as mean ± SEM of 10-18 slices from more than four mice per condition. PPR slope: control (1.697 ± 0.054, n=17), BHB (1.808 ± 0.056; n=9), vehicle (1.778 ± 0.074, n=12), PA (1.733 ± 0.060, n=17) and PA+BHB (1.739 ± 0.077, n=12). PPR amplitude: control (1.789 ± 0.059, n=18), BHB (1.938 ± 0.064; n=10), vehicle (1.786 ± 0.057, n=12), PA (1.707 ± 0.052, n=17) and PA+BHB (1.778 ± 0.077, n=12). Statistical analysis was performed by one-way ANOVA followed by Bonferroni's post correction.

Considering all the effects are occurring at a postsynaptic level, I/O curves were conducted to evaluate how the treatments affect the response of neurons to various levels of stimulation. Figure 49 shows that PA treatment decreases I/O slope and amplitude indicating that this fatty acid diminishes the excitability and the intensity response of neurons while BHB increases them. Interestingly, BHB is able to reverse palmitate negative effects.

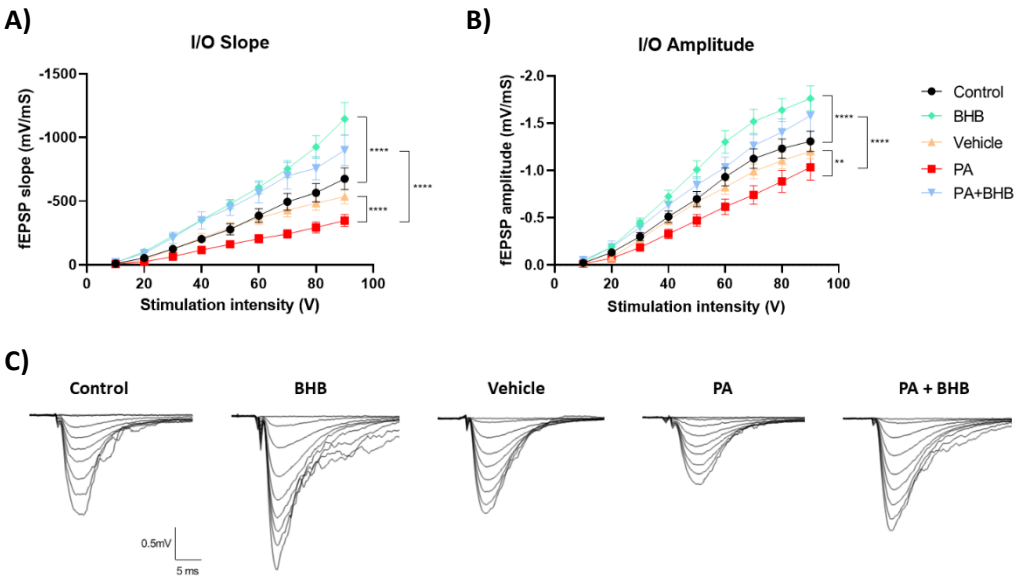

Figure 49. I/O curves in the CA1 region of hippocampal slices. A) The input/output curve plotted with the increased fEPSP slopes corresponding to the enhanced stimulating intensities. B) The input/output curve plotted with the increased fEPSP amplitudes corresponding to the enhanced stimulating intensities. C) Superimposed fEPSP traces induced by a series of stimulating pulses with an increase of 10 V applied to the SC fiber. n = 10-17 slices from more than four male mice (P26±5) per condition. Statistical analysis was performed by two-way ANOVA followed by Bonferroni's post correction. **p<0.01, ****p<0.0001.

To verify that these observed effects can only be attributed to AMPARs and are not influenced by other types of receptors, an AMPA/NMDA ratio was performed. This ratio is calculated by comparing the amplitudes of AMPA-mediated EPSCs and the amplitudes of NMDA-mediated EPSCs. These type of recordings were conducted by Ernesto Griego Melo at the Albert Einstein College of Medicine.

As it can be shown in figure 50, palmitate induced a significant decrease in the AMPA/NMDA ratio. There is not any difference between control and vehicle group. Therefore, the palmitate's I/O curve effects are exclusively due to a decrease in AMPARs, not NMDARs. In the case of BHB, a slight upward tendency can be observed.

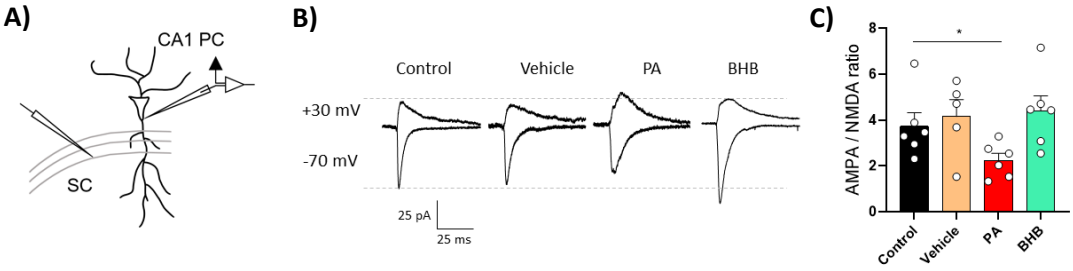

Figure 50. Palmitate decreased AMPA/NMDA ratio at the CA3-CA1 synapse. A) Targeted patch-clamp recordings from CA1 pyramidal cells at stratum radiatum while stimulating SC fibers. B) Representative traces of AMPA and NMDA receptor mediated postsynaptic currents recorded at -70 and +30 mV, respectively. C) Summary bar graph showing the effect of the different treatments on the AMPA/NMDA ratio. Data are represented as mean ± SEM, n=5-6 cells from 3-5 male mice (P26±5) per condition. Control (3.732 ± 0.589, n=6), vehicle (4.158 ± 0.736, n=5), PA (2.245 ± 0.307, n=6) and BHB (4.398 ± 0.655, n=6). Statistical significance was performed by Student t-test by only comparing each condition with the control. *p<0.05. CA1 PC: CA1 pyramidal cell. SC: Schaffer collateral.

Hence, fatty acids and ketone bodies impact postsynaptic functions rather than presynaptic mechanisms. Notably, BHB has demonstrated the capability to counteract the adverse effects induced by the palmitate, leading to the restoration of neuronal excitability in the presence of a stimulating current. However, synaptic plasticity is less affected by the treatments, perhaps due to the relatively brief incubation with the nutrients (2h). Finally, it is noteworthy that these effects are mediated through AMPARs.

4.3. Behavioral tests

Finally, to study whether the beneficial effects of BHB over the palmitate's also affect cognitive levels, we decided to perform *in vivo* experiments. We explored whether daily administration of BHB could reverse the detrimental effects of SFAD on memory tasks' performance. For this purpose, 5 weeks-old mice were fed with SD or SFAD for 7 weeks. At the same time, they were intragastrically administrated with vehicle (equal amount of water) or BHB (100 mg/kg/day). Their weights were monitored to observe the evolution of both male and female mice over 7 weeks of controlled food intake (figure 51). In the case of males, they did show an

increased tendency in their body weight. However, female mice did not have this tendency in weight over time.

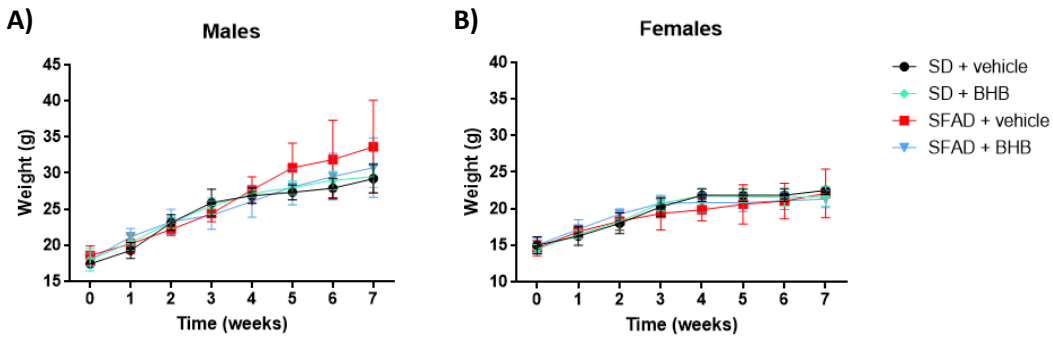

Figure 51. Body weight of male and female mice over 7 weeks fed with SD or SFAD and treated with vehicle or BHB. A) Male mice body weight. B) Female mice body weight. Data are represented as mean ± SD, 5 weeks-old male and female mice, n=5-7/group. Statistical analysis was performed by two-way ANOVA followed by Bonferroni's post correction.

As mentioned before, several behavioral tests were conducted in order to examine the cognitive impact of the diets at the end of the treatment (figure 52). After a habituation period, short-term memory was analyzed with NORT using DI, which is a value that indicates the animal's ability to recognize and remember a previously encountered object. Mice fed with SD and BHB improved their cognitive abilities compared to SD with vehicle. Moreover, animals fed with SFAD showed important cognitive impairments, which were reversed by the concomitant administration of BHB. Long-term memory was also evaluated with NORT. The same results were obtained regarding the SFAD-mediated impairment and BHB restoration. However, no significance differences were found among SD groups.

In addition, spatial learning was evaluated with OLT (figure 52C). A great significant different was found in the DI between SD and SFAD corroborating the negative effects of saturated fatty acids on brain functions. BHB counteracts the detrimental effects of SFAD, while no changes were observed in SD groups. Finally, locomotor activity was also tested with OFT (figure 52D). The ketone body, in the presence of SFAD,

increases the distance travelled by mice compared with the rest of the groups.

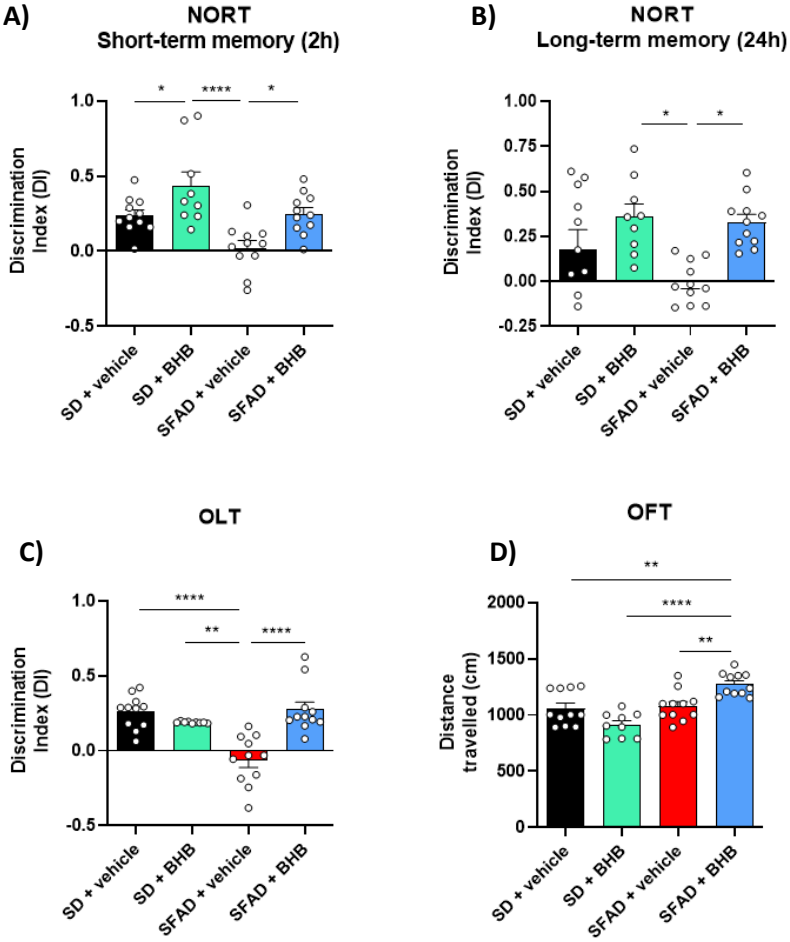

Figure 52. Behavioral results for the novel object recognition test (NORT), object location test (OLT) and open field test (OFT) in male and female mice at 12 weeks-old fed with SD or SFAD and treated with vehicle or BHB. A) Summary of NORT discrimination index (DI) from short-term memory (2h). SD + vehicle (0.240 ± 0.036, n=11), SD + BHB (0.436 ± 0.092, n=9), SFAD + vehicle (0.024 ± 0.048, n=11) and SFAD + BHB (0.250 ± 0.041, n=11). B) Summary of NORT discrimination index (DI) from long-term memory (24h). SD + vehicle (0.176 ± 0.110, n=11), SD + BHB (0.359 ± 0.070, n=9), SFAD + vehicle (-0.006 ± 0.035, n=11) and SFAD + BHB (0.330 ± 0.043, n=11). C) Summary of OLT DI. SD + vehicle (0.260 ± 0.036, n=11), SD + BHB (0.190 ± 0.002, n=9), SFAD + vehicle (-0.061 ± 0.050, n=11) and SFAD + BHB (0.275 ± 0.049, n=11). D) Summary of the distance travelled in OFT. SD + vehicle (1060 ± 46.34, n=11), SD + BHB (913.8 ± 36.30, n=9), SFAD + vehicle (1079 ± 40.34, n=11) and SFAD + BHB (1274 ± 30.57, n=11). Data are represented as mean ± SEM.

Statistical analysis was performed by two-way ANOVA followed by Bonferroni's post correction. *p<0.05, **p<0.01, ****p<0.0001.

These results reveal the translational effect of BHB on cognitive processes. It can counteract the negative impact of a SFAD *in vivo*.

5. The involvement of malonyl-CoA – CPT1C axis in nutrients' effects

Here, we aimed to explore whether malonyl-CoA – CPT1C axis participates in cognitive impairment associated with a high-fat diet. It is well-known that palmitate is an inhibitor of ACC, the enzyme that synthesizes malonyl-CoA (Hunkeler et al., 2018). Taking into account these previous results, it was hypothesized that this axis may contribute to the regulation of AMPAR vesicular trafficking and synaptic plasticity mediated by diet-induced malonyl-CoA fluctuations.

5.1. Enzymes of malonyl-CoA metabolism

To examine whether malonyl-CoA levels could be modified by nutrients, an analysis of upstream pathway was conducted in cortical neurons. The ratio of p(S79)-ACC/ACC was studied as ACC enzyme is the responsible to synthetize malonyl-CoA and it is inactivated by phosphorylation. Moreover, ACC activity can also be modulated by the allosteric binding of specific metabolites, such as acetate, which is an activator, and palmitate, being an inhibitor (Rubink & Winder, 2005). FAS enzyme, whose function is to catalyze the synthesis of long-chain fatty acids from malonyl-CoA, was also studied.

Furthermore, it has been published that phosphorylated CREB and BDNF decreased with HFD (Spinelli et al., 2020), so these two proteins were analyzed too with some treatments. They are related to the regulation of the expression and function of GluA1. On the one hand, CREB is a transcription factor that can regulate the expression of various genes, including those related to glutamate receptors. For instance, activation of CREB can increase the expression of GluA1 contributing to synaptic plasticity and brain function (Middei et al., 2013). On the other hand, BDNF

is a neurotrophic factor which can increase the synthesis and insertion of GluA1 into synapses enhancing communication between neurons (Jung et al., 2020).

As it is shown in figure 53A-D, the presence of palmitate for 2h did not induce any change in the protein levels of ACC, FAS, CREB and BDNF. With a 24h incubation, there was an increase in the ratio p(S79)-ACC/ACC indicating ACC is phosphorylated and the subsequent inhibition of malonyl-CoA synthesis (figure 53E). This suggests that in the presence of palmitate, the synthesis of malonyl-CoA and long-chain fatty acids is halted. Moreover, this agrees with the fact that palmitate directly inhibits ACC enzyme.

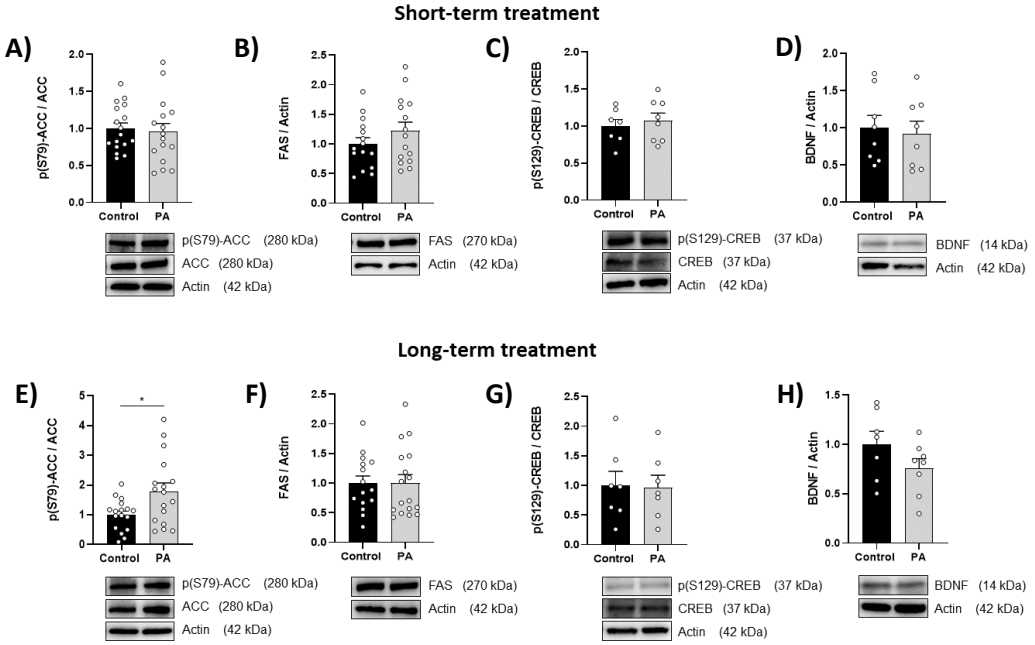

Figure 53. Levels of different proteins with 200 µM palmitate's short-term treatment of 2h (A-D) and long-term treatment of 24h (E-H). Actin was used as housekeeping to normalize protein levels. Data are represented as mean ± SEM, n=7-17 from two (ratio pCREB and BDNF) to four (ratio pACC and FAS) independent experiments. Short-term treatment: ratio of p(S79)-ACC (control: 1.000 ± 0.074, n=17 and PA: 0.954 ± 0.111, n=16), FAS (control: 1.000 ± 0.108, n=15 and PA: 1.222 ± 0.146, n=15), ratio of p(S129)-CREB (control: 1.000 ± 0.088, n=7 and PA: 1.075 ± 0.100, n=8) and BDNF (control: 1.000 ± 0.169, n=8 and PA: 0.926 ± 0.167, n=8). Long-term treatment: ratio of p(S79)-ACC (control: 1.000 ± 0.127, n=17 and PA: 1.791 ± 0.278, n=17), FAS (control: 1.000 ± 0.121, n=15 and PA: 1.003 ± 0.142, n=17), ratio of p(S129)-CREB (control: 1.000 ± 0.235, n=7 and

PA: 0.965 ± 0.208, n=7) and BDNF (control: 1.000 ± 0.133, n=7 and PA: 0.761 ± 0.094, n=8). Statistical significance was performed by Student t-test. *p<0.05.

Nevertheless, the monounsaturated fatty acid led to an increase in p(S79)-ACC with short-term treatment (figure 54A) indicating that the synthesis of malonyl-CoA is partially decreased. However, the levels of FAS were reduced as well (figure 54B), suggesting that malonyl-CoA is not used for fatty acid synthesis and, therefore, some accumulation of the metabolite might occur.

A similar result to that of the short-term treatment was obtained with 24h incubation. Data in figure 54C-D indicate an increase in phosphorylated ACC, which leads to inhibition of malonyl-CoA synthesis and a reduction in FAS levels, which suggest that malonyl-CoA synthesis is decreased, but also its utilization in the subsequent step for fatty acid synthesis. Therefore, it is difficult to infer whether malonyl-CoA levels are changed by oleate treatment.

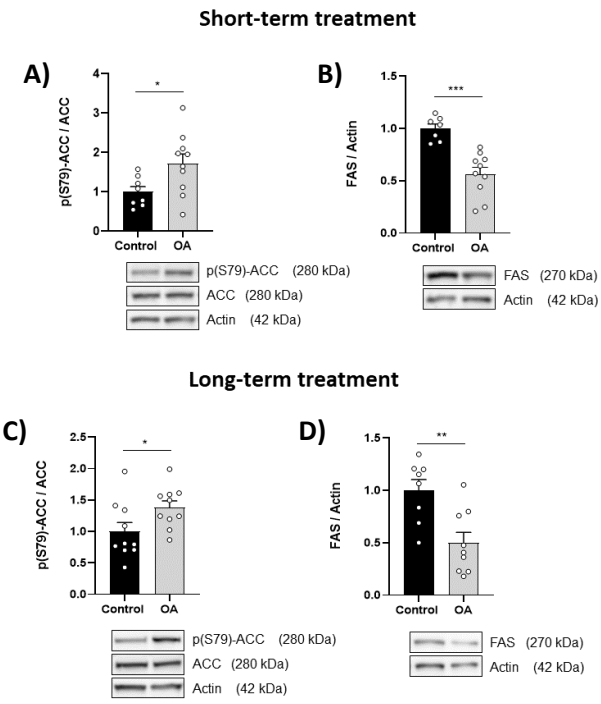

Figure 54. Levels of different proteins with 200 µM oleate's short-term treatment of 2h (A-B) and long-term treatment of 24h (C-D). Actin was used as housekeeping to normalize protein levels. Data are represented as mean ± SEM, n=7-10 from two independent experiments. Short-term treatment: ratio of p(S79)-ACC (control: 1.000 ± 0.133, n=8 and OA: 1.717 ± 0.246, n=10) and FAS (control: 1.000 ± 0.043, n=7 and OA: 0.563 ± 0.066, n=10). Long-term treatment: ratio of p(S79)-ACC (control: 1.000 ± 0.143, n=10 and OA: 1.382 ± 0.104, n=10) and FAS (control: 1.000 ± 0.104, n=8 and OA: 0.498 ± 0.102, n=9). Statistical significance was performed by Student t-test. *p<0.05, **p<0.01, ***p<0.001.

In the case of the polyunsaturated fatty acid, the DHA's incubation for 2h did not result in any modification in protein levels of ACC, FAS, CREB and BDNF (figure 55). Strikingly in figure 55E-H, the same results were obtained indicating that there is not any change in the synthesis of malonyl-CoA.

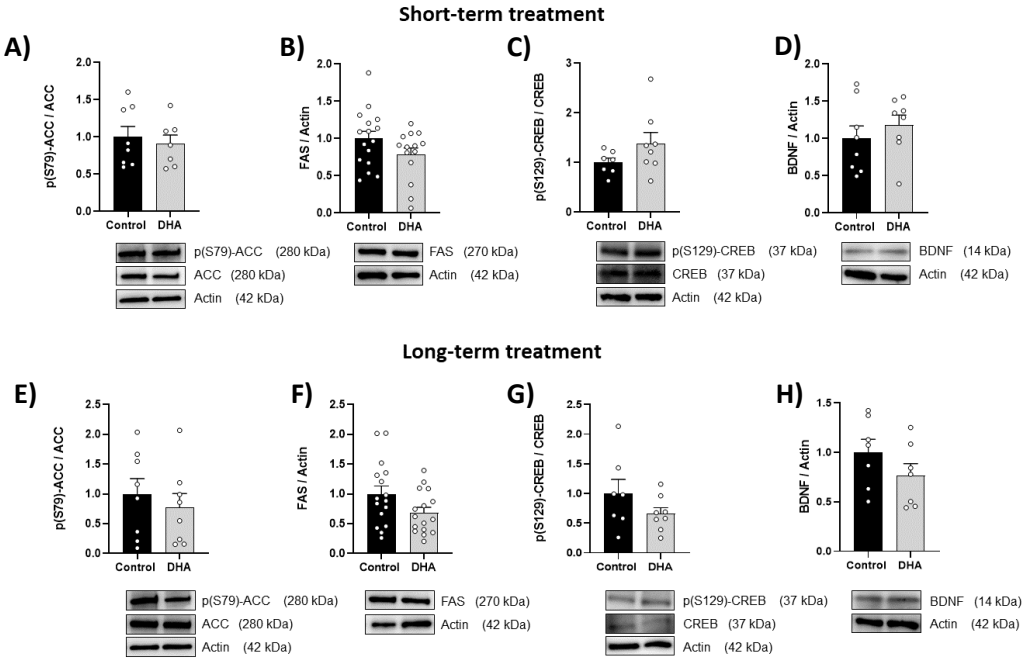

Figure 55. Levels of different proteins with 200 µM DHA's short-term treatment of 2h (A-D) and long-term treatment of 24h (E-H). Actin was used as housekeeping to normalize protein levels. Data are represented as mean ± SEM, n=7-16 from two (ratio pACC, ratio pCREB and BDNF) to four (FAS) independent experiments. Short-term treatment: ratio of p(S79)-ACC (control: 1.000 ± 0.141, n=8 and DHA: 0.909 ± 0.117, n=7), FAS (control: 1.000 ± 0.096, n=16 and DHA: 0.782 ± 0.091, n=14), ratio of p(S129)-CREB (control: 1.000 ± 0.088, n=7 and DHA: 1.384 ± 0.222, n=8) and BDNF (control: 1.000 ± 0.169, n=8 and DHA: 1.179 ± 0.136, n=8). Long-term treatment: ratio of p(S79)-ACC (control: 1.000 ± 0.257, n=8 and DHA: 0.775

± 0.232, n=8), FAS (control: 1.000 ± 0.135, n=16 and DHA: 0.687 ± 0.089, n=16), ratio of p(S129)-CREB (control: 1.000 ± 0.235, n=7 and DHA: 0.658 ± 0.103, n=8) and BDNF (control: 1.000 ± 0.133, n=7 and DHA: 0.765 ± 0.121, n=7). Statistical significance was performed by Student t-test. *p<0.05.

As indicated in figure 56A-D, data reveal that with short-term BHB treatment, none of the proteins are modified either. In the case of 24h incubation, FAS levels decreased suggesting a possible inhibition in the long-chain fatty acids synthesis and, consequently, an accumulation of malonyl-CoA, the substrate of FAS.

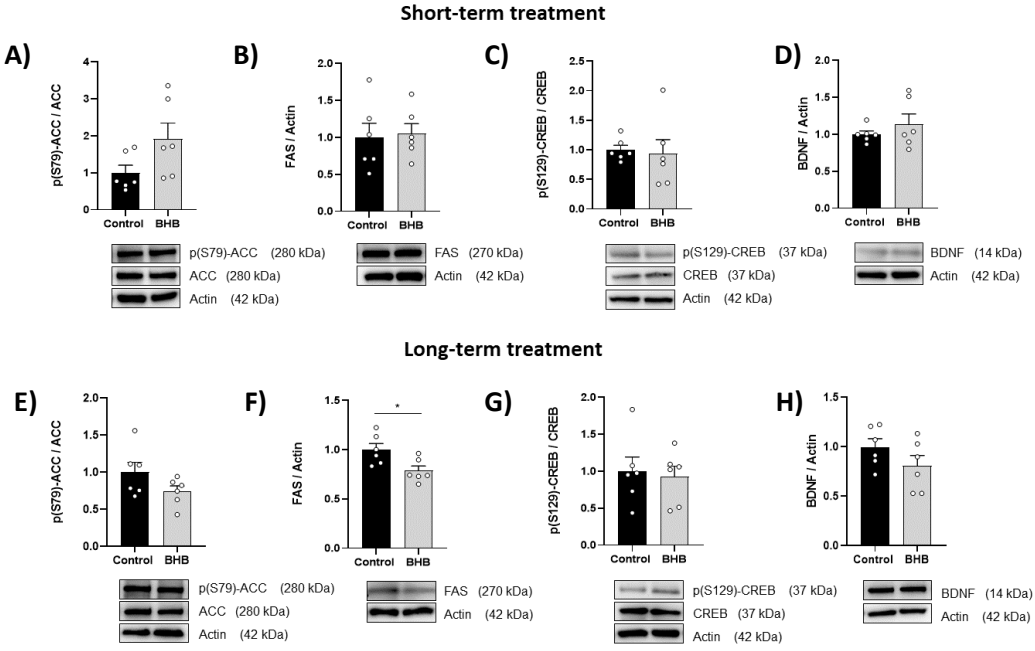

Figure 56. Levels of different proteins with 5 mM BHB's short-term treatment of 2h (A-D) and long-term treatment of 24h (E-H). Actin was used as housekeeping to normalize protein levels. Data are represented as mean ± SEM, n=6 from two independent experiments. Short-term treatment: ratio of p(S79)-ACC (control: 1.000 ± 0.206, n=6 and BHB: 1.920 ± 0.427, n=6), FAS (control: 1.000 ± 0.190, n=6 and BHB: 1.050 ± 0.136, n=6), ratio of p(S129)-CREB (control: 1.000 ± 0.077, n=6 and BHB: 0.934 ± 0.241, n=6) and BDNF (control: 1.000 ± 0.044, n=6 and BHB: 1.138 ± 0.136, n=6). Long-term treatment: ratio of p(S79)-ACC (control: 1.000 ± 0.135, n=6 and BHB: 0.741 ± 0.076, n=6), FAS (control: 1.000 ± 0.063, n=6 and BHB: 0.787 ± 0.048, n=6), ratio of p(S129)-CREB (control: 1.000 ± 0.191, n=6 and BHB: 0.922 ± 0.147, n=6) and BDNF (control: 1.000 ± 0.202, n=6 and BHB: 0.808 ± 0.255, n=6). Statistical significance was performed by Student t-test. *p<0.05.

In summary, results suggest that malonyl-CoA levels in cultured neurons might be decreased by palmitate, while they might be increased by BHB (table 14). This data agrees with the fact that palmitate decreases the trafficking of GluA1 to the plasma membrane, whereas BHB increase it.

Table 14. Summarized protein levels regarding the upstream malonyl-CoA – CPT1C pathway.

Treatment	Protein	Short-term treatment (2h)	Long-term treatment (24h)	Putative malonyl-CoA levels
PA	p(S79)-ACC/ACC	=	↑	**↓**
	FAS	=	=	
	p(S129)-CREB/CREB	=	=	
	BDNF	=	=	
OA	p(S79)-ACC/ACC	↑	↑	**=**
	FAS	↓	↓	
	p(S129)-CREB/CREB	-	-	
	BDNF	-	-	
DHA	p(S79)-ACC/ACC	=	=	**=**
	FAS	=	=	
	p(S129)-CREB/CREB	=	=	
	BDNF	=	=	
BHB	p(S79)-ACC/ACC	=	=	**↑**
	FAS	=	↓	
	p(S129)-CREB/CREB	=	=	
	BDNF	=	=	

5.2. Modulation of malonyl-CoA levels

It has been corroborated in our group that a decrease of malonyl-CoA by the ACC inhibitor, 5-tetradecyloxy-2-furoic acid (TOFA), reduces surface GluA1 levels with only 2h. However, it can be toxic for cells within a long-term incubation (Casas et al., 2020).

To continue exploring whether malonyl-CoA – CPT1C axis is involved in PA or BHB effects, cortical neurons were silenced with a lentiviral vector carrying either a control (shRandom) or CPT1C-silencing sequence (shCPT1C) at 7 DIV. As it can be seen in figure 57, shCPT1C viruses can inhibit the production of this protein in infected cells in about 50%.

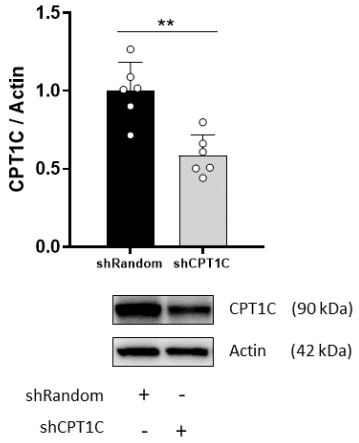

Figure 57. CPT1C-silencing verification in cortical neurons. Representative image of CPT1C levels quantified by Western blot. Cortical neurons were infected at 7 DIV with 1 MOI of either shRandom or shCPT1C. CPT1C-silencing was checked at 14 DIV. Data are represented as mean ± SEM, n=6 from two independent experiments. shRandom (1.000 ± 0.184, n=6) and shCPT1C (0.588 ± 0.131, n=6). Statistical significance was performed by Student t-test. **p<0.01.

Once the silencing was checked, primary cortical neurons were infected with shRandom or shCPT1C viruses at 7 DIV. After another week, cells were treated with 200 µM palmitate, 200 µM malonyl-CoA or both for 24h.

Figure 58 shows (in green) that all selected neurons to be analyzed were infected with viruses. On the one hand (part A), palmitate treatment decreased surface GluA1 in agreement with the previous result (figure 37A). Moreover, malonyl-CoA showed that it can increase them. However, malonyl-CoA treatment was no able to reverse palmitate's effects on surface GluA1.

On the other hand, in cells where CPT1C was downregulated (part B), palmitate still decreased surface GluA1 levels, although the effect was not significant (p=0.0996). In absence of CPT1C, malonyl was able to enhance surface GluA1 levels and reverse the impact of palmitate. Overall, these data indicate that palmitate's effect on surface GluA1 is independent of the malonyl-CoA – CPT1C pathway.

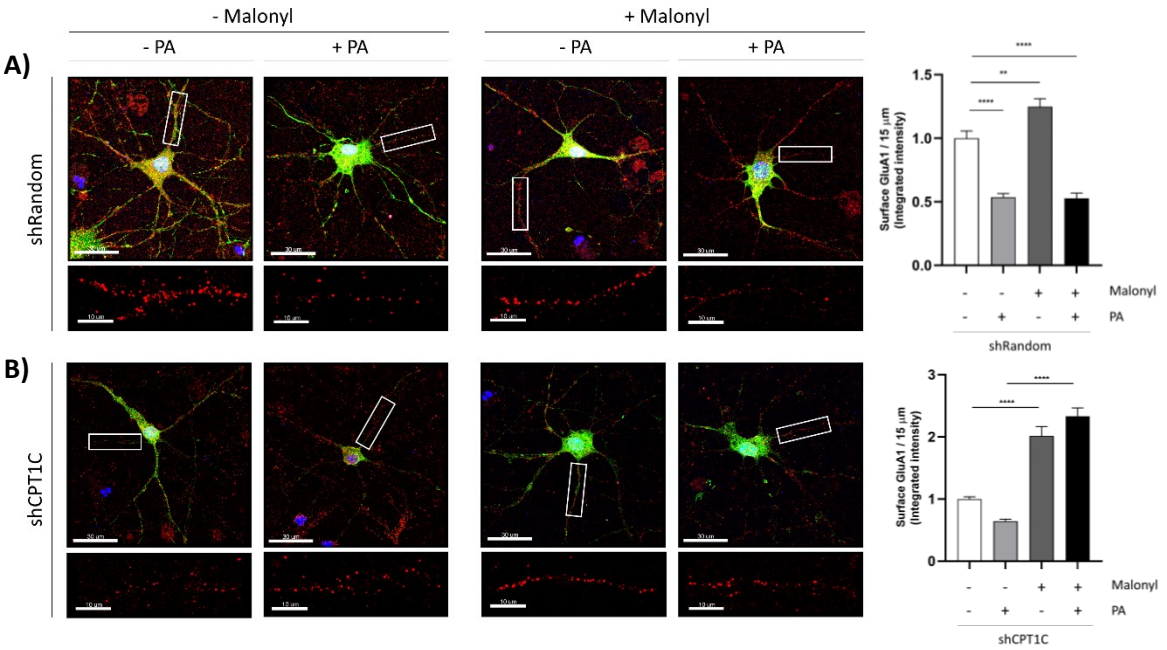

Figure 58. Palmitate's and malonyl-CoA's long-term effects on surface GluA1 in cortical neurons with or without the presence of CPT1C. A) Surface GluA1 quantified by immunocytochemistry in cortical neurons (n=45 cells) under 24h palmitate (200 µM) and malonyl (200 µM) treatment. Control (1.000 ± 0.058, n=98), PA (0.537 ± 0.028, n=101), malonyl-CoA (1.250 ± 0.062, n=102) and malonyl-CoA + PA (0.528 ± 0.040, n= 82). B) Surface GluA1 quantified by immunocytochemistry in CPT1C silenced cortical neurons (n=45 cells) under 24h palmitate (200 µM) and malonyl (200 µM) treatment. Control (1.000 ± 0.036, n=107), PA (0.643 ± 0.035, n=76), malonyl-CoA (2.017 ± 0.149, n=98) and malonyl-CoA + PA (2.331 ± 0.1136, n= 80). Scale bar = 30 µm; scale bar of inset magnifications = 10 µm. Hoechst was used to detect nuclei. Results of integrated intensity in 15 µm of primary dendrites were normalized by the control treatment. Data are represented as mean ± SEM of 90 dendrites from three independent experiments. Statistical analysis was performed by one-way ANOVA followed by Bonferroni's post correction. **p<0.01, ****p<0.0001.

In the case of BHB, it was also checked that all neurons were infected with viruses (figure 59). As it has been demonstrated before (figure 36A), BHB treatment for 2h in control neurons increased surface GluA1. It is also observed a reduction in surface GluA1 caused by TOFA treatment. When both treatments were applied at the same time, TOFA blocked the actions of BHB, suggesting that BHB's effects could be mediated by malonyl-CoA

– CPT1C axis. Accordingly, when CPT1C was downregulated (figure 59B), the effects of ketone body were blunted. Therefore, data suggest that BHB's effects on surface GluA1 levels can be mediated by the malonyl-CoA – CPT1C pathway.

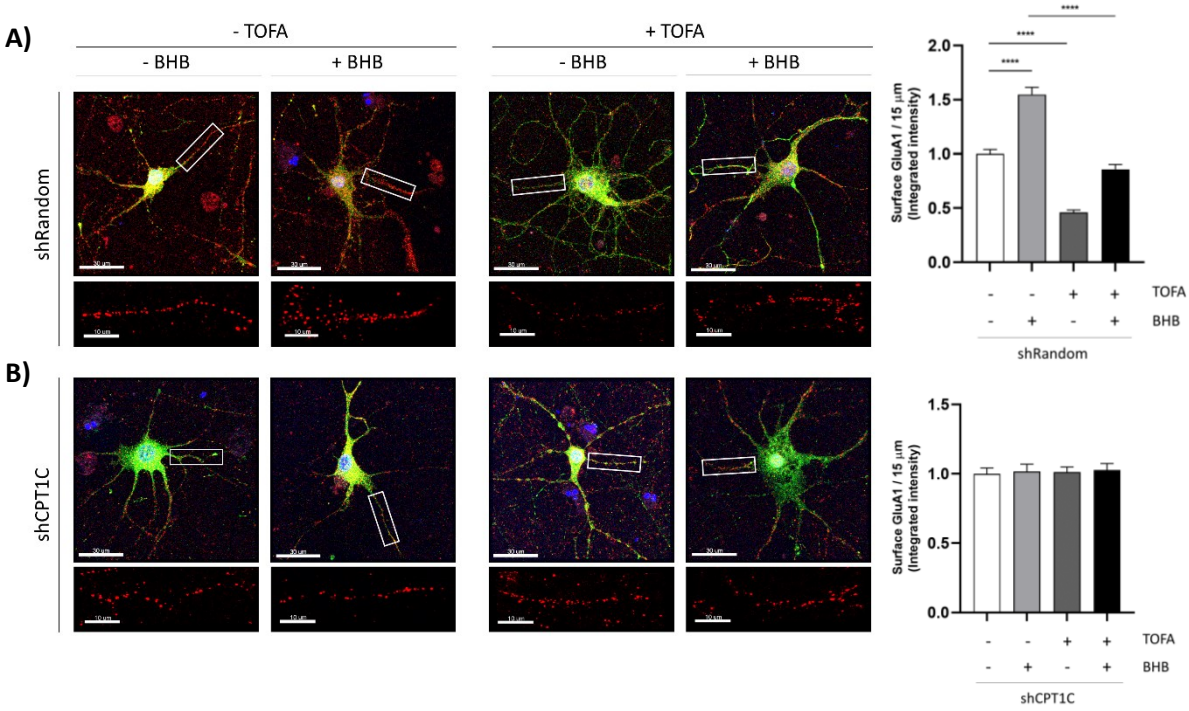

Figure 59. BHB's and TOFA's short-term effects on surface GluA1 in cortical neurons with or without the presence of CPT1C. A) Surface GluA1 quantified by immunocytochemistry in cortical neurons (n=45 cells) under 2h BHB (5 mM) and TOFA (20 µg/mL) treatment. Control (1.000 ± 0.040, n=78), BHB (1.548 ± 0.065, n=73), TOFA (0.461 ± 0.022, n=80) and TOFA + BHB (0.858 ± 0.044, n= 73). B) Surface GluA1 quantified by immunocytochemistry in CPT1C silenced cortical neurons (n=45 cells) under 2h BHB (5 mM) and TOFA (20 µg/mL) treatment. Control (1.000 ± 0.042, n=82), BHB (1.017 ± 0.053, n=73), TOFA (1.011 ± 0.038, n=84) and TOFA + BHB (1.027 ± 0.048, n= 76). Scale bar = 30 µm; scale bar of inset magnifications = 10 µm. Hoechst was used to detect nuclei. Results of integrated intensity in 15 µm of primary dendrites were normalized by the control treatment. Data are represented as mean ± SEM of 90 dendrites from three independent experiments. Statistical analysis was performed by one-way ANOVA followed by Bonferroni's post correction. ****p<0.0001.

6. Results summary of chapter I

This chapter has focused on the impact that fatty acids and ketone bodies have on surface GluA1 levels, synaptic transmission and cognition. Firstly, their effects have been analyzed *in vivo* (mice) and then, *in vitro* (primary culture of neurons and brain slices). Also the role of malonyl-CoA – CPT1C axis in nutrients' effects has been explored. Results are summarized in figure 60.

Diets (HFD, SFAD and MUFAD) have not shown a strong impact on GluA1 and its phosphorylation in residues of serine 845 and 831 in mice cortex and hippocampus. Moreover, *in vitro* cortical neurons have been treated with different nutrients considered as diets' analogues. The results obtained are more significant with a long-term incubation than with a short-term one. The saturated fatty acid (palmitate) decreases surface GluA1, while the unsaturated fatty acids (oleate and DHA) and the ketone body (BHB) increase them. Moreover, differentiated SH-SY5Y cells mimic these results being a suitable alternative model for the study.

Palmitate has the capacity to decrease both surface and synaptic levels of GluA1, whereas BHB only increases surface levels without affecting synaptic ones. This implies that palmitate exerts a pronounced detrimental effect, while BHB demonstrates a partially beneficial effect. BHB does not directly increase synaptic levels but ensures that GluA1 is readily available on the surface, enabling rapid synaptic delivery when required. This important contribution to GluA1 availability could explain BHB capacity to counteract PA deleterious effects, as demonstrated also through electrophysiological recordings. In addition, *in vivo* results showed that SFAD-fed mice improved memory performance due to BHB administration.

Regarding malonyl-CoA – CPT1C axis, the reversion experiments showed that palmitate's impact is not mediated by this pathway. This fact implies that there are others, more significant mechanisms at play, such as the palmitoylation of GluA1. However, it appears that the malonyl-CoA – CPT1C axis does play a role in mediating the effects of BHB, at least to some extent.

Altogether, there is evidence that palmitate and BHB can modulate synaptic transmission. Although saturated fatty acid, like palmitate,

presents a detrimental effect on AMPA receptors, BHB can counteract it through the regulation of surface GluA1.

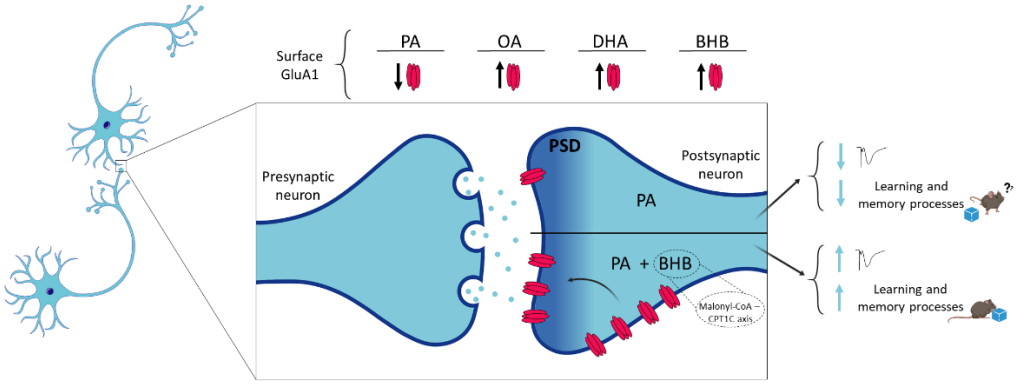

Figure 60. Graphical abstract of chapter I. Main results of the study of the impact of fatty acids and ketone body on synaptic transmission. PA decreases synaptic GluA1, whereas BHB increases surface GluA1.

Chapter II

Study of SAC1-CPT1C interaction

As it was mentioned in the introduction section, SAC1 and CPT1C proteins are able to interact regulating several processes within neurons (Brechet et al., 2017). However, the interacting region of both proteins is still unknown. Dr. José Luis Domínguez Mejide, a bioinformatician from Núria Casals's group, conducted *in silico* experiments to simulate the interaction between these two proteins, using cytosolic SAC1 (residues from 1 to 520) and the N-terminal domain of CPT1C (residues from 1 to 52). This approach suggested that residues 331-333 of SAC1's N-terminal region interact with residues 13-15 of CPT1C's N-terminal domain (data not published).

In this chapter, we wanted to explore which regions of the SAC1 protein are involved in the binding with CPT1C. Therefore, to address it, deletions of the N-terminal region of SAC1 were performed. The interaction was studied with two different experimental approaches: 1) FRET and 2) pull-down.

1. Validation of SAC1's constructs

SAC1's constructs were developed as described in methodology (see section 3.2.). The first step was to verify that the truncated proteins were expressed correctly in transfected cells and to check their cellular localization. For this purpose, HEK293T were transfected and, after 2 days, a western blot was conducted. This validation was very important because some truncated proteins do not express in an appropriate way.

The initial approach was the positioning of the fluorescent tag (mTurquoise2) after SAC1 protein in the C-terminus. For this purpose, HEK293T were transfected with 3 constructs: C1 (1-587aa, the full-length protein), C2 (89-587aa, deletion of the first 88 aa), and C3 (189-587aa, deletion of the first 188 aa). Despite the fact that SAC1(C1)-mTurquoise2 is completely expressed (it is the full-length protein as mentioned before), the western blot analysis revealed no expression for the truncated C2 and C3 variants (figure 61). This suggested that the combination of SAC1 truncations in the N-terminal domain with a tag in the C-terminus results in impaired expression of the recombinant proteins.

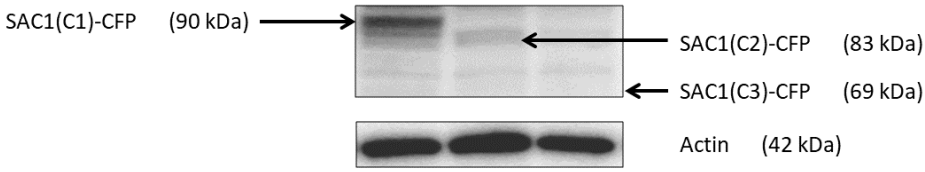

Figure 61. Expression of SAC1's truncated proteins with the fluorescent tag in the C-terminus in transfected HEK293T. Western blot was conducted for three constructs: C1 (1-587aa), C2 (89-587aa) and C3 (189-587aa). Actin was used as a housekeeping protein to verify that the same amount of protein was charged.

The absence of protein expression upon cell transfection with the truncated variants can be attributed to potential disruptions in the protein's structural integrity or in its essential functional domains. Truncations may lead to misfolding, improper localization, impaired interactions with binding partners or quick degradation due to the loss of stabilizing motifs. These factors collectively contribute to the observed absence of protein expression, underscoring the intricate relationship between protein structure, function and cellular context.

On the other hand, FRET interaction studies between full-length proteins CPT1C-mTurq2 and SAC1-EYFP were performed and no interaction was observed (figure 62) suggesting that the position of the tag at the C-terminal region of SAC1 was causing some kind of stearic impediment for the proper interaction.

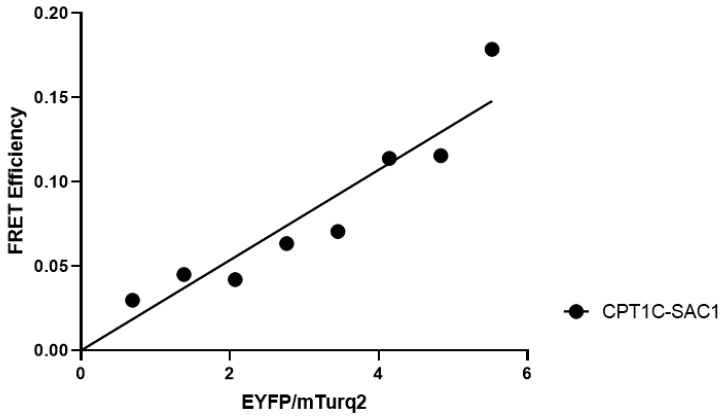

Figure 62. FRETse of CPT1C-mTurq2 and SAC1-EYFP in living cells. The experiments were conducted 48 hours after transfection in HEK293T cells expressing full-length CPT1C-mTurq2 using increasing amounts of SAC1-EYFP plasmidic DNA.

Subsequently, it was decided to place the fluorescent tag at the N-terminal domain of SAC1. HEK293T were transfected with the 7 new constructs: C1 (1-587aa, the full-length protein), C2 (89-587aa), C3 (189-587aa), C4 (275-587aa), C5 (378-587), C6 (436-587aa) and C7 (520-587aa). Figure 63 shows a scheme of all the constructs. It is important to take into account that each construct is smaller than the previous one, so the amount of plasmid used was adjusted to moles.

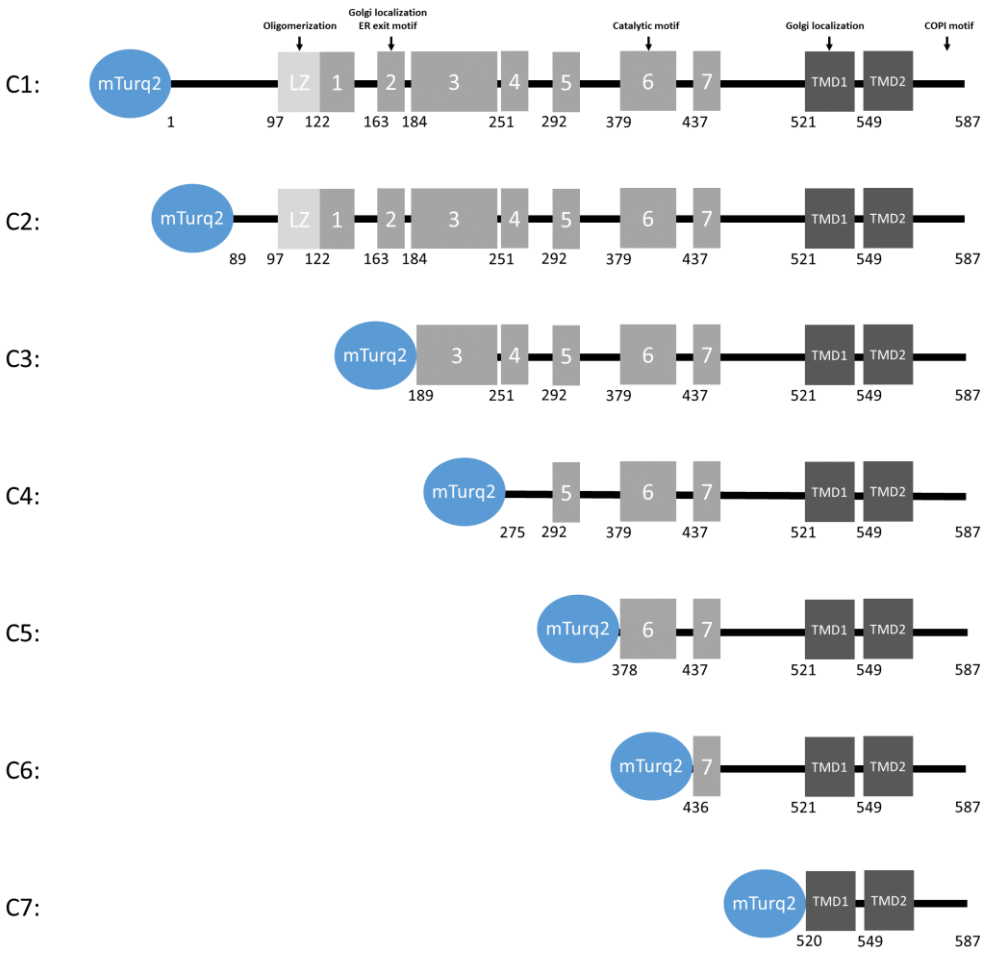

Figure 63. Schematic representation of SAC1 protein domains of the different constructs: C1 (1-587aa), C2 (89-587aa), C3 (189-587aa), C4 (275-587aa), C5 (378-587), C6 (436-587aa) and C7 (520-587aa). mTurq2 was added to the N-terminal region as fluorochrome. Numbers 1-7 refer to conserved motifs in the phosphatase domain. LZ: leucine zipper. TMD: transmembrane domain.

As it can be observed in figure 64, all constructs were well-expressed with this second approach. However, they were expressed in different quantities although the same amount of plasmid (in moles) was used for all the transfections. In addition, the full-length SAC1 (C1) has a higher expression that the other proteins. Unexpectedly, the smallest protein (C7) was highly expressed too although it completely lacks the N-terminal region.

The molecular weights shown in figure 64 correspond to those of the specific proteins together with mTurq2, the fluorescent protein fused to SAC1 constructs, whose molecular weight is 25 kDa.

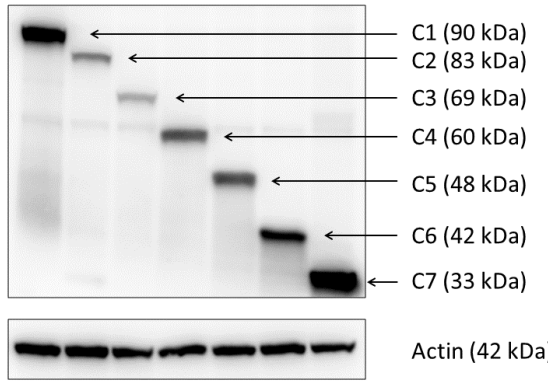

Figure 64. Expression of SAC1's truncated proteins with the fluorescent tag in its N-terminus in transfected HEK293T. Western blot was conducted for the seven constructs from C1 to C7: C1 (1-587aa), C2 (89-587aa), C3 (189-587aa), C4 (275-587aa), C5 (378-587), C6 (436-587aa) and C7 (520-587aa). Actin was used as a housekeeping protein to verify that the same amount of protein was charged.

It is important to take into account that not only a correct expression of SAC1 constructs must be corroborated, but also the right subcellular localization. For this purpose, cells were visualized under confocal microscopy after immunocytochemistry against mTurq2 (detected by an anti-GFP antibody) and calnexin, an ER resident protein.

As shown in figure 65, SAC1 and the truncated proteins showed a reticular pattern suggesting an ER localization. This agrees with the fact that all constructs maintain the two transmembrane domains. In all the cases a partial colocalization with the ER marker calnexin was observed, suggesting that SAC1 and the truncated proteins are also found in other organelles such as the Golgi apparatus, as expected for SAC1 protein. In

any case, the localization pattern of all the constructs was very similar. These results indicate that partial or complete deletion of SAC1 N-terminal domain does not dramatically change protein localization.

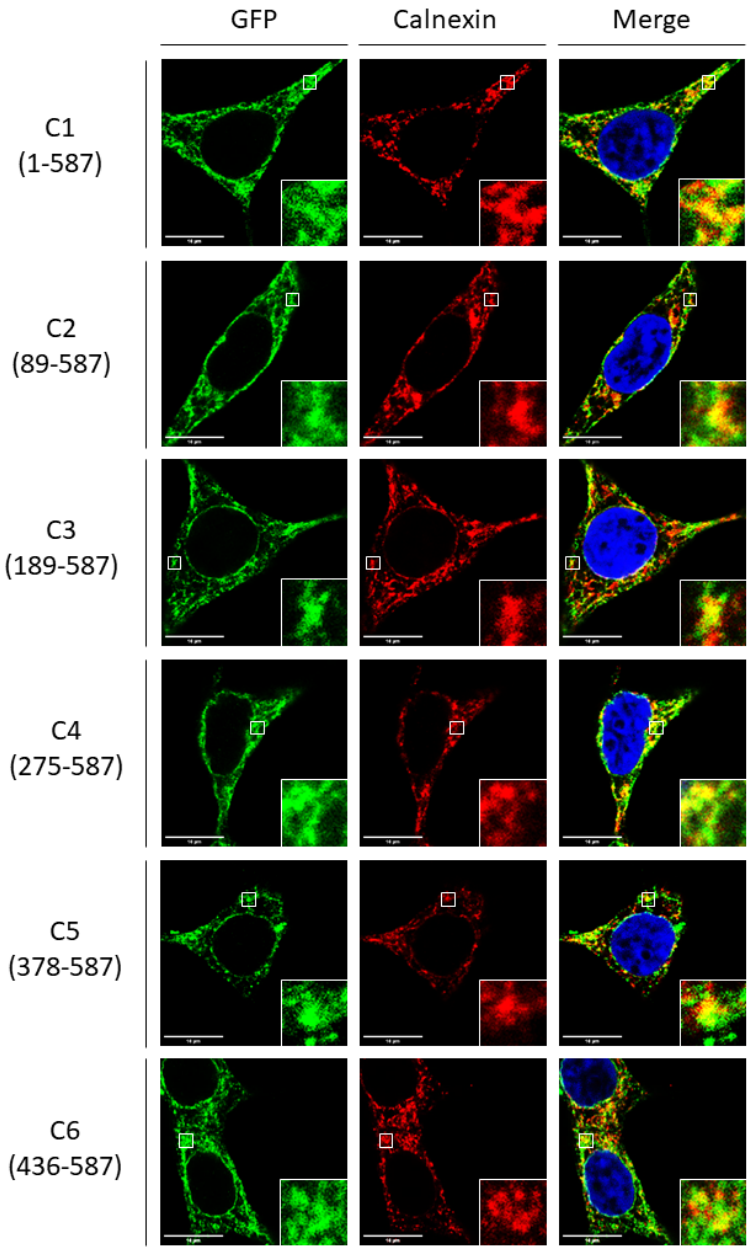

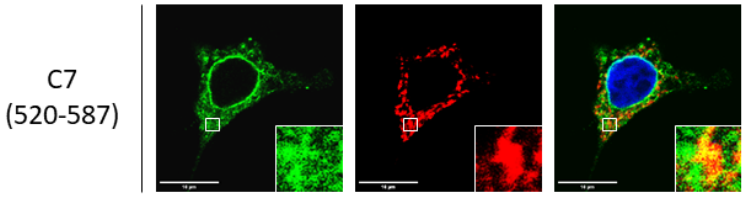

Figure 65. Representative images of the different constructs of SAC1. HEK293T were transfected with the same amount in moles of the different constructs. Immunocytochemistry was conducted against GFP, calnexin and Hoechst to detect SAC1, ER and nucleus, respectively. Scale bar = 10 µm. The crop images correspond to a cytoplasmic area where the co-localization of the proteins can be observed.

2. Region of SAC1 interacting with CPT1C

2.1. Analysis of interaction via FRET

To start exploring the specific region of SAC1 that interacts with the CPT1C, first of all, a FRETap approach was conducted. This technique is based on the increase in donor fluorescence after the complete acceptor photobleaching in a specific area of the fixed cell. To carry out the experiment it was necessary to use controls transfecting cells with only one fluorophore either the acceptor (in this case, CPT1C-EYFP) or the donor (in this case, mTurq2-SAC1 or the truncated forms). Once established the conditions to conduct the photobleaching, the images were taken.

The figure 66 shows the images where a region of the cells was photobleached in the acceptor channel (yellow) and the fluorescence intensity for the donor channel (blue) increased. KDEL and Sec61 were used as negative controls of the interaction with CPT1C. Sec61 is an ER-resident protein, whereas KDEL is a target peptide sequence that drives proteins to the ER.

Results demonstrate that the three constructs of SAC1 interact with CPT1C in the same way. However, this FRET approach is not sensitive enough because one of the negative controls did not exhibit significant differences compared to C1, which was used as a positive control. Furthermore, a significant internal variability was observed in each construct. Even though, significant differences between the truncated proteins and the

negative controls suggest that the initial 188 amino acids of SAC1 may not be the responsible for the interaction with CPT1C.

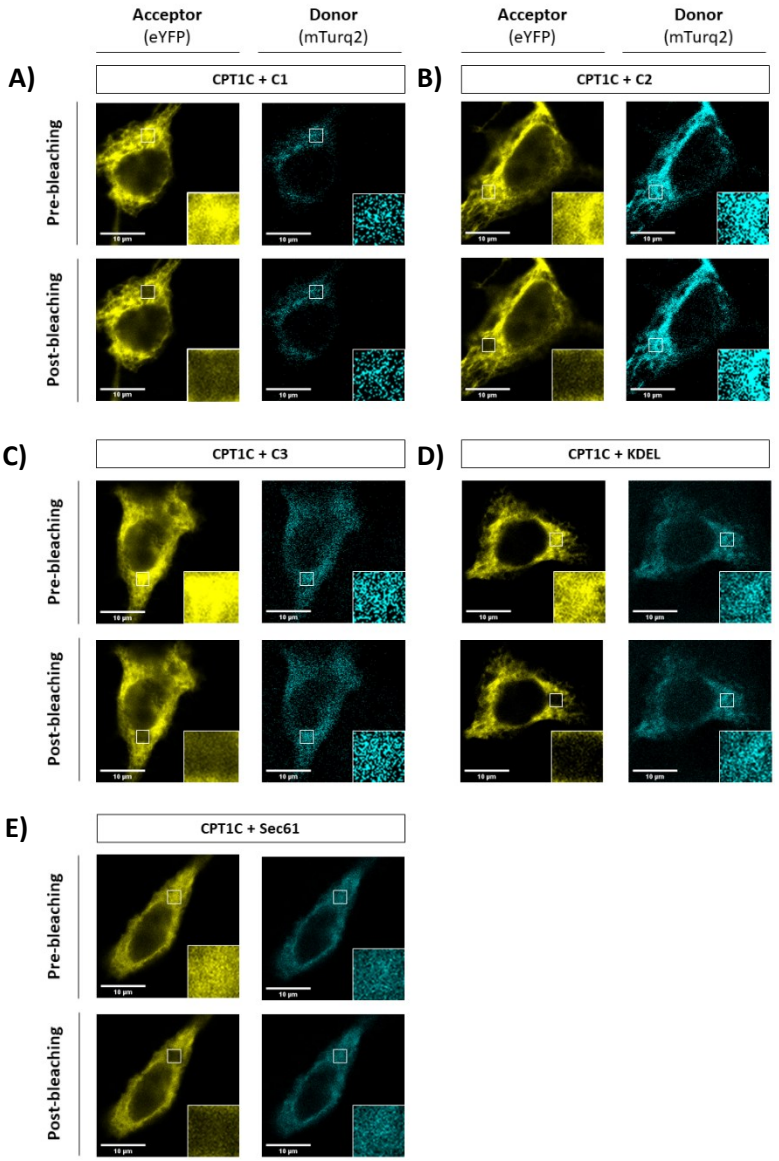

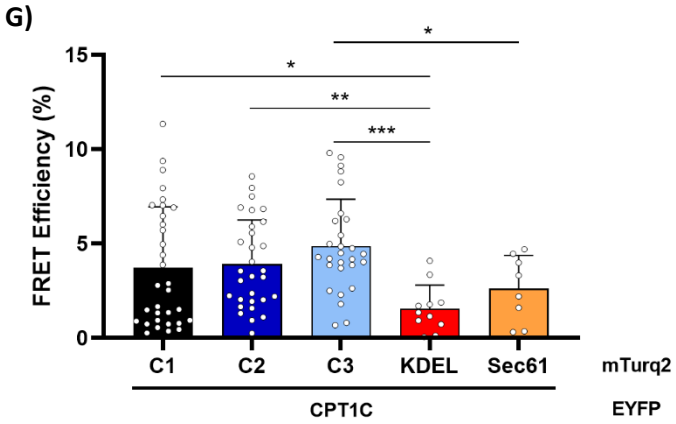

Figure 66. FRET acceptor photobleaching examining the SAC1 (C1, C2, C3)-CPT1C interaction. A-F) Representative images of FRET efficiency. Scale bar = 10 µm. G) FRET efficiency of CPT1C-EYFP with mTurq2-SAC1(C1), mTurq2-SAC1(C2) and mTurq2-SAC1(C3); and with mTurq2-KDEL, mTurq2-Calnexin and mTurq2-Sec61 as negative FRET interactions. Percentage of FRET was measured by the increase in donor intensity after photobleaching (n=8-32). Data are represented as mean ± SD. The results are from one (Sec61) to three independent experiments. *p<0.05, **p<0.01, ***p<0.001 indicate a significant difference. Statistical significance was performed by Student t-test by only comparing each condition with the corresponding negative control.

Then, a more precise alternative approach was chosen for further investigating the interaction: the FRETse technique. This assay was performed in order to detect interactions too, but unlike the previous approach, which involved the photobleaching of fixed cells, FRETse uses live cells without any photobleaching. The obtained result is a saturated curve when interaction occurs and a linear pattern when it does not. Moreover, this approach had already been used in our group to assay the interaction between CPT1C and another partner, ABHD6 (Miralpeix et al., 2021).

For this purpose, HEK293T cells were transfected with different acceptor and donor proteins to validate the interaction between SAC1 and CPT1C using this approach. ABHD6 was used as positive interactor of CPT1C, while KDEL and Sec61 were used as negative controls.

Results demonstrate that, as expected, the FRETse efficiency between the pair SAC1/CPT1C and SAC1/ABHD6 was higher compared to the negative

control pairs KDEL/CPT1C and Sec61/CPT1C (figure 67). Moreover, the curve of positive interactors becomes saturated, whereas the ones of negative interactors does not. The FRETse curve observed for SAC1/CPT1C interaction is not significantly different from the ABHD6/CPT1C curve, indicating that SAC1-CPT1C interaction can be effectively addressed using this approach.

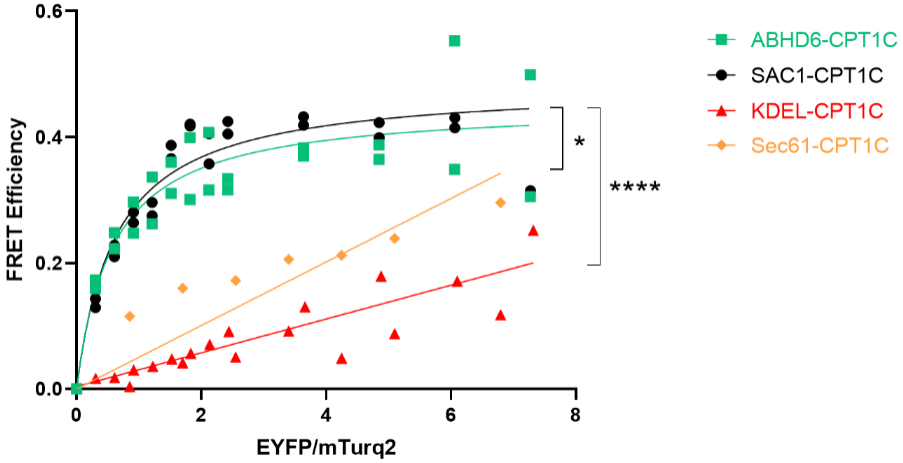

Figure 67. Full-length SAC1 interacts with CPT1C by FRETse. FRETse of CPT1C with either ABHD6, SAC1, KDEL or Sec61 in living cells. The experiments were conducted 48 hours after transfection of HEK293T cells. Cells were transfected with plasmids coding for ABHD6-mTurq2, mTurq2-SAC1, mTurq2-KDEL and mTurq2-Sec61 as donor proteins, and with increasing amounts of CPT1C-EYFP as an acceptor protein. The results are from one to four independent experiments (Sec61-CPT1C one experiment, KDEL-CPT1C three experiments, ABHD6-CPT1C and SAC1-CPT1C four experiments). *p<0.05, ****p<0.0001 indicates a significant difference. Statistical significance was performed by one-way ANOVA followed by Bonferroni's post correction test.

Then, the study between SAC1 truncated constructs and full-length CPT1C was conducted with FRETse assay. As it can be observed in figure 68, the N-terminal domain of SAC1 seems not to be the responsible for the interaction with CPT1C because all the results draw a curve, the characteristic of a positive interaction. Negative interactions result in a lineal pattern.

Nevertheless, the curve representing FRET efficiency between SAC1(C7) and CPT1C shows a significant difference comparing to the full-length SAC1(C1). SAC1(C7) protein seems to have a lower interaction with CPT1C. However, in SAC1(C7) construct, the fluorescent tag is positioned extremely close to the transmembrane domains, perhaps reducing its mobility or sterically interfering with SAC1-CPT1C interaction. It cannot be ruled out that these differences in FRETse between SAC1(C1) and SAC1(C7) are false negative, related with the chosen experimental approach. Moreover, comparing FRET efficiency of SAC1(C7)-CPT1C with the negative controls (KDEL-CPT1C or Sec61-CPT1C), statistical differences are found (figure 68B), suggesting that SAC1(C7) is still able to bind CPT1C.

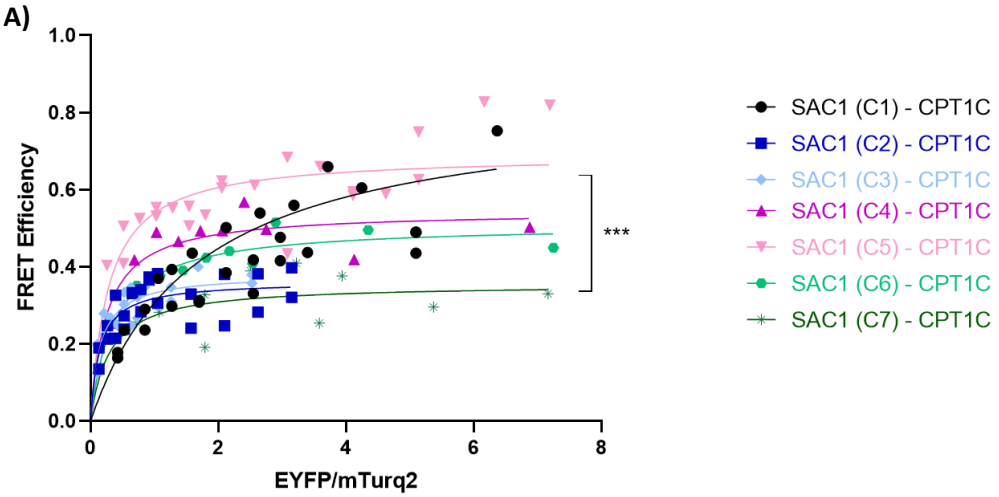

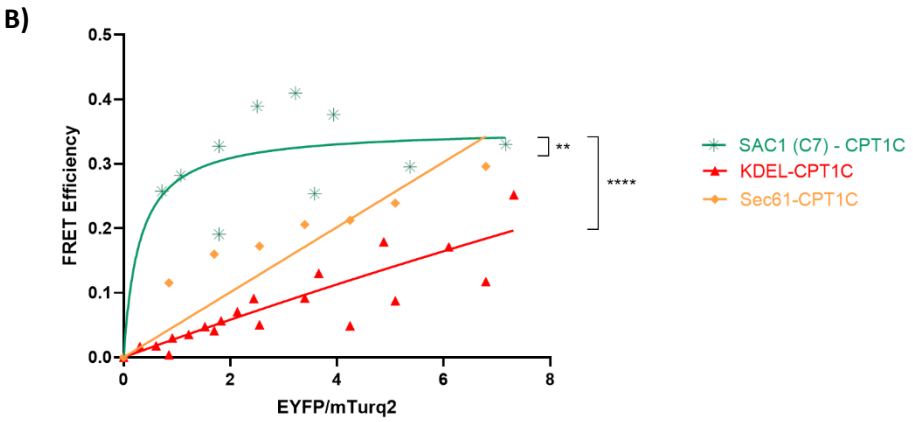

Figure 68. The N-terminal region of SAC1 seems not to be the responsible for its interaction with CPT1C. A) FRETse of CPT1C with either SAC1 C1 (1-587aa), C2 (89-587aa), C3 (189-587aa), C4 (275-587aa), C5 (378-587), C6 (436-587aa) or C7 (520-587aa) in living cells. B) FRETse of CPT1C with either SAC1 C7 (520-587aa), KDEL and Sec61 in living cells. The experiments were conducted 48 hours after transfection of HEK293T cells. Cells were transfected with plasmids coding for mTurq2-SAC1(C1-C7), mTurq2-KDEL and mTurq2-Sec61 as donor proteins, and with increasing amounts of CPT1C-EYFP as an acceptor protein. The results are from one to three independent experiments (one experiment for Sec61-CPT1C, and three experiments for KDEL-CPT1C and SAC1-CPT1C). ***p<0.001, ****p<0.0001 indicates a significant difference. Statistical significance was performed by one-way ANOVA followed by Bonferroni's post correction test.

2.2. Analysis of interaction via pull-down

To confirm these results, a very different approach was needed. Therefore, pull-down studies were performed with streptavidin tagged-CPT1C or streptavidin tagged-calnexin and C5, C6 and C7 constructs of SAC1. Streptavidin-tagged proteins were purified by using the Strep-Tactin® Superflow® high capacity resin. Moreover, SAC1 variants were tagged with mTurq2 and mCPT1C and calnexin, with eGFP. The full-length SAC1 was used as the positive control and calnexin, as the negative one.

Once proteins are retained in the resin due to the streptavidin tag, they were solubilized using GDN detergent generating the pull-downs which contain the possible interacting proteins. GDN was the chosen solubilization buffer because previous studies in the group, performed by Xavier Fontanals Palacios, indicated it is the best detergent to efficiently solubilize these membrane proteins due to its physical properties.

Then, pull-down proteins and their interacting partners were detected by western blot. As it can be observed in figure 69A, obtained pull-down were revealed with three different antibodies: α-mCPT1C, α-calnexin and α-GFP, the last one used to visualize all proteins, since this antibody recognizes both GFP and mTurq2 fluorescent tags.

In the case of α-GFP antibody, a 115 kDa band corresponding to mCPT1C-eGFP-streptavidin or calnexin-eGFP-streptavidin (depending on the condition) is identified at the top of the membrane. It is worth mentioning that calnexin's pull-down is more efficient than CPT1C's pull-down

because calnexin is more stable (as it is a chaperone) facilitating its better expression. Below it, an unspecific band is observed in all lanes (at 90 KDa, approximately). Directly underneath, the bands corresponding to the different constructs of SAC1 are detected. It has to be pointed out that SAC1(C1) is identified in the pull-down of calnexin, when it should not be, since these two proteins are not intended to interact. This means that some contamination of insoluble membranes can occur in the pull-down fraction. Therefore, the amount of SAC1 present in the pull-down was normalized by the amount of the streptavidin-tagged protein present in the same pull-down.

Figure 69B shows the quantity of interacting SAC1 normalized by the pull-down proteins, mCPT1C and calnexin, respectively. Proportionally, the amount of SAC1 interacting with calnexin is extremely low, confirming that calnexin does not interact with SAC1. By contrast, all the truncated proteins interact with mCPT1C with a similar or higher strength than full-length SAC1, confirming the results obtained with FRETse analysis.

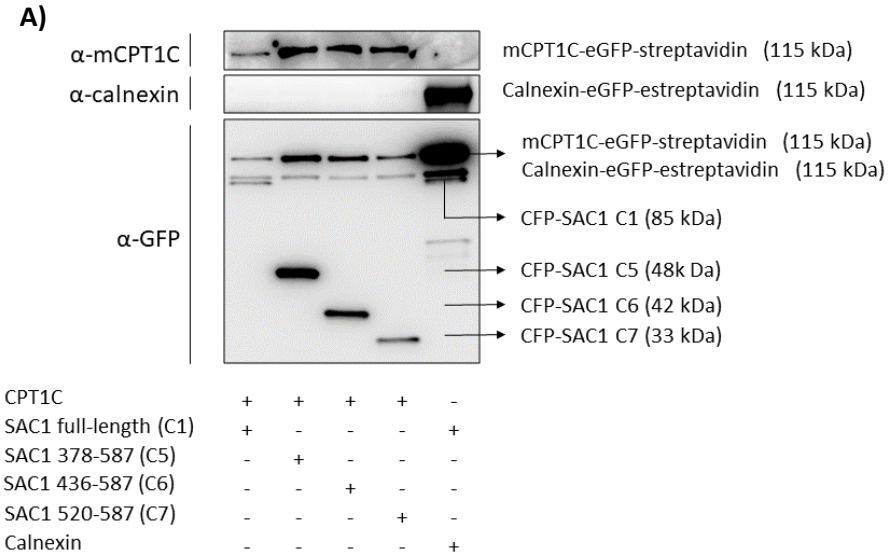

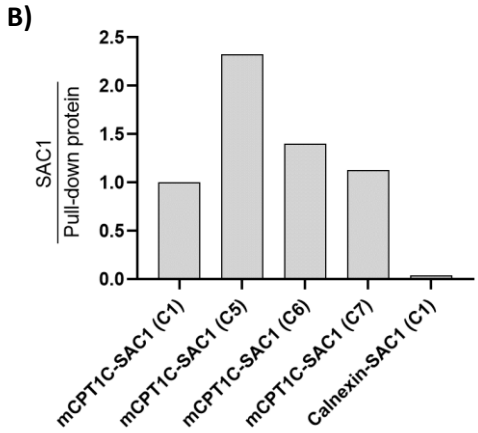

Figure 69. Pull-down assay characterizing the SAC1-CPT1C interaction. A) CPT1C, calnexin and SAC1 levels in pull-down samples. B) Quantification of purified SAC1 normalized to the levels of pull-down proteins, CPT1C or calnexin, both tagged with streptavidin. The results are from one independent experiment.

Interestingly, all these results suggest that the N-terminal domain of SAC1 is not the responsible for its interaction with CPT1C. Several deletions for this N-terminus were done and none of them showed a loss of interaction with CPT1C. Despite the fact that C7 (520-587), the truncated protein with only the two transmembrane domains and the C-terminus, showed lower FRETse efficiency, it was demonstrated with the pull-down approach that this truncated protein still interacts with CPT1C.

3. Results summary of chapter II

In this chapter, it has been studied the interaction between the two proteins of interest: SAC1 and CPT1C. The first step was to verify the correct expression of the truncated forms of SAC1 (C2, C3, C4, C5, C6 and C7). All of them are expressed in the appropriate way when the fluorescent tag (mTurq2) is placed before the N-terminus. They are mostly located in the ER as it was expected.

A first FRETse with SAC1 tagged at the C-terminus resulted in a very low efficiency indicating the protein cannot interact with CPT1C when the tag

is placed in this position. This fact implies that the position occupied by the fluorochrome is important in techniques like FRETse.

The results of the possible interacting region of SAC1 to CPT1C are summarized in figure 70. It seems that neither of SAC1's deletions of N-terminal domain impair the interaction. There were some doubts about the C7 truncated protein (520-587aa) with FRETse assay but they were solved with the pull-down approach, and the results point out that amino acids from 1 to 519 are not the responsible for the interaction.

These findings reinforce the idea that the N-terminal domain of SAC1 is not implicated in the interaction, suggesting that the C-terminal region or even the TMDs could be involved in SAC1-CPT1C binding.

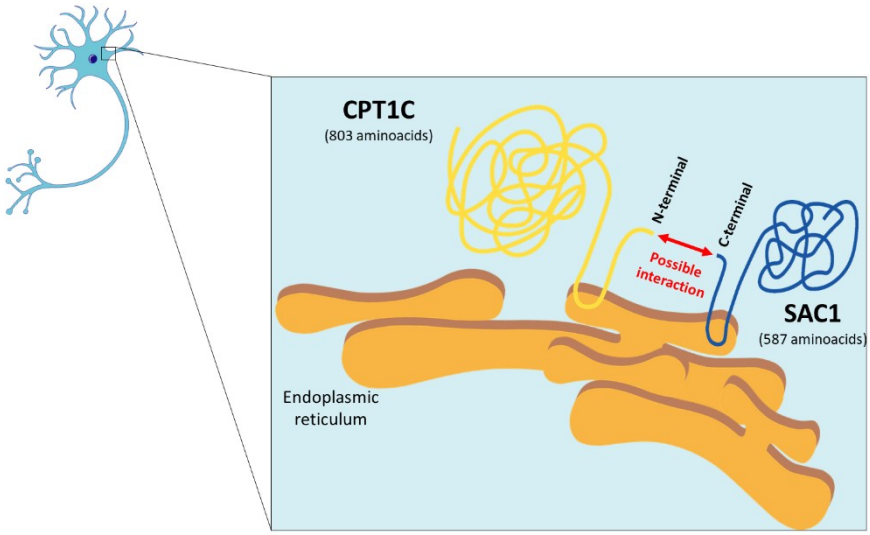

Figure 70. Graphical abstract of chapter II. The interaction between SAC1 and CPT1C proteins in the endoplasmic reticulum can be through the C-terminal domain of SAC1 and, perhaps, the N-terminus of CPT1C.

DISCUSSION

The brain, often regarded as the most complex organ in the human body, is a vast network composed of billions of neurons which are interconnected by synapses. Scientific research is continuously revealing the brain's incredible adaptability and plasticity, demonstrating its capacity to rewire and reorganize in response to learning, experiences and, even, recovery from injury. A relatively new area of study is increasingly highlighting the crucial influence of diets in brain function. Nutrients derived from our diet play a key role in shaping the brain's structure and functionality.

This thesis tries to give new insights about the close connection between nutrition and cognition, focusing specially in AMPAR subunit GluA1 due to its importance in this process. Moreover, our group has previously published that the transport of GluA1 to the plasma membrane during the synapse is regulated by malonyl-CoA, a metabolite whose levels fluctuate depending on the presence of nutrients (Casas et al., 2020). In this thesis, it has been studied the impact of different diets *in vivo* and the effects of nutrients that mimic those diets *in vitro*.

Previously, it had been shown that saturated fatty acids negatively influence neurotransmission. At cellular level, PA decreases the trafficking of GluA1 subunits toward the plasma membrane (Spinelli et al., 2017) and alters neuronal morphology (McLean et al., 2019). On the contrary, unsaturated fatty acids had the opposite effect on synaptic processes, specially ω-3 PUFAs (Loehfelm et al., 2020). Moreover, upon a fasting situation or with a ketogenic diet, GluA1 levels increase in hippocampal neurons (Grillo et al., 2011; Hu et al., 2018; Rojic-Becker et al., 2019). Here, it has been demonstrated that saturated fats decrease the trafficking of GluA1 to the plasma membrane, whereas unsaturated fats and BHB increase it. Specifically, it has been described for the first time that a ketone body, BHB, can counteract the detrimental effect of saturated fats on GluA1 trafficking, synaptic transmission and cognition.

Taking into account that the malonyl-CoA – CPT1C axis has been demonstrated to regulate GluA1 trafficking depending on energetic conditions, the involvement of this axis in PA and BHB effects was also studied. Finally, since the main partner of CPT1C in mediating AMPAR trafficking regulation is SAC1 and, little is known about the interaction between both proteins, we performed a series of deletions in the

sequence of SAC1 to identify the region involved in the binding to CPT1C. With all these approaches, this thesis has contributed to the understanding of nutrient's effects on AMPAR trafficking, synaptic plasticity and cognition.

1. Exploring dietary influence on AMPARs

Considering the crucial role that CPT1C plays in the regulation of GluA1 receptor trafficking in response to energetic status, we first analyzed the levels of GluA1 and its phosphorylations in the cortex of CPT1C KO mice. It is expected that in the absence of CPT1C protein, total GluA1 levels are reduced, as it has been published before (Fado et al., 2015). However, this fact was observed in hippocampal GluA1 but no in cortical one, suggesting that cortex does not regulate GluA1 synthesis, but it could be modulating its transport to the plasma membrane. Therefore, the phosphorylation of GluA1 was analyzed.

Post-translational modifications are one of the mechanisms responsible for the regulation of AMPARs trafficking to perisynaptic sites and synapses (Diering & Huganir, 2018), being phosphorylations at S831 and S845 the best studied ones. Only levels of GluA1 phosphorylated at S845 decreased in cortical samples of CPT1C KO mice. Less p(S845)-GluA1 suggests an impairment in exocytosis processes, as expected in the absence of CPT1C because this protein has been related with GluA1's canonical trafficking towards the plasma membrane (Casas et al., 2020). By contrast, p(S831)-GluA1 is related with channel conductance, playing a critical role in the receptor's functionality (Summers et al., 2019). The absence of changes in S831 phosphorylation in CPT1C KO mice correlates perfectly with the fact that CPT1C is not modulating GluA1's channel properties (Gratacos-Batlle et al., 2015). Therefore, it seems that GluA1 trafficking is impaired in the cortex, whereas its synthesis is altered in the hippocampus. Although it cannot be discarded that the trafficking is not altered in the hippocampus because phosphorylation levels have not been analyzed in this region. Despite CPT1C modulates GluA1 and GluA2 hippocampal synthesis (Fado et al., 2015), this thesis has specifically focused on the trafficking of GluA1 subunit as it is the only one to be regulated by CPT1C (Casas et al., 2020).

Taking into account that CPT1C in the hypothalamus has a protective role against HFD-induced obesity and CPT1C KO mice are more prone to gaining body weight (Rodriguez-Rodriguez et al., 2019; Wolfgang et al., 2008), we decided to explore whether HFD could affect cognition through CPT1C. Feeding WT animals with HFD for one week is not enough to affect GluA1 levels or its phosphorylation rate. Moreover, the observed decrease in GluA1 phosphorylation in CPT1C KO cortex compared to WT did not occur in the presence of a short-term HFD. This could suggest that dietary fats are able to increase GluA1 phosphorylation to normal levels in cortex of CPT1C deficient mice. It is noteworthy that the specific fat composition of this type of diet is usually left unspecified. Typically, HFD is characterized by a combination of saturated and unsaturated fatty acids, where saturated fats tend to be in a higher proportion than unsaturated ones. In line with this, it was assumed that unsaturated fatty acids were probably mitigating the effects of saturated fats. Because of that, the next step was to analyze GluA1 levels with different types of HFD: the SFAD and the MUFAD. Neither short-term or long-term diets (1 week and 1 month respectively) showed any alteration in total GluA1 levels or phosphorylated ones. This fact indicated that there were not changes at tissue levels, at least, within this intake period. Nevertheless, p(S845)-GluA1 decreased with a SFAD based on 60% of fats for 6 weeks (Spinelli et al., 2017), indicating the importance of the fatty dose. It can be suggested that longer periods of time are needed to have a negative impact on cortical brain function with the SFAD used in this thesis (based on 49% of fats). Moreover, as just a few receptors are phosphorylated (Diering et al., 2016; Hosokawa et al., 2015; Oh et al., 2006), the experimental approach used may not allow us to know what really occurs with their transport. That is why we decided to performed the study at the cellular level.

To simulate SFAD and MUFAD at this level, different fatty acids were chosen: PA as a represent for SFAD and OA, for MUFAD. Moreover, we were also interested to find out what happen with ω-3 PUFAs, so DHA treatment was also administered. ω-6 PUFAs, such as araquidonic acid, were excluded because they have been related to inflammatory response (D'Angelo et al., 2020).

The results are in concordance with the hypothesis that saturated fatty acids impair GluA1 trafficking and unsaturated ones, enhance it. A high abundance of PA led to a decrease in surface GluA1 levels. Its effects

seemed to be more intense with long-term treatment (24h). This might be attributed to the body's ability to adapt and maintain homeostasis. In the short-term period, it may prioritize immediate energy needs and allocate resources to cope with the high fat intake without causing important cognitive changes. Over time, as high-fat diets persist, the cumulative impact on the brain and cognitive functions become more apparent. In addition, HFD has also led to a decrease in the total levels of PSD95 (Spinelli et al., 2017). Therefore, this reduction in surface GluA1 due to PA may be associated with the downregulation of proteins within AMPAR macrocomplex.

It has been published that PA halts the trafficking of AMPARs toward the plasma membrane through the palmitoylation of GluA1 subunit (Spinelli et al., 2017) although other mechanisms can be involved too. Nevertheless, not all the surface GluA1 is participating in synapses. In the case of the saturated fatty acid PA, it also decreased synaptic GluA1 suggesting that it has a direct consequence on neuronal signaling.

On the other hand, the positive effect of unsaturated fatty acids (OA and DHA) needed more time to impact on GluA1 levels. They might carry out their beneficial effects through more complex mechanisms than saturated fatty acids. They could also accumulate in tissues, which could explain the light tendency of increased phosphorylated GluA1 levels that it was observed with the long-term MUFAD. Therefore, their impact may be more gradual and sustained over time.

Furthermore, the ketone body BHB, produced from fatty acids in fasting situation, has also been studied. BHB showed its positive effects on surface GluA1 levels with both short- and long-term treatment, indicating a rapid impact on neurotransmission no matters the duration of the treatment. This suggests that it not only serves as energy source but also potentially has a direct impact on synaptic plasticity. This effect could enhance alertness in mice and enables them, for instance, to look for food faster. However, BHB did not change synaptic GluA1 levels as it was firstly expected. It seems that the ketone body improves AMPARs trafficking, yet GluA1 remains in extrasynaptic regions probably ready until it is needed. Taking into account that BHB levels are very low in a normal situation and they increase with ketogenic state, we were interested in studying the effects of different doses of this ketone body. Strikingly, lower concentrations of BHB increased surface GluA1 too although, again, no changes in synaptic GluA1 were observed.

In line with the observation that PA causes axonal blebbing reducing dendritic arborization, while DHA can reverse these effects returning neurons to their typical morphology (Loehfelm et al., 2020; McLean et al., 2019), we decided to explore whether BHB could exert a similar effect reversal. It is already known that BHB can ameliorate adverse effects in the presence of brain damage (Di Majo et al., 2022; Henderson et al., 2009; Manville et al., 2020; Newport et al., 2015; Tieu et al., 2003), so we wondered about its potential role about counteracting the deleterious impact of PA in GluA1 trafficking.

As it was hypothesized, BHB was able to reverse the negative effects caused by PA on synaptic GluA1 levels. Surprisingly, with 5 mM BHB, the highest concentration, the reversion was not observed. It is important to point out that this concentration is not found in blood at physiological conditions. Another intriguing perspective to explore would have been initially subjecting neurons to PA treatment, allowing the manifestation of any adverse effects and, subsequently, administrating BHB. This approach could have shed light on the potential for BHB to mitigate negative consequences of PA once they have been developed. An alternative strategy could have involved the longitudinal observations of treatments, such as conducting a washout period for both PA and BHB, followed by an analysis of the changes in surface and synaptic GluA1. Accordingly, it could be determined whether the unique effects gradually diminish over time or persist indefinitely.

Despite the fact that this thesis focused on GluA1 subunit of AMPARs, highlighting the specific effects of different nutrients on membrane targeting, it raises the question of what impact these nutrients might have on other glutamatergic receptors, like GluA2 or NMDA-type glutamate receptors, and other synaptic proteins, like PSD95.

Moreover, an alternative cellular model to primary cultures was developed to corroborate these results. Even though no significant differences were obtained with short-term treatments, nutrients had the same effects on differentiated SH-SY5Y confirming our previous results. These cells represent a compelling model to avoid animal sacrifice in scientific research. Their use aligns with ethical considerations and may streamline experimental procedures enhancing the efficiency of research.

2. Diet-related impacts on synaptic plasticity

In the last years, there have been an increasing interest about how our dietary habits affect cognition. The recognition that our diets play a key role in shaping cognitive abilities and processes has led to a surge in studies investigating the effects of specific nutrients (Gómez-Pinilla, 2008; Klimova et al., 2020; Puri et al., 2023). Once we established the effect of fatty acids and the ketone body in surface and synaptic GluA1 levels, we decided to further explore their role in neurotransmission. In line with the absence of any detected modifications in synaptic GluA1 levels with BHB treatment, there was no enhancement in mEPSCs recordings in cultured neurons. By contrast, PA clearly decreased the amplitude of mEPSCs, corroborating the results obtained in synaptic GluA1 levels. In fact, there was a notable change in the amplitude distribution toward lower values in this case. Moreover, the analyzed kinetic parameters exhibited no appreciable alterations either, so AMPARs subtype composition remained consistent. The frequency of these mEPSCs did not show any change indicating that the effects of PA and BHB occur at a postsynaptic level. Considering that NMDA inhibitors were used when recording mEPSCs, we can specifically attribute PA effects to the regulation of AMPARs.

Given these results, we then wanted to study the nutrient's effect in a more physiological context, conducting electrophysiological recordings in hippocampal slices. The absence of changes in PPR results also confirmed the postsynaptic effects of these nutrients. For these reasons, we examined neuronal excitability and the response of neurons to various levels of stimulation. Neurons became more excitable and fired more action potentials generating a larger response as the input increased with BHB treatment. This can be explained by considering the presence of a greater quantity of AMPARs in the plasma membrane ready to receive neurotransmitters.

Although no changes were observed with BHB, PA induced a significant decrease in AMPA/NMDA ratio, indicating the changes in synaptic transmission resulting from the presence of this saturated fatty acid are mostly attributed to alterations in AMPARs.

In order to evaluate the influence of PA and BHB in synaptic plasticity, LTP was studied too. The outcomes were not conclusive due to the large variability in the LTP magnitude and the relatively small sample size tested.

However, it is known that ketogenic diets do not affect synaptic plasticity (Huang et al., 2019). On the other hand, LTP is reduced following an 8-week SFAD dietary regimen (Fernandez-Felipe et al., 2021), which is a longer duration compared to the short-term treatment used in the experiments conducted in this thesis. Furthermore, it might be of significant interest to investigate the effects of these two nutrients on several other forms of synaptic plasticity, such as LTD.

3. Diet-related impacts on cognition

Once electrophysiological approaches were done, it was relevant to perform behavioral tests to examine cognitive processes. Taking into account that the deleterious effects of fatty acids are mostly observed with a dietary regimen of 2 months, we decided to feed mice with SFAD (49% of saturated fats) during that time. To mitigate this effect, BHB was administrated intragastrically to ensure consistent daily doses. In addition, blood BHB levels vary depending on the nutritional situation: they oscillate between 0.5-3 mmol/L with ketogenic diets (Lowder et al., 2023) and can reach up to 1 mmol/L in the brain with a short-term fasting (Pan et al., 2000). In accordance with this, the chosen dose was 100 mg/kg/day, determined based on previously published data (Hu et al., 2018), in which they administered 60nmg/kg twice daily. We used a slightly lower dose injected in the morning to prevent administering on an empty stomach and to avoid potential ketosis.

BHB reverses deleterious effects of the diet. Furthermore, this fact is in line with the results previously mentioned, indicating that BHB alone does not affect synaptic transmission or synaptic GluA1. The consistent outcomes were replicated when assessing spatial learning. Altogether these results highlight that BHB can counteract PA's effects at a cellular and cognitive level. So far, there have not been any available study about the role of BHB counteracting PA effect. This thesis has described for the first time the potential role of BHB over the detrimental effect of PA on cognition. BHB appears to function as a highly effective energy source in comparison to glucose. One possible explanation for this could be that BHB improves mitochondrial functions increasing cognitive performance with the extra energy. BHB, besides serving as a crucial energetic metabolite for neurons as demonstrated in this thesis, enhances

perisynaptic GluA1. This could play a vital role in facilitating the rapid replacement of GluA1 that is endocytosed due to palmitate, thereby helping to prevent the negative effects of the fatty acid. In addition, the energetic surplus may serve as a protection for neurons, safeguarding them against damage and degeneration, while also offering antioxidant and anti-inflammatory effects in challenging situations (Marosi et al., 2016; Rojas-Morales et al., 2020).

In the context of fasting, the body enters an atypical state, prompting the production of ketone bodies to provide energy for the brain and mitigate any adverse consequences. PA is released from adipose tissue and BHB, from the liver. Both metabolites reach the brain together explaining why intermittent fasting is not detrimental to the brain, rather, it is quite the opposite. Moreover, BHB emerges as the most efficient ketone body. Acetoacetate, which precedes BHB and acetone in the ketone synthesis pathway, might exhibit milder cognitive effects compared to BHB. Acetone, being a volatile compound rapidly eliminated from the body, is unlikely to exert the same strong impact as BHB.

Based on these findings, one could consider the option to commercialize BHB for mitigating HFD-mediated cognitive impairment. Nevertheless, it could be interesting also to analyze AMPARs and NMDARs in the postsynaptic density zone and in synaptosomes. This could provide valuable extra insights into the functioning of synapses and neurons under the effects of PA and BHB.

Regarding *in vivo* studies, for the purpose of extending the applicability of the concepts presented here, it is advisable to replicate the analysis using older mice. It has been described that disparities in synaptic plasticity exist between young and elderly individuals (Fado et al., 2022). Furthermore, we need to delve into the specific quantities of BHB required to trigger these reversal effects. It is very important to ascertain the precise levels of BHB in both the bloodstream and the brain to observe and understand this phenomenon.

4. Implication of malonyl-CoA – CPT1C axis in nutrients-mediated regulation of AMPARs

As it was mentioned before, CPT1C plays a key role in regulating AMPARs. Once studied several nutritional situations, the next step was to find out whether malonyl-CoA – CPT1C axis was involved in AMPARs changes related with diets.

Malonyl-CoA, a fatty acid precursor, is under the influence of several regulating enzymes such as ACC and FAS. ACC assumes a critical role in the control of malonyl-CoA synthesis and can be modulated through its phosphorylation. ACC exhibited nuances when exposed to different nutritional factors. Both PA and OA induce the inactivation of ACC inhibiting the synthesis of fatty acids. Remarkably, DHA and BHB, in contrast, did not seem to impart any significant alteration. On the other hand, FAS downregulates malonyl-CoA levels because it catalyzes its conversion to long-chain fatty acids, such as PA. In this context, it is intriguing to note the PA and DHA had no discernible impact on FAS levels, whereas OA and BHB provoked a noticeable reduction. The results revealed that monounsaturated fatty acids uniquely possessed the capacity to concurrently regulate both ACC and FAS, consequently maintaining malonyl-CoA levels at a steady equilibrium. Considering these findings, it becomes plausible to speculate that the putative levels of malonyl-CoA would witness a decline in the presence of PA, indicating a state of low energy availability and promoting the oxidation of fatty acids. The presence of BHB could potentially result in an increase of malonyl-CoA levels, facilitating fatty acid synthesis to store energy.

Moreover, we delved into the analysis of additional proteins, specifically focusing on CREB and BDNF, both of which have previously demonstrated alterations in response to HFD (Spinelli et al., 2020). No significant differences were observed in the levels of BDNF or the activation of CREB, neither with short- or long-term treatments. These findings underscore the complexity of the interplay between dietary factors and the molecular pathways governed by these proteins, warranting further exploration and a deeper understanding of their regulatory mechanisms.

It has been published that malonyl-CoA increases surface GluA1 levels (Casas et al., 2020). In agreement with this, we supposed that PA might

exert its impact on malonyl-CoA levels, given its role as an inhibitor of ACC, decreasing surface GluA1 levels. This points out an exploration into whether malonyl-CoA could potentially mitigate the adverse effects induced by PA, which we hypothesized might be linked to an alteration in the malonyl-CoA – CPT1C axis. Remarkably, our results demonstrated that malonyl-CoA led to an increase in surface GluA1 levels. However, it became evident this metabolite alone was unable to fully reverse the detrimental impact of PA. This outcome raised interesting questions about the potential mechanisms at play. Indeed, even in the absence of CPT1C, PA continued to have a slight reduction in surface GluA1 levels, although not statistically significant. Malonyl-CoA's influence on surface GluA1 levels remained evident, regardless of CPT1C's presence. As it increases the synthesis of fatty acids, this process could probably cause a remodeling of the plasma membrane influencing, at the same time, the amount of surface GluA1. In the absence of CPT1C, there are more free malonyl-CoA molecules possibly enhancing the trafficking of GluA1 under this situation.

These findings strongly suggest that the malonyl-CoA – CPT1C pathway might not be the responsible for PA's effects. A noteworthy hypothesis emerges from this observation: it is plausible that an excess of PA may lead to palmitoylation of GluA1 subunits, a phenomenon previously mentioned. Consequently, the effects of PA on GluA1 may be independent of the malonyl-CoA – CPT1C pathway.

In order to investigate the potential influence of BHB on GluA1 via the malonyl-CoA – CPT1C axis, we used TOFA, an inhibitor of the ACC enzyme responsible for malonyl-CoA synthesis. When these two molecules, BHB and TOFA, were administered at the same time, it was observed that TOFA effectively blocked the actions of BHB, underscoring the interplay between these components. Even so, when CPT1C was absent, BHB failed to cause any noticeable alterations, suggesting a pivotal role of CPT1C in this process. These findings provide reasonable evidences to suggest that the malonyl-CoA – CPT1C axis is implicated in BHB’s effect, particularly along the well-established canonical pathway of AMPARs trafficking.

Nevertheless, these nutrients can generate indirect effects, thereby introducing a layer of complexity that requires careful consideration when postulating a mechanistic explanation.

5. Interaction between SAC1 and CPT1C

It is well-accepted that AMPARs are macromolecular complexes whose regulation rely on the proteins that co-assemble with these receptors (Brechet et al., 2017; Schwenk et al., 2019; Schwenk et al., 2012). Two proteins this thesis was focused on were SAC1 and CPT1C, as they modulate the transport of AMPARs toward the plasma membrane depending on the nutritional status of neurons (Casas et al., 2020). However, there is limited knowledge about the interaction between them. We engineered constructs of truncated SAC1 in order to identify the domain of SAC1 involved in it.

The fact that locating the fluorescent tag (mTurq2) at the end of the truncated SAC1 resulted in no protein expression is possibly due to issues like misfolding or cellular stress. In addition, the tag at the C-terminus of the non-truncated SAC1 also prevented the binding to CPT1C, probably due to a stearic impediment. Therefore, to stabilize the truncated proteins and avoid this stearic impediment, mTurq2 was replaced in the N-terminus of SAC1 for all the following experiments.

Results evidenced that all the truncated proteins still maintained the interaction with CPT1C, indicating that the domain of SAC1 involved in the interaction is not the N-terminal region but the transmembrane domain or the C-terminus. The hindrance observed in the interaction between both proteins due to the placement of the fluorescent tag at the C-terminal domain of SAC1 suggests that this specific short C-terminal region is involved in this interaction.

Our results do not agree with *in silico* studies because both the transmembrane and C-terminal domains were excluded from the analysis. In this way, SAC1 was forced to interact through its N-terminus. This fact underlies the importance of validating results by other techniques, such as FRET and pull-down.

Therefore, we concluded that SAC1 does not interact through its N-terminal domain with CPT1C. When hypothesizing about their interaction, two scenarios come to mind. One possibility is a cis interaction, in which SAC1 may interact via its transmembrane domains or C-terminus with CPT1C within the ER. The alternative option is a trans interaction, where SAC1 in the Golgi apparatus uses its C-terminal domain to establish contact

with CPT1C in a distinct subcellular compartment. However, SAC1's C-terminus is formed by just 17 aa complicating the interaction through this domain with another protein located in another cellular organelle (Zewe et al., 2018), like the ER in the case of CPT1C.

Thus, to fully describe the interaction of these two proteins, it would be recommended to engineer a new construct without SAC1's C-terminal domain. Other possibility to consider could involve the deletion of its transmembrane domains although it could not be such a good idea as SAC1 needs these domains to be tethered to the membrane. Their removal could result in SAC1 degradation. Finally, the same interaction studies (FRETs and pull-downs) should be done with truncated CPT1C. Previous research has already described that the last 40 aa, a unique characteristic that sets this protein apart from the other family members, do not play a role in mediating the interaction with SAC1 (Casas et al., 2020). Therefore, it could be suggested to engineer a truncated CPT1C without its N-terminal segment. Nonetheless, we have to consider the possibility that the rest of the voluminous C-terminal domain still plays a role in the interaction. Consequently, the same cloning strategy used for SAC1 (involving the removal of specific motifs) should be explored for CPT1C too.

6. Concluding remarks

Overall, this thesis has focused on the role of fatty acids and ketone bodies in AMPARs trafficking. Saturated fatty acids, as previously shown, have been found to significantly reduce surface GluA1 levels, thereby providing an explanation for their adverse impact on cognitive functions. Conversely, unsaturated fatty acids and ketone bodies have been observed to elevate the levels of this specific AMPAR subunit. In addition, it is worth noting that PA was able to affect synaptic GluA1 levels, whereas BHB seemed to predominantly affect extrasynaptic ones.

These dietary components caused an impact at postsynaptic level, specifically through the modulation of AMPARs. More importantly, these effects observed by PA and BHB extend beyond receptor dynamics and correlate with alterations in learning and memory processes. Here, we demonstrated that BHB can counteract the detrimental effects of PA *in*

vitro and *in vivo* in mice. Furthermore, a potential mechanistic pathway for the BHB actions has been proposed involving the malonyl-CoA – CPT1C axis. Finally, ongoing studies have been directed toward elucidating the specific motifs underlying the interaction between SAC1 and CPT1C.

Altogether, these results have contributed to a better understanding of the impact of nutrients in brain functions and cognitive processes. They have given new insights into the cellular mechanisms which can be implicated, as it is shown in figure 71.

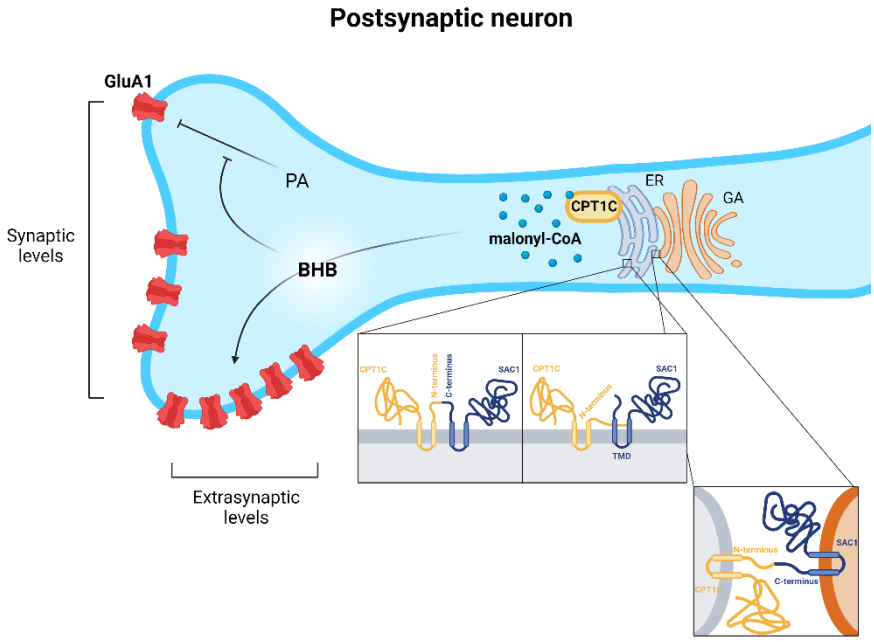

Figure 71. Graphical abstract of thesis concluding remarks. Schematic summary of main conclusions of chapter I and II of results. BHB's effects are dependent of malonyl-CoA – CPT1C axis. The three possible interactions of SAC1 and CPT1C are represented. ER: endoplasmic reticulum. GA: Golgi apparatus. TMD: transmembrane domain.

CONCLUSIONS

1. GluA1 phosphorylation at S845 is compromised within the cortex of CPT1C KO mice, whereas GluA1 synthesis is reduced in the hippocampus.

2. SFAD and MUFAD, based on 49% of fats, have no effects on GluA1 protein levels and phosphorylation at S845 or S831, regardless of whether the feeding period was one week or one month.

3. PA treatment for 24h decreases surface GluA1 levels while OA, DHA and BHB increase them in cultured cortical neurons. Short-term (2h) effects are similar to the long-term ones but milder.

4. The alternative cellular model of differentiated SH-SY5Y successfully replicates nutrients' effects on surface GluA1 levels as in primary neuronal cultures.

5. PA has the capacity to reduce synaptic GluA1 levels in cultured hippocampal neurons, while BHB does not. However, BHB counteracts PA-mediated downregulation of synaptic GluA1 in these neurons.

6. PA negatively regulates AMPARs-mediated excitatory postsynaptic currents in cultured cortical neurons.

7. BHB restores the adverse effects of PA on neuronal excitability in hippocampal slices. The detrimental effects of PA are mostly due to AMPARs, not NMDARs.

8. Daily oral BHB administration for two months counteracts the detrimental effects of SFAD in spatial learning and recognition memory.

9. BHB, but not PA, regulates surface GluA1 levels through the malonyl-CoA – CPT1C axis.

10. SAC1 does not interact with CPT1C through its N-terminal domain.

REFERENCES

Acker, C. D., Hoyos, E., & Loew, L. M. (2016). EPSPs Measured in Proximal Dendritic Spines of Cortical Pyramidal Neurons. *eNeuro*, *3*(2). https://doi.org/10.1523/ENEURO.0050-15.2016

Andersen, J. V., Markussen, K. H., Jakobsen, E., Schousboe, A., Waagepetersen, H. S., Rosenberg, P. A., & Aldana, B. I. (2021). Glutamate metabolism and recycling at the excitatory synapse in health and neurodegeneration. *Neuropharmacology*, *196*, 108719. https://doi.org/10.1016/j.neuropharm.2021.108719

Araque, A., Parpura, V., Sanzgiri, R. P., & Haydon, P. G. (1999). Tripartite synapses: glia, the unacknowledged partner. *Trends Neurosci*, *22*(5), 208-215. https://doi.org/10.1016/s0166-2236(98)01349-6

Attwell, D., & Laughlin, S. B. (2001). An energy budget for signaling in the grey matter of the brain. *J Cereb Blood Flow Metab.*, *21*(10), 1133-1145. https://doi.org/10.1097/00004647-200110000-00001

Bakr, M., Jullie, D., Krapivkina, J., Paget-Blanc, V., Bouit, L., Petersen, J. D., Retailleau, N., Breillat, C., Herzog, E., Choquet, D., & Perrais, D. (2021). The vSNAREs VAMP2 and VAMP4 control recycling and intracellular sorting of post-synaptic receptors in neuronal dendrites. *Cell Rep*, *36*(10), 109678. https://doi.org/10.1016/j.celrep.2021.109678

Barry, M. F., & Ziff, E. B. (2002). Receptor trafficking and the plasticity of excitatory synapses. *Curr Opin Neurobiol*, *12*(3), 279-286. https://doi.org/10.1016/s0959-4388(02)00329-x

Bats, C., Groc, L., & Choquet, D. (2007). The interaction between Stargazin and PSD-95 regulates AMPA receptor surface trafficking. *Neuron*, *53*(5), 719-734. https://doi.org/10.1016/j.neuron.2007.01.030

Bauer, I., Hughes, M., Rowsell, R., Cockerell, R., Pipingas, A., Crewther, S., & Crewther, D. (2014). Omega-3 supplementation improves cognition and modifies brain activation in young adults. *Hum Psychopharmacol*, *29*(2), 133-144. https://doi.org/10.1002/hup.2379

Baym, C. L., Khan, N. A., Monti, J. M., Raine, L. B., Drollette, E. S., Moore, R. D., Scudder, M. R., Kramer, A. F., Hillman, C. H., & Cohen, N. J. (2014). Dietary lipids are differentially associated with hippocampal-dependent relational memory in prepubescent children. *Am J Clin Nutr*, *99*(5), 1026-1032. https://doi.org/10.3945/ajcn.113.079624

Bedoukian, M. A., Weeks, A. M., & Partin, K. M. (2006). Different domains of the AMPA receptor direct stargazin-mediated trafficking and stargazin-mediated modulation of kinetics. *J Biol Chem*, *281*(33), 23908-23921. https://doi.org/10.1074/jbc.M600679200

Beilharz, J. E., Kaakoush, N. O., Maniam, J., & Morris, M. J. (2016). The effect of short-term exposure to energy-matched diets enriched in fat or sugar on memory, gut microbiota and markers of brain inflammation and plasticity. *Brain Behav Immun*, *57*, 304-313. https://doi.org/10.1016/j.bbi.2016.07.151

Beique, J. C., & Andrade, R. (2003). PSD-95 regulates synaptic transmission and plasticity in rat cerebral cortex. *J Physiol*, *546*(Pt 3), 859-867. https://doi.org/10.1113/jphysiol.2002.031369

Bissen, D., Foss, F., & Acker-Palmer, A. (2019). AMPA receptors and their minions: auxiliary proteins in AMPA receptor trafficking. *Cell Mol Life Sci*, *76*(11), 2133-2169. https://doi.org/10.1007/s00018-019-03068-7

Blackstone, C., O'Kane, C. J., & Reid, E. (2011). Hereditary spastic paraplegias: membrane traffic and the motor pathway. *Nat Rev Neurosci*, *12*(1), 31-42. https://doi.org/10.1038/nrn2946

Blagoveshchenskaya, A., Cheong, F. Y., Rohde, H. M., Glover, G., Knodler, A., Nicolson, T., Boehmelt, G., & Mayinger, P. (2008). Integration of Golgi trafficking and growth factor signaling by the lipid phosphatase SAC1. *J Cell Biol*, *180*(4), 803-812. https://doi.org/10.1083/jcb.200708109

Blagoveshchenskaya, A., & Mayinger, P. (2009). SAC1 lipid phosphatase and growth control of the secretory pathway. *Mol Biosyst*, *5*(1), 36-42. https://doi.org/10.1039/b810979f

Blaise, J. H., Ruskin, D. N., Koranda, J. L., & Masino, S. A. (2015). Effects of a ketogenic diet on hippocampal plasticity in freely moving juvenile rats. *Physiol Rep*, *3*(5). https://doi.org/10.14814/phy2.12411

Boudkkazi, S., Brechet, A., Schwenk, J., & Fakler, B. (2014). Cornichon2 dictates the time course of excitatory transmission at individual hippocampal synapses. *Neuron*, *82*(4), 848-858. https://doi.org/10.1016/j.neuron.2014.03.031

Boutry, M., Morais, S., & Stevanin, G. (2019). Update on the Genetics of Spastic Paraplegias. *Curr Neurol Neurosci Rep*, *19*(4), 18. https://doi.org/10.1007/s11910-019-0930-2

Bowen, A. B., Bourke, A. M., Hiester, B. G., Hanus, C., & Kennedy, M. J. (2017). Golgi-independent secretory trafficking through recycling endosomes in neuronal dendrites and spines. *Elife*, *6*. https://doi.org/10.7554/eLife.27362

Brechet, A., Buchert, R., Schwenk, J., Boudkkazi, S., Zolles, G., Siquier-Pernet, K., Schaber, I., Bildl, W., Saadi, A., Bole-Feysot, C., Nitschke, P., Reis, A., Sticht, H., Al-Sanna'a, N., Rolfs, A., Kulik, A., Schulte, U., Colleaux, L., Abou Jamra, R., & Fakler, B. (2017).

AMPA-receptor specific biogenesis complexes control synaptic transmission and intellectual ability. *Nat Commun*, *8*, 15910. https://doi.org/10.1038/ncomms15910

Brice, S. E., Alford, C. W., & Cowart, L. A. (2009). Modulation of sphingolipid metabolism by the phosphatidylinositol-4-phosphate phosphatase Sac1p through regulation of phosphatidylinositol in Saccharomyces cerevisiae. *J Biol Chem*, *284*(12), 7588-7596. https://doi.org/10.1074/jbc.M808325200

Butler, M. J., Cole, R. M., Deems, N. P., Belury, M. A., & Barrientos, R. M. (2020). Fatty food, fatty acids, and microglial priming in the adult and aged hippocampus and amygdala. *Brain Behav Immun*, *89*, 145-158. https://doi.org/10.1016/j.bbi.2020.06.010

Buzsáki, G., & Watson, B. O. (2012). Brain rhythms and neural syntax: implications for efficient coding of cognitive content and neuropsychiatric disease. *Dialogues Clin Neurosci*, *14*(4), 345-367. https://doi.org/10.31887/DCNS.2012.14.4/gbuzsaki

Cai, Y., Deng, Y., Horenkamp, F., Reinisch, K. M., & Burd, C. G. (2014). Sac1-Vps74 structure reveals a mechanism to terminate phosphoinositide signaling in the Golgi apparatus. *J Cell Biol*, *206*(4), 485-491. https://doi.org/10.1083/jcb.201404041

Canhada, S., Castro, K., Perry, I. S., & Luft, V. C. (2018). Omega-3 fatty acids' supplementation in Alzheimer's disease: A systematic review. *Nutr Neurosci*, *21*(8), 529-538. https://doi.org/10.1080/1028415X.2017.1321813

Cansev, M., Wurtman, R. J., Sakamoto, T., & Ulus, I. H. (2008). Oral administration of circulating precursors for membrane phosphatides can promote the synthesis of new brain synapses. *Alzheimers Dement*, *4*(1 Suppl 1), S153-168. https://doi.org/10.1016/j.jalz.2007.10.005

Caporale, N., & Dan, Y. (2008). Spike timing-dependent plasticity: a Hebbian learning rule. *Annu Rev Neurosci*, *31*, 25-46. https://doi.org/10.1146/annurev.neuro.31.060407.125639

Carrasco, P., Jacas, J., Sahun, I., Muley, H., Ramirez, S., Puisac, B., Mezquita, P., Pie, J., Dierssen, M., & Casals, N. (2013). Carnitine palmitoyltransferase 1C deficiency causes motor impairment and hypoactivity. *Behav Brain Res*, *256*, 291-297. https://doi.org/10.1016/j.bbr.2013.08.004

Carrasco, P., Sahun, I., McDonald, J., Ramirez, S., Jacas, J., Gratacos, E., Sierra, A. Y., Serra, D., Herrero, L., Acker-Palmer, A., Hegardt, F. G., Dierssen, M., & Casals, N. (2012). Ceramide levels regulated by carnitine palmitoyltransferase 1C control dendritic spine

maturation and cognition. *J Biol Chem*, *287*(25), 21224-21232. https://doi.org/10.1074/jbc.M111.337493

Casals, N., Zammit, V., Herrero, L., Fado, R., Rodriguez-Rodriguez, R., & Serra, D. (2016). Carnitine palmitoyltransferase 1C: From cognition to cancer. *Prog Lipid Res*, *61*, 134-148. https://doi.org/10.1016/j.plipres.2015.11.004

Casas, M., Fado, R., Dominguez, J. L., Roig, A., Kaku, M., Chohnan, S., Sole, M., Unzeta, M., Minano-Molina, A. J., Rodriguez-Alvarez, J., Dickson, E. J., & Casals, N. (2020). Sensing of nutrients by CPT1C controls SAC1 activity to regulate AMPA receptor trafficking. *J Cell Biol*, *219*(10). https://doi.org/10.1083/jcb.201912045

Chen, X., Tomchick, D. R., Kovrigin, E., Araç, D., Machius, M., Südhof, T. C., & Rizo, J. (2002). Three-dimensional structure of the complexin/SNARE complex. *Neuron*, *33*(3), 397-409. https://doi.org/10.1016/s0896-6273(02)00583-4

Cheong, F. Y., Sharma, V., Blagoveshchenskaya, A., Oorschot, V. M., Brankatschk, B., Klumperman, J., Freeze, H. H., & Mayinger, P. (2010). Spatial regulation of Golgi phosphatidylinositol-4-phosphate is required for enzyme localization and glycosylation fidelity. *Traffic*, *11*(9), 1180-1190. https://doi.org/10.1111/j.1600-0854.2010.01092.x

Chernomordik, L. V., & Kozlov, M. M. (2008). Mechanics of membrane fusion. *Nat Struct Mol Biol*, *15*(7), 675-683. https://doi.org/10.1038/nsmb.1455

Choquet, D., & Triller, A. (2013). The dynamic synapse. *Neuron*, *80*(3), 691-703. https://doi.org/10.1016/j.neuron.2013.10.013

Chung, J., Torta, F., Masai, K., Lucast, L., Czapla, H., Tanner, L. B., Narayanaswamy, P., Wenk, M. R., Nakatsu, F., & De Camilli, P. (2015). PI4P/phosphatidylserine countertransport at ORP5- and ORP8-mediated ER-plasma membrane contacts. *Science*, *349*(6246), 428-432. https://doi.org/10.1126/science.aab1370

Citri, A., & Malenka, R. C. (2008). Synaptic plasticity: multiple forms, functions, and mechanisms. *Neuropsychopharmacology*, *33*(1), 18-41. https://doi.org/10.1038/sj.npp.1301559

Cutuli, D., De Bartolo, P., Caporali, P., Laricchiuta, D., Foti, F., Ronci, M., Rossi, C., Neri, C., Spalletta, G., Caltagirone, C., Farioli-Vecchioli, S., & Petrosini, L. (2014). n-3 polyunsaturated fatty acids supplementation enhances hippocampal functionality in aged mice. *Front Aging Neurosci*, *6*, 220. https://doi.org/10.3389/fnagi.2014.00220

D'Angelo, S., Motti, M. L., & Meccariello, R. (2020). omega-3 and omega-6 Polyunsaturated Fatty Acids, Obesity and Cancer. *Nutrients*, *12*(9). https://doi.org/10.3390/nu12092751

Dai, Y., Wolfgang, M. J., Cha, S. H., & Lane, M. D. (2007). Localization and effect of ectopic expression of CPT1c in CNS feeding centers. *Biochem Biophys Res Commun*, *359*(3), 469-474. https://doi.org/10.1016/j.bbrc.2007.05.161

Del Bel, L. M., & Brill, J. A. (2018). Sac1, a lipid phosphatase at the interface of vesicular and nonvesicular transport. *Traffic*, *19*(5), 301-318. https://doi.org/10.1111/tra.12554

Demaugre, F., Bonnefont, J. P., Cepanec, C., Scholte, J., Saudubray, J. M., & Leroux, J. P. (1990). Immunoquantitative Analysis of Human Carnitine Palmitoyltransferase I and I1 Defects. *Pediatr Res.*, *27(5)*, 497-500. https://doi.org/10.1203/00006450-199005000-00016

Di Maio, V. (2008). Regulation of information passing by synaptic transmission: a short review. *Brain Res*, *1225*, 26-38. https://doi.org/10.1016/j.brainres.2008.06.016

Di Majo, D., Cacciabaudo, F., Accardi, G., Gambino, G., Giglia, G., Ferraro, G., Candore, G., & Sardo, P. (2022). Ketogenic and Modified Mediterranean Diet as a Tool to Counteract Neuroinflammation in Multiple Sclerosis: Nutritional Suggestions. *Nutrients*, *14*(12). https://doi.org/10.3390/nu14122384

Diering, G. H., Heo, S., Hussain, N. K., Liu, B., & Huganir, R. L. (2016). Extensive phosphorylation of AMPA receptors in neurons. *Proc Natl Acad Sci U S A*, *113*(33), E4920-4927. https://doi.org/10.1073/pnas.1610631113

Diering, G. H., & Huganir, R. L. (2018). The AMPA Receptor Code of Synaptic Plasticity. *Neuron*, *100*(2), 314-329. https://doi.org/10.1016/j.neuron.2018.10.018

Dippold, H. C., Ng, M. M., Farber-Katz, S. E., Lee, S. K., Kerr, M. L., Peterman, M. C., Sim, R., Wiharto, P. A., Galbraith, K. A., Madhavarapu, S., Fuchs, G. J., Meerloo, T., Farquhar, M. G., Zhou, H., & Field, S. J. (2009). GOLPH3 bridges phosphatidylinositol-4-phosphate and actomyosin to stretch and shape the Golgi to promote budding. *Cell*, *139*(2), 337-351. https://doi.org/10.1016/j.cell.2009.07.052

Dyall, S. C., Michael, G. J., Whelpton, R., Scott, A. G., & Michael-Titus, A. T. (2007). Dietary enrichment with omega-3 polyunsaturated fatty acids reverses age-related decreases in the GluR2 and NR2B glutamate receptor subunits in rat forebrain. *Neurobiol Aging*, *28*(3), 424-439. https://doi.org/10.1016/j.neurobiolaging.2006.01.002

Ehrlich, I., Klein, M., Rumpel, S., & Malinow, R. (2007). PSD-95 is required for activity-driven synapse stabilization. *Proc Natl Acad Sci*, *104*(10), 4176-4181. https://doi.org/10.1073/pnas.0609307104

Ennaceur, A., & Meliani, K. (1992). A new one-trial test for neurobiological studies of memory in rats. III. Spatial vs. non-spatial working memory. *Behav Brain Res*, *51*(1), 83-92. https://doi.org/10.1016/s0166-4328(05)80315-8

Esser, V., Brown, N. F., Cowan, A. T., Foster, D. W., & McGarry, J. D. (1996). Expression of a cDNA Isolated from Rat Brown Adipose Tissue and Heart Identifies the Product as the Muscle Isoform of Carnitine Palmitoyltransferase I (M-CPT I). *The Journal of Biological Chemistry*, *271(12)*, 6972-6977. https://doi.org/10.1074/jbc.271.12.6972

Esteves da Silva, M., Adrian, M., Schatzle, P., Lipka, J., Watanabe, T., Cho, S., Futai, K., Wierenga, C. J., Kapitein, L. C., & Hoogenraad, C. C. (2015). Positioning of AMPA Receptor-Containing Endosomes Regulates Synapse Architecture. *Cell Rep*, *13*(5), 933-943. https://doi.org/10.1016/j.celrep.2015.09.062

Fado, R., Molins, A., Rojas, R., & Casals, N. (2022). Feeding the Brain: Effect of Nutrients on Cognition, Synaptic Function, and AMPA Receptors. *Nutrients*, *14*(19). https://doi.org/10.3390/nu14194137

Fado, R., Rodriguez-Rodriguez, R., & Casals, N. (2021). The return of malonyl-CoA to the brain: Cognition and other stories. *Prog Lipid Res*, *81*, 101071. https://doi.org/10.1016/j.plipres.2020.101071

Fado, R., Soto, D., Minano-Molina, A. J., Pozo, M., Carrasco, P., Yefimenko, N., Rodriguez-Alvarez, J., & Casals, N. (2015). Novel Regulation of the Synthesis of alpha-Amino-3-hydroxy-5-methyl-4-isoxazolepropionic Acid (AMPA) Receptor Subunit GluA1 by Carnitine Palmitoyltransferase 1C (CPT1C) in the Hippocampus. *J Biol Chem*, *290*(42), 25548-25560. https://doi.org/10.1074/jbc.M115.681064

Fado, R., Zagmutt, S., Herrero, L., Muley, H., Rodriguez-Rodriguez, R., Bi, H., Serra, D., & Casals, N. (2023). To be or not to be a fat burner, that is the question for cpt1c in cancer cells. *Cell Death Dis*, *14*(1), 57. https://doi.org/10.1038/s41419-023-05599-1

Fernández-Chacón, R., Königstorfer, A., Gerber, S. H., García, J., Matos, M. F., Stevens, C. F., Brose, N., Rizo, J., Rosenmund, C., & Südhof, T. C. (2001). Synaptotagmin I functions as a calcium regulator of release probability. *Nature*, *410*(6824), 41-49. https://doi.org/10.1038/35065004

Fernandez-Felipe, J., Merino, B., Sanz-Martos, A. B., Plaza, A., Contreras, A., Naranjo, V., Morales, L., Chowen, J. A., Cano, V., Ruiz-Gayo, M., & Del Olmo, N. (2021). Saturated and unsaturated fat diets impair hippocampal glutamatergic transmission in adolescent mice. *Psychoneuroendocrinology*, *133*, 105429. https://doi.org/10.1016/j.psyneuen.2021.105429

Fernandez-Monreal, M., Brown, T. C., Royo, M., & Esteban, J. A. (2012). The balance between receptor recycling and trafficking toward lysosomes determines synaptic strength during long-term depression. *J Neurosci*, *32*(38), 13200-13205. https://doi.org/10.1523/JNEUROSCI.0061-12.2012

Fink, J. K. (2013). Hereditary spastic paraplegia: clinico-pathologic features and emerging molecular mechanisms. *Acta Neuropathol*, *126*(3), 307-328. https://doi.org/10.1007/s00401-013-1115-8

Forrest, S., Chai, A., Sanhueza, M., Marescotti, M., Parry, K., Georgiev, A., Sahota, V., Mendez-Castro, R., & Pennetta, G. (2013). Increased levels of phosphoinositides cause neurodegeneration in a Drosophila model of amyotrophic lateral sclerosis. *Hum Mol Genet*, *22*(13), 2689-2704. https://doi.org/10.1093/hmg/ddt118

Fox, K., & Stryker, M. (2017). Integrating Hebbian and homeostatic plasticity: introduction. *Philos Trans R Soc Lond B Biol Sci*, *372*(1715). https://doi.org/10.1098/rstb.2016.0413

Fujii, S., Tanaka, H., & Hirano, T. (2018). Suppression of AMPA Receptor Exocytosis Contributes to Hippocampal LTD. *J Neurosci*, *38*(24), 5523-5537. https://doi.org/10.1523/JNEUROSCI.3210-17.2018

Fukushima, A., Ogura, Y., Furuta, M., Kakehashi, C., Funabashi, T., & Akema, T. (2015). Ketogenic diet does not impair spatial ability controlled by the hippocampus in male rats. *Brain Res*, *1622*, 36-42. https://doi.org/10.1016/j.brainres.2015.06.016

Furukawa, H., Singh, S. K., Mancusso, R., & Gouaux, E. (2005). Subunit arrangement and function in NMDA receptors. *Nature*, *438*(7065), 185-192. https://doi.org/10.1038/nature04089

Gao, S., Zhu, G., Gao, X., Wu, D., Carrasco, P., Casals, N., Hegardt, F. G., Moran, T. H., & Lopaschuk, G. D. (2011). Important roles of brain-specific carnitine palmitoyltransferase and ceramide metabolism in leptin hypothalamic control of feeding. *Proc Natl Acad Sci U S A*, *108*(23), 9691-9696. https://doi.org/10.1073/pnas.1103267108

Gao, X. F., Chen, W., Kong, X. P., Xu, A. M., Wang, Z. G., Sweeney, G., & Wu, D. (2009). Enhanced susceptibility of Cpt1c knockout mice to glucose intolerance induced by a high-fat diet involves elevated hepatic gluconeogenesis and decreased skeletal muscle glucose

uptake. *Diabetologia*, *52*(5), 912-920. https://doi.org/10.1007/s00125-009-1284-0

Gardener, S. L., & Rainey-Smith, S. R. (2018). The Role of Nutrition in Cognitive Function and Brain Ageing in the Elderly. *Curr Nutr Rep*, *7*(3), 139-149. https://doi.org/10.1007/s13668-018-0229-y

Gibson, E. L., Barr, S., & Jeanes, Y. M. (2013). Habitual fat intake predicts memory function in younger women. *Front Hum Neurosci*, *7*, 838. https://doi.org/10.3389/fnhum.2013.00838

Golomb, B. A., & Bui, A. K. (2015). A Fat to Forget: Trans Fat Consumption and Memory. *PLoS One*, *10*(6), e0128129. https://doi.org/10.1371/journal.pone.0128129

Gómez-Pinilla, F. (2008). Brain foods: the effects of nutrients on brain function. *Nat Rev Neurosci*, *9*(7), 568-578. https://doi.org/10.1038/nrn2421

Granger, A. J., Shi, Y., Lu, W., Cerpas, M., & Nicoll, R. A. (2013). LTP requires a reserve pool of glutamate receptors independent of subunit type. *Nature*, *493*(7433), 495-500. https://doi.org/10.1038/nature11775

Granholm, A. C., Bimonte-Nelson, H. A., Moore, A. B., Nelson, M. E., Freeman, L. R., & Sambamurtia, K. (2008). Effects of a saturated fat and high cholesterol diet on memory and hippocampal morphology in the middle-aged rat. *J Alzheimer's Dis*, *14*(2), 133-145. https://doi.org/10.3233/jad-2008-14202

Gratacos-Batlle, E., Yefimenko, N., Cascos-Garcia, H., & Soto, D. (2015). AMPAR interacting protein CPT1C enhances surface expression of GluA1-containing receptors. *Front Cell Neurosci*, *8*, 469. https://doi.org/10.3389/fncel.2014.00469

Gray, E. E., Guglietta, R., Khakh, B. S., & O'Dell, T. J. (2014). Inhibitory interactions between phosphorylation sites in the C terminus of alpha-Amino-3-hydroxy-5-methyl-4-isoxazolepropionic acid-type glutamate receptor GluA1 subunits. *J Biol Chem*, *289*(21), 14600-14611. https://doi.org/10.1074/jbc.M114.553537

Greger, I. H., Watson, J. F., & Cull-Candy, S. G. (2017). Structural and Functional Architecture of AMPA-Type Glutamate Receptors and Their Auxiliary Proteins. *Neuron*, *94*(4), 713-730. https://doi.org/10.1016/j.neuron.2017.04.009

Greger, I. H., Ziff, E. B., & Penn, A. C. (2007). Molecular determinants of AMPA receptor subunit assembly. *Trends Neurosci*, *30*(8), 407-416. https://doi.org/10.1016/j.tins.2007.06.005

Griffiths, N. W., Del Bel, L. M., Wilk, R., & Brill, J. A. (2020). Cellular homeostasis in the Drosophila retina requires the lipid

phosphatase Sac1. *Mol Biol Cell*, *31*(11), 1183-1199. https://doi.org/10.1091/mbc.E20-02-0161

Grillo, C. A., Piroli, G. G., Evans, A. N., Macht, V. A., Wilson, S. P., Scott, K. A., Sakai, R. R., Mott, D. D., & Reagan, L. P. (2011). Obesity/hyperleptinemic phenotype adversely affects hippocampal plasticity: effects of dietary restriction. *Physiol Behav*, *104*(2), 235-241. https://doi.org/10.1016/j.physbeh.2010.10.020

Grinan-Ferre, C., Codony, S., Pujol, E., Yang, J., Leiva, R., Escolano, C., Puigoriol-Illamola, D., Companys-Alemany, J., Corpas, R., Sanfeliu, C., Perez, B., Loza, M. I., Brea, J., Morisseau, C., Hammock, B. D., Vazquez, S., Pallas, M., & Galdeano, C. (2020). Pharmacological Inhibition of Soluble Epoxide Hydrolase as a New Therapy for Alzheimer's Disease. *Neurotherapeutics*, *17*(4), 1825-1835. https://doi.org/10.1007/s13311-020-00854-1

Grinan-Ferre, C., Palomera-Avalos, V., Puigoriol-Illamola, D., Camins, A., Porquet, D., Pla, V., Aguado, F., & Pallas, M. (2016). Behaviour and cognitive changes correlated with hippocampal neuroinflammaging and neuronal markers in female SAMP8, a model of accelerated senescence. *Exp Gerontol*, *80*, 57-69. https://doi.org/10.1016/j.exger.2016.03.014

Guo, C., & Ma, Y. Y. (2021). Calcium Permeable-AMPA Receptors and Excitotoxicity in Neurological Disorders. *Front Neural Circuits*, *15*, 711564. https://doi.org/10.3389/fncir.2021.711564

Guo, S., Stolz, L. E., Lemrow, S. M., & York, J. D. (1999). SAC1-like domains of yeast SAC1, INP52, and INP53 and of human synaptojanin encode polyphosphoinositide phosphatases. *J Biol Chem*, *274*(19), 12990-12995. https://doi.org/10.1074/jbc.274.19.12990

Hahm, J. R., Jo, M. H., Ullah, R., Kim, M. W., & Kim, M. O. (2020). Metabolic Stress Alters Antioxidant Systems, Suppresses the Adiponectin Receptor 1 and Induces Alzheimer's Like Pathology in Mice Brain. *Cells*, *9*(1). https://doi.org/10.3390/cells9010249

Hangen, E., Cordelieres, F. P., Petersen, J. D., Choquet, D., & Coussen, F. (2018). Neuronal Activity and Intracellular Calcium Levels Regulate Intracellular Transport of Newly Synthesized AMPAR. *Cell Rep*, *24*(4), 1001-1012 e1003. https://doi.org/10.1016/j.celrep.2018.06.095

Hardie, D. G. (2015). AMPK: positive and negative regulation, and its role in whole-body energy homeostasis. *Curr Opin Cell Biol*, *33*, 1-7. https://doi.org/10.1016/j.ceb.2014.09.004

Hebb, D. O. (1949). The organization of behavior. *New York: Wiley & Sons*.

Heim, L. R., Shoob, S., de Marcas, L., Zarhin, D., & Slutsky, I. (2022). Measuring synaptic transmission and plasticity with fEPSP recordings in behaving mice. *STAR Protoc*, *3*(1), 101115. https://doi.org/10.1016/j.xpro.2021.101115

Henderson, S. T., Vogel, J. L., Barr, L. J., Garvin, F., Jones, J. J., & Costantini, L. C. (2009). Study of the ketogenic agent AC-1202 in mild to moderate Alzheimer's disease: a randomized, double-blind, placebo-controlled, multicenter trial. *Nutr Metab (Lond)*, *6*, 31. https://doi.org/10.1186/1743-7075-6-31

Herguedas, B., Garcia-Nafria, J., Cais, O., Fernandez-Leiro, R., Krieger, J., Ho, H., & Greger, I. H. (2016). Structure and organization of heteromeric AMPA-type glutamate receptors. *Science*, *352*(6285), aad3873. https://doi.org/10.1126/science.aad3873

Hernandez, A. R., Hernandez, C. M., Campos, K., Truckenbrod, L., Federico, Q., Moon, B., McQuail, J. A., Maurer, A. P., Bizon, J. L., & Burke, S. N. (2018). A Ketogenic Diet Improves Cognition and Has Biochemical Effects in Prefrontal Cortex That Are Dissociable From Hippocampus. *Front Aging Neurosci*, *10*, 391. https://doi.org/10.3389/fnagi.2018.00391

Hill, T. C., & Zito, K. (2013). LTP-induced long-term stabilization of individual nascent dendritic spines. *J Neurosci*, *33*(2), 678-686. https://doi.org/10.1523/JNEUROSCI.1404-12.2013

Hirano, T. (2018). Visualization of Exo- and Endocytosis of AMPA Receptors During Hippocampal Synaptic Plasticity Around Postsynaptic-Like Membrane Formed on Glass Surface. *Front Cell Neurosci*, *12*, 442. https://doi.org/10.3389/fncel.2018.00442

Hodgkin, A. L., & Huxley, A. F. (1952). A quantitative description of membrane current and its application to conduction and excitation in nerve. *J Physiol*, *117*(4), 500-544. https://doi.org/10.1113/jphysiol.1952.sp004764

Hong, D., Cong, L., Zhong, S., Liu, L., Xu, Y., & Zhang, J. (2019). A novel CPT1C variant causes pure hereditary spastic paraplegia with benign clinical course. *Ann Clin Transl Neurol*, *6*(3), 610-614. https://doi.org/10.1002/acn3.717

Hosokawa, T., Mitsushima, D., Kaneko, R., & Hayashi, Y. (2015). Stoichiometry and phosphoisotypes of hippocampal AMPA-type glutamate receptor phosphorylation. *Neuron*, *85*(1), 60-67. https://doi.org/10.1016/j.neuron.2014.11.026

Hu, E., Du, H., Zhu, X., Wang, L., Shang, S., Wu, X., Lu, H., & Lu, X. (2018). Beta-hydroxybutyrate Promotes the Expression of BDNF in Hippocampal Neurons under Adequate Glucose Supply.

Neuroscience, *386*, 315-325. https://doi.org/10.1016/j.neuroscience.2018.06.036

Huang, J., Li, Y. Q., Wu, C. H., Zhang, Y. L., Zhao, S. T., Chen, Y. J., Deng, Y. H., Xuan, A., & Sun, X. D. (2019). The effect of ketogenic diet on behaviors and synaptic functions of naive mice. *Brain Behav*, *9*(4), e01246. https://doi.org/10.1002/brb3.1246

Hume, R. I., Dingledine, R., & Heinemann, S. F. (1991). Identification of a site in glutamate receptor subunits that controls calcium permeability. *Science*, *253*(5023), 1028-1031. https://doi.org/doi.org/10.1126/science.1653450

Hunkeler, M., Hagmann, A., Stuttfeld, E., Chami, M., Guri, Y., Stahlberg, H., & Maier, T. (2018). Structural basis for regulation of human acetyl-CoA carboxylase. *Nature*, *558*(7710), 470-474. https://doi.org/10.1038/s41586-018-0201-4

Iacovides, S., Goble, D., Paterson, B., & Meiring, R. M. (2019). Three consecutive weeks of nutritional ketosis has no effect on cognitive function, sleep, and mood compared with a high-carbohydrate, low-fat diet in healthy individuals: a randomized, crossover, controlled trial. *Am J Clin Nutr*, *110*(2), 349-357. https://doi.org/10.1093/ajcn/nqz073

Iborra-Lazaro, G., Djebari, S., Sanchez-Rodriguez, I., Gratacos-Batlle, E., Sanchez-Fernandez, N., Radosevic, M., Casals, N., Navarro-Lopez, J. D., Soto Del Cerro, D., & Jimenez-Diaz, L. (2023). CPT1C is required for synaptic plasticity and oscillatory activity that supports motor, associative and non-associative learning. *J Physiol*. https://doi.org/10.1113/JP284248

Jung, Y., Seo, J. Y., Ryu, H. G., Kim, D. Y., Lee, K. H., & Kim, K. T. (2020). BDNF-induced local translation of GluA1 is regulated by HNRNP A2/B1. *Sci Adv*, *6*(47), eabd2163. https://doi.org/10.1126/sciadv.abd2163

Jurado, S., Goswami, D., Zhang, Y., Molina, A. J., Sudhof, T. C., & Malenka, R. C. (2013). LTP requires a unique postsynaptic SNARE fusion machinery. *Neuron*, *77*(3), 542-558. https://doi.org/10.1016/j.neuron.2012.11.029

Kapitein, L. C., Schlager, M. A., Kuijpers, M., Wulf, P. S., van Spronsen, M., MacKintosh, F. C., & Hoogenraad, C. C. (2010). Mixed microtubules steer dynein-driven cargo transport into dendrites. *Curr Biol*, *20*(4), 290-299. https://doi.org/10.1016/j.cub.2009.12.052

Kashiwaya, Y., Pawlosky, R., Markis, W., King, M. T., Bergman, C., Srivastava, S., Murray, A., Clarke, K., & Veech, R. L. (2010). A ketone ester diet increases brain malonyl-CoA and Uncoupling proteins 4 and 5 while decreasing food intake in the normal Wistar

Rat. *J Biol Chem*, *285*(34), 25950-25956. https://doi.org/10.1074/jbc.M110.138198

Katz, B. (1969). The release of neural transmitter substances. *Liverpool University Press*.

Kim, J. M., Lee, U., Kang, J. Y., Park, S. K., Kim, J. C., & Heo, H. J. (2020). Matcha Improves Metabolic Imbalance-Induced Cognitive Dysfunction. *Oxid Med Cell Longev*, *2020*, 8882763. https://doi.org/10.1155/2020/8882763

Kimura, R., Ma, L. Y., Wu, C., Turner, D., Shen, J. X., Ellsworth, K., Wakui, M., Maalouf, M., & Wu, J. (2012). Acute exposure to the mitochondrial complex I toxin rotenone impairs synaptic long-term potentiation in rat hippocampal slices. *CNS Neurosci Ther*, *18*(8), 641-646. https://doi.org/10.1111/j.1755-5949.2012.00337.x

Klimova, B., Dziuba, S., & Cierniak-Emerych, A. (2020). The Effect of Healthy Diet on Cognitive Performance Among Healthy Seniors - A Mini Review. *Front Hum Neurosci*, *14*, 325. https://doi.org/10.3389/fnhum.2020.00325

Kochendörfer, K. U., Then, A. R., Kearns, B. G., Bankaitis, V. A., & Mayinger, P. (1999). Sac1p plays a crucial role in microsomal ATP transport, which is distinct from its function in Golgi phospholipid metabolism. *EMBO J.*, *18*(6), 1506-1515. https://doi.org/10.1093/emboj/18.6.1506

Kolb, H., Kempf, K., Rohling, M., Lenzen-Schulte, M., Schloot, N. C., & Martin, S. (2021). Ketone bodies: from enemy to friend and guardian angel. *BMC Med*, *19*(1), 313. https://doi.org/10.1186/s12916-021-02185-0

Konrad, G., Schlecker, T., Faulhammer, F., & Mayinger, P. (2002). Retention of the yeast Sac1p phosphatase in the endoplasmic reticulum causes distinct changes in cellular phosphoinositide levels and stimulates microsomal ATP transport. *J Biol Chem*, *277*(12), 10547-10554. https://doi.org/10.1074/jbc.M200090200

Krijnse-Locker, J., Parton, R. G., Fuller, S. D., Griffiths, G., & G., D. C. (1995). The organization of the endoplasmic reticulum and the intermediate compartment in cultured rat hippocampal neurons. *Mol Biol Cell*, *6*, 1315-1332. https://doi.org/doi.org/10.1091/mbc.6.10.1315

Krikorian, R., Shidler, M. D., Dangelo, K., Couch, S. C., Benoit, S. C., & Clegg, D. J. (2012). Dietary ketosis enhances memory in mild cognitive impairment. *Neurobiol Aging*, *33*(2), 425 e419-427. https://doi.org/10.1016/j.neurobiolaging.2010.10.006

Kristensen, A. S., Jenkins, M. A., Banke, T. G., Schousboe, A., Makino, Y., Johnson, R. C., Huganir, R., & Traynelis, S. F. (2011). Mechanism of Ca2+/calmodulin-dependent kinase II regulation of AMPA receptor gating. *Nat Neurosci*, *14*(6), 727-735. https://doi.org/10.1038/nn.2804

Kulzow, N., Witte, A. V., Kerti, L., Grittner, U., Schuchardt, J. P., Hahn, A., & Floel, A. (2016). Impact of Omega-3 Fatty Acid Supplementation on Memory Functions in Healthy Older Adults. *J Alzheimers Dis*, *51*(3), 713-725. https://doi.org/10.3233/JAD-150886

Kwak, S., Hideyama, T., Yamashita, T., & Aizawa, H. (2010). AMPA receptor-mediated neuronal death in sporadic ALS. *Neuropathology*, *30*(2), 182-188. https://doi.org/10.1111/j.1440-1789.2009.01090.x

Lauretti, E., Nenov, M., Dincer, O., Iuliano, L., & Pratico, D. (2020). Extra virgin olive oil improves synaptic activity, short-term plasticity, memory, and neuropathology in a tauopathy model. *Aging Cell*, *19*(1), e13076. https://doi.org/10.1111/acel.13076

Lee, A. Y., Choi, J. M., Lee, J., Lee, M. H., Lee, S., & Cho, E. J. (2016). Effects of Vegetable Oils with Different Fatty Acid Compositions on Cognition and Memory Ability in Abeta(25-35)-Induced Alzheimer's Disease Mouse Model. *J Med Food*, *19*(10), 912-921. https://doi.org/10.1089/jmf.2016.3737

Lee, H. K., Takamiya, K., Han, J. S., Man, H., Kim, C. H., Rumbaugh, G., Yu, S., Ding, L., He, C., Petralia, R. S., Wenthold, R. J., Gallagher, M., & Huganir, R. (2003). Phosphorylation of the AMPA receptor GluR1 subunit is required for synaptic plasticity and retention of spatial memory. *112*(5), 631-643. https://doi.org/10.1016/s0092-8674(03)00122-3

Lee, H. K., Takamiya, K., He, K., Song, L., & Huganir, R. L. (2010). Specific roles of AMPA receptor subunit GluR1 (GluA1) phosphorylation sites in regulating synaptic plasticity in the CA1 region of hippocampus. *J Neurophysiol*, *103*(1), 479-489. https://doi.org/10.1152/jn.00835.2009

Lee, J., Park, S., Lee, J. Y., Yeo, Y. K., Kim, J. S., & Lim, J. (2012). Improved spatial learning and memory by perilla diet is correlated with immunoreactivities to neurofilament and alpha-synuclein in hilus of dentate gyrus. *Proteome Sci*, *10*(1), 72. https://doi.org/10.1186/1477-5956-10-72

Lee, S., Goodson, M. L., Vang, W., Rutkowsky, J., Kalanetra, K., Bhattacharya, M., Barile, D., & Raybould, H. E. (2021). Human milk oligosaccharide 2'-fucosyllactose supplementation improves gut barrier function and signaling in the vagal afferent pathway in

mice. *Food Funct*, *12*(18), 8507-8521. https://doi.org/10.1039/d1fo00658d

Lee, S., Kim, S., Nahm, M., Kim, E., Kim, T. I., Yoon, J. H., & Lee, S. (2011). The phosphoinositide phosphatase Sac1 is required for midline axon guidance. *Mol Cells*, *32*(5), 477-482. https://doi.org/10.1007/s10059-011-0168-6

Leonard, A. S., Davare, M. A., Horne, M. C., Garner, C. C., & Hell, J. W. (1998). SAP97 is associated with the alpha-amino-3-hydroxy-5-methylisoxazole-4-propionic acid receptor GluR1 subunit. *J Biol Chem*, *273*(31), 19518-19524. https://doi.org/10.1074/jbc.273.31.19518

Leyh, J., Winter, K., Reinicke, M., Ceglarek, U., Bechmann, I., & Landmann, J. (2021). Long-term diet-induced obesity does not lead to learning and memory impairment in adult mice. *PLoS One*, *16*(9), e0257921. https://doi.org/10.1371/journal.pone.0257921

Lilliu, V., Pernas-Alonso, R., Trelles, R. D., di Porzio, U., Zuddas, A., & Perrone-Capano, C. (2001). Ontogeny of AMPA receptor gene expression in the developing rat midbrain and striatum. *Brain Res Mol Brain Res*, *96*(1-2), 133-141. https://doi.org/10.1016/s0169-328x(01)00280-7

Liu, K., Kong, L., Graham, D. B., Carey, K. L., & Xavier, R. J. (2021). SAC1 regulates autophagosomal phosphatidylinositol-4-phosphate for xenophagy-directed bacterial clearance. *Cell Rep*, *36*(4), 109434. https://doi.org/10.1016/j.celrep.2021.109434

Liu, Y., Boukhelifa, M., Tribble, E., Morin-Kensicki, E., Uetrecht, A., Bear, J. E., & Bankaitis, V. A. (2008). The Sac1 phosphoinositide phosphatase regulates Golgi membrane morphology and mitotic spindle organization in mammals. *Mol Biol Cell*, *19*(7), 3080-3096. https://doi.org/10.1091/mbc.e07-12-1290

Loehfelm, A., Elder, M. K., Boucsein, A., Jones, P. P., Williams, J. M., & Tups, A. (2020). Docosahexaenoic acid prevents palmitate-induced insulin-dependent impairments of neuronal health. *FASEB J*, *34*(3), 4635-4652. https://doi.org/10.1096/fj.201902517R

Lomeli, H., Mosbacher, J., Melcher, T., Höger, T., Geiger, J. R., Kuner, T., Monyer, H., Higuchi, M., Bach, A., & Seeburg, P. H. (1994). Control of kinetic properties of AMPA receptor channels by nuclear RNA editing. *Science*, *266*(5191), 1709-1713. https://doi.org/10.1126/science.7992055

Lopez-Taboada, I., Gonzalez-Pardo, H., & Conejo, N. M. (2020). Western Diet: Implications for Brain Function and Behavior. *Front Psychol*, *11*, 564413. https://doi.org/10.3389/fpsyg.2020.564413

Louail, A., Bengoetxea de Tena, I., Rojas, R., & Casals, N. (2023). XIth Cajal Conference: New frontiers in neuron-glial plasticity in health and disease. *Eur J Neurosci*, *57*(9), 1447-1465. https://doi.org/10.1111/ejn.15960

Lowder, J., Fallah, S., Venditti, C., Musa-Veloso, K., & Kotlov, V. (2023). An open-label, acute clinical trial in adults to assess ketone levels, gastrointestinal tolerability, and sleepiness following consumption of (R)-1,3-butanediol (Avela). *Front Physiol*, *14*, 1195702. https://doi.org/10.3389/fphys.2023.1195702

Luscher, C., & Malenka, R. C. (2012). NMDA receptor-dependent long-term potentiation and long-term depression (LTP/LTD). *Cold Spring Harb Perspect Biol*, *4*(6). https://doi.org/10.1101/cshperspect.a005710

Lynch, M. A. (2004). Long-term potentiation and memory. *Physiol Rev*, *84*(1), 87-136. https://doi.org/10.1152/physrev.00014.2003

Maalouf, M., & Rho, J. M. (2008). Oxidative impairment of hippocampal long-term potentiation involves activation of protein phosphatase 2A and is prevented by ketone bodies. *J Neurosci Res*, *86*(15), 3322-3330. https://doi.org/10.1002/jnr.21782

Magee, J. C., & Grienberger, C. (2020). Synaptic Plasticity Forms and Functions. *Annu Rev Neurosci*, *43*, 95-117. https://doi.org/10.1146/annurev-neuro-090919-022842

Malinow, R., & Malenka, R. C. (2002). AMPA receptor trafficking and synaptic plasticity. *Annu Rev Neurosci*, *25*, 103-126. https://doi.org/10.1146/annurev.neuro.25.112701.142758

Manford, A., Xia, T., Saxena, A. K., Stefan, C., Hu, F., Emr, S. D., & Mao, Y. (2010). Crystal structure of the yeast Sac1: implications for its phosphoinositide phosphatase function. *EMBO J*, *29*(9), 1489-1498. https://doi.org/10.1038/emboj.2010.57

Manville, R. W., Papanikolaou, M., & Abbott, G. W. (2020). M-Channel Activation Contributes to the Anticonvulsant Action of the Ketone Body beta-Hydroxybutyrate. *J Pharmacol Exp Ther*, *372*(2), 148-156. https://doi.org/10.1124/jpet.119.263350

Marosi, K., Kim, S. W., Moehl, K., Scheibye-Knudsen, M., Cheng, A., Cutler, R., Camandola, S., & Mattson, M. P. (2016). 3-Hydroxybutyrate regulates energy metabolism and induces BDNF expression in cerebral cortical neurons. *J Neurochem*, *139*(5), 769-781. https://doi.org/10.1111/jnc.13868

Martin, A. A., Davidson, T. L., & McCrory, M. A. (2018). Deficits in episodic memory are related to uncontrolled eating in a sample of healthy adults. *Appetite*, *124*, 33-42. https://doi.org/10.1016/j.appet.2017.05.011

Martínez-Lapiscina, E. H., Clavero, P., Toledo, E., Estruch, R., Salas-Salvadó, J., San Julián, B., Sanchez-Tainta, A., Ros, E., Valls-Pedret, C., & Martinez-Gonzalez, M. Á. (2013). Mediterranean diet improves cognition: the PREDIMED-NAVARRA randomised trial. *J Neurol Neurosurg Psychiatry*, *84*(12), 1318-1325. https://doi.org/10.1136/jnnp-2012-304792

Mayer, M. L. (2006). Glutamate receptors at atomic resolution. *Nature*, *440*(7083), 456-462. https://doi.org/10.1038/nature04709

Mayinger, P. (2009). Regulation of Golgi function via phosphoinositide lipids. *Semin Cell Dev Biol*, *20*(7), 793-800. https://doi.org/10.1016/j.semcdb.2009.03.016

McGarry, J. D., & Brown, N. F. (1997). The mitochondrial carnitine palmitoyltransferase system. From concept to molecular analysis. *Eur J Biochem*, *244*, 1-14. https://doi.org/10.1111/j.1432-1033.1997.00001.x

McLean, F. H., Campbell, F. M., Sergi, D., Grant, C., Morris, A. C., Hay, E. A., MacKenzie, A., Mayer, C. D., Langston, R. F., & Williams, L. M. (2019). Early and reversible changes to the hippocampal proteome in mice on a high-fat diet. *Nutr Metab (Lond)*, *16*, 57. https://doi.org/10.1186/s12986-019-0387-y

Middei, S., Houeland, G., Cavallucci, V., Ammassari-Teule, M., D'Amelio, M., & Marie, H. (2013). CREB is necessary for synaptic maintenance and learning-induced changes of the AMPA receptor GluA1 subunit. *Hippocampus*, *23*(6), 488-499. https://doi.org/10.1002/hipo.22108

Miles, K. N., & Skelton, M. R. (2020). Male mice placed on a ketogenic diet from postnatal day (P) 21 through adulthood have reduced growth, are hypoactive, show increased freezing in a conditioned fear paradigm, and have spatial learning deficits. *Brain Res*, *1734*, 146697. https://doi.org/10.1016/j.brainres.2020.146697

Miralpeix, C., Reguera, A. C., Fosch, A., Casas, M., Lillo, J., Navarro, G., Franco, R., Casas, J., Alexander, S. P. H., Casals, N., & Rodriguez-Rodriguez, R. (2021). Carnitine palmitoyltransferase 1C negatively regulates the endocannabinoid hydrolase ABHD6 in mice, depending on nutritional status. *Br J Pharmacol*, *178*(7), 1507-1523. https://doi.org/10.1111/bph.15377

Moretto, E., & Passafaro, M. (2018). Recent Findings on AMPA Receptor Recycling. *Front Cell Neurosci*, *12*, 286. https://doi.org/10.3389/fncel.2018.00286

Moser von Filseck, J., Copic, A., Delfosse, V., Vanni, S., Jackson, C. L., Bourguet, W., & Drin, G. (2015). Phosphatidylserine transport by

ORP/Osh proteins is driven by phosphatidylinositol 4-phosphate. *Science*, *349*, 432-436. https://doi.org/10.1126/science.aab1346

Moser von Filseck, J., Vanni, S., Mesmin, B., Antonny, B., & Drin, G. (2015). A phosphatidylinositol-4-phosphate powered exchange mechanism to create a lipid gradient between membranes. *Nat Commun*, *6*, 6671. https://doi.org/10.1038/ncomms7671

Muley, H., Valencia, K., Casas, J., Moreno, B., Botella, L., Lecanda, F., Fado, R., & Casals, N. (2023). Cpt1c Downregulation Causes Plasma Membrane Remodelling and Anthracycline Resistance in Breast Cancer. *Int J Mol Sci*, *24*(2). https://doi.org/10.3390/ijms24020946

Nakano, R., Nakayama, T., & Sugiya, H. (2020). Biological Properties of JNK3 and Its Function in Neurons, Astrocytes, Pancreatic beta-Cells and Cardiovascular Cells. *Cells*, *9*(8). https://doi.org/10.3390/cells9081802

Negrete-Diaz, J. V., Falcon-Moya, R., & Rodriguez-Moreno, A. (2022). Kainate receptors: from synaptic activity to disease. *FEBS J*, *289*(17), 5074-5088. https://doi.org/10.1111/febs.16081

Nemoto, Y., Kearns, B. G., Wenk, M. R., Chen, H., Mori, K., Alb, J. G., Jr., De Camilli, P., & Bankaitis, V. A. (2000). Functional characterization of a mammalian Sac1 and mutants exhibiting substrate-specific defects in phosphoinositide phosphatase activity. *J Biol Chem*, *275*(44), 34293-34305. https://doi.org/10.1074/jbc.M003923200

Newman, J. C., Covarrubias, A. J., Zhao, M., Yu, X., Gut, P., Ng, C. P., Huang, Y., Haldar, S., & Verdin, E. (2017). Ketogenic Diet Reduces Midlife Mortality and Improves Memory in Aging Mice. *Cell Metab*, *26*(3), 547-557 e548. https://doi.org/10.1016/j.cmet.2017.08.004

Newport, M. T., VanItallie, T. B., Kashiwaya, Y., King, M. T., & Veech, R. L. (2015). A new way to produce hyperketonemia: use of ketone ester in a case of Alzheimer's disease. *Alzheimers Dement*, *11*(1), 99-103. https://doi.org/10.1016/j.jalz.2014.01.006

Niswender, C. M., & Conn, P. J. (2010). Metabotropic glutamate receptors: physiology, pharmacology, and disease. *Annu Rev Pharmacol Toxicol*, *50*, 295-322. https://doi.org/10.1146/annurev.pharmtox.011008.145533

Novick, P., Osmond, B. C., & Botstein, D. (1989). Suppressors of yeast actin mutations. *Genetics*, *121*(4), 659-674. https://doi.org/10.1093/genetics/121.4.659

Oh, M. C., Derkach, V. A., Guire, E. S., & Soderling, T. R. (2006). Extrasynaptic membrane trafficking regulated by GluR1 serine 845 phosphorylation primes AMPA receptors for long-term

potentiation. *J Biol Chem*, *281*(2), 752-758. https://doi.org/10.1074/jbc.M509677200

Okereke, O. I., Rosner, B. A., Kim, D. H., Kang, J. H., Cook, N. R., Manson, J. E., Buring, J. E., Willett, W. C., & Grodstein, F. (2012). Dietary fat types and 4-year cognitive change in community-dwelling older women. *Ann Neurol*, *72*(1), 124-134. https://doi.org/10.1002/ana.23593

Osborne, D. M., Fitzgerald, D. P., O'Leary, K. E., Anderson, B. M., Lee, C. C., Tessier, P. M., & McNay, E. C. (2016). Intrahippocampal administration of a domain antibody that binds aggregated amyloid-beta reverses cognitive deficits produced by diet-induced obesity. *Biochim Biophys Acta*, *1860*(6), 1291-1298. https://doi.org/10.1016/j.bbagen.2016.03.005

Ota, M., Matsuo, J., Ishida, I., Takano, H., Yokoi, Y., Hori, H., Yoshida, S., Ashida, K., Nakamura, K., Takahashi, T., & Kunugi, H. (2019). Effects of a medium-chain triglyceride-based ketogenic formula on cognitive function in patients with mild-to-moderate Alzheimer's disease. *Neurosci Lett*, *690*, 232-236. https://doi.org/10.1016/j.neulet.2018.10.048

Palomo-Guerrero, M., Fado, R., Casas, M., Perez-Montero, M., Baena, M., Helmer, P. O., Dominguez, J. L., Roig, A., Serra, D., Hayen, H., Stenmark, H., Raiborg, C., & Casals, N. (2019). Sensing of nutrients by CPT1C regulates late endosome/lysosome anterograde transport and axon growth. *Elife*, *8*. https://doi.org/10.7554/eLife.51063

Pan, J. W., Rothman, T. L., Behar, K. L., Stein, D. T., & Hetherington, H. P. (2000). Human brain beta-hydroxybutyrate and lactate increase in fasting-induced ketosis. *J Cereb Blood Flow Metab.*, *20*(10), 1502-1507. https://doi.org/10.1097/00004647-200010000-00012

Paolicelli, R. C., & Gross, C. T. (2011). Microglia in development: linking brain wiring to brain environment. *Neuron Glia Biol*, *7*(1), 77-83. https://doi.org/10.1017/S1740925X12000105

Parcerisas, A., Pujadas, L., Ortega-Gasco, A., Perello-Amoros, B., Viais, R., Hino, K., Figueiro-Silva, J., La Torre, A., Trullas, R., Simo, S., Luders, J., & Soriano, E. (2020). NCAM2 Regulates Dendritic and Axonal Differentiation through the Cytoskeletal Proteins MAP2 and 14-3-3. *Cereb Cortex*, *30*(6), 3781-3799. https://doi.org/10.1093/cercor/bhz342

Park, J. (2018). Phosphorylation of the AMPAR-TARP Complex in Synaptic Plasticity. *Proteomes*, *6*(4). https://doi.org/10.3390/proteomes6040040

Parkinson, G. T., & Hanley, J. G. (2018). Mechanisms of AMPA Receptor Endosomal Sorting. *Front Mol Neurosci*, *11*, 440. https://doi.org/10.3389/fnmol.2018.00440

Power, R., Nolan, J. M., Prado-Cabrero, A., Roche, W., Coen, R., Power, T., & Mulcahy, R. (2022). Omega-3 fatty acid, carotenoid and vitamin E supplementation improves working memory in older adults: A randomised clinical trial. *Clin Nutr*, *41*(2), 405-414. https://doi.org/10.1016/j.clnu.2021.12.004

Pozo, M., Rodriguez-Rodriguez, R., Ramirez, S., Seoane-Collazo, P., Lopez, M., Serra, D., Herrero, L., & Casals, N. (2017). Hypothalamic Regulation of Liver and Muscle Nutrient Partitioning by Brain-Specific Carnitine Palmitoyltransferase 1C in Male Mice. *Endocrinology*, *158*(7), 2226-2238. https://doi.org/10.1210/en.2017-00151

Price, N., van der Leij, F., Jackson, V., Corstorphine, C., Thomson, R., Sorensen, A., & Zammit, V. (2002). A novel brain-expressed protein related to carnitine palmitoyltransferase I. *Genomics*, *80*(4), 433-442. https://doi.org/10.1006/geno.2002.6845

Puchalska, P., & Crawford, P. A. (2017). Multi-dimensional Roles of Ketone Bodies in Fuel Metabolism, Signaling, and Therapeutics. *Cell Metab*, *25*(2), 262-284. https://doi.org/10.1016/j.cmet.2016.12.022

Puri, S., Shaheen, M., & Grover, B. (2023). Nutrition and cognitive health: A life course approach. *Front Public Health*, *11*, 1023907. https://doi.org/10.3389/fpubh.2023.1023907

Purkey, A. M., & Dell'Acqua, M. L. (2020). Phosphorylation-Dependent Regulation of Ca(2+)-Permeable AMPA Receptors During Hippocampal Synaptic Plasticity. *Front Synaptic Neurosci*, *12*, 8. https://doi.org/10.3389/fnsyn.2020.00008

Qian, J., Yao, B., & Wu, C. (2014). Fluorescence resonance energy transfer detection methods: Sensitized emission and acceptor bleaching. *Exp Ther Med*, *8*(5), 1375-1380. https://doi.org/10.3892/etm.2014.1928

Ramirez, S., Martins, L., Jacas, J., Carrasco, P., Pozo, M., Clotet, J., Serra, D., Hegardt, F. G., Dieguez, C., Lopez, M., & Casals, N. (2013). Hypothalamic ceramide levels regulated by CPT1C mediate the orexigenic effect of ghrelin. *Diabetes*, *62*(7), 2329-2337. https://doi.org/10.2337/db12-1451

Rangel-Huerta, O. D., & Gil, A. (2018). Effect of omega-3 fatty acids on cognition: an updated systematic review of randomized clinical trials. *Nutr Rev*, *76*(1), 1-20. https://doi.org/10.1093/nutrit/nux064

Rao, J. N., Warren, G. Z. L., Estolt-Povedano, S., Zammit, V. A., & Ulmer, T. S. (2011). An environment-dependent structural switch underlies the regulation of carnitine palmitoyltransferase 1A. *J Biol Chem*, *286*(49), 42545-42554. https://doi.org/10.1074/jbc.M111.306951

Richardson, M. J., & Silberberg, G. (2008). Measurement and analysis of postsynaptic potentials using a novel voltage-deconvolution method. *J Neurophysiol*, *99*(2), 1020-1031. https://doi.org/10.1152/jn.00942.2007

Rinaldi, C., Schmidt, T., Situ, A. J., Johnson, J. O., Lee, P. R., Chen, K. L., Bott, L. C., Fado, R., Harmison, G. H., Parodi, S., Grunseich, C., Renvoise, B., Biesecker, L. G., De Michele, G., Santorelli, F. M., Filla, A., Stevanin, G., Durr, A., Brice, A., . . . Fischbeck, K. H. (2015). Mutation in CPT1C Associated With Pure Autosomal Dominant Spastic Paraplegia. *JAMA Neurol*, *72*(5), 561-570. https://doi.org/10.1001/jamaneurol.2014.4769

Roa-Mansergas, X., Fado, R., Atari, M., Mir, J. F., Muley, H., Serra, D., & Casals, N. (2018). CPT1C promotes human mesenchymal stem cells survival under glucose deprivation through the modulation of autophagy. *Sci Rep*, *8*(1), 6997. https://doi.org/10.1038/s41598-018-25485-7

Rodenas-Gonzalez, F., Blanco-Gandia, M. C., Minarro, J., & Rodriguez-Arias, M. (2022). Cognitive profile of male mice exposed to a Ketogenic Diet. *Physiol Behav*, *254*, 113883. https://doi.org/10.1016/j.physbeh.2022.113883

Rodriguez-Rodriguez, R., Miralpeix, C., Fosch, A., Pozo, M., Calderon-Dominguez, M., Perpinya, X., Vellvehi, M., Lopez, M., Herrero, L., Serra, D., & Casals, N. (2019). CPT1C in the ventromedial nucleus of the hypothalamus is necessary for brown fat thermogenesis activation in obesity. *Mol Metab*, *19*, 75-85. https://doi.org/10.1016/j.molmet.2018.10.010

Rohde, H. M., Cheong, F. Y., Konrad, G., Paiha, K., Mayinger, P., & Boehmelt, G. (2003). The human phosphatidylinositol phosphatase SAC1 interacts with the coatomer I complex. *J Biol Chem*, *278*(52), 52689-52699. https://doi.org/10.1074/jbc.M307983200

Rojas-Morales, P., Pedraza-Chaverri, J., & Tapia, E. (2020). Ketone bodies, stress response, and redox homeostasis. *Redox Biol*, *29*, 101395. https://doi.org/10.1016/j.redox.2019.101395

Rojic-Becker, D., Portero-Tresserra, M., Marti-Nicolovius, M., Vale-Martinez, A., & Guillazo-Blanch, G. (2019). Caloric restriction modulates the monoaminergic and glutamatergic systems in the hippocampus, and attenuates age-dependent spatial memory

decline. *Neurobiol Learn Mem*, *166*, 107107. https://doi.org/10.1016/j.nlm.2019.107107

Rothman, J. S., & Silver, R. A. (2018). NeuroMatic: An Integrated Open-Source Software Toolkit for Acquisition, Analysis and Simulation of Electrophysiological Data. *Front Neuroinform*, *12*, 14. https://doi.org/10.3389/fninf.2018.00014

Rubink, D. S., & Winder, W. W. (2005). Effect of phosphorylation by AMP-activated protein kinase on palmitoyl-CoA inhibition of skeletal muscle acetyl-CoA carboxylase. *J Appl Physiol (1985)*, *98*(4), 1221-1227. https://doi.org/10.1152/japplphysiol.00621.2004

Samanta, S., Situ, A. J., & Ulmer, T. S. (2014). Structural characterization of the regulatory domain of brain carnitine palmitoyltransferase 1. *Biopolymers*, *101*(4), 398-405. https://doi.org/10.1002/bip.22396

Sampaio, L. P. (2016). Ketogenic diet for epilepsy treatment. *Arq Neuropsiquiatr*, *74*(10), 842-848. https://doi.org/10.1590/0004-282X20160116

Sanchez-Macedo, N., Feng, J., Faubert, B., Chang, N., Elia, A., Rushing, E. J., Tsuchihara, K., Bungard, D., Berger, S. L., Jones, R. G., Mak, T. W., & Zaugg, K. (2013). Depletion of the novel p53-target gene carnitine palmitoyltransferase 1C delays tumor growth in the neurofibromatosis type I tumor model. *Cell Death Differ*, *20*(4), 659-668. https://doi.org/10.1038/cdd.2012.168

Sans, N., Racca, C., Petralia, R. S., Wang, Y., McCallum, J., & Wenthold, R. J. (2001). Synapse-Associated Protein 97 Selectively Associates with a Subset of AMPA Receptors Early in their Biosynthetic Pathway. *J Neurosci*, *21*(19), 7506-7516. https://doi.org/10.1523/JNEUROSCI.21-19-07506.2001

Sayer, R. J., Friedlander, M. J., & Redman, S. J. (1990). The time course and amplitude of EPSPs evoked at synapses between pairs of CA3/CA1 neurons in the hippocampal slice. *J Neurosci*, *10*(3), 826-836. https://doi.org/10.1523/JNEUROSCI.10-03-00826.1990

Schafer, D. P., Lehrman, E. K., & Stevens, B. (2013). The "quad-partite" synapse: microglia-synapse interactions in the developing and mature CNS. *Glia*, *61*(1), 24-36. https://doi.org/10.1002/glia.22389

Schafer, J. H., Korner, C., Esch, B. M., Limar, S., Parey, K., Walter, S., Januliene, D., Moeller, A., & Frohlich, F. (2023). Structure of the ceramide-bound SPOTS complex. *Nat Commun*, *14*(1), 6196. https://doi.org/10.1038/s41467-023-41747-z

Schorr, M., Then, A., Tahirovic, S., Hug, N., & Mayinger, P. (2001). The phosphoinositide phosphatase Sac1p controls trafficking of the

yeast Chs3p chitin synthase. *Curr. Biol.*, *11*(18), 1421-1426. https://doi.org/10.1016/s0960-9822(01)00449-3

Schwenk, J., Boudkkazi, S., Kocylowski, M. K., Brechet, A., Zolles, G., Bus, T., Costa, K., Kollewe, A., Jordan, J., Bank, J., Bildl, W., Sprengel, R., Kulik, A., Roeper, J., Schulte, U., & Fakler, B. (2019). An ER Assembly Line of AMPA-Receptors Controls Excitatory Neurotransmission and Its Plasticity. *Neuron*, *104*(4), 680-692 e689. https://doi.org/10.1016/j.neuron.2019.08.033

Schwenk, J., Harmel, N., Brechet, A., Zolles, G., Berkefeld, H., Muller, C. S., Bildl, W., Baehrens, D., Huber, B., Kulik, A., Klocker, N., Schulte, U., & Fakler, B. (2012). High-resolution proteomics unravel architecture and molecular diversity of native AMPA receptor complexes. *Neuron*, *74*(4), 621-633. https://doi.org/10.1016/j.neuron.2012.03.034

Schwenk, J., Harmel, N., Zolles, G., Bildl, W., Kulik, A., Heimrich, B., Chisaka, O., Jonas, P., Schulte, U., Fakler, B., & Klöcker, N. (2009). Functional proteomics identify cornichon proteins as auxiliary subunits of AMPA receptors. *Science*, *323*(5919), 1313-1319. https://doi.org/10.1126/science.1167852

Seebohm, G., Wrobel, E., Pusch, M., Dicks, M., Terhag, J., Matschke, V., Rothenberg, I., Ursu, O. N., Hertel, F., Pott, L., Lang, F., Schulze-Bahr, E., Hollmann, M., Stoll, R., & Strutz-Seebohm, N. (2014). Structural basis of PI(4,5)P2-dependent regulation of GluA1 by phosphatidylinositol-5-phosphate 4-kinase, type II, alpha (PIP5K2A). *Pflugers Arch*, *466*(10), 1885-1897. https://doi.org/10.1007/s00424-013-1424-8

Selvakumar, B., Jenkins, M. A., Hussain, N. K., Huganir, R. L., Traynelis, S. F., & Snyder, S. H. (2013). S-nitrosylation of AMPA receptor GluA1 regulates phosphorylation, single-channel conductance, and endocytosis. *Proc Natl Acad Sci U S A*, *110*(3), 1077-1082. https://doi.org/10.1073/pnas.1221295110

Shatz, C. J. (1992). The developing brain. *Sci Am*, *267*(3), 60-67. https://doi.org/10.1038/scientificamerican0992-60

Shen, L., Liang, F., Walensky, L. D., & Huganir, R. L. (2000). Regulation of AMPA receptor GluR1 subunit surface expression by a 4. 1N-linked actin cytoskeletal association. *J Neurosci*, *20*(21), 7932-7940. https://doi.org/10.1523/JNEUROSCI.20-21-07932.2000

Sierra, A. Y., Gratacos, E., Carrasco, P., Clotet, J., Urena, J., Serra, D., Asins, G., Hegardt, F. G., & Casals, N. (2008). CPT1c is localized in endoplasmic reticulum of neurons and has carnitine palmitoyltransferase activity. *J Biol Chem*, *283*(11), 6878-6885. https://doi.org/10.1074/jbc.M707965200

Sikalidis, A. K., Kelleher, A. H., & Kristo, A. S. (2021). Mediterranean Diet. *Encyclopedia*, *1*(2), 371-387. https://doi.org/10.3390/encyclopedia1020031

Silva, M. C., Rocha, J., Pires, C. S., Ribeiro, L. C., Brolese, G., Leite, M. C., Almeida, L. M., Tramontina, F., Ziegler, D. R., & Goncalves, C. A. (2005). Transitory gliosis in the CA3 hippocampal region in rats fed on a ketogenic diet. *Nutr Neurosci*, *8*(4), 259-264. https://doi.org/10.1080/10284150500475032

Söllner, T., Bennett, M. K., Whiteheart, S. W., Scheller, R. H., & Rothman, J. E. (1993). A protein assembly-disassembly pathway in vitro that may correspond to sequential steps of synaptic vesicle docking, activation, and fusion. *Cell*, *75*(3), 409-418. https://doi.org/10.1016/0092-8674(93)90376-2

Sommer, B., Keinänen, K., Verdoorn, T. A., Wisden, W., Burnashev, N., Herb, A., Köhler, M., Takagi, T., Sakmann, B., & Seeburg, P. H. (1990). Flip and flop: a cell-specific functional switch in glutamate-operated channels of the CNS. *Science*, *249*(4976), 1580-1585. https://doi.org/10.1126/science.1699275

Spencer, S. J., Korosi, A., Laye, S., Shukitt-Hale, B., & Barrientos, R. M. (2017). Food for thought: how nutrition impacts cognition and emotion. *NPJ Sci Food*, *1*, 7. https://doi.org/10.1038/s41538-017-0008-y

Spinelli, M., Fusco, S., Mainardi, M., Scala, F., Natale, F., Lapenta, R., Mattera, A., Rinaudo, M., Li Puma, D. D., Ripoli, C., Grassi, A., D'Ascenzo, M., & Grassi, C. (2017). Brain insulin resistance impairs hippocampal synaptic plasticity and memory by increasing GluA1 palmitoylation through FoxO3a. *Nat Commun*, *8*(1), 2009. https://doi.org/10.1038/s41467-017-02221-9

Spinelli, M., Natale, F., Rinaudo, M., Leone, L., Mezzogori, D., Fusco, S., & Grassi, C. (2020). Neural Stem Cell-Derived Exosomes Revert HFD-Dependent Memory Impairment via CREB-BDNF Signalling. *Int J Mol Sci*, *21*(23). https://doi.org/10.3390/ijms21238994

Stampanoni Bassi, M., Iezzi, E., Gilio, L., Centonze, D., & Buttari, F. (2019). Synaptic Plasticity Shapes Brain Connectivity: Implications for Network Topology. *Int J Mol Sci*, *20*(24). https://doi.org/10.3390/ijms20246193

Stefan, C. J., Manford, A. G., Baird, D., Yamada-Hanff, J., Mao, Y., & Emr, S. D. (2011). Osh proteins regulate phosphoinositide metabolism at ER-plasma membrane contact sites. *Cell*, *144*(3), 389-401. https://doi.org/10.1016/j.cell.2010.12.034

Stuart, G. J., & Häusser, M. (2001). Dendritic coincidence detection of EPSPs and action potentials. *Nat Neurosci*, *4*(1), 63-71. https://doi.org/10.1038/82910

Summers, K. C., Bogard, A. S., & Tavalin, S. J. (2019). Preferential generation of Ca(2+)-permeable AMPA receptors by AKAP79-anchored protein kinase C proceeds via GluA1 subunit phosphorylation at Ser-831. *J Biol Chem*, *294*(14), 5521-5535. https://doi.org/10.1074/jbc.RA118.004340

Tahirovic, S., Schorr, M., & Mayinger, P. (2005). Regulation of intracellular phosphatidylinositol-4-phosphate by the Sac1 lipid phosphatase. *Traffic*, *6*(2), 116-130. https://doi.org/10.1111/j.1600-0854.2004.00255.x

Tani, M., & Kuge, O. (2010). Requirement of a specific group of sphingolipid-metabolizing enzyme for growth of yeast Saccharomyces cerevisiae under impaired metabolism of glycerophospholipids. *Mol Microbiol*, *78*(2), 395-413. https://doi.org/10.1111/j.1365-2958.2010.07340.x

Tani, M., & Kuge, O. (2014). Involvement of Sac1 phosphoinositide phosphatase in the metabolism of phosphatidylserine in the yeast Saccharomyces cerevisiae. *Yeast*, *31*(4), 145-158. https://doi.org/10.1002/yea.3004

Taub, A. H., Katz, Y., & Lampl, I. (2013). Cortical balance of excitation and inhibition is regulated by the rate of synaptic activity. *J Neurosci*, *33*(36), 14359-14368. https://doi.org/10.1523/JNEUROSCI.1748-13.2013

Thomas, M. H., Paris, C., Magnien, M., Colin, J., Pelleieux, S., Coste, F., Escanye, M. C., Pillot, T., & Olivier, J. L. (2017). Dietary arachidonic acid increases deleterious effects of amyloid-beta oligomers on learning abilities and expression of AMPA receptors: putative role of the ACSL4-cPLA(2) balance. *Alzheimers Res Ther*, *9*(1), 69. https://doi.org/10.1186/s13195-017-0295-1

Tieu, K., Perier, C., Caspersen, C., Teismann, P., Wu, D.-C., Yan, S.-D., Naini, A., Vila, M., Jackson-Lewis, V., Ramasamy, R., & Przedborski, S. (2003). D-β-Hydroxybutyrate rescues mitochondrial respiration and mitigates features of Parkinson disease. *Journal of Clinical Investigation*, *112*(6), 892-901. https://doi.org/10.1172/jci200318797

Tokuda, E., Itoh, T., Hasegawa, J., Ijuin, T., Takeuchi, Y., Irino, Y., Fukumoto, M., & Takenawa, T. (2014). Phosphatidylinositol 4-phosphate in the Golgi apparatus regulates cell-cell adhesion and invasive cell migration in human breast cancer. *Cancer Res*, *74*(11), 3054-3066. https://doi.org/10.1158/0008-5472.CAN-13-2441

Tokutake, Y., Onizawa, N., Katoh, H., Toyoda, A., & Chohnan, S. (2010). Coenzyme A and its thioester pools in fasted and fed rat tissues. *Biochem Biophys Res Commun*, *402*(1), 158-162. https://doi.org/10.1016/j.bbrc.2010.10.009

Tomita, S., Shenoy, A., Fukata, Y., Nicoll, R. A., & Bredt, D. S. (2007). Stargazin interacts functionally with the AMPA receptor glutamate-binding module. *Neuropharmacology*, *52*(1), 87-91. https://doi.org/10.1016/j.neuropharm.2006.07.012

Traynelis, S. F., Wollmuth, L. P., McBain, C. J., Menniti, F. S., Vance, K. M., Ogden, K. K., Hansen, K. B., Yuan, H., Myers, S. J., & Dingledine, R. (2010). Glutamate receptor ion channels: structure, regulation, and function. *Pharmacol Rev*, *62*(3), 405-496. https://doi.org/10.1124/pr.109.002451

Turrigiano, G. G., & Nelson, S. B. (2004). Homeostatic plasticity in the developing nervous system. *Nat Rev Neurosci*, *5*(2), 97-107. https://doi.org/10.1038/nrn1327

Twomey, E. C., Yelshanskaya, M. V., & Sobolevsky, A. I. (2019). Structural and functional insights into transmembrane AMPA receptor regulatory protein complexes. *J Gen Physiol*, *151*(12), 1347-1356. https://doi.org/10.1085/jgp.201812264

Vadakkan, K. I. (2016). The functional role of all postsynaptic potentials examined from a first-person frame of reference. *Rev Neurosci*, *27*(2), 159-184. https://doi.org/10.1515/revneuro-2015-0036

Vandenberghe, W., Nicoll, R. A., & Bredt, D. S. (2005). Interaction with the unfolded protein response reveals a role for stargazin in biosynthetic AMPA receptor transport. *J Neurosci*, *25*(5), 1095-1102. https://doi.org/10.1523/JNEUROSCI.3568-04.2005

Venditti, R., Masone, M. C., Rega, L. R., Di Tullio, G., Santoro, M., Polishchuk, E., Serrano, I. C., Olkkonen, V. M., Harada, A., Medina, D. L., La Montagna, R., & De Matteis, M. A. (2019). The activity of Sac1 across ER-TGN contact sites requires the four-phosphate-adaptor-protein-1. *J Cell Biol*, *218*(3), 783-797. https://doi.org/10.1083/jcb.201812021

Wagh, D. A., Rasse, T. M., Asan, E., Hofbauer, A., Schwenkert, I., Durrbeck, H., Buchner, S., Dabauvalle, M. C., Schmidt, M., Qin, G., Wichmann, C., Kittel, R., Sigrist, S. J., & Buchner, E. (2006). Bruchpilot, a protein with homology to ELKS/CAST, is required for structural integrity and function of synaptic active zones in Drosophila. *Neuron*, *49*(6), 833-844. https://doi.org/10.1016/j.neuron.2006.02.008

Wakana, Y., Kotake, R., Oyama, N., Murate, M., Kobayashi, T., Arasaki, K., Inoue, H., & Tagaya, M. (2015). CARTS biogenesis requires VAP-

lipid transfer protein complexes functioning at the endoplasmic reticulum-Golgi interface. *Mol Biol Cell*, *26*(25), 4686-4699. https://doi.org/10.1091/mbc.E15-08-0599

Wang, D., & Mitchell, E. S. (2016). Cognition and Synaptic-Plasticity Related Changes in Aged Rats Supplemented with 8- and 10-Carbon Medium Chain Triglycerides. *PLoS One*, *11*(8), e0160159. https://doi.org/10.1371/journal.pone.0160159

Wang, J., Chen, J., Enns, C. A., & Mayinger, P. (2013). The first transmembrane domain of lipid phosphatase SAC1 promotes Golgi localization. *PLoS One*, *8*(8), e71112. https://doi.org/10.1371/journal.pone.0071112

Wang, J., Freire, D., Knable, L., Zhao, W., Gong, B., Mazzola, P., Ho, L., Levine, S., & Pasinetti, G. M. (2015). Childhood and adolescent obesity and long-term cognitive consequences during aging. *J Comp Neurol*, *523*(5), 757-768. https://doi.org/10.1002/cne.23708

Wang, S., Li, Y., Gong, J., Ye, S., Yang, X., Zhang, R., & Ma, C. (2019). Munc18 and Munc13 serve as a functional template to orchestrate neuronal SNARE complex assembly. *Nat Commun*, *10*(1), 69. https://doi.org/10.1038/s41467-018-08028-6

Wang, X. J., & Buzsáki, G. (1996). Gamma oscillation by synaptic inhibition in a hippocampal interneuronal network model. *J Neurosci*, *16*(20), 6402-6413. https://doi.org/10.1523/JNEUROSCI.16-20-06402.1996

Wang, Z., Ge, Q., Wu, Y., Zhang, J., Gu, Q., & Han, J. (2020). Impairment of Long-term Memory by a Short-term High-fat Diet via Hippocampal Oxidative Stress and Alterations in Synaptic Plasticity. *Neuroscience*, *424*, 24-33. https://doi.org/10.1016/j.neuroscience.2019.10.050

Watt, A. J., Sjostrom, P. J., Hausser, M., Nelson, S. B., & Turrigiano, G. G. (2004). A proportional but slower NMDA potentiation follows AMPA potentiation in LTP. *Nat Neurosci*, *7*(5), 518-524. https://doi.org/10.1038/nn1220

Wei, H. C., Sanny, J., Shu, H., Baillie, D. L., Brill, J. A., Price, J. V., & Harden, N. (2003). The Sac1 lipid phosphatase regulates cell shape change and the JNK cascade during dorsal closure in Drosophila. *Curr Biol*, *13*(21), 1882-1887. https://doi.org/10.1016/j.cub.2003.09.056

Whitters, E. A., Cleves, A. E., McGee, T. P., Skinner, H. B., & Bankaitis, V. A. (1993). SAC1p is an integral membrane protein that influences the cellular requirement for phospholipid transfer protein function and inositol in yeast. *J Cell Biol*, *122*(1), 79-94. https://doi.org/10.1083/jcb.122.1.79

Wolfgang, M. J., Cha, S. H., Millington, D. S., Cline, G., Shulman, G. I., Suwa, A., Asaumi, M., Kurama, T., Shimokawa, T., & Lane, M. D. (2008). Brain-specific carnitine palmitoyl-transferase-1c: role in CNS fatty acid metabolism, food intake, and body weight. *J Neurochem*, *105*(4), 1550-1559. https://doi.org/10.1111/j.1471-4159.2008.05255.x

Wolfgang, M. J., Kurama, T., Dai, Y., Suwa, A., Asaumi, M., Matsumoto, S. I., Cha, S. H., Shimokawa, T., & Lane, M. D. (2006). The brain-specific carnitine palmitoyltransferase-1c regulates energy homeostasis. *Proc Natl Acad Sci U S A*, *103*, 7282–7287. https://doi.org/10.1073/pnas.0602205103

Wood, C. S., Hung, C. S., Huoh, Y. S., Mousley, C. J., Stefan, C. J., Bankaitis, V., Ferguson, K. M., & Burd, C. G. (2012). Local control of phosphatidylinositol 4-phosphate signaling in the Golgi apparatus by Vps74 and Sac1 phosphoinositide phosphatase. *Mol Biol Cell*, *23*(13), 2527-2536. https://doi.org/10.1091/mbc.E12-01-0077

Wood, C. S., Schmitz, K. R., Bessman, N. J., Setty, T. G., Ferguson, K. M., & Burd, C. G. (2009). PtdIns4P recognition by Vps74/GOLPH3 links PtdIns 4-kinase signaling to retrograde Golgi trafficking. *J Cell Biol*, *187*(7), 967-975. https://doi.org/10.1083/jcb.200909063

Wu, M., Liao, M., Huang, R., Chen, C., Tian, T., Wang, H., Li, J., Li, J., Sun, Y., Wu, C., Li, Q., & Xiao, X. (2022). Hippocampal overexpression of TREM2 ameliorates high fat diet induced cognitive impairment and modulates phenotypic polarization of the microglia. *Genes Dis*, *9*(2), 401-414. https://doi.org/10.1016/j.gendis.2020.05.005

Xu, Y., Jiang, C., Wu, J., Liu, P., Deng, X., Zhang, Y., Peng, B., & Zhu, Y. (2021). Ketogenic diet ameliorates cognitive impairment and neuroinflammation in a mouse model of Alzheimer's disease. *CNS Neurosci Ther*, *28*(4), 580-592. https://doi.org/10.1111/cns.13779

Yang, G., & Cynader, M. S. (2014). Regulation of protein trafficking: JNK3 at the Golgi complex. *Cell Cycle*, *13*(1), 5-6. https://doi.org/10.4161/cc.27019

Yang, G., Zhou, X., Zhu, J., Liu, R., Zhang, S., Coquinco, A., Chen, Y., Wen, Y., Kojic, L., Jia, W., & Cynader, M. S. (2013). JNK3 couples the neuronal stress response to inhibition of secretory trafficking. *6*(283), ra57. https://doi.org/10.1126/scisignal.2003727

Yin, J. X., Maalouf, M., Han, P., Zhao, M., Gao, M., Dharshaun, T., Ryan, C., Whitelegge, J., Wu, J., Eisenberg, D., Reiman, E. M., Schweizer, F. E., & Shi, J. (2016). Ketones block amyloid entry and improve cognition in an Alzheimer's model. *Neurobiol Aging*, *39*, 25-37. https://doi.org/10.1016/j.neurobiolaging.2015.11.018

Yomogida, Y., Matsuo, J., Ishida, I., Ota, M., Nakamura, K., Ashida, K., & Kunugi, H. (2021). An fMRI Investigation into the Effects of Ketogenic Medium-Chain Triglycerides on Cognitive Function in Elderly Adults: A Pilot Study. *Nutrients*, *13*(7). https://doi.org/10.3390/nu13072134

Yoon, Y. J., White, S. L., Ni, X., Gokin, A. P., & Martin-Caraballo, M. (2012). Downregulation of GluA2 AMPA receptor subunits reduces the dendritic arborization of developing spinal motoneurons. *PLoS One*, *7*(11), e49879. https://doi.org/10.1371/journal.pone.0049879

Zaugg, K., Yao, Y., Reilly, P. T., Kannan, K., Kiarash, R., Mason, J., Huang, P., Sawyer, S. K., Fuerth, B., Faubert, B., Kalliomaki, T., Elia, A., Luo, X., Nadeem, V., Bungard, D., Yalavarthi, S., Growney, J. D., Wakeham, A., Moolani, Y., . . . Mak, T. W. (2011). Carnitine palmitoyltransferase 1C promotes cell survival and tumor growth under conditions of metabolic stress. *Genes Dev*, *25*(10), 1041-1051. https://doi.org/10.1101/gad.1987211

Zewe, J. P., Wills, R. C., Sangappa, S., Goulden, B. D., & Hammond, G. R. (2018). SAC1 degrades its lipid substrate PtdIns4P in the endoplasmic reticulum to maintain a steep chemical gradient with donor membranes. *Elife*, *7*. https://doi.org/10.7554/eLife.35588

Zhang, H., Zhou, J., Xiao, P., Lin, Y., Gong, X., Liu, S., Xu, Q., Wang, M., Ren, H., Lu, M., Wang, Y., Zhu, J., Xie, Z., Li, H., & Lu, K. (2021). PtdIns4P restriction by hydrolase SAC1 decides specific fusion of autophagosomes with lysosomes. *Autophagy*, *17*(8), 1907-1917. https://doi.org/10.1080/15548627.2020.1796321

Zhang, J., Cao, Q., Li, S., Lu, X., Zhao, Y., Guan, J. S., Chen, J. C., Wu, Q., & Chen, G. Q. (2013). 3-Hydroxybutyrate methyl ester as a potential drug against Alzheimer's disease via mitochondria protection mechanism. *Biomaterials*, *34*(30), 7552-7562. https://doi.org/10.1016/j.biomaterials.2013.06.043

Zhao, Q., Stafstrom, C. E., Fu, D. D., Hu, Y., & Holmes, G. L. (2004). Detrimental effects of the ketogenic diet on cognitive function in rats. *Pediatr Res*, *55*(3), 498-506. https://doi.org/10.1203/01.PDR.0000112032.47575.D1

Zhong, S., Hsu, F., Stefan, C. J., Wu, X., Patel, A., Cosgrove, M. S., & Mao, Y. (2012). Allosteric activation of the phosphoinositide phosphatase Sac1 by anionic phospholipids. *Biochemistry*, *51*(15), 3170-3177. https://doi.org/10.1021/bi300086c

Zhou, Q., Homma, K. J., & Poo, M. M. (2004). Shrinkage of dendritic spines associated with long-term depression of hippocampal synapses.

Neuron, *44*(5), 749-757. https://doi.org/10.1016/j.neuron.2004.11.011

Zhu, J. J., Esteban, J. A., Hayashi, Y., & Malinow, R. (2000). Postnatal synaptic potentiation: delivery of GluR4-containing AMPA receptors by spontaneous activity. *Nat Neurosci*, *3*(11), 1098-1106. https://doi.org/10.1038/80614

Zucker, R. S., & Regehr, W. G. (2002). Short-term synaptic plasticity. *Annu Rev Physiol*, *64*, 355-405. https://doi.org/10.1146/annurev.physiol.64.092501.114547

ABBREVIATIONS

2-AG	2-arachidoniyglycerol
A	Acceptor
aa	Amino acid
AA	Araquidonic acid
ACC	Acetyl-CoA carboxylase
aCSF	Artificial cerebrospinal fluid
AMPAR	α-amino-3-hydroxy-5-methyl-4-isoxazolepropionic acid receptor
AMPK	AMP-activated protein kinase
BHB	β-hydroxybutyrate
CAMKII	Ca^{2+}/calmodulin-dependent kinase II
CNIH	Cornichon protein
CNS	Central nervous system
COPI	Coat protein I
COPII	Coat protein II
COT	Carnitine octanoyltransferase
CPT	Carnitine palmitoyltransferase
CrAT	Carnitine acetyltransferase
CTD	C-terminal domain
D	Donor
D-AP5	D-(-)-2-amino-5-phosphonopentanoic acid
DEPC	Diethyl pyrocarbonate
DHA	Docosahexaenoic acid
DI	Discrimination index
DIO	Diet-induced obesity
DMEM	Dulbecco's Modified Eagle Medium
DMSO	Dimethyl sulfoxide
ECR	Extracellular region
EGTA	Ethylene glycol tetraacetic acid
Em	Emission
EPSP	Excitatory postsynaptic potential
ER	Endoplasmic reticulum
Ex	Excitation
FACS	Fluorescent-activated cell sorting
FAS	Fatty acid synthase
FBS	Fetal bovine serum
fEPSP	Field excitatory postsynaptic potential
FRET	Föster resonance energy transfer
FRETap	FRET acceptor photobleaching

FRETse	FRET sensitized emission
GABA	γ-aminobutyric
HBSS	Hank's balanced salt solution
HEK293T	Human embryonic kidney 293T
HFD	High-fat diet
HFS	High-frequency stimulation
HSP	Hereditary spastic paraplegia
I/O	Input/output
ICR	Intracellular region
icv	Intracerebroventricular
IPSP	Inhibitory postsynaptic potential
JNK3	c-Jun N-terminal kinase 3
KO	Knock-out
LBD	Ligand-binding domain
LTD	Long-term depression
LTP	Long-term potentiation
mEPSC	Miniature excitatory synaptic current
ms	Milliseconds
MUFAD	Mono-unsaturated fatty acid diet
mV	Millivolts
MWM	Morris water maze
MΩ	Megaohmios
NMDAR	N-methyl-D-aspartate receptor
NORT	Novel object recognition test
NTD	N-terminal domain
OA	Oleic acid
OFT	Open field test
OLT	Object location test
PA	Palmitic acid
pA	Picoamperes
PAK3	p21-activated kinase 3
PBS	Dulbecco's Phosphate Buffered Saline
PCR	Polymerase chain reaction
PEI	Polyethylenimine
PI	Phosphatidylinositol
PI4P	Phosphatidylinositol 4-phosphate
PKA	cAMP-dependent kinase
PKC	Protein kinase C
PPR	Paired-pulse ratio

PS	Phosphatidylserine
PSD95	Postsynaptic density protein 95
PTX	Picrotoxin
PTX	Picrotoxin
rpm	Revolutions per minute
Rs	Series resistance
RT	Room temperature
SAP97	Synapse-associated protein 97
SC	Schaffer collateral
SD	Standard diet
SFAD	Saturated fatty acid diet
SNARE	soluble N-ethylmaleimide-sensitive factor attachment protein receptors
TARP	Transmembrane AMPA-regulatory protein
TGN	Trans Golgi network
TM(D)	Transmembrane domain
TOFA	5-tetradecyloxy-2-furoic acid
TTX	Tetrodotoxin
V	Volts
WT	Wild type

LISTS OF FIGURES AND TABLES

Figures

Tables

LISTS OF REACTIVES AND ANTIBODIES

Reactives

Product	Reference	Distributor
40 µm cell strainer	542040	ddBiolab
β-hydroxybutyrate	H6501	Sigma
B27	17504044	ThermoFisher
BamHI	R3136	New England BioLabs
Benzonase	Sigma	E1014
Borosilicate glass	GC120F-10	Harvard Apparatus
Bradford (Bio-Rad Protein Assay Dye Reagent)	5000006	Bio-Rad
BSA	10735078001	Roche
Collagen type I	354236	Corning
D-AP5	ab120003	Abcam
Deffated BSA	126575	Millipore
DEPC	D5758	Sigma-Aldrich
Desthiobiotin	2-1000-001	IBA Lifesciences
DMEM	D5671	Sigma-Aldrich
DMSO	1029521011	Merck
DNase	4716728001	Merk
Docosahexanoic acid sodium salt	D8768	Sigma
Ethidium bromide	GX12420	Genaxis
FBS	FBS12A	Capricorn Scientific
Filtered tubes	VS2042	Sartorius
Fluoromount-G®	0100-01	Southern Biotech
GDN detergent	GDN101	Anatrace
Glutamax	X0551-100	Biowest
Goat serum	g-9023	Sigma-Aldrich
HBSS	14052-050	Fisher
Hoescht	14530	Sigma-Aldrich
Horse serum	10368902	Fisher

KpnI	R3142	New England BioLabs
Luminata Forte Western HRP substrate	WBLUF0500	Merck
Malonyl-CoA	M4263	Sigma-Aldrich
Maxiprep DNA purification kit	740414.50	Cultek
Midiprep DNA purification kit	MB14101	NZYtech
Neurobasal	21103049	ThermoFisher
Paraformaldehyde	252549	Sigma-Aldrich
PBS10X	D1408	Sigma-Aldrich
PEI	24765	Polysciences
Penicillin-streptomycin	P0781	Sigma-Aldrich
Phosphatase inhibitor	A32957	Fisher Scientific
Picrotoxin	P1675	Sigma-Aldrich
Pierce® Centrifuge Columns (2 mL)	89896	Thermo Scientific
Pierce™ BCA Protein Assay Kit	23225	ThermoFisher
Polyacrylamide gels	Midi-PROTEAN	BioRad
Poly-D-lysine	P7886	Sigma-Aldrich
Protease inhibitor	A32955	Fisher Scientific
PVDF membrane	IPVH00010	Merck
Retinoic acid	R2622	Sigma
Sodium oleate	O7501	Sigma
Sodium palmitate	P9767	Sigma
Strep-Tactin® Superflow® high capacity resin	2-1208-002	IBA Lifesciences
Tetrodotoxin	ab120054	Abcam
TOFA	ab141578	Abcam
Triton	X100	Sigma-Aldrich
Trypsin	15400054	ThermoFisher
Tween20	P9416	Sigma-Aldrich
Type F immersion liquid	11513859	Leica
Whatman paper	11330744	Fisher Scientific

Antibodies

Product	Reference	Distributor
α-β-actin	ma1-91399	Fisher
α-ACC	3676	Cell Signalling
α-BDNF	SC-546	Santa Cruz
α-calnexin	ab22595	abcam
α-chicken 488	A11039	Invitrogen
α-CPT1C	Produced by Dolors Serra's laboratory	Produced by Dolors Serra's laboratory
α-CREB	sc-58	Santa Cruz
α-FAS	sc-48357	Santa Cruz
α-GFP	2956S	Cell Signalling
α-GFP	ab13970	abcam
α-GluA1	PC246	Millipore
α-GluA1	ab174785	abcam
α-mouse 488	A11001	Invitrogen
α-mouse-HRP	115-035-003	Jackson
α-p(Ser129)-CREB	sc-101662	Santa Cruz
α-p(Ser79)-ACC	3661	Cell Signalling
α-p(Ser831)-GluA1	ab76321	abcam
α-p(Ser845)-GluA1	ab109464	abcam
α-PDD95	ab18258	abcam
α-rabbit 568	A11011	Invitrogen
α-rabbit-HRP	111-035-144	Jackson
α-SAC1	13033-1-AP	ProteinTech

APPENDIX

1. Participation in congresses

6th MetNet International Annual Meeting 2020: The key role of crosstalk in metabolic control. 28-29 September 2020, Barcelona (Catalan Society of Biology) – Assistant

7th MetNet International Annual Meeting 2021: Multifaceted metabolism in human disease. 8 October 2021, Barcelona (Catalan Society of Biology) – Assistant

Seeing is believing: imaging the molecular processes of life. 5-8 October 2021, online (EMBO-EMBL) – Assistant

19th National Meeting of the Spanish Society of Neuroscience. 3-5 November 2021, Lleida (SENC) – Poster

XI Cajal Conference: New frontiers in neuron-glial plasticity in health and disease. 18-20 May, Sant Feliu de Guixols (SENC) – Oral communication and poster

XII Neurobiology Symposium: Towards translational medicine. 7-8 June, Barcelona (Catalan Society of Biology) – Oral communication

2. Publications

First authorship shared – Louail, A., Bengoetxea de Tena, I., Rojas, R., & Casals, N. (2023). XIth Cajal Conference: New frontiers in neuron-glial plasticity in health and disease. *Eur J Neurosci*, 57(9), 1447-1465. doi.org/10.1111/ejn.15960

Contributing author – Fado, R., Molins, A., Rojas, R., & Casals, N. (2022). Feeding the Brain: Effect of Nutrients on Cognition, Synaptic Function, and AMPA Receptors. *Nutrients*, 14(19). doi.org/10.3390/nu14194137